Escola de Camins
Escola Tècnica Superior d'Enginyeria de Camins, Canals i Ports
UPC BARCELONATECH

Evaluation of 3D Dynamic Effects Induced by High-speed Trains on Double-track Slab Bridges

TREBALL FINAL DE MÀSTER

Treball realitzat per:
Assís Arañó Barenys

Dirigit per:
José Manuel González López

Màster en:
Enginyeria de Camins, Canals i Ports

Barcelona, juny de 2016

Departament d'Enginyeria Civil i Ambiental (ECA)

Evaluation of 3D Dynamic Effects Induced by High-speed Trains on Double-track Slab Bridges

Assís Arañó Barenys
June 2016

Polytechnic University of Catalonia (UPC)
Department of Civil and Environmental Engineering
Barcelona, Spain, 2016

Abstract

The present work describes a dynamic analysis which has to be performed in addition to static design for rail-way bridges where the maximum permissible train speed exceeds 200 km/h. This analysis requires a lot of computing time. For this reason Svedholm and Andersson (2016) have developed a simple tool describing the relationship between the first eigenfrequency of the bridge, the span length and the minimum mass to fulfil the regulation specified in EN-1990.

However, these diagrams are based on 2D beam models in which the 3D dynamic effects are not considered. An evaluation of the torsional modes has been performed by analysing parametrized 3D bridge models, in order to obtain design diagrams including these effects.

Therefore, a frequency domain analysis has been implemented, based on a steady-state step previously performed in a FEM software. This approach provides a fast way to solve the equation of motion due to the Fourier transform properties, and allows the application of several load configurations which are convenient for a parametric study.

From this analysis it can be concluded that the thickness to fulfil the demands is larger for 3D models than for 2D. On one hand, contribution of torsional modes of vibration is more significant for the shortest span length, and on the other hand shear-lag effects lead to a reduction of the total resisting bending section.

Keywords: Dynamics, Frequency analysis, 3D model, Design diagrams, Torsional modes of vibration

Resumen

El presente trabajo describe el análisis dinámico necesario que se debe realizar en puentes para trenes, con una velocidad máxima admisible superior a 200 km/h, además del correspondiente análisis estático. Éste análisis requiere una gran cantidad de tiempo de cálculo por lo que Svedholm and Andersson (2016) desarrollaron unos diagramas para el pre diseño del puente. Dichos diagramas describen la relación entre la primera frecuencia natural del puente, la luz de vano, y la masa mínima necesaria para satisfacer la normativa especificada en EN-1990.

El cuerpo del trabajo mejora los actuales diagramas desarrollados basados en modelos bidimensionales, dónde no se consideran los efectos dinámicos producidos en un análisis tridimensional, como los efectos de torsión. Ésta aplicación se realiza mediante el estudio de diferentes modelos de puentes evaluando los efectos dinámicos producidos e incorporándolos en los nuevos diagramas.

Para éste análisis, se ha realizado un estudio de dominio de la frecuencia, llevado a cabo en base al análisis dinámico previamente realizado en un programa de elementos finitos. La ecuación de movimiento se resuelve de manera más rápida utilizando las propiedades de la transformada de Fourier. Adicionalmente, ésta aproximación permite la aplicación de varias configuraciones de carga, lo que resulta conveniente para poder realizar un estudio paramétrico.

Finalmente, comparando los modelos se puede concluir que el espesor mínimo obtenido que cumple la normativa, es mayor en los modelos tridimensionales, desarrollados en éste trabajo, frente a los bidimensionales, punto de partida del mismo.

Como conclusiones adicionales, por un lado, la contribución de los modos de vibración torsionales es más significativa para luces más cortas ; y por otro lado, el arrastre por cortante en las secciones transversales se traduce en una reducción de su sección resistente a flexión.

Palabras clave : Dinámica estructural, Análisis de frecuencia, Modelo 3D, Diagramas de Pre diseño, Torsión.

Preface

This master thesis was initiated at the Department of Civil and Architectural engineering at the Royal Institute of Technology (KTH), in collaboration with Tyréns, division of Structural Engineering and Bridges.

I would like to give my sincere gratitude to my inspiring supervisors, Mahir Ülker-Kaustell and Andreas Andersson for their support, the time spent and all the advice provided which was very valuable for me. A special thanks to Prof. Raid Karoumi for helping me with the formulation of the thesis.

I would also like to thank Tyréns AB for the opportunity of carrying out my thesis in the bridge department, with the support of the people working there.

I would like to thank Cristiana Golfetto and Yuri Impens for reading my thesis and giving me suggestions.

Finally, I would like to thank my family for their love, support and encouragement.

Notations

Notation	Description	Unit
ξ	Damping ratio	[%]
δ	Deflection	[m]
ν	Poisson's ratio	[-]
ρ_{b}	Density of ballast	[kg/m^3]
ρ_{c}	Density of concrete	[kg/m^3]
θ_1	Rotation over the ends of the deck	[rad/s]
θ_2	Rotation over the mid-supports	[rad/s]
ω	Angular frequency	[rad/s]
ω_1	First natural frequency	[rad/s]
ω_{n}	Natural frequency	[rad/s]
a	Acceleration	[m/s^2]
c	Damping coefficient	[Ns/m]
E	Young modulus	[Pa]
F	Force amplitude	[N]
f_{n}	Natural frequency	[Hz]
f_{s}	Sampling frequency	[Hz]
H	Complex frequency response function	[m/Ns^2]
k	Stiffness	[N/m]
L	Length of the main span	[m]
L_{b}	Total length of the bridge	[m]
m	Mass	[kg]
n_0	First eigenfrequency of the bridge	[rad/s]
T	Total time of the analysis	[s]
U	Fourier transform of displacement	[m]
u	Displacement	[m]
v	Speed of the train	[km/h]

Abbreviations

Abbreviation	Description
2D	Two-dimensional
3D	Three-dimensional
DAF	Dynamic amplification factor
DFT	Discrete Fourier Transform
DOF	Degree of freedom
FE	Finite element
FEM	Finite element method
FEA	Finite element analysis
FFT	Fast Fourier Transform
GUI	Graphical User Interface
MDOF	Multiple degrees of freedom
ODB	Output database file
SDOF	Single degree of freedom

Contents

Chapter 1

Introduction

1.1 General background

Public transportations have a crucial role in the organization of a country and while Sweden has been growing, the country's rail network has been expanding. Demands for faster and environmentally friendly transports are rising. For these reasons, the Swedish government decided in 2012 to start building new high-speed railway lines between Södertälje in the area of Stockholm and Linköping in less than one hour. The long-term objective is to connect Stockholm central station with Göteborg in two hours. To reach this goal, this project will involve the construction of more than 155 new bridges with a total length of 10 km.

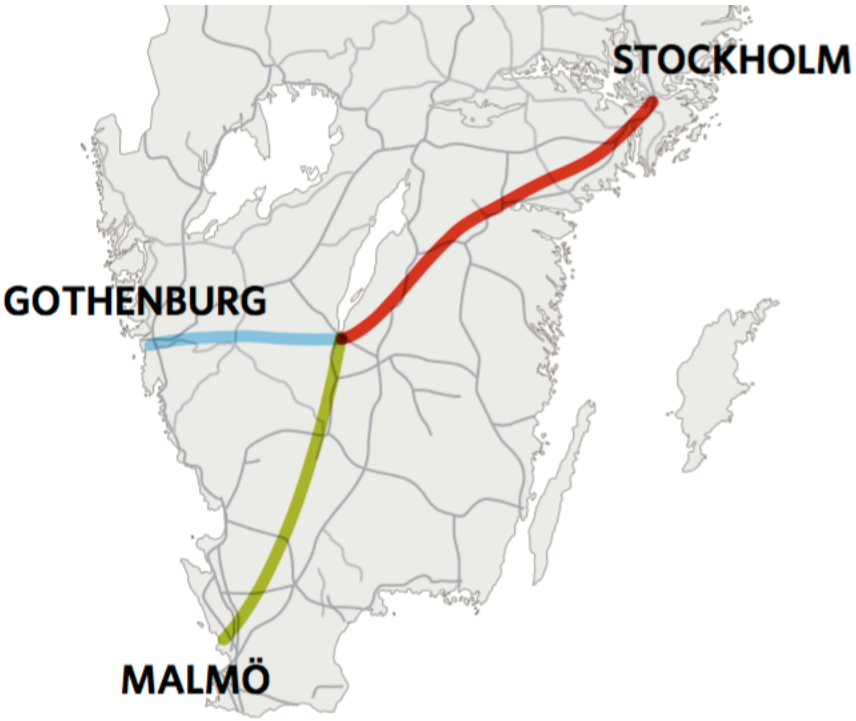

Figure 1.1 – Ostlänken project

In addition to a static design, high-speed railway bridges require a dynamic analysis if the maximum permissible speed at the site is greater than 200 km/h. To ensure passenger comfort and traffic safety, maximum vertical deflection and acceleration have to be controlled as the rotation of the deck over the supports. All the requirements regarding a dynamic analysis are defined in EN 1991-2, section 6.4.6 and according to EN 1990 A.2.4.4 have to be applied to each new construction in Europe.

Estimating these effects often require a lot of time and computer resources. Besides, these analyses are very sensitive to different parameters such as the mass of the bridge, the stiffness or the type of boundary conditions. Thus wrong assumptions can easily lead to poor results. Moreover, a conservative static design can result in a dynamic design on the unsafe side.

1.2 Previous studies

In order to save time in the preliminary stage of the design, Svedholm and Andersson (2016) have developed a simple tool to check if a given bridge fulfils the dynamic requirements according to Eurocode. In these diagrams the relationship between the span length and the first eigenfrequency of the bridge are presented, from which the necessary mass or stiffness to satisfy the demands can be deduced.

Besides, some sections representing slab or beam bridges are presented with the minimum dimensions to fulfil the dynamic requirements. It provides a fast way to check if a section is satisfactory in a preliminary design stage, which is very useful for engineers.

However, those diagrams have been obtained under certain assumptions:

- Results are based on 2D beam models with constant mass and stiffness with given proportions in the span lengths for three and four span bridges.
- Diagrams are obtained for a maximum permissible speed at the site equal to 320 km/h.
- Only un-ballasted tracks are considered.
- The static design is not checked.

1.3 Aims and scope

In addition to the rules formulated previously, the Swedish transport administration Trafikverket (2014) has listed some other demands. Regarding them, 3D effects and torsional modes of vibration that could engender more dynamic effects should be taken into consideration, unless it can be shown that 2D models are on the safe side.

The purpose of this thesis is to study the dynamic effects due to 3D bridge models for ballast free tracks, which are not considered in 2D beam models. Another purpose is to figure out to what extent 2D diagrams can be used, and how they can be interpreted when adding modes of vibration coming from 3D effects.

The topic will cover slab bridges composed of several spans up to 4 spans, with span lengths from 10 to 30 meters. No substructure interacting with the bridge has been considered.

Chapter 2

Theoretical background

2.1 Structural Dynamics Theory

2.1.1 Single-Degree-of-Freedom Systems

The SDOF systems are those in which the motion of the system is defined in only one coordinate. An example of SDOF system is a cantilever subjected to a vertical point load, applied at the endpoint. Since the displacement on the horizontal direction is really small, the motion of the cantilever is considered to be in the vertical direction.

The three basic components of all mechanical systems are spring, damper and mass. By exposing each of these components to a constant force, a constant displacement, constant velocity and constant acceleration are obtained.

The structural dynamic analysis is focused on the evaluation of the displacement time-histories of a structure subjected to a certain load that varies with time. The equations of motion are the mathematical expressions which define these dynamic displacements, giving as a solution the time-histories of the displacement.

fig. 2.1 shows an example of a SDoF system. fig. 2.1a presents a representation of the spring, the damper and the mass and in fig. 2.1b the free-body diagram is shown, with the forces to which it is subjected.

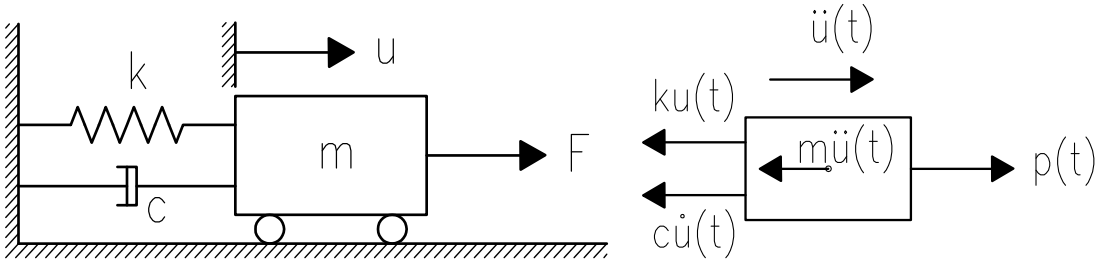

(a) Single-Degree-of-Freedom system (b) Free-body diagram of the SDOF system

Figure 2.1 – Example of a SDOF system and its free-body diagram

In order for the system to reach equilibrium, the equation which needs to be fulfilled is the following:

$$m\,\ddot{u}(t) + c\,\dot{u}(t) + k\,u(t) = p(t) \tag{2.1}$$

If the damping is ignored in eq. (2.1), the natural frequency ω_n can be calculated as:

$$\omega_n = \sqrt{\frac{k}{m}} \tag{2.2}$$

If the damping is considered, eq. (2.2) does not fully describe the oscillation in the system. Thus, the damped natural frequency can be calculated as:

$$\omega_d = \omega_n \sqrt{1 - \xi^2} \tag{2.3}$$

However, eq. (2.3) is only valid when the damping ration defined in eq. (2.4) is less than 1.

$$\xi = \frac{c}{2\sqrt{km}} \tag{2.4}$$

2.1.2 Multi-Degree-of-Freedom Systems

In this section the discretization of the structure is explained and definitions for the different forces are given.

- **Discretization**

  First of all, it is needed to define the DOFs of the structure. As explained in the FEM section, a general frame structure can be idealized as different elements (beams, columns...) assembled and connected through nodes. A two-dimensional frame has three DOFs, two translations and one rotation. A three-dimensional frame has six DOFs, three translations and three rotations, one in each axis (x, y and z).

- **Elastic forces**

  These types of forces are related with the structure stiffness. The stiffness matrix $\mathbf{K}$ relates the external forces f_{Sj} on the stiffness component of the structure to the displacements u_j. To obtain it, a unit displacement is applied along DOF j, holding all other displacements to zero. Each coefficient k_{ij} can be seen as the force that should be applied in DOF i to get a zero displacement

when a unit displacement is applied in DOF j. The following is obtained by superposition:

$$f_{Si} = k_{i1}u_1 + k_{i2}u_2 + \cdots + k_{ij}u_j + \cdots + k_{iN}u_N \tag{2.5}$$

This equation exists for each $i = 1$ to N. The system of equations can be written in matrix form:

$$\begin{bmatrix} f_{S1} \\ f_{S2} \\ \vdots \\ f_{SN} \end{bmatrix} = \begin{bmatrix} k_{11} & k_{12} & \dots & k_{1j} & \dots & k_{1N} \\ k_{21} & k_{22} & \dots & k_{2j} & \dots & k_{2N} \\ \vdots & \vdots & & \vdots & & \vdots \\ k_{N1} & k_{N2} & \dots & k_{Nj} & \dots & k_{NN} \end{bmatrix} \begin{Bmatrix} u_1 \\ u_2 \\ \vdots \\ u_N \end{Bmatrix}$$

or,

$$\mathbf{f}_S = \mathbf{k}\mathbf{u} \tag{2.6}$$

Where $\mathbf{k}$ is the *stiffness matrix* of the structure, and is a symmetric matrix ($k_{ij} = k_{ji}$).

- **Damping forces**

As previously explained, damping in the structure dissipates the energy of a vibrating structure. The damping matrix $\mathbf{C}$ relates the external forces f_{Dj} acting on the damping component of the structure to the velocities $\dot{u}_j$. In this case, a velocity unit is applied along DOF j, while all the others are zero. Each coefficient c_{ij} can be seen as the force that should be applied in the node i to get a null velocity when a unit velocity is applied in node j. The following is obtained by superposition:

$$f_{Di} = c_{i1}\dot{u}_1 + c_{i2}\dot{u}_2 + \cdots + c_{ij}\dot{u}_j + \cdots + c_{iN}\dot{u}_N \tag{2.7}$$

This equation exist for each $i = 1$ to N. The system of equations can be written in matrix form:

$$\begin{bmatrix} f_{D1} \\ f_{D2} \\ \vdots \\ f_{DN} \end{bmatrix} = \begin{bmatrix} c_{11} & c_{12} & \dots & c_{1j} & \dots & c_{1N} \\ c_{21} & c_{22} & \dots & c_{2j} & \dots & c_{2N} \\ \vdots & \vdots & & \vdots & & \vdots \\ c_{N1} & c_{N2} & \dots & c_{Nj} & \dots & c_{NN} \end{bmatrix} \begin{Bmatrix} \dot{u}_1 \\ \dot{u}_2 \\ \vdots \\ \dot{u}_N \end{Bmatrix}$$

or,

$$\mathbf{f}_D = \mathbf{c}\dot{\mathbf{u}} \tag{2.8}$$

Where $\mathbf{c}$ is the *damping matrix* of the structure.

- **Inertia forces**

Inertia forces are related with the mass of the structure. The mass matrix $\mathbf{M}$

relates the external forces f_{Ij} acting on the mass component of the structure to the accelerations $\ddot{u}_j$. To obtain it, unit acceleration is applied along DOF j, keeping the acceleration on the rest of DOFs with a value of zero. Each coefficient m_{ij} represents the external force that should be applied to equilibrate inertia forces in the node i to keep a zero acceleration when a unit acceleration in node j is applied. The following is obtained by superposition:

$$f_{Ii} = m_{i1}\ddot{u}_1 + m_{i2}\ddot{u}_2 + \cdots + m_{ij}\ddot{u}_j + \cdots + m_{iN}\ddot{u}_N \tag{2.9}$$

This equation exist for each $i = 1$ to N. The system of equations can be written in matrix form:

$$\begin{bmatrix} f_{I1} \\ f_{I2} \\ \vdots \\ f_{IN} \end{bmatrix} = \begin{bmatrix} m_{11} & m_{12} & \dots & m_{1j} & \dots & m_{1N} \\ m_{21} & m_{22} & \dots & m_{2j} & \dots & m_{2N} \\ \vdots & \vdots & & \vdots & & \vdots \\ m_{N1} & m_{N2} & \dots & m_{Nj} & \dots & m_{NN} \end{bmatrix} \begin{Bmatrix} \ddot{u}_1 \\ \ddot{u}_2 \\ \vdots \\ \ddot{u}_N \end{Bmatrix}$$

or,

$$\mathbf{f}_I = \mathbf{m}\ddot{\mathbf{u}} \tag{2.10}$$

Where $\mathbf{m}$ is the *mass matrix* of the structure. As the stiffness matrix, the mass matrix is symmetric ($m_{ij} = m_{ji}$).

- **External forces**

Finally, once the forces are described, the equation of motion for a MDF system can be written when external dynamic forces $\mathbf{p}(t)$ are applied on it. As has been described, these external forces are applied in three components of the structure: $\mathbf{f}_S(t)$ to the stiffness component, $\mathbf{f}_D(t)$ to the damping component and $\mathbf{f}_I(t)$ to the mass component.

$$\mathbf{f}_I + \mathbf{f}_D + \mathbf{f}_S = \mathbf{p}(t) \tag{2.11}$$

So if all the components are taken into consideration, the following is obtained:

$$\mathbf{m}\ddot{\mathbf{u}} + \mathbf{c}\dot{\mathbf{u}} + \mathbf{k}\mathbf{u} = \mathbf{p}(t) \tag{2.12}$$

This is the equation of motion for a MDF system. It is equivalent to the one obtained for a SDF system, each scalar in the SDF becomes a vector or a matrix of order N, the number of DOFs in the MDF system.

2.2 Fourier Transform

2.2.1 Definition

From any arbitrary periodic signal $f(t)$, the Fourier series can be constructed as a sum of many different periodic functions, with different frequencies. Thus, the Fourier transform of the original signal can be written as:

$$f(t) = \frac{a_0}{2} + \sum_{n=1}^{\infty}[a_n \cos(n\omega t) + b_n \sin(n\omega t)] \tag{2.13}$$

Where,

$$a_n = \frac{2}{T}\int_{-T/2}^{T/2} f(t)\cos(n\omega t)dt \qquad n \in \mathbb{N} \tag{2.14}$$

And,

$$b_n = \frac{2}{T}\int_{-T/2}^{T/2} f(t)\sin(n\omega t)dt \qquad n \in \mathbb{N} \tag{2.15}$$

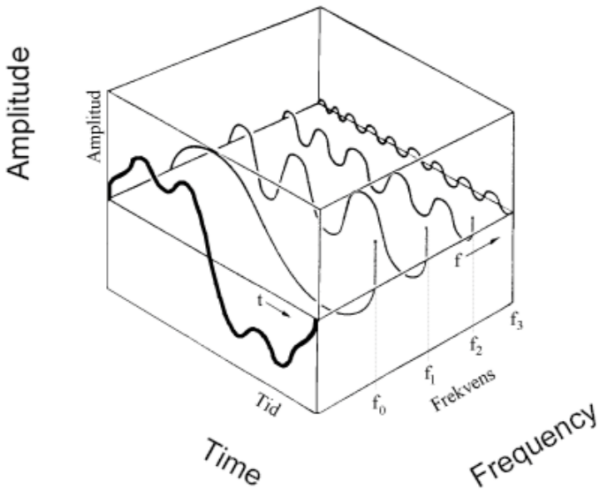

Figure 2.2 – Fourier decomposition of a signal. Karoumi (2008).

The Fourier transform is a generalization of the complex Fourier series, thus the complex Fourier series is an expansion of a periodic function that can be written as an infinite sum of complex exponential:

$$f(t) = \sum_{n=-\infty}^{\infty} A_n e^{2i\pi nt/L} \tag{2.16}$$

Where A_n are:

$$A_n = \frac{1}{L}\int_{-L/2}^{L/2} f(t)e^{-2i\pi nt/L} \tag{2.17}$$

In the limits, as $L \to \infty$, the sum of n becomes an integral. Therefore, the discrete coefficients A_n are replaced by the continuous functions $F(k)dk$ where $k = n/L$. Thus, the equation defining the complex Fourier transform become:

$$f(t) = \int_{-\infty}^{\infty} F(k) e^{-2i\pi kt} dk \tag{2.18}$$

This process is called the forward Fourier transform.

$$F(k) = \frac{1}{2\pi} \int_{-\infty}^{\infty} f(t) e^{2i\pi kt} dt \tag{2.19}$$

And this process is called the inverse Fourier transform.

However, these equations apply to continuous functions and in signal analysis, most of the time the input is discrete. It means that the signal is sampled at regularly spaced time points. For that reason, the algorithm of discrete Fourier transform (DFT) is used. For a N-periodic function:

$$X_k = \sum_{n=0}^{N-1} x_n e^{-2i\pi kn/N} \qquad k \in \mathbb{Z} \tag{2.20}$$

And the inverse is given by:

$$x_n = \frac{1}{N} \sum_{k=0}^{N-1} X_k e^{2i\pi kn/N} \qquad n \in \mathbb{Z} \tag{2.21}$$

It's also important to notice that *Matlab* uses another algorithm to calculate a Fourier transform which is called Fast Fourier Transform. It provides a fast way to do the transformation developed by Cooley and Turkey in 1965.

2.2.2 Basic properties of the Fourier transform

2.2.2.1 Linearity

For any complex number a and b that satisfy this equation, with f, g and h continuous functions: $h(x) = af(x) + bg(x)$

The Fourier transform of h is: $H(k) = aF(k) + bG(k)$

2.2.2.2 Derivation

If x is a real number, then: $\mathcal{F}(\frac{d^n}{dx^n} f(x)) = (jk)^n F(k)$

2.2.2.3 Time-Shifting

If x_0 is a real number, the properties of the Fourier transform allow to translate a function as defined below:

If $h(x) = f(x - x_0)$, then $H(k) = F(k - k_0) = e^{-2i\pi x_0 k} F(k)$

This property is very useful and will be used later on in the thesis to build the load function.

2.3 Frequency domain approach

According to Newton's second law of motion, for a viscously damped system subjected to an external force F(t) the equation of motion is:

$$M\ddot{u}(t) + C\dot{u}(t) + Ku(t) = F(t) \tag{2.22}$$

Where,

- M is the mass matrix of the system
- C is the damping matrix
- K is the stiffness matrix
- u is the displacement vector

For this system, the steady-state response will be harmonic motion at a given frequency. Thus, the load and the displacement are assumed to be harmonic, which means that the different physical quantities can be written as:

$$F(t) = F(\omega) \cdot e^{i\omega t} \tag{2.23}$$

$$u(t) = H(\omega) \cdot e^{i\omega t} \tag{2.24}$$

With,

F the amplitude of the external force in frequency domain applied to each node, and H the amplitude of the displacement which remains to be determined.

Then, the differentials of the displacement give:

$$\dot{u}(t) = i\omega \cdot H_u(\omega) \cdot e^{i\omega t} = i\omega \cdot u(t) \qquad \ddot{u}(t) = -\omega^2 \cdot H_u \cdot e^{i\omega t} = -\omega^2 \cdot u(t) \tag{2.25}$$

Once substituted in eq. (2.22):

$$(-\omega^2 M + i\omega C + K) \cdot u(\omega) = F(\omega) \tag{2.26}$$

eq. (2.26) can also be expressed as:

$$u(\omega) = H(\omega) \cdot F(\omega) \tag{2.27}$$

Where,

$$H(\omega) = \frac{1}{[-\omega^2 M + i\omega C + K]} \tag{2.28}$$

$H(\omega)$ is the frequency response function of the system that can be written as:

$$H(\omega) = \frac{1}{k} \cdot \frac{1}{[1 - (\omega/\omega_n)^2] + i\,[2\xi(\omega/\omega_n)]} \tag{2.29}$$

Where $\omega_n = \sqrt{k/m}$ is the natural frequency if vibration and $\xi = c/(2m\omega_n)$ the damping ratio of the system.

It means that the displacement can be obtained in the frequency domain by multiplying the frequency response function with the load function. Thus, the desired solution in time domain is obtained by the inverse Fourier transform of $u(\omega)$:

$$u(t) = \frac{1}{2\pi} \int_{-\infty}^{\infty} H(\omega).F(\omega)e^{i\omega t} d\omega \tag{2.30}$$

This way, if the frequency response function is obtained, a load function can easily be computed and thus the desired displacement can be obtained.

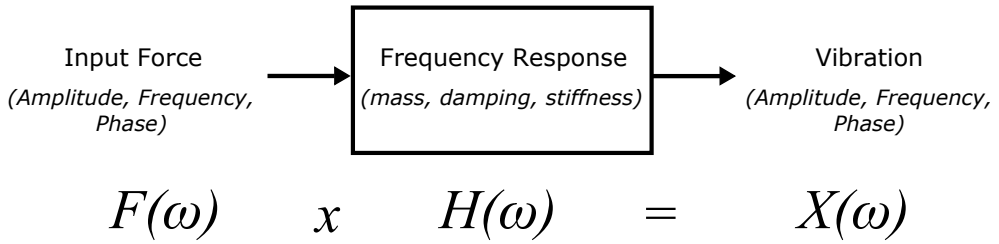

Figure 2.3 – Principle of the frequency domain approach

This method provides a fast way to compare different alternatives or parameters set, which is convenient for this study. It also provides a relatively efficient solution to the equations of motion for the HSLM load systems, a set of train load models. These load systems will be described later on.

2.4 Simply supported beam subjected to constant moving forces

A simply supported beam subjected to constant moving forces is considered. This classical case has been studied for many years by different authors because it is one of the few moving load problems that can be solved analytically. Krylov (1905) was the first to propose an analytical solution for this problem, and other solutions have been proposed using different methods of integral transformations.

2.4.1 Formulation

It is considered that the span length of the beam is equal to L, E is the modulus of elasticity and I the constant moment of inertia of the cross section of the beam. In addition, the beam is subjected to a row of N punctual forces F_n, $n \in [\![1, N]\!]$, with a constant speed c.

Frýba (2001) presents the Euler-Bernoulli partial differential equation governing the behaviour of a beam for a movement of a row of forces along the beam.

$$EI\frac{\partial^4 v(x,t)}{\partial x^4} + m\frac{\partial^2 v(x,t)}{\partial t^2} + 2m\omega\frac{\partial v(x,t)}{\partial t} = \sum_{n=1}^{N} \varepsilon_n(t)\delta(x - x_n)F_n \tag{2.31}$$

Where,

- v(x,t) is the vertical deflection of the beam at the spatial coordinate x and time t
- m the constant mass of the beam per unit of length
- ω the natural circular frequency

And,

$$\varepsilon_n(t) = h(t - t_n) - h(t - T_n) \tag{2.32}$$

$$t_n = d_n/c \tag{2.33}$$

$$T_n = (L + d_n)/c \tag{2.34}$$

With h the Heaviside unit function defined in eq. (2.35)

$$h(t) = \begin{cases} 0 & \text{for } t < 0 \\ 1 & \text{for } t \geq 0 \end{cases} \tag{2.35}$$

$\delta(x)$ is the Dirac delta function used to activate or deactivate the punctual load acting on the beam, with d_n the distance between the first load and the nth one.

$$x_n = ct - d_n \tag{2.36}$$

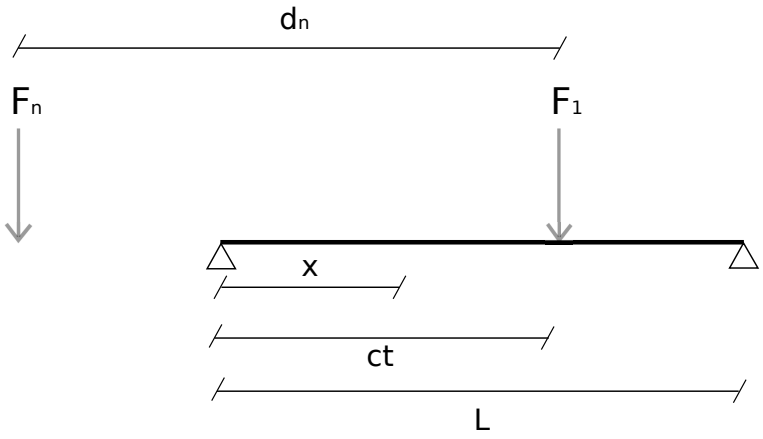

Figure 2.4 – Simply supported beam subjected to a row of moving punctual forces

2.4.2 Solution of the problem

The solution obtained by Frýba presented in this thesis is detailed in Frýba (1999), in the case where a single punctual load is applied in eq. (2.37).

$$y(x,t) = \frac{FL^3}{48EI}\frac{96}{\pi^4}\sum_{i=1}^{\infty}\frac{1}{i^4\left[1-(\alpha/i)^2\right]}\left[\sin(i\frac{\pi c}{L}t) - \frac{\alpha}{i}\sin(\omega_i t)\right]\sin(\frac{i\pi x}{L}) \tag{2.37}$$

Where i is the mode number and ω_i the corresponding circular frequency of vibration, and α a non-dimensional speed parameter.

$$\omega_i = \left(\frac{i\pi}{L}\right)^2\sqrt{\frac{EI}{m}} \tag{2.38}$$

$$\alpha = \frac{\pi c}{\omega_1 L} \tag{2.39}$$

A solution for a row of punctual forces is obtained by combining the different loads with the Heaviside functions as presented in eq. (2.40).

$$\begin{aligned} y(x,t) =& v_0\frac{96}{\pi^4}\sum_{i=1}^{\infty}\sum_{n=1}^{N}\frac{1}{i^4\left[1-(\alpha/i)^2\right]} \\ & \left[f(t-t_n)h(t-t_n) - (-1)^i f(t-T_n)h(t-T_n)\right]\sin(\frac{i\pi x}{L}) \end{aligned} \tag{2.40}$$

Where,

$$f(t) = \sin(i\frac{\pi c}{L}t) - \frac{\alpha}{i}\sin(\omega_i t) \tag{2.41}$$

And,

$$v_0 = \frac{FL^3}{48EI} \tag{2.42}$$

From displacement, acceleration is calculated by differentiating twice y(x,t):

$$\begin{aligned} y(x,t) =& v_0 \frac{96}{\pi^4} \sum_{i=1}^{\infty} \sum_{n=1}^{N} \frac{1}{i^4\left[1-(\alpha/i)^2\right]} \\ & \left[f''(t-t_n)h(t-t_n) - (-1)^i f''(t-T_n)h(t-T_n)\right] \sin(\frac{i\pi x}{L}) \end{aligned} \tag{2.43}$$

With,

$$f''(t) = -\left(\frac{i\pi c}{L}\right)^2 \sin(i\frac{\pi c}{L}t) + \frac{\alpha}{i}\omega_i^2 \sin(\omega_i t) \tag{2.44}$$

2.5 Finite Element Method

2.5.1 Introduction to FEM

An overview of the FEM method is provided in this section, based on Oñate (1992). The majority of the structures in the engineering field are continuous, so it's behaviour cannot be accurately described as a function of a small number of discrete variables. In order to perform a rigorous analysis it is needed to integrate the differential equations that consider the equilibrium of one generic differential element on them. These continuous structures are pretty common in civil engineering, such us damns, bridges, etc., (fig. 2.5). Although continuous structures are inherently three-dimensional, in some cases their behaviour can be studied using two-dimensional or uni-dimensional models.

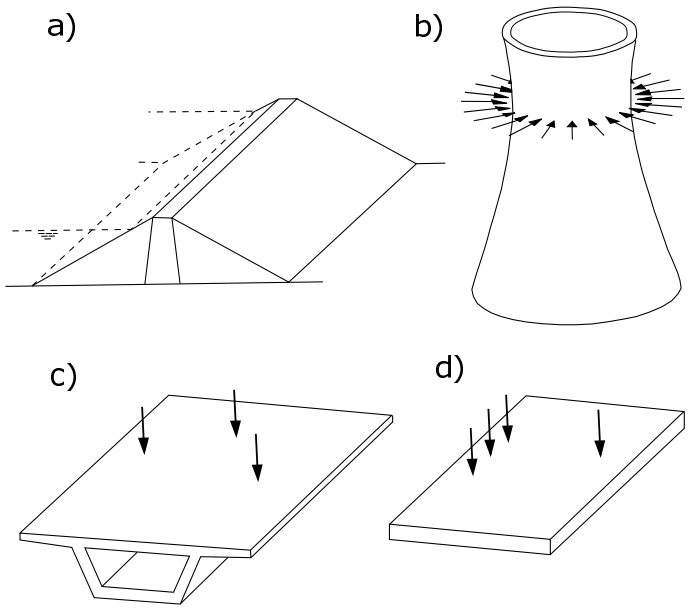

Figure 2.5 – Some continuum structures: a)Dam, b)Nuclear reactor, c)Bridge, d)Plate. Oñate (1992)

The finite element method (FEM) is the most powerful method to perform an analysis nowadays of any kind of uni-, two- or three-dimensional structure, when several external actions interact with them.

2.5.2 Beam theory

A beam element reduces a three-dimensional continuum to one dimension mathematically, where the primary solution variables are functions of position along the beam axis only. This assumption is only applicable when the dimensions of the cross-section are small compared to typical lengths along the axis. The main advantage of beams is their geometrical simplicity and efficiency, requiring a few degrees of freedom. In fig. 2.6 a representation of the beam assumption is shown.

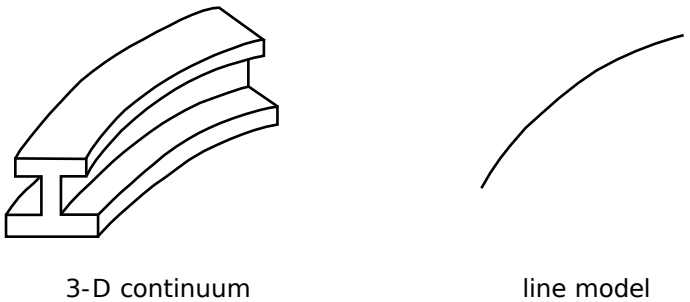

Figure 2.6 – Beam element assumption

The simplest approach to beam theory is the classical Euler-Bernoulli assumption. This assumption considers that plane-cross sections initially normal to the beam's

axis remain plane, normal and undistorted to the axis. This approximation can also be used to formulate beams for large axial strains as well as large rotations.

The beam element used in Abaqus is B31, which uses linear interpolation, is based on such a formulation. In addition, this element also allows "transverse shear strain", where the cross-section may not necessarily remain normal to the beam axis. This extension leads to the Timoshenko beam theory, generally considered useful for thicker beams. The B31 element is formulated in Abaqus so that they are efficient for thin beams-where the Euler-Bernoulli theory is accurate-as well as for thick beams, becoming one the most effective and commonly used elements in Abaqus.

The large-strain formulation in these elements allows axial strains of arbitrary magnitude; but quadratic terms in the nominal torsional strain are neglected compared to unity, and the axial strain is assumed to be small in the calculation of the torsional shear strain. Thus, while the axial strain may be arbitrarily large, only a "moderately large" torsional strain is modelled correctly, and then only when the axial strain is not large. It is assumed that, throughout the motion, the radius of curvature of the beam is large compared to distances in the cross-section: the beam cannot fold into a tight hinge. A further assumption is that the strain in the beam's cross-section is the same in any direction in the cross-section and throughout the section.

2.5.3 Shell elements

Shell elements are developed based on the shell theory that approximates a thin 3D continuum (small thickness compared to lateral dimensions) using a 2D formulation. A shell element allows the modelling of curved, intersecting shells that can exhibit nonlinear material response and undergo large overall motions (translations and rotations). They can also model the bending behaviour of composites. In fig. 2.7 a representation of the beam assumption is shown.

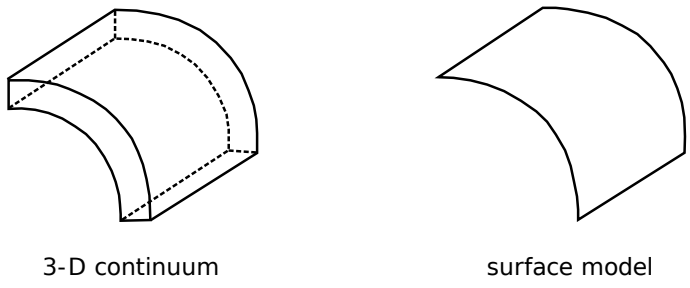

Figure 2.7 – Shell element assumption

There are three categories of elements consisting of general-purpose, thin and thick shell elements. Thin shell elements provide solutions to shell problems that are adequately described by classical (Kirchhoff) shell theory while thick shell elements yield solutions for structures that are best modelled by shear flexible (Mindin) shell theory. General-purpose shell elements can provide solutions to both thin and thick

shell problems. All shell elements use bending strain measures that are approximations to those Koiter-Sanders shell theory.

Depending on the ration between thickness and lateral directions dimensions different theories have been developed. Conventional shell elements have been used, in which 2D geometry is defined in the reference surfaces while thickness is defined by section property.

The general-purpose shell element S4R has been used. The general-purpose shell elements provide robust and accurate solutions in all loading conditions for thin and thick shell modes. This element considers finite membrane strains, and uses reduced-order integration, which allow for fast and cheap calculation of the element matrices. Abaqus uses reduced integration for first-order elements, with only one Gauss-point to calculate the element matrices. This also minimizes the computational expense of element calculation.

Chapter 3

Requirements and demands

3.1 Requirements for a dynamic analysis

For railway bridges where the train speed can exceed 200 km/h, a dynamic analysis has to be performed according to EN 1991-2. The main difference with a static design is that resonance phenomenon can appear, involving large vertical displacements and accelerations.

In addition, dynamic analysis can vary a lot according to the mass of the bridge, the stiffness of the deck and the kind of boundary conditions. For these reasons, incorrect assumptions in the modelling process can lead to wrong results.

Moreover, a conservative static design can produce unexpected dynamic effects that could occasionally results in an unsafe ride. For this reason, an accurate study has to be carried out taking into consideration both static and dynamic contributions.

3.1.1 Parameters for a dynamic analysis

All the requirements for a dynamic analysis regarding the load and properties of the bridge can be found in EN 1991-2, section 6.4.6.

3.1.1.1 Loading

Dynamic effects vary a lot according to the load applied, thus a general load model is defined in section 6.4.6.1 for European high speed lines. The HSLM-A load model is defined by a range of 10 different trains (from HSLM-A1 to HSLM-A10) and shall be taken into account for continuous structure complex structures where the span length is larger than 7 m. Characteristics of these trains are presented in fig. 3.1 and in table 3.1.

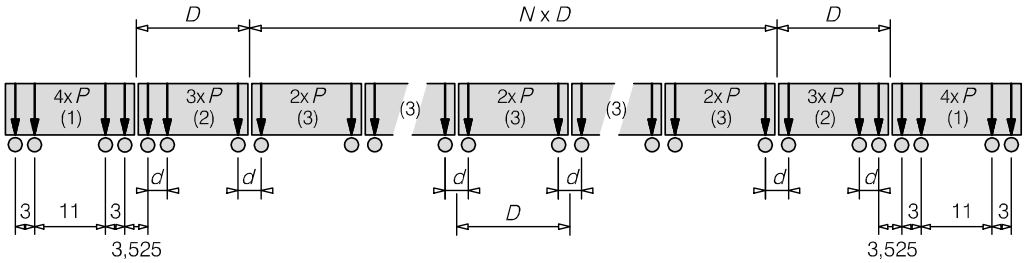

Key
(1) Power car (leading and trailing power cars identical)
(2) End coach (leading and trailing end coaches identical)
(3) Intermediate coach

Figure 3.1 – HSLM A, EN-1991-2, figure 6.12

Table 3.1 – HSLM A, EN-1991-2, table 6.3

Universal train	Number of intermediate coaches N	Coach length D (m)	Bogie axle spacing d (m)	Point force P (kN)
A1	18	18	2.0	170
A2	17	19	3.5	200
A3	16	20	2.0	180
A4	15	21	3.0	190
A5	14	22	2.0	170
A6	13	23	2.0	180
A7	13	24	2.0	190
A8	12	25	2.5	190
A9	11	26	2.0	210
A10	11	27	2.0	210

In addition, each point load may be distributed over three rail support as in fig. 3.2

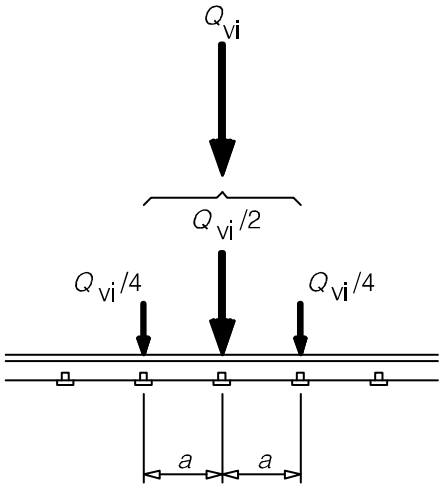

Figure 3.2 – Longitudinal repartition of a point force, EN-1991-2, figure 6.4

Where Q_{vi} is the point force on each rail and a the distance between rail support points.

Besides, each train shall be run at a series of speeds up to the maximum design speed equal to 1.2xMPVS (Maximum Permitted Vehicle Speed at the site). In this study, HSLM A trains will run up to a speed of 384 km/h, since MPVS is equal to 320 km/h.

3.1.1.2 Structural damping

The structural damping that shall be used for a dynamic analysis is defined in table 3.2.

Table 3.2 – Lower limit values of damping ξ (%) to be assumed, EN-1991-2, table 6.6

Bridge type	L < 20 m	L ≥ 20 m
Steel and composite	0.5 + 0.125(20 - L)	0.5
Prestressed concrete	1.0 + 0.07(20 - L)	1.0
Filler beam and reinforced concrete	1.5 + 0.07(20 - L)	1.5

Furthermore, for span lengths shorter than 30 m the damping may be increased by considering an extra damping $\Delta\xi$ where $\xi_{TOTAL} = \xi + \Delta\xi$. However, this reduction will not be considered in this report.

3.1.1.3 Dynamic factor

Due to track defects and vehicle imperfections, a dynamic factor DF shall be applied by multiplying the dynamic effects by DF. For carefully maintained tracks, DAF is equal to $1 + 0.5\phi''$. This factor depends on the first eigenfrequency of the bridge and can be found in EN 1991-2, Annex C.

3.1.2 Vertical acceleration of the deck

A maximum vertical acceleration of the deck is defined in order to satisfy passenger comfort criteria and traffic safety. This value depends on the track system and is equal to 3.5 m/s^2 for un-ballasted tracks and 5 m/s^2 for ballasted tracks, as defined in A.2.4.4.2.1(4).

In addition, consideration of associated mode shapes is taken into account since the higher frequency n_{max} shall be equal to $n_{max} = \max(30\text{ Hz}, 1.5\text{x}n_0, n_2)$ where n_0 is the frequency of the first mode of vibration, and n_2 the frequency of the third mode of vibration. In this report, n_{max} will always be taken equal to 30 Hz.

3.1.3 Vertical deformation of the deck

Maximum permissible vertical deformation is defined in A.2.4.4.3 and depends on the span length. It corresponds to a permissible vertical acceleration of 1 m/s^2. Values of L/δ are provided in fig. 3.3.

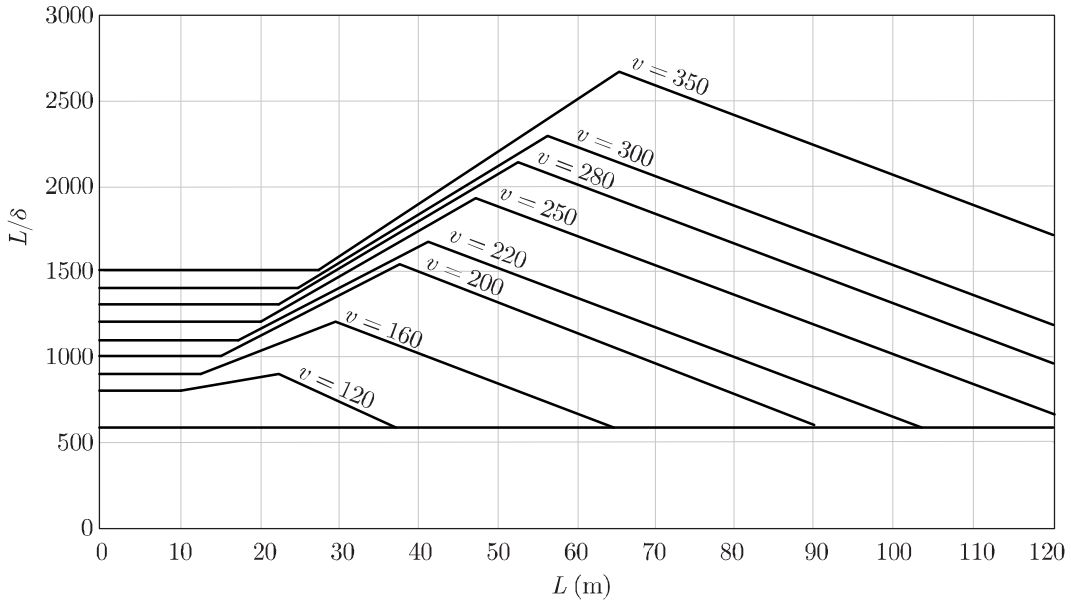

Figure 3.3 – Maximum permissible vertical deflection δ for railway bridges, EN-1990, figure A.2.3

However, the values presented are given for a succession of simply supported beams with three spans or more. Simply-supported beams or continuous beams with two spans are considered by multiplying L/δ by a factor of 0.7, while continuous beams with three or more spans shall be multiplied by 0.9.

In addition, angular rotations at the end of decks as defined in fig. 3.4 should be controlled but the limitation is implicit in Eurocode and comes from the maximum vertical deformation. However, this limitation is only valid for ballasted tracks. In TRVK Bro 11, maximum rotations allowed are defined for ballast-free tracks and depend on the distance $h_{(m)}$ from the centre of rotation of the bearing to the top of the rail (see fig. 3.5). Limit values are $\theta_1 = 2.10^{-3}/h_{(m)}$ for the rotation at the end supports of the bridge, and $\theta_2 = 4.10^{-3}/h_{(m)}$ for the middle supports.

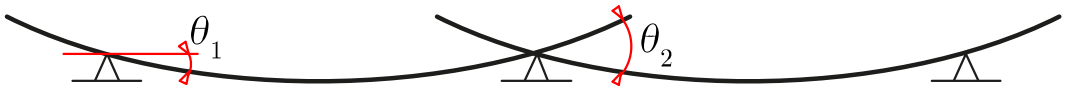

Figure 3.4 – Definition of angular rotations at the end of decks, EN-1990, figure A.2.2

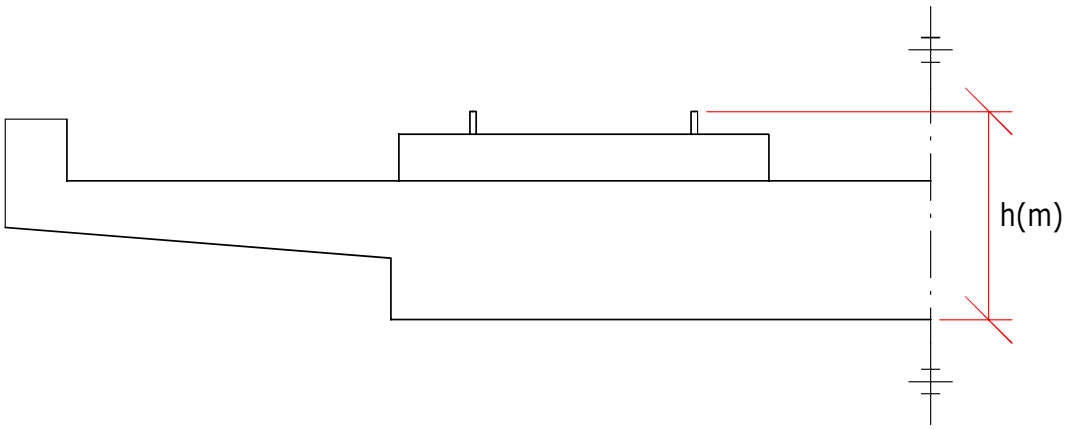

Figure 3.5 – Distance from the centre of rotation of the bearing to the top of the rail

3.2 Resistance verification for slab deck bridges

In order to obtain a complete design of a section, a static design stage and a dynamic analysis are required for high speed railways. Based on some assumptions, a resistance verification has been performed for slab bridges to obtain the minimum thickness to ensure a static design. Details of these calculations are provided in appendix A.

3.2.1 Construction rules

The static design will be performed in accordance with applicable standards:

- Eurocode 0 : Annex A2, Application for bridges
- Eurocode 1 : Part 2, Traffic loads on bridges (EN 1991-2)
- Eurocode 2 : Part 1, Design of concrete structures

Nevertheless, in order to simplify the static design, not all the limits have been checked and some have been omitted deliberately since the static design is not the main aim of this thesis. Next, the verifications that have been checked will be presented.

3.2.1.1 Ultimate Limit State

$$A_s > A_{s_{min}} \tag{3.1}$$

With, $A_{s_{min}}$ the minimum quantity of steel calculated in accordance with Eurocode.

$$A_s < A_{s_{max}} = 0.04.A_c \tag{3.2}$$

Where, $A_{s_{max}}$ represents the maximum quantity of steel for the section of concrete A_c.

3.2.1.2 Serviceability Limit State

$$\sigma_{c,quasi-permanent} \leq 0.45.f_{ck} \tag{3.3}$$

$$\sigma_{c,rare} \leq 0.6.f_{ck} \tag{3.4}$$

$$\sigma_{s,rare} \leq 0.8.f_{yk} \tag{3.5}$$

Where, $\sigma_{c,quasi-permanent}$ is the maximum stress in concrete due to quasi-permanent loading, and $\sigma_{c,rare}$ represents the maximum stress in concrete due to rare loading.

Consequently, the maximum vertical deflection will not be checked, neither will the maximum crack width.

3.2.2 Loads and load combinations

3.2.2.1 Loads

Vertical loads

Vertical loads will be applied in accordance with the train loads defined in Eurocode 1. Thus two tracks will be loaded with LM71 in order to obtain the most unfavourable effects.

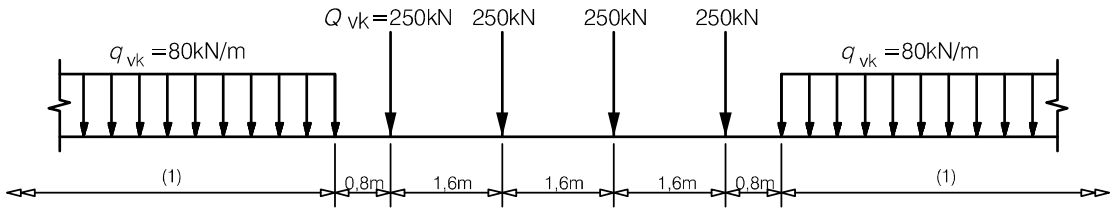

Key
(1) No limitation

Figure 3.6 – Load model LM71

In addition, the self-weight will be applied.

Horizontal loads

In order to take horizontal forces due to the train acceleration or braking into account, such as temperature effects, one unique conservative horizontal force will be applied with a magnitude of 6000 kN.

3.2.2.2 Load combinations

According to Eurocode 0, loads have to be combined with the following equation in the ultimate limit state:

$$E_d(6.10) = \sum_{j\geq 1} \gamma_{G,j} + \gamma_P P + \gamma_{Q,1}\psi_{0,1}Q_{k,1} + \sum_{j>1} \gamma_{Q,i}\psi_{0,i}Q_{k,i} \tag{3.6}$$

Where,

$\gamma = 1.35$ or $\gamma = 1$ for the self-weight, and $\gamma = 1.45$ or $\gamma = 0$ for the LM71.

In the serviceability limit state, two different combinations have to be applied for the quasi-permanent loading and the rare loading.

For the combinations:

$$E_d(6.14) = \sum_{j\geq 1} \gamma_{Gk,j} + P + Q_{k,1} + \sum_{j>1} \psi_{0,i}Q_{k,i} \tag{3.7}$$

And quasi-permanent combinations:

$$E_d(6.16) = \sum_{j\geq 1} \gamma_{Gk,j} + P + Q_{k,1} + \sum_{j>1} \psi_{2,i}Q_{k,i} \tag{3.8}$$

For LM71, $\psi_0 = 0.8$ and $\psi_2 = 0$.

3.2.3 Preliminary static design curves

Preliminary static design curves have been obtained with *Matlab*, for different span lengths. An increment of 1 centimeter has been used for the thickness. However, these curves cannot be considered precisely since not all the verifications have been checked. They give an overview of the thickness, with a certain margin of error due to the assumptions made.

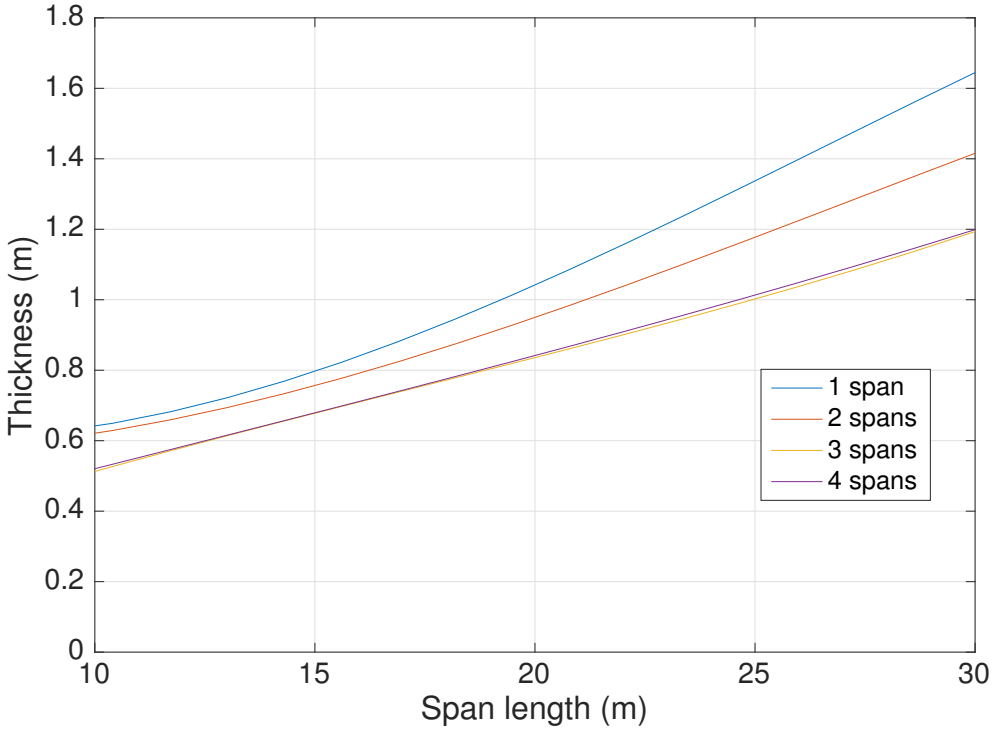

Figure 3.7 – Preliminary static design curves for slab deck bridges

Chapter 4

Geometry and materials

In this section three parameters will be studied in order to compare 3D with 2D models: span length, number of spans and thickness of the deck. There will be a description of the geometry considered and the scope of these parameters.

4.1 Geometry

4.1.1 Overall geometry

The structure is an un-ballasted railway bridge for high-speed trains with two tracks. The bridge consists of a slab deck with two edge beams. A more detailed description of the cross section is presented in the next subsection.

Slab sections are commonly used for short span length bridges, up to 30 meters. For larger span lengths it is suggested to use other type of sections, such as beam bridges. Following this criterion and the diagrams for 2D models, span lengths between 10 and 30 metres have been analysed. Due to a simplification of the modelling process, it has been decided to compute cases every 1.3 meters.

Another important parameter is the number of spans of the bridge. For every span length, a different number of spans from 1 to 4 has been checked. If 2 spans are considered, the span length is the same ($L_1 = L_2$). For the cases with 3 and 4 spans, a reduction of the span length in the outer spans has been considered. fig. 4.1 shows the two different lengths considered.

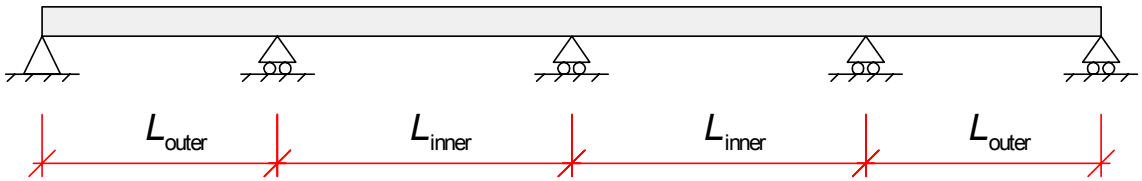

Figure 4.1 – Different span lengths

The whole length is considered in the inner spans, while the outer spans' length is reduced ($L_{outer} = 0.8L_{inner}$). This is commonly used in real bridges' design in order to have the same bending moment in each span at the midpoint.

4.1.2 Cross section

The cross section of the bridge consists in a slab deck and two beams placed at the top of the deck, one at each side. The section has a total width of B = 12 m. The slab deck has a central part in which the thickness is constant (h) and lateral parts where the thickness varies (from $t_{max,flange}$ to $t_{min,flange}$). The edge beams have a square profile, filled in the inner part. In fig. 4.2 the cross section of the bridge is presented, and the dimensions of the different parameters are defined in table 4.1.

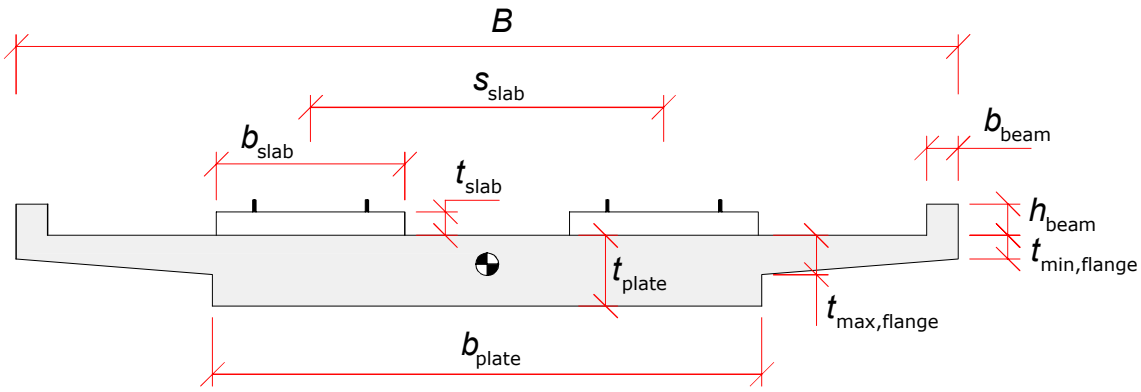

Figure 4.2 – Cross section from Svedholm and Andersson (2016)

Table 4.1 – Dimensions cross section

Parameter	Value	[]
B	12,0	m
b_{plate}	7,0	m
S_{slab}	4,5	m
b_{slab}	2,4	m
t_{slab}	0,3	m
$t_{max,flange}$	0,5	m
$t_{min,flange}$	0,3	m
b_{beam}	0,4	m
h_{beam}	0,4	m

The dimensions presented have been chosen according to the 2D models presented in Svedholm and Andersson (2016), in order to compare two models as much similar as possible.

As previously said, the central part of the deck has a constant thickness (t_{plate}). Models are used to figure out which is the minimum thickness value that fulfils the regulation considerations, and several values have been computed. For each span length and number of spans, a range of thickness has been considered, analysing 12 cases with 5 centimetres of difference between two values. The range has been defined differently for each span length and number of spans, according to the values defined in the 2D beam models.

For each case, it has been checked that the minimum value of the range was not smaller than the minimum value obtained from the static design. It was expected that the minimum thickness considering the dynamic effects is higher than the static one.

4.2 Materials

The materials used have been chosen according to the 2D models. However, in the 2D analysis the Poisson's ratio of the material was not taken into account. This parameter was considered for the 3D analysis performed in this project in order to study a more realistic case.

table 4.2 reports the values for concrete's Young's modulus, Poisson's ratio and density used.

Table 4.2 – Material properties

Parameter	Value	[]
E_c	34	Gpa
v	0,2	-
ρ_c	2500	kg/m^3

As seen in fig. 4.2, there are the two tracks on the top of the cross-section in question. The concrete used for the sleepers is considered to be the same for the rest of the section. These tracks are not considered in the model, whereas the load is applied in several surfaces along the deck. However, in order to compare this model with the 2D models, an altered density of the material has been computed to get a similar mass per unit of length. An extra-mass of 3.6 ton/m has been considered, corresponding to the mass of the two sleepers.

An analysis comparing the total mass between 2D and 3D models has been performed to check the density modification was properly defined. The analysis is presented in table 4.3.

Table 4.3 – Total model mass comparison for different span lengths and each number of spans

	1 span				
L (m)	**10**	**15**	**20**	**25**	**30**
h (m)	0,80	1,16	1,48	1,84	2,03
m_{2D} (ton/m)	23,37	29,79	35,28	41,62	44,99
m_{3D} (ton/m)	23,40	29,70	35,30	41,60	44,93
Error (%)	0,14	0,29	0,05	0,05	0,14

(a) 1 span

	2 spans				
L (m)	**10**	**15**	**20**	**25**	**30**
h (m)	0,59	0,88	1,16	1,24	1,39
m_{2D} (ton/m)	19,76	24,83	29,79	31,04	33,78
m_{3D} (ton/m)	19,73	24,80	29,70	31,10	33,73
Error (%)	0,19	0,12	0,29	0,19	0,17

(b) 2 spans

	3 spans				
L (m)	**10**	**15**	**20**	**25**	**30**
h (m)	0,55	0,77	0,96	1,19	1,39
m_{2D} (ton/m)	18,97	22,96	26,27	30,20	33,78
m_{3D} (ton/m)	19,03	22,88	26,20	30,23	33,73
Error (%)	0,29	0,36	0,28	0,10	0,17

(c) 3 spans

	4 spans				
L (m)	**10**	**15**	**20**	**25**	**30**
h (m)	0,54	0,75	0,96	1,08	1,22
m_{2D} (ton/m)	18,88	22,56	26,27	28,23	30,83
m_{3D} (ton/m)	18,85	22,52	26,20	28,30	30,75
Error (%)	0,13	0,15	0,28	0,26	0,25

(d) 4 spans

The damping of the bridge has been applied when the material properties were defined as structural damping. As explained in chapter 2, the structural damping is twice the value of the modal damping. The modal damping considered is presented in table 3.2 and its value depends on the material of the structure.

Chapter 5

Frequency domain analysis

5.1 General process

The aim of this chapter is to describe the methodology that has been implemented for this analysis, and presented in fig. 5.1. The method is organized in two main steps with a pre-process step and a post-process step. *Brigade* constitutes the pre-process step and provides the FRF which is an input for the analysis. On the other side, the train load is formulated in *Matlab* and corresponds to the second input. From these two quantities the equation of motion is solved in a post-process step which is *Matlab*, to end up with the desired quantity in time domain.

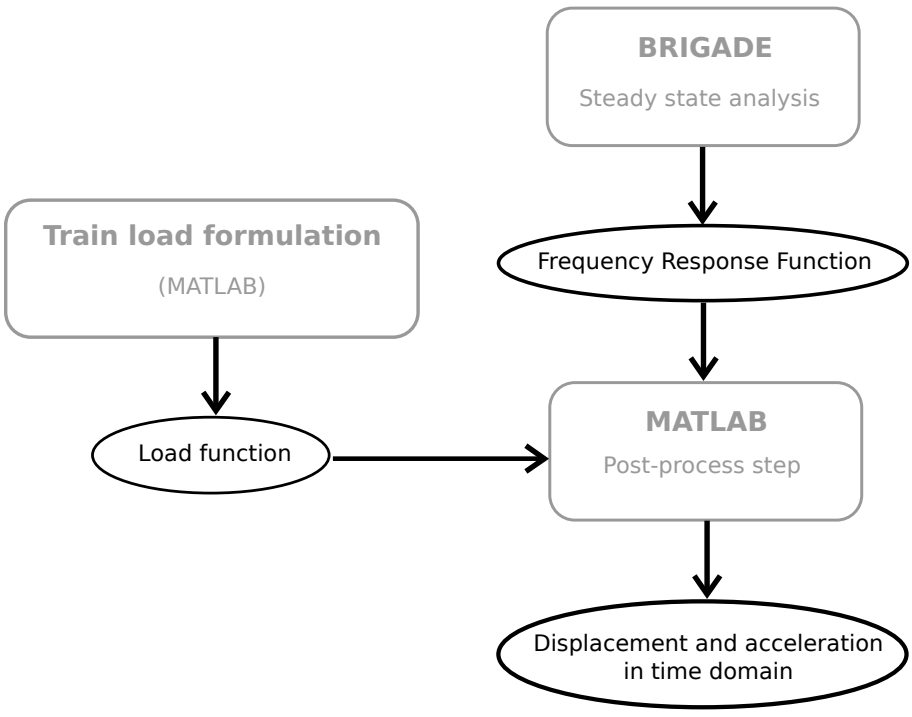

Figure 5.1 – General analysis process

5.2 *Brigade*/Plus Modelling Procedures

In this section the first part of the method is explained, which consists of the modelling process. A description of the 3D software is provided as well as an explanation on how the frequency response function is obtained. Finally, an overview is given concerning the generalized python script used to create the different cases.

5.2.1 Modules

Brigade uses modules in which the different aspects of the model are generated and assigned. Each of them has specific functions, clearly defining the steps followed to model the studied structures.

5.2.1.1 Part and Property

The Part module is used to create the different parts of which the initial structure consists of. Depending on the typology of structure, different types of parts can be used, as described in chapter 2. When creating a new part, it is necessary to define a modelling space, shape and type of the base feature. For this specific study, a 3D deformable shell planar part has been used to represent the deck while a 2D planar deformable wire has been used to model the edge beams.

As explained in chapter 4, a simplified section has been considered, which can be modelled more easily. fig. 5.2 shows the simplification made, with the beam and shell elements used to model the section in *Brigade*.

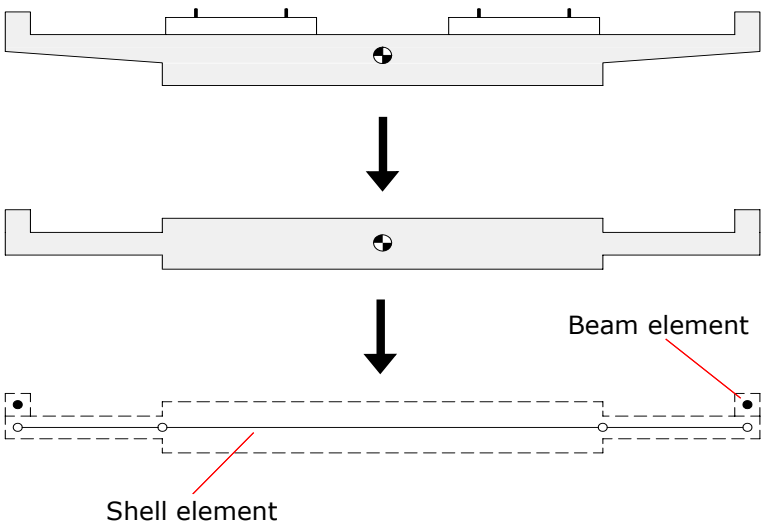

Figure 5.2 – Section and model simplifications

The geometry is generated defining parameters such as the width, thickness, length,

etc. This module also defines *partitions*, which are basically used to divide surfaces or lines. They have been used to divide the deck in different regions (one central and two lateral regions), in order to define different thickness values. Creating several partitions, nodes are generated in the intersection between them and used to define properties of the model of the structure and regions where the results are obtained.

In the property module, materials and properties of different parts of the bridge are defined. Sections with different materials or properties need to be created and they are used to assign the corresponding properties to each particular region. fig. 5.3 shows an example of a part with different sections assigned.

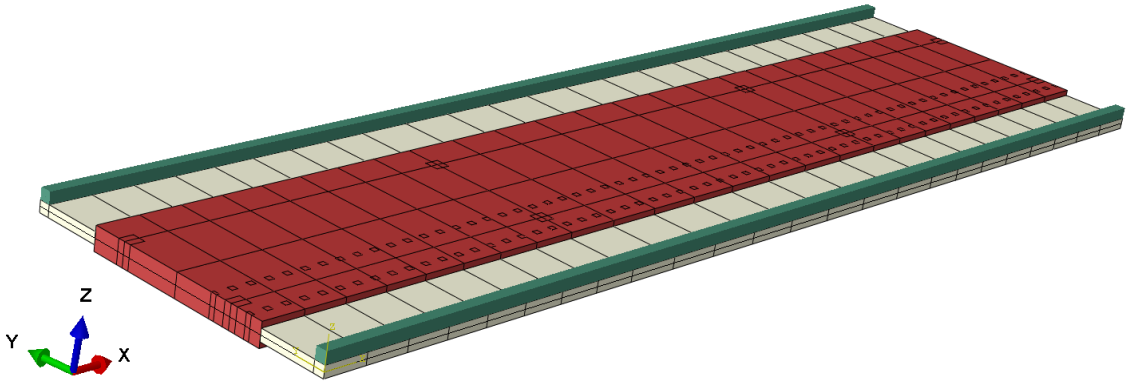

Figure 5.3 – Different sections of the model

In the case of the beams, it is also necessary to create their profiles and define the proper orientation.

5.2.1.2 Assembly

The Assembly module is used to assemble the different parts that have been created. They are assembled as different instances. In this module the whole structure can be visualized three-dimensionally.

One specific part can be assembled more than once as many instances. In this case, the part is created and then assembled in several locations. However, even if there are two features with the same properties, they can be created together as one single part, such as the beams. fig. 5.3 presents the whole structure assembled for a particular studied case.

Besides that, *sets* are also defined in this module. A set is a region of a single or group of entities, used to assign properties, to define loads and boundary conditions, to requested outputs from specific regions, etc.

5.2.1.3 Step

The Step module has been used to create the different steps of the analysis and specify output requests. Different kinds of steps have been used, performing analysis in different domains. For the time-domain analysis the *Modal Dynamics step* has been used. However, for the frequency-domain analysis *Frequency Step*, *Steady-state Direct Dynamic Step* and *Steady-state Modal Dynamic Step* have been used. The *initial step* is defined by default.

- **Initial Step:**it is always the first step of the modelling process. When more than one step is used to perform different analysis in the same model, the general aspects such as the boundary conditions, are defined in this step and then propagated in the other steps used.
- **Modal dynamics Step:**it has been used to perform the analysis in the time-domain. It is important to define the total computing time and a proper time step for the analysis.
- **Frequency Step:** it has been used to perform a frequency extraction, which is a linear perturbation procedure that performs an eigenvalue extraction to calculate the natural frequencies and the corresponding modes of shapes of a system. In this case, as previously said, a maximum frequency of 30Hz is used and all the eigenfrequencies included in that frequency range will be computed. In this case, this step is needed for the following Steady State Steps, where eigenfrequencies and eigenmodes are used.
- **Steady-state Direct Dynamic Step:** this step is in frequency domain, computing a harmonic response in terms of degrees of freedom of the model and using the mass, damping and stiffness matrices of the system.
- **Steady-state Modal Dynamic Step:** it has been used to perform the frequency-domain analysis. In this analysis, the response is based on modal superposition techniques. A previous frequency step is needed in order to obtain them. The type of frequency spacing can be specified as well as the number of frequencies where results will be required.

Due to a pronounced decrease on the computing time, the Steady-state Modal Dynamic Step has been used to compute the different cases studied. section 5.4.3 describes an analysis comparing the results from the two steady-state step analyses (direct and modal dynamic).

When an analysis is performed it is needed to define the region where the solution is desired. In lieu of computing the results in the whole model, some node regions have been specified. This is implemented in order to reduce computing time as well as space in the memory due to the size of the files.

5.2.1.4 Interaction

The Interaction module is used to define and manage the interaction between different regions from the model created, such as mechanical and thermal interactions between regions or springs and dash pots between two points.

In the main model created the interaction has been defined using two types of constraints: tie and coupling constraint.

- **Tie constraint:** this type of constraint fuses together two regions, making the three displacements and three rotations null between them. In the main model, this constraint has been used to define the interaction between the beams and the deck of the bridge, which can be seen in fig. 5.4-a.

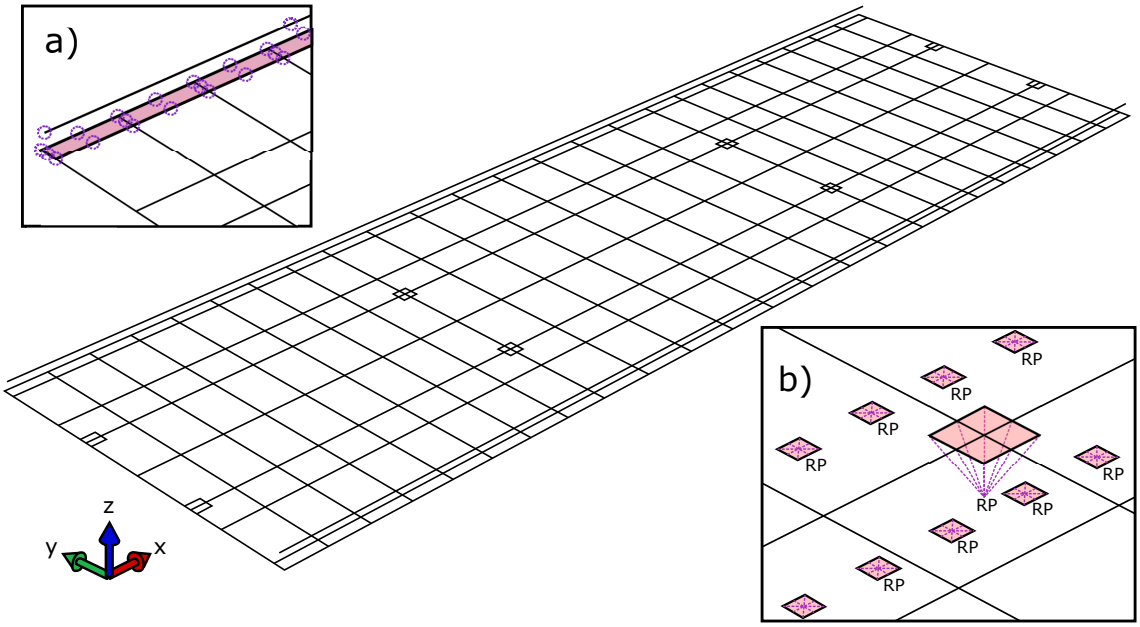

Figure 5.4 – Constraints defined in the interaction module: a) Tie, b) Coupling

- **Coupling constraint:** defining this constraint to a surface, its motion is constrained to the motion of a single point. This constraint is used when defining the surfaces concerning the supports and the rail insertion surfaces. fig. 5.4-b shows the coupling interaction in the supports and surfaces.

5.2.1.5 Load and Boundary Conditions

The Load module is the module where loads and boundary conditions are defined as prescribed conditions. If several analysis steps are computed, it is necessary to define in which ones these conditions are applied. Load Cases are used to combine different loads created.

For a specific transversal section, half of the point load is applied in each rail,

considering half of the contribution that the load produces to the structure. The load has been considered to be applied in surfaces, to make the interaction load-structure more realistic. Due to the rails and sleepers the region affected by the point load is not a single point but a surface. fig. 5.4-b shows the coupling interaction to distribute the load into the surfaces.

A reference point has been created in the middle of each surface, where the load has been applied to. Then, using the coupling described in the *Interaction module*, the load is distributed through all the surface. fig. 5.5 shows the point loads defined in the model and a load case.

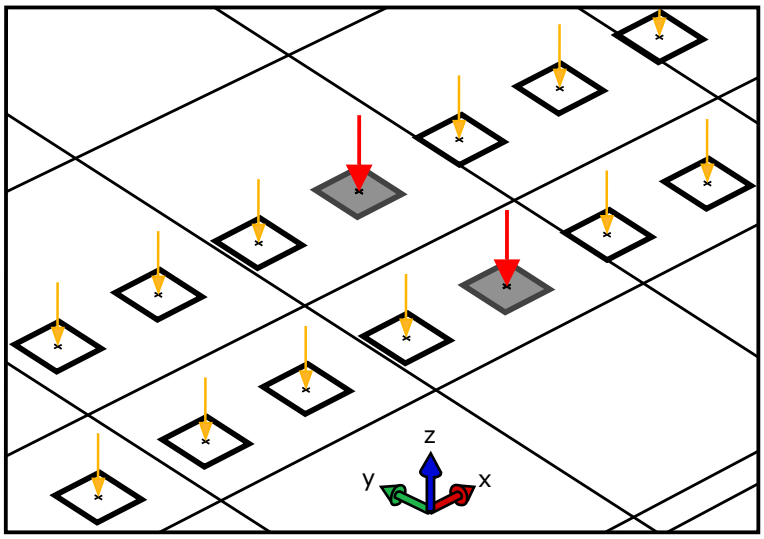

Figure 5.5 – Point loads along the bridge

On the other hand, the boundary conditions can also be defined in the Load module. They are defined to allow or restrict some degrees of freedom in certain regions of the structure modelled.

In the main model, the boundary conditions consist of two supports placed in each centre of the two rails. They have been placed at the beginning and at the end of each span defined. In all the supports the vertical displacement is restricted, while there is free rotation in all the directions. For this type of bridge, the common support design regarding the horizontal displacement of the bridge fixes one support and allows the movement in the others. fig. 5.6 shows a representation of the allowed and restricted movements along the deck.

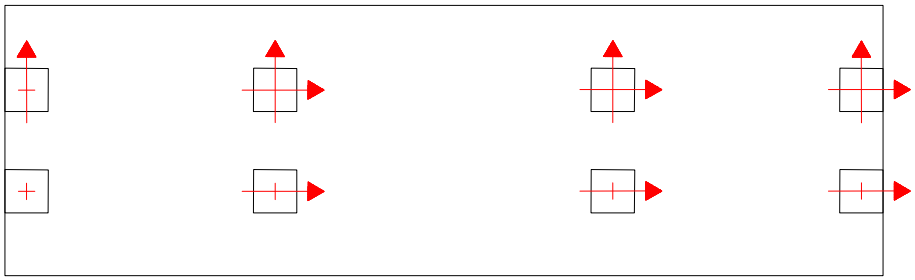

Figure 5.6 – Restriction of movements along the supports

There is one horizontal movement in the longitudinal direction and another one in the transversal direction. It has been decided to fix the longitudinal movement in the supports placed at the beginning of the first span. Concerning the transversal movement, it has been fixed for those supports placed in the side of the bridge where the track of the train is modelled, which is more unfavourable than on the other side.

5.2.1.6 Mesh

In the Mesh module, the mesh and its properties are defined for all the parts and assemblies previously created. The type and size of element needs to be defined in order to generate the mesh. There is also an option to verify and check that the mesh generated is not too deformed to compute the solution. Depending on the type of problem, there are elements that work in a better way than others, due to the theory behind them. For this problem, linear quadrilateral shell elements *S4R* and linear beam elements *B31* have been used.

It is important to perform some convergence analysis to find the optimal element size. Although a thin mesh usually provides results more precisely, it also takes more computing time. A good solution to deal with the trade-off between accuracy and computing time is to define different mesh sizes depending on the position in the structure. This alternative has been used, defining a smaller element size in those parts where the load is applied to due to the complexity of the geometry and the interaction between load and structure. A bigger element has been used in those parts where the geometry is simpler. fig. 5.7 shows an example of mesh, where this solution has been used.

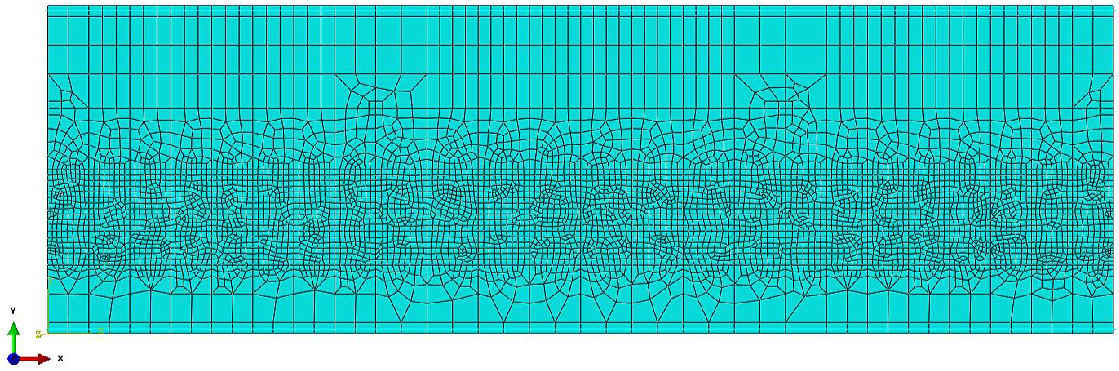

Figure 5.7 – Mesh of the model

The smallest element size used to define the mesh is $0.2m$, located in the region where all the surfaces for the load application are defined. The biggest element size, situated in the region on the opposite side of the bridge, is $1.0m$. In section 5.4.4 the analysis performed to define these values is described.

5.2.2 Frequency Response Function

The Frequency response function (FRF) is the response for a certain number of points when a load system is applied. The points where this response is computed are called **output** points, while the different load systems applied are called **inputs**. Since a steady-state analysis is performed, this response is computed for every frequency step analysed in the frequency range. The response computed for all the cases is the vertical displacement.

The outputs points have been placed in the middle point of the surfaces, where the point load is applied. Output points in the two rails along the length of the bridge have been considered. The different inputs are all the load cases defined. As previously explained, every load case consists of a harmonic unit point load split equally between the two rails. fig. 5.8 represents the load system applied with the input and output points described.

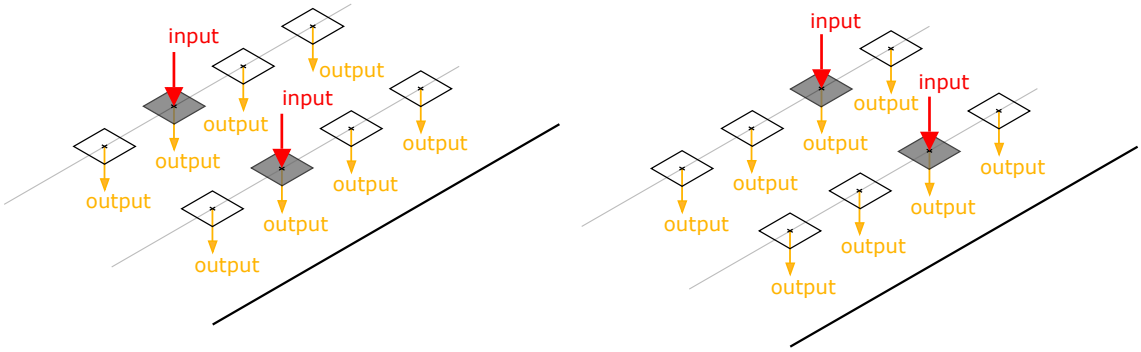

Figure 5.8 – Input and output points for different load cases

During the first frequency step, when the first input is applied, the response due to the load system is computed for all the output points along the bridge. For the rest of the inputs, the displacement is computed in the same way. When all the inputs have been computed, this process is repeated for every frequency defined in all the frequency ranges. In the end, a three-dimensional matrix with all the values is obtained, which is the FRF. fig. 5.9 shows an illustration of the frequency response function, with the parameters previously described.

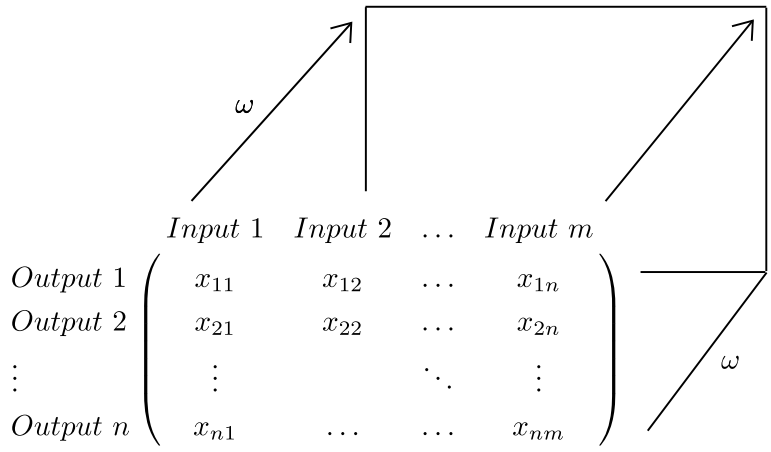

Figure 5.9 – Frequency Response Function

During the pre-process, the effects on the two rails have been studied separately, obtaining a FRF for each rail. This choice was made to simplify the analysis of the data during the post-process. For this reason, all the FRF computed have the same number of load cases and output points, resulting in a square matrix for each frequency step.

As previously described, the FRF stores the response of the bridge for a unit load applied. When we want to analyse which is the response of the bridge for a load with a different magnitude, it is only needed to multiply the unit response by the magnitude of the load. In this way, the response of the bridge can be obtained for a moving load representing a passing train.

Then, one of the main advantages is that different load systems can be applied by just changing the magnitude of the different loads applied. Once the FRF for a particular bridge with defined properties is obtained, the effect of different load systems applied to it can be evaluated without the necessity of computing the FRF again.

In a general case, a bridge subjected to m different inputs is considered. If n is the number of outputs requested and k the number of frequency steps, data exported from *Brigade* are organized in the following structure:

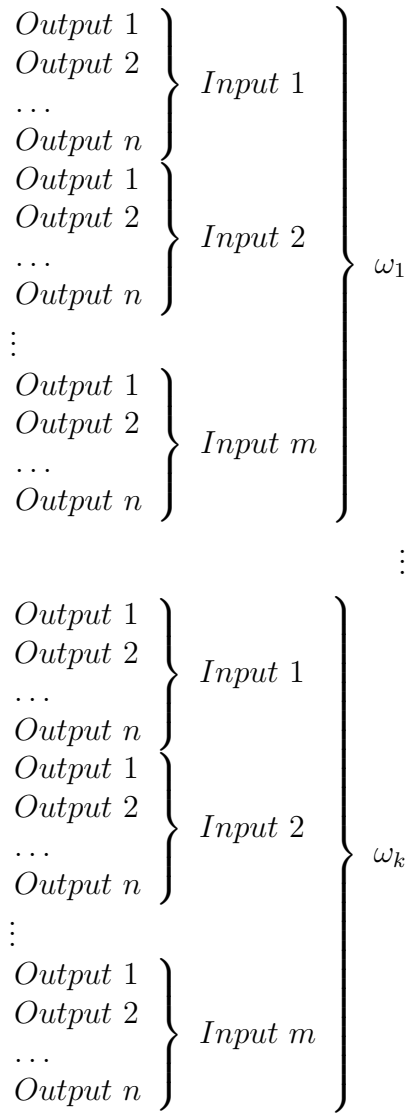

5.2.3 Parametric study

The process previously described is used to create a single and particular model. In this project several cases from the same model are studied, where the only change is the thickness of the slab deck. Moreover, the differences between other models are also the span length and the number of spans considered. Taking into account the unreasonable amount of time to model hundreds of cases, a script has been created to parametrize the study.

The Python programming language has been used to create a general script able to model the different cases depending on the parameters defined. In the script, a text file including all the different cases with their specific parameter values is read by the software. With these values, it creates the *input* file for each case with all the information necessary to compute it. The script also creates a *bat* file containing all

the cases prepared to be computed.

After the computing process, two more Python scripts have been created to extract the results. The first one opens the *odb* file created from *Brigade* and writes the data to a *npz* file. Afterwards, the other script converts all the *npz* files into *mat* files in order to process all the data in *Matlab* and analyse it. In the following section the post-process is explained.

5.3 *Matlab* post-process

5.3.1 General description

After describing the pre-process step, the post-process step will be explained in detail. On one hand, a Fourier transform is performed on the load to end up with a train load formulation in frequency-domain. On the other hand, a linear interpolation is implemented on the data coming from *Brigade* to obtain the final FRF used during the analysis.

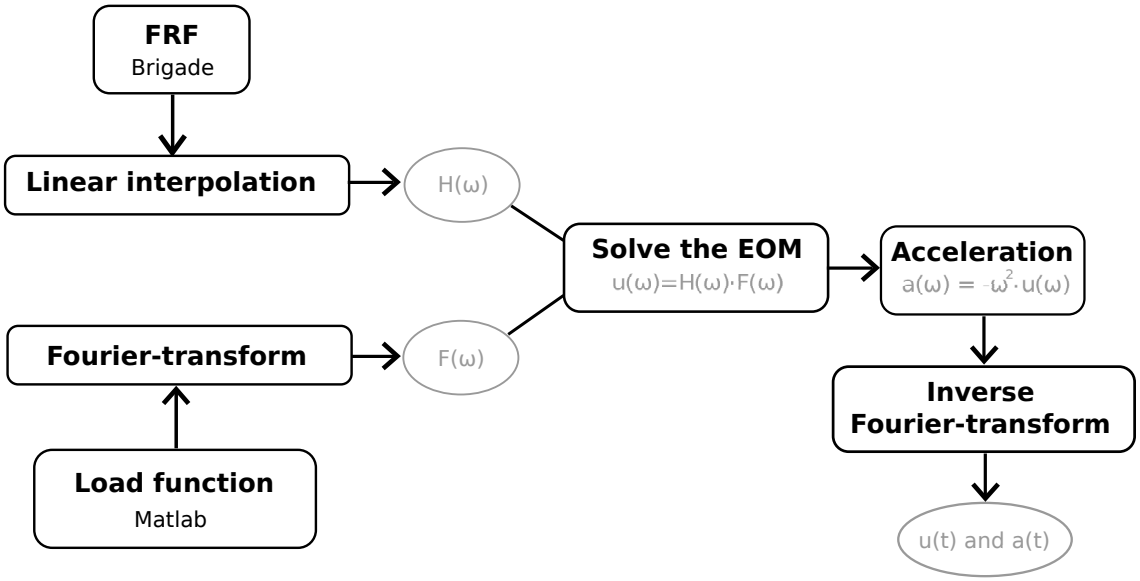

Figure 5.10 – *Matlab* post-process step

This process is illustrated in fig. 5.10, in the case when the output coming from *Brigade* is the displacement. From the load and FRF, the equation of motion can be solved to obtain the displacement in frequency-domain. Then, the acceleration is computed using the Fourier transform properties. Finally, displacement and acceleration are obtained in time-domain performing an inverse Fourier transform.

5.3.2 Train load formulation

In order to fulfil the requirements formulated in chapter 3 for the load, HSLM-A trains have to be computed. Point loads have been used to describe train bogies, with a linear variation of the load between the neighbouring nodes, and a maximum value P at the considered node (see fig. 5.11).

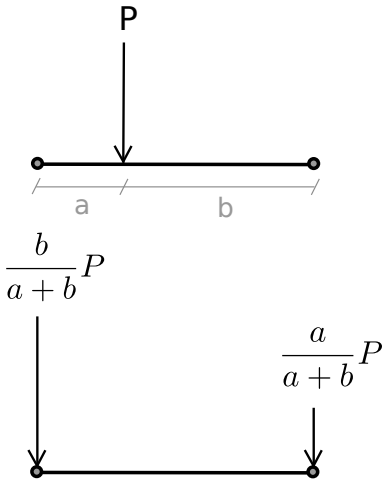

Figure 5.11 – Load distribution between two considered nodes

Thus, the load received by each node due to a single point load moving along the bridge can be represented over the time as seen in fig. 5.12.

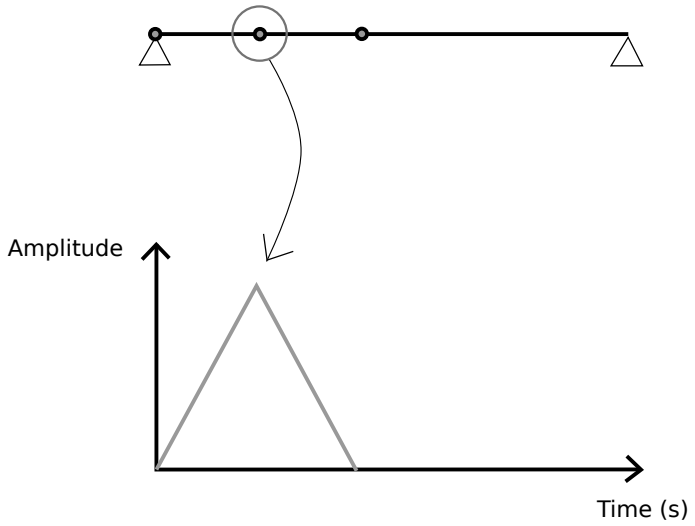

Figure 5.12 – Amplitude of the load received by one node over the time

In this way, the load received by the following node is obtained by time-shifting this function. This shift depends on the speed of the train v and the distance between two nodes d. For the next node, the shift is equal to $\frac{d}{v}$. For the *nth* node, the shift is $\frac{d}{v}(n-1)$.

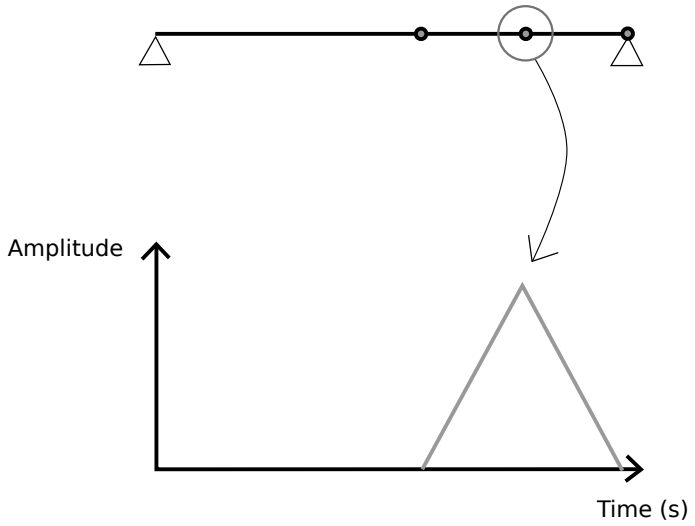

Figure 5.13 – Time shift of the load function for one node

Finally, one HSLM-A train is obtained by adding several point loads, and repeating this process for each node along the bridge as represented in fig. 5.14.

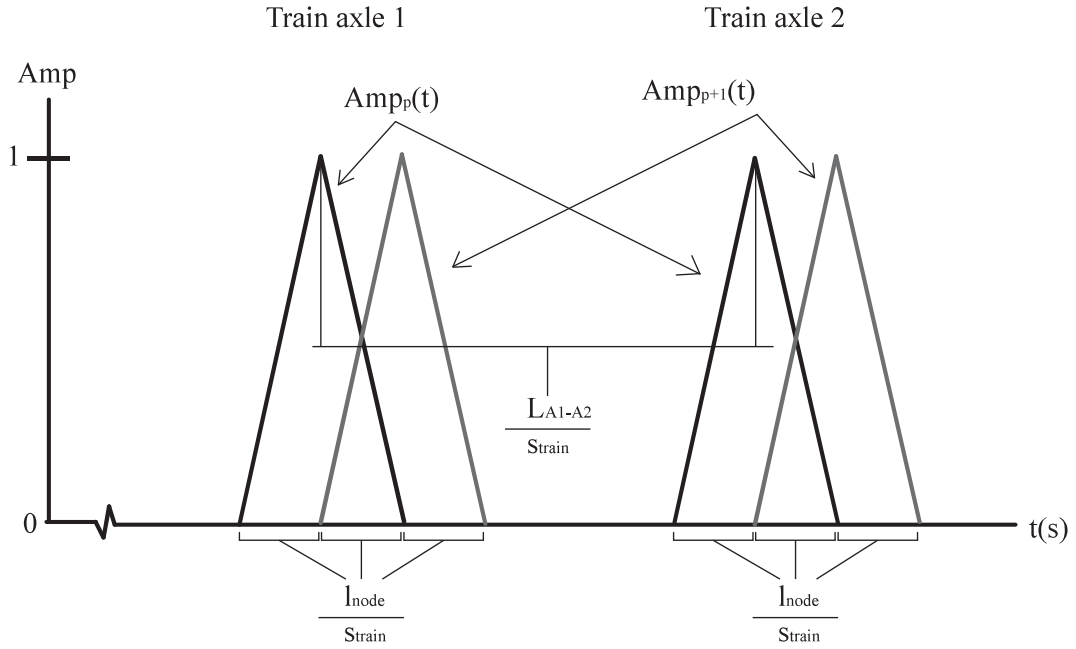

Figure 5.14 – Schematic figure of the nodes for several point loads applied, from Kylén (2010)

In order to solve the equation of motion in frequency-domain as presented in the theoretical part, different variables in eq. (2.22) have to be transposed from time to frequency-domain using the Fast Fourier Transform provided by *Matlab*.

Thus, the load function representing the passage of a train for one node has to be computed at each node for each train speed and HSLM-A train. Consequently, this

operation requires a lot of computing time. However, using the Fourier transform properties, only the first node needs to be computed since the others can be obtained by translating the first node. If F_1 and F_2 are respectively the Fourier transform of the first and second node, F_2 is obtained with eq. (5.1).

$$F_2(\omega) = e^{-2i\pi(x_{node2}-x_{node1})\omega} F_1(\omega) \tag{5.1}$$

Where x_{node1} and x_{node2} refer to the spatial coordinate of nodes 1 and 2.

Afterwards, the maximum frequency considered in the Fourier transform of the load has to be the same as the maximum frequency f_{max} considered for the analysis, which is also considered in the FRF. For this reason, frequencies greater than f_{max} are removed from the original signal. It is also important to notice that the frequency step of the load is equal to the frequency step of the FRF, since the total time T is the same in both cases.

5.3.3 Linear interpolation

5.3.3.1 Bias option in *Brigade*

The first approach to solve a dynamic problem in frequency domain, is to compute a frequency response function for different frequencies, equally spaced in all the frequency ranges.

However, although this method provides accurate results if the frequency step is small enough to describe the behaviour of the structure at different frequencies, it requires a lot of computing time in a steady-state analysis. In addition, the resonance phenomenon leads to very sharp peaks at different eigenfrequencies. This means that the frequency step has to be small enough in order not to miss them, which has a significant influence on the results.

In order to prevent this, an option called *bias* is included in the FEM software. It allows the subdivision of the total frequency interval in several frequency intervals defined by the different eigenfrequencies. A closer spacing of the results towards the outer limits of each interval gives a more accurate way to discrete the peaks and thus the eigenmodes. A lot of computing time can be saved defining a larger spacing of the points between the peaks where the contribution on the results is not pronounced. An illustration of the subdivision of an interval in fig. 5.15 shows how data points are located in the frequency interval.

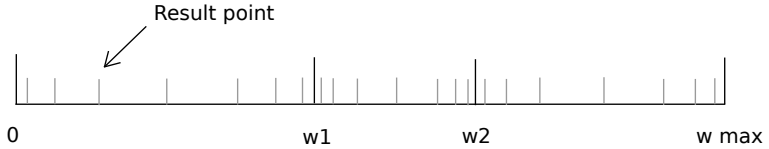

Figure 5.15 – Subdivision of an interval with the bias option

Furthermore, it is also possible to fix the frequency spacing in each subinterval by changing the value of this parameter. A value equal to 1 equally spaces the frequency in the interval, whereas a value greater than 1 induces close spacing between points towards the end of the interval. A few examples in fig. 5.16 show the effect of this parameter.

Figure 5.16 – Effects of the bias parameter on the frequency spacing

It is also possible to define the number of points inside each interval. Combining the bias parameter together with the number of points the frequency interval is represented.

5.3.3.2 Interpolation between data points

Once the data is imported to *Matlab*, although the frequency interval is well discretized, some operations are required to be able to perform an analysis in frequency domain.

On one hand, the frequency step changes within each interval. On the other hand, the spacing between the frequencies in the middle of each interval is too large, thus it is inappropriate for a frequency analysis. This means that from the procedure used to save computing time and amount of data, new points need to be regenerated in this post-process step.

Firstly, a linear interpolation is performed between each frequency. Since the largest spaces are located between the peaks, small errors committed due to this linear interpolation are negligible.

fig. 5.17 shows the imaginary part of a frequency response function at midspan for a 3D model of a slab bridge, to illustrate the interpolation between the frequencies.

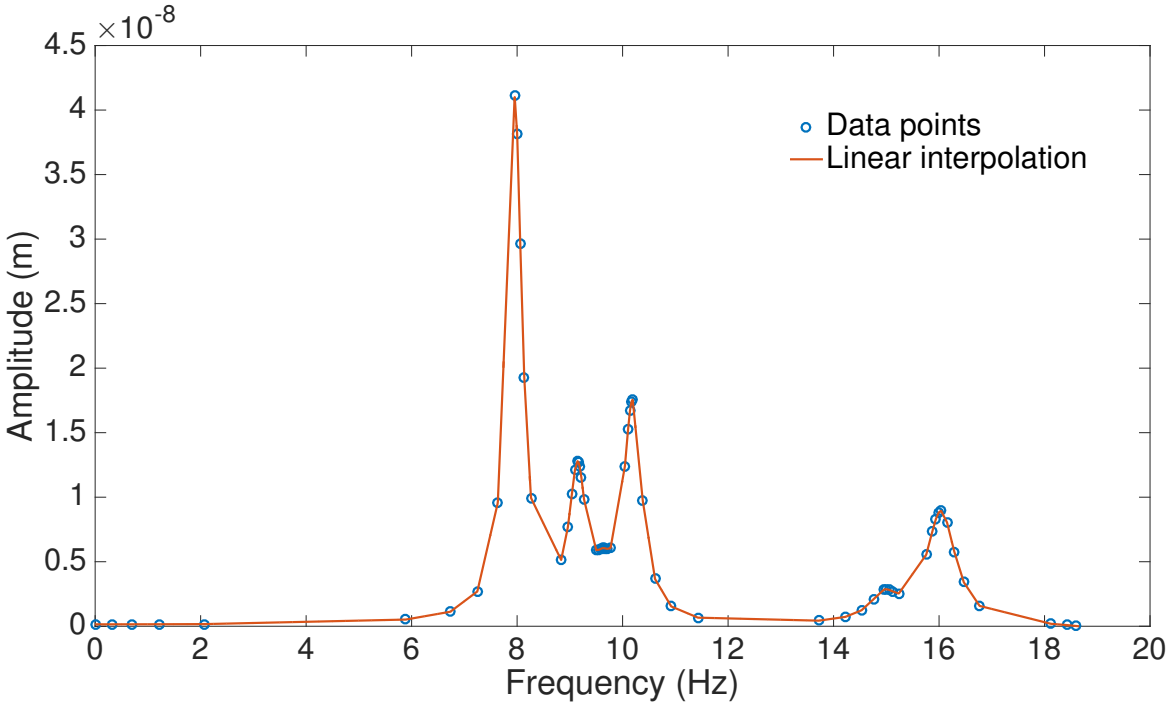

Figure 5.17 – Linear interpolation between data points

Thus, the frequency response function is built by interpolating the real part and the imaginary part of a complex number for positive frequencies. Nevertheless, negative frequencies have also to be considered when performing a Fourier transform. For the real part, the matrix is symmetric in relation to zero, which means that the negative part is obtained by flipping the positive part as illustrated in fig. 5.18a. For the imaginary part, since the matrix is antisymmetric, the negative part is obtained taking the conjugate of the positive one (see fig. 5.18b).

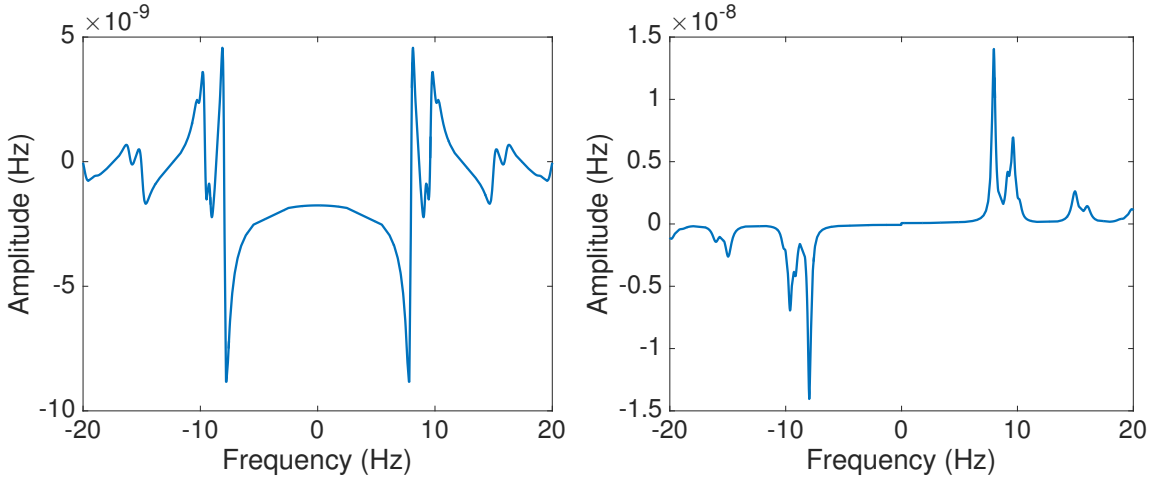

(a) Real part

(b) Imaginary part

Figure 5.18 – Example of a FRF for a 3D slab bridge at the midspan, for one load case

Moreover, a constant frequency step is defined by fixing the total time of the analysis, since the frequency step is obtained by the relation $\Delta f = \frac{1}{T}$. In this way, requested points will be taken for each frequency step, as illustrated in fig. 5.19.

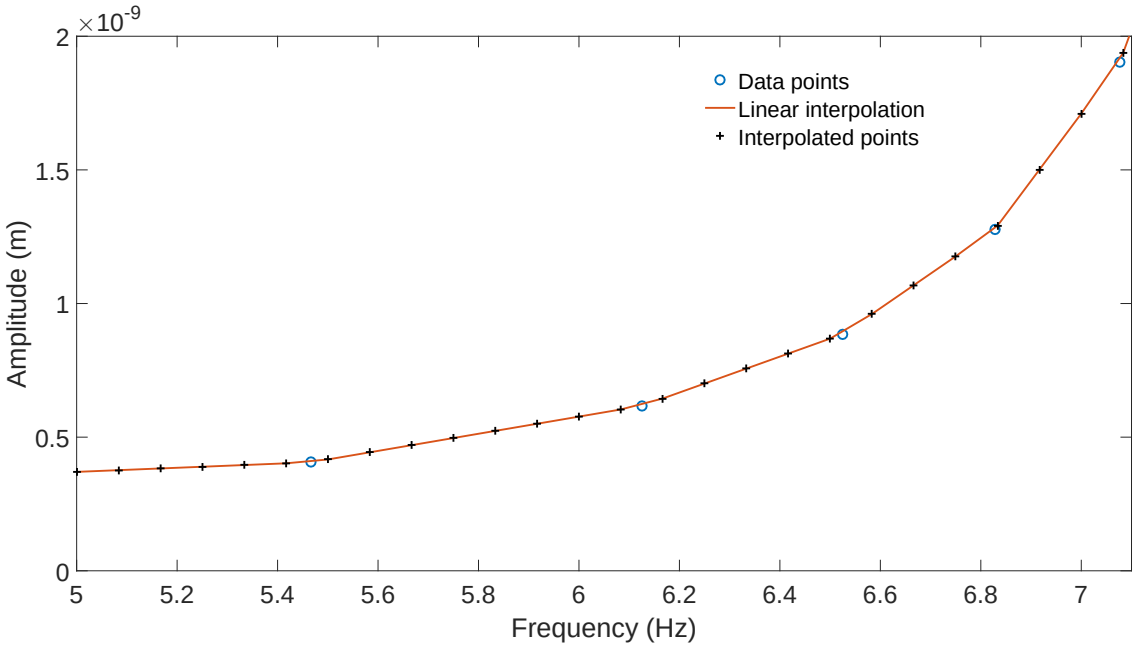

Figure 5.19 – Illustration of the frequency step

5.4 Influence of parameters

In this section, all the convergence analyses performed are explained. These analyses have been used to define parameters used in *Brigade*, concerning the type of step, the frequency range or the kind of mesh.

5.4.1 Selection of the frequency step

This section is focused on the influence of the frequency step on a 3D slab bridge model where the modes of vibration are more frequent compared to a 2D model, especially because of the torsional modes of vibration.

Different frequency steps have been computed using all the load systems for a slab bridge with two spans, and the envelope of the maximum acceleration for each speed is presented in fig. 5.20. In this way, the maximum value of the acceleration used for the design of the section can be seen from a dynamic point of view.

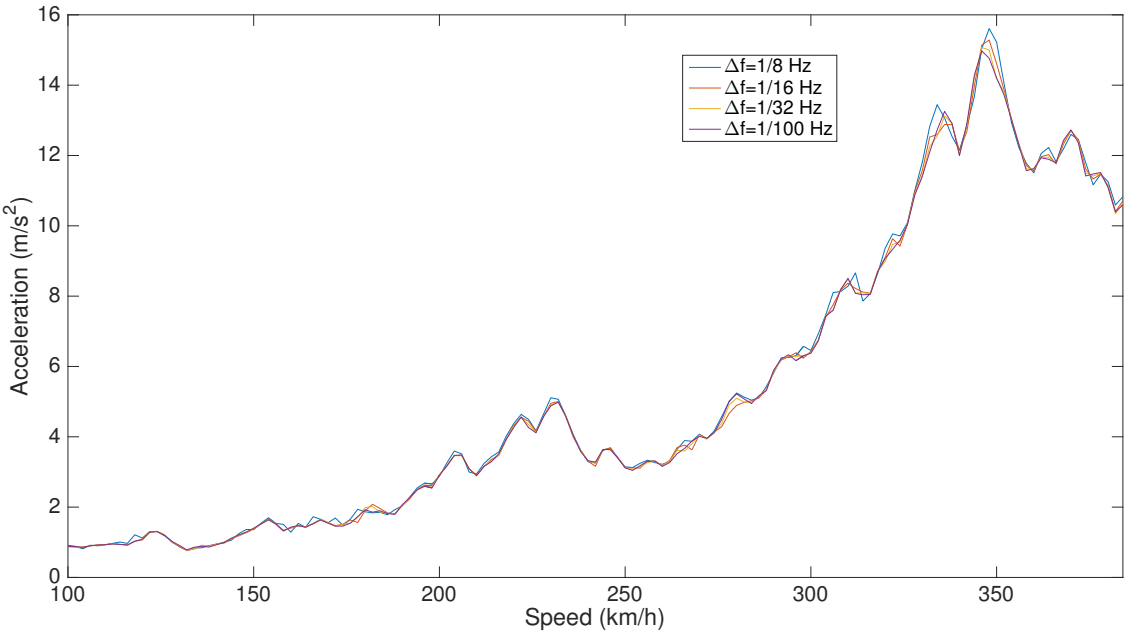

Figure 5.20 – Influence of the frequency step on the acceleration for a 3D slab bridge

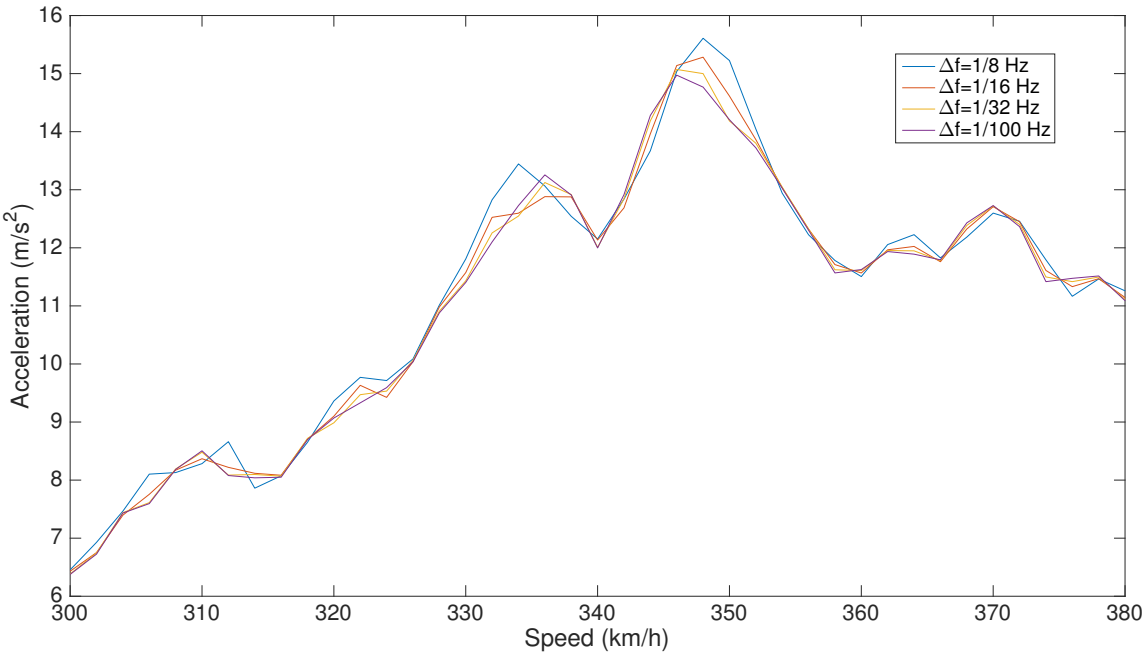

Figure 5.21 – Close-up of the frequency step influence on the acceleration for a 3D slab bridge

Besides, the computing time to obtain these envelopes is reported in table 5.1

Table 5.1 – Time to compute the envelope for different frequency steps

Δf (Hz)	Computing time (s)
1/8	187,4
1/16	343,3
1/32	634,8
1/100	1753,8

It is necessary to find the correct compromise between, large frequency step and a smaller value. The first case leads to accurate results where a lot of computing time is required while the second one requires less computing time but poor results. Considering a very small value will have an effect on the frequency response function as illustrated in fig. 5.22.

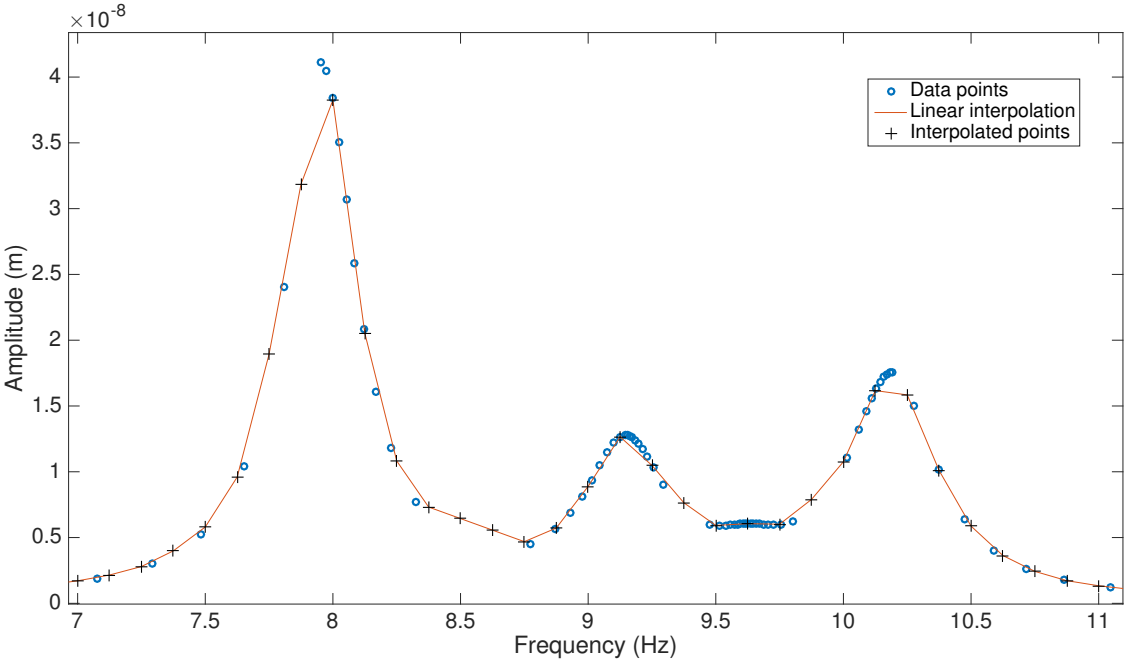

Figure 5.22 – Effects of a very small frequency step on the FRF

Data points represented in blue correspond to the frequencies imported in *Matlab* from *Brigade* with the bias option. The black crosses are the points linearly interpolated in the post-process step, where the frequency step is chosen by fixing the total time. Thus, the FRF will not be correctly represented if the frequency step is not large enough, since some points will not be considered during the interpolation process. This results in a poor approximation of the peaks by missing data points, but also in the maximum value of the resonance which has a relevant contribution on the final results.

In the end, considering the computing time and the accuracy of the results, a frequency step of $1/32$ s is the best compromise for this parametric study. The difference obtained with $\Delta f = 1/100$ Hz is not so relevant, whereas the computing time is three times lower.

5.4.2 Influence of the bias

5.4.2.1 Bias value

For an eigenfrequency interval, the default bias parameter is set equal to 3 by *Brigade*. However, it is interesting to see the influence of this parameter on the results. A few cases have been compared using also values 2 and 4 for the bias parameter. The difference obtained between them is not relevant enough to use another value than 3.

5.4.2.2 Number of points per interval

Once the frequency range has been subdivided into subintervals, it is necessary to define the number of points per interval. As previously explained, the best compromise needs to be determined.

The influence of this parameter is studied in fig. 5.23 where the envelope of the acceleration for the same 2D beam model is shown.

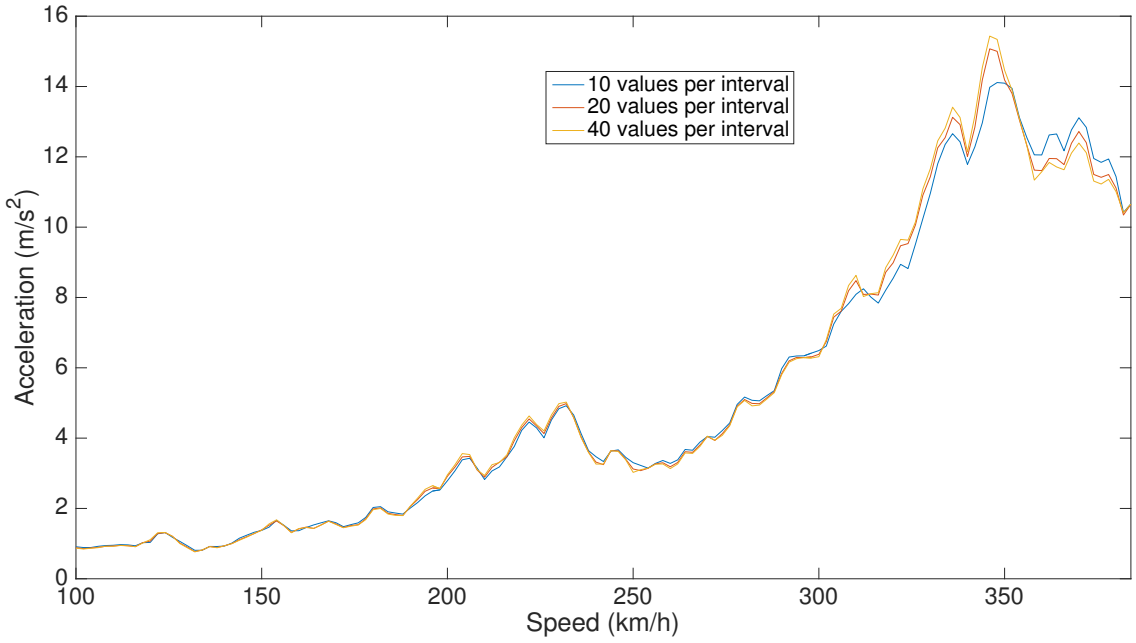

Figure 5.23 – Influence of the number of points per interval for a 3D slab bridge

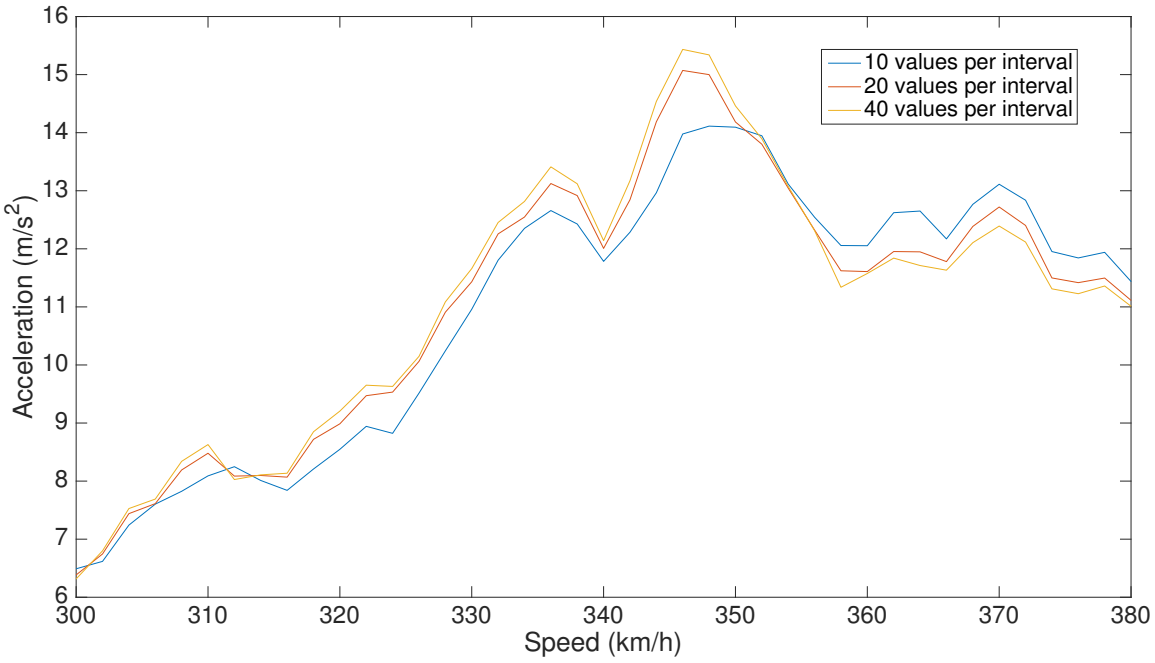

Figure 5.24 – Close-up of the number of points influence per interval for a 3D slab bridge

As previously mentioned, if the number of values per interval is not big enough has an effect on the FRF, especially for bridges with a high first eigenfrequency. Indeed, in this case the first interval is quite large, and then the space between the values close to the end of the interval will lead to a bad approximation of the first peak. In addition, most of the time this peak corresponds to the first vertical mode of vibration which is the most important for the resonance. This phenomenon is illustrated in fig. 5.25.

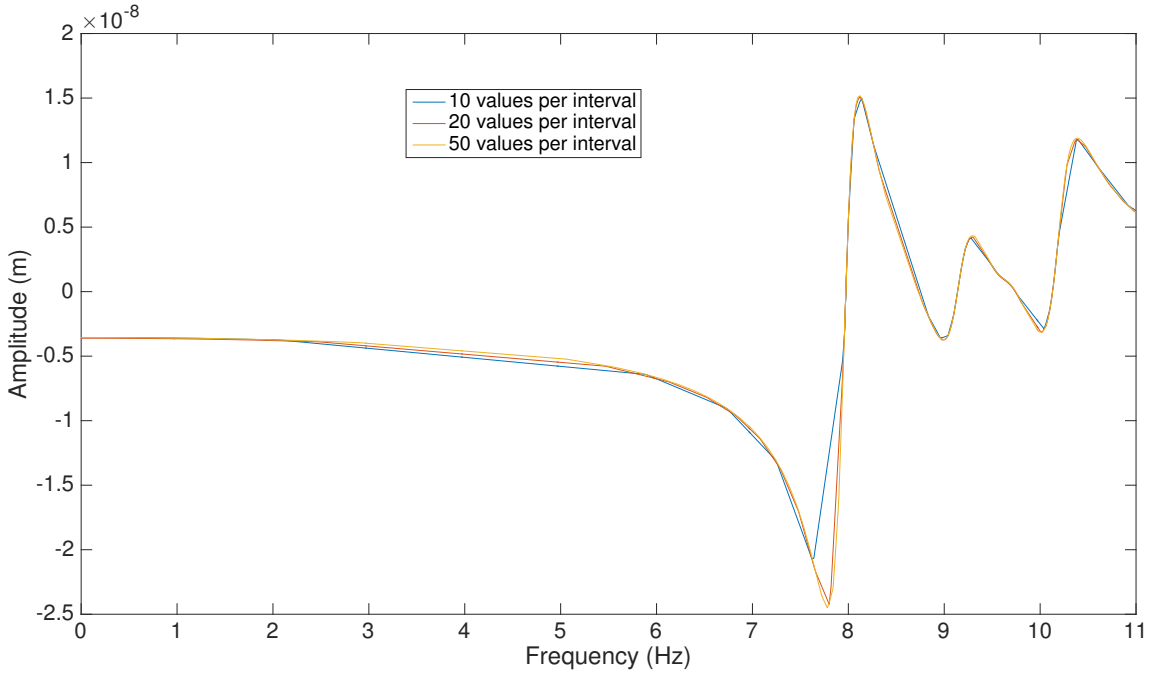

Figure 5.25 – Illustration of a different number of values per interval and the effect on the real part of the FRF

As becomes clear, using 10 points leads to inaccurate results close to the peaks, where the contribution is more pronounced. However, the results obtained using 20 or 50 points are similar. Consequently, 20 data points per intervals will be considered.

5.4.3 Steady-state Dynamic Step

The frequency approach used in this project needs a steady-state dynamic analysis to be previously performed in the different cases studied. This kind of analysis can be done using a *direct* or *mode-based* solution. The *direct* solution provides more accurate results than the *mode-based* one. The difference between the two solutions is increased when a highly frequency-dependent material damping or viscoelastic material behaviour is present in the structure. On the other hand, the *mode-based* solution is much faster, so the total computing time is reduced.

The type of structure analysed has no elements with a significant damping such as dashpots or springs, so the two solutions should be similar. An analysis comparing the two solutions has been performed to study the influence on the values obtained. The envelope for acceleration for a given bridge has been compared (L=10.4m, 2 spans). fig. 5.26 shows the comparison between the two solutions.

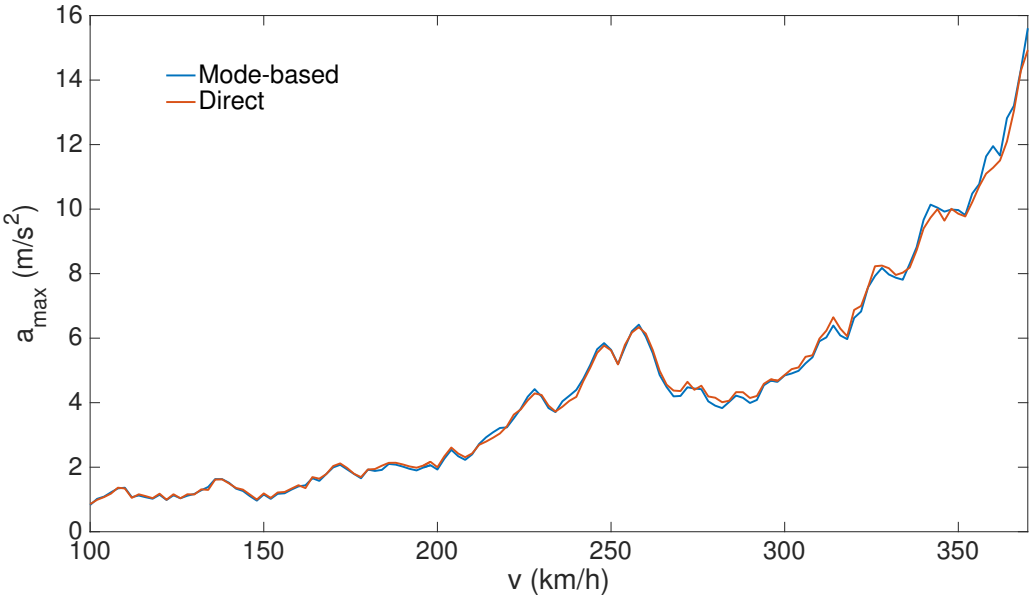

Figure 5.26 – Comparison between direct and mode-based solutions

Analysing the figure, the envelope for acceleration obtained with the two different alternatives is very similar, with no relevant difference between them. Moreover, an additional analysis has been performed to compare the computing time between the two steps. The extreme cases, corresponding to the shortest and largest span length, have been computed. The results are shown in table 5.2.

Table 5.2 – Computing time comparison between direct and modal Steady-state dynamics solution

			COMPUTING TIME		
L (m)	Spans	Total length (m)	Direct solution (h)	Modal solution (h)	Relationship (N times faster)
10,4	1	10,4	0,05	0,00	17,69
	2	20,8	0,22	0,01	22,83
	3	27,0	0,34	0,02	21,94
	4	37,4	0,73	0,02	29,38
29,9	1	29,9	0,69	0,03	25,87
	2	59,8	3,39	0,10	34,65
	3	77,7	6,81	0,21	32,71
	4	107,6	12,81	0,43	29,62

As can be seen, the modal solution is approximately between 20 and 30 times faster than the direct solution. This faster computing time has been the main motivation to use the Steady-state Modal dynamics step to perform further analyses.

5.4.4 Mesh parameters

Two different analyses have been performed concerning the shell element type used in the mesh. On one hand, the influence of the element type of the mesh has been studied. On the other hand, a convergence analysis comparing different element sizes has been performed.

There are different types of mesh element that can be used in *Brigade* for this type of problem. Different shell elements have been used to compute the solution: linear triangular (S3R), linear quadrilateral (S4R), quadratic triangular (STRI65) and quadratic quadrilateral (S8R). Then, the values obtained have been compared as well as computing time.

The analysis consisted in a comparison of the envelope of vertical displacement and acceleration for the particular case of two spans with a span length of L=10.4 metres. In fig. 5.27 and fig. 5.28 the comparison is shown for the passage of a HSLM-A1 train.

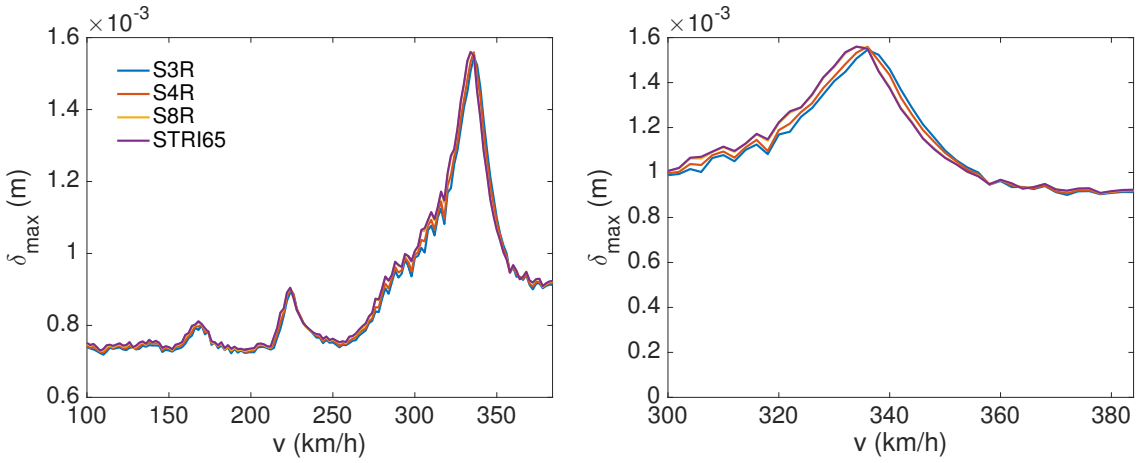

Figure 5.27 – Maximum deflection comparison between different element types

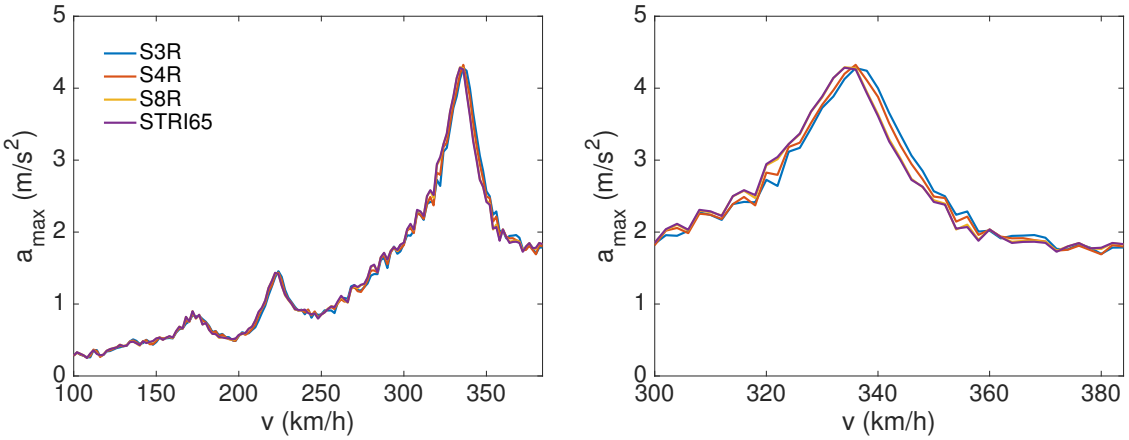

Figure 5.28 – Maximim acceleration comparison between different element types

As can be seen, for the displacement there is no relevant difference between the 4 different elements, while for the acceleration there is a slight difference in some peaks. fig. 5.28b shows a close-up of the peak where the maximum value is obtained. Although the solution using the quadratic elements is more accurate than the one using linear elements, the difference is not so relevant.

table 5.3 shows the computing time of the different elements for the case.

Element type		Computing time (s)
Linear	Triangular (S3R)	44,30
	Quadrilateral (S4R)	46,20
Quadratic	Triangular (STRI65)	52,20
	Quadrilateral (S8R)	52,60

Table 5.3 – Computing time different element types

Analysing table 5.3 using quadratic elements leads to a higher computing time compared to linear elements, as it was expected since the solution is more complex. The difference on the computing time is not so big when a modal solution is used for the steady-state analysis. However, the difference is increased when a direct solution is used, which is not described in the present report. Moreover, quadrilateral shell elements provide better solution than triangular elements for this problem and analyses performed.

Taking into account the results obtained, linear quadrilateral shell elements (S4R) will be used for the mesh.

A second analysis is performed to define the mesh element size used. The element size is generally chosen regarding the geometry of the model.

The small surfaces defined to represent the insertion points of the loads require a thin mesh in order to obtain an accurate solution. However, it is not necessary a refined mesh on the other side of the bridge to obtain the same accuracy. For this reason, different mesh sizes are defined depending on the location along the surface.

As previously presented, element mesh sizes used vary between 1.0, 0.5 and 0.2 metres. The chosen mesh has been compared with a finer mesh (constant value of 0.2 metres) and a denser mesh (constant value of 0.5 metres). The value of n_0 has been compared for each number of spans with span lengths of L=10, L=20 and L=30 metres. table 5.4 shows the results obtained.

Cases		n_0 (Hz)			Error (%)		Computing time (s)		
Spans	L (m)	0,5 m	variable	0,2 m	0,5 m	variable	0,5 m	variable	0,2 m
1	10	10,98	10,88	10,85	1,14	0,29	0,4	1,0	1,6
	20	5,51	5,50	5,50	0,21	0,04	0,6	1,7	5,3
	30	3,42	3,42	3,42	0,13	0,02	0,5	2,6	8,3
2	10	8,69	8,60	8,56	1,46	0,40	0,5	1,7	4,5
	20	4,20	4,19	4,19	0,21	0,04	0,7	4,3	12,1
	30	2,26	2,26	2,26	0,13	0,04	1,2	6,8	16,2
3	10	10,32	10,33	10,27	0,46	0,51	0,4	2,7	6,3
	20	4,37	4,35	4,35	0,28	0,04	1,1	5,7	13,9
	30	2,84	2,84	2,84	0,15	0,03	1,3	8,3	17,6
4	10	9,75	9,61	9,58	1,79	0,32	0,6	4,1	9,9
	20	3,98	3,97	3,97	0,26	0,04	1,4	7,5	23,8
	30	2,26	2,26	2,26	0,15	0,04	2,0	14,4	32,0

Table 5.4 – Computing time and n_0 for different element size meshes

As can be seen, the values obtained using different meshes are similar. Comparing the relative error it becomes clear that the values obtained using variable element size are almost the same than using the finer mesh.

In addition, there is a pronounced difference between the computing time using the denser and finer mesh. The computer time is approximately 50 per cent reduced using the variable element size mesh.

For these reasons, a variable element size mesh has been used to compute the different bridge cases.

Chapter 6

Verification of the frequency domain analysis

6.1 Description of the bridge

The Banafjäl bridge is a simply supported bridge with a span length of 42 m. The deck is a composite structure made of steel and concrete. table 6.1 presents the general parameters used to define the model.

Table 6.1 – General parameters used in the models

Parameter		Value	[]
Span length	*L*	42,0	m
Young's modulus	*E*	2,1E+11	Pa
Poisson ratio	*v*	0,0	-
Moment of inertia	*I*	0,62	m^4
Mass	*m*	18140	kg/m
Area	*A*	0.57	m^2

Figure 6.1 – *Banafjäl* railway bridge

6.2 Results obtained in time domain with *Brigade*

In this section a verification of the 2D model is performed. It has been carried out in two different ways: using the analytical solution and another FEM software. The results that have been compared are the vertical displacement and acceleration in the point located at midspan (L/2).

6.2.1 Analytical solution

For the first verification, the model has been compared with the analytical solution for a simply supported beam subjected to the passage of a train (HSLM A1). The solution described in section 2.4 has been implemented in *Matlab* to compare the results.

The maximum displacement and acceleration have been obtained with the analytical solution for a speed range from 100 km/h up to 300 km/h and these values are represented in fig. 6.2. Then, two solutions for two train speeds have been compared, one in resonance (156 km/h) and another out of resonance (200 km/h). These two train speeds have been chosen according to fig. 6.2.

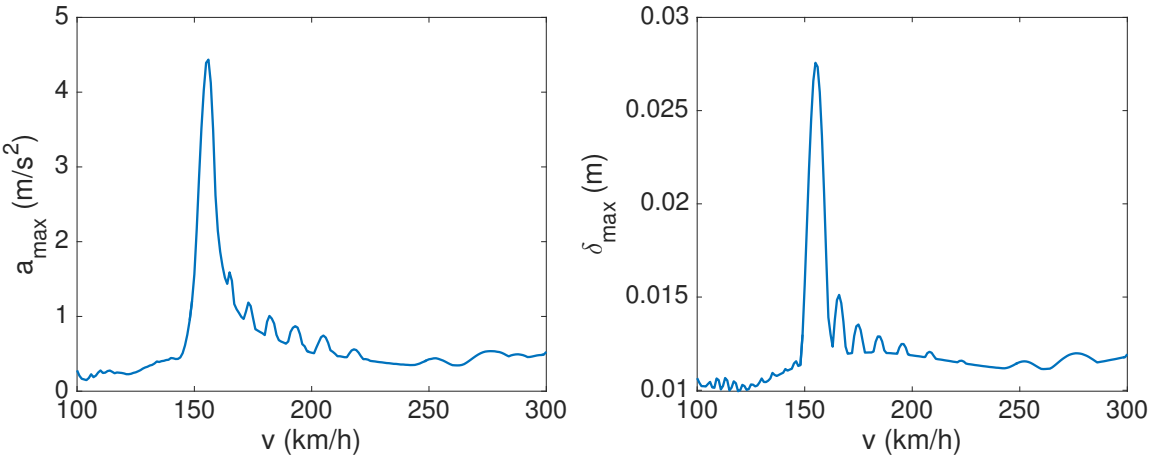

(a) Maximum acceleration (b) Maximum displacement

Figure 6.2 – Envelopes for displacement and acceleration - Banafjäl bridge

fig. 6.3 and fig. 6.4 show the results of vertical displacement and acceleration at midspan for the resonance speed. This location and speed are expected to be the most unfavourable case.

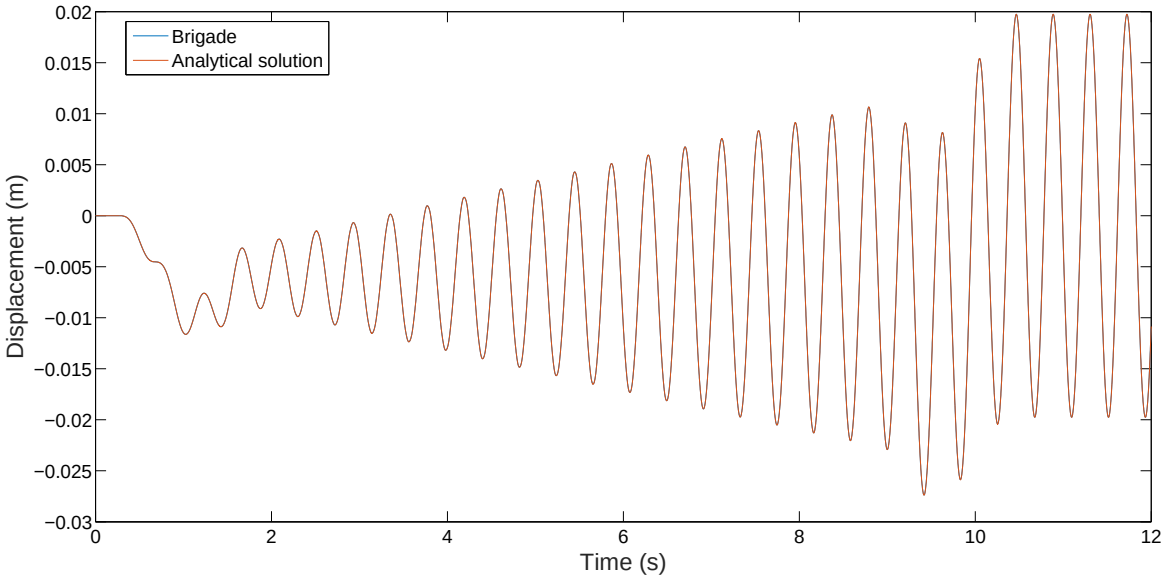

Figure 6.3 – Comparison *Brigade*-Analytical Vertical displacement at midspan for resonance speed

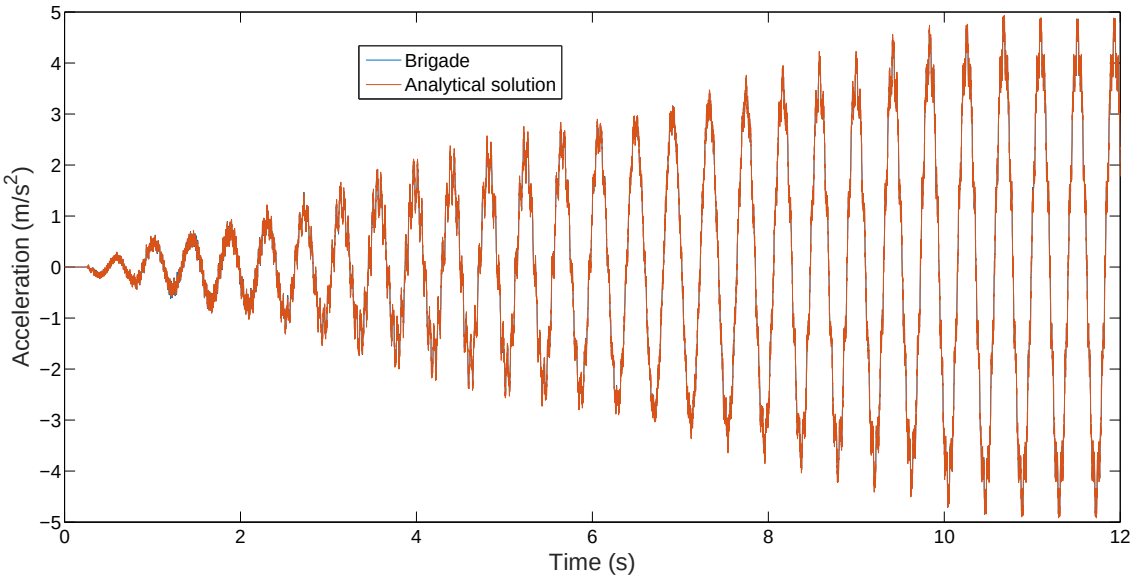

Figure 6.4 – Comparison *Brigade*-Analytical Vertical acceleration at midspan for resonance speed

As shown in these figures, the results obtained with the model in *Brigade* are very similar to the analytical solution. The free vibration can be observed in the last part of the graphs, where the amplitude is constant due to the fact that no damping is applied.

As it was expected, vertical displacement results are better than acceleration ones,

due to the faster convergence achieved. Regarding the displacement results, no difference can be recognized between the two solutions presented. Regarding the acceleration, the solution obtained with the *Brigade* model is very similar to the analytical one. fig. 6.5 shows a close-up of fig. 6.4.

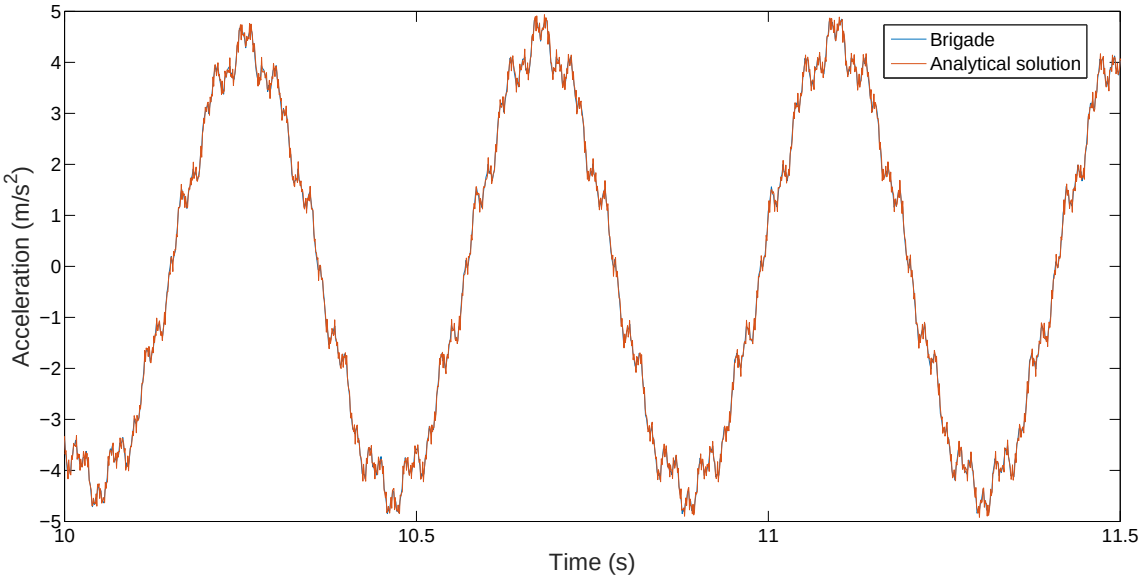

Figure 6.5 – Close-up of comparison *Brigade*-Analytical vertical acceleration at midspan for resonance speed

Although not all the small peaks have been computed in the *Brigade* solution due to the time-step used, the tendency and shape between the two solutions are the same. Therefore, the difference is small enough to conclude that the two solutions behave in the same way.

6.2.2 FEM software

Since the analytical solution can be used only for undamped problems, the model from *Brigade* has been compared with other FEM software. The solution from *Solvia* has been used.

For this second comparison the damping on the structure has been taken into account. Due to the results available from *Solvia*, vertical displacement and acceleration at midspan have been computed for the two speeds used in the previous comparison. When comparing the two methods the same values for parameters such as material properties, modal damping or mesh element type and size have been defined. Regarding the time step, a smaller value has been used in *Brigade* due to the load definition. table 6.2 presents the values considered.

Table 6.2 – Specific parameters used in the FEM models

Parameter		Value	[]
Time step (BRIGADE)	Δt	1,5E-03	s
Time step (SOLVIA)	Δt	2,5E-03	s
Damping	ξ	0,5	%
Eigenmodes		5	-
Element type		Euler-Bernoulli	-
Mesh size		0,2	m

fig. 6.6 and fig. 6.7 show the comparison for the vertical displacement and acceleration at midspan for the resonance speed.

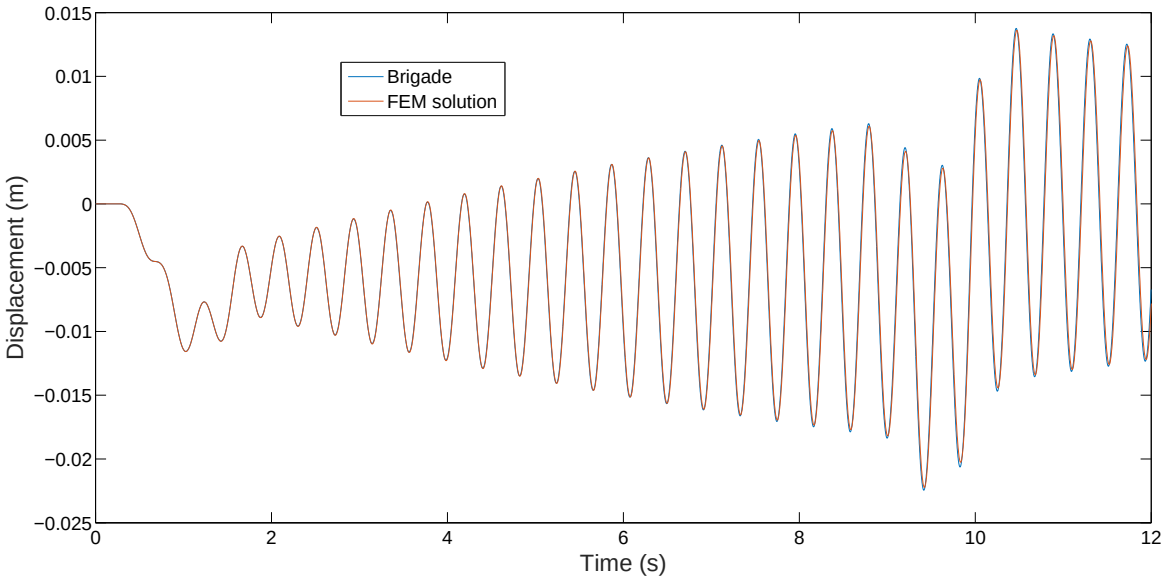

Figure 6.6 – Comparison *Brigade-Solvia* Vertical displacement at midspan for resonance speed

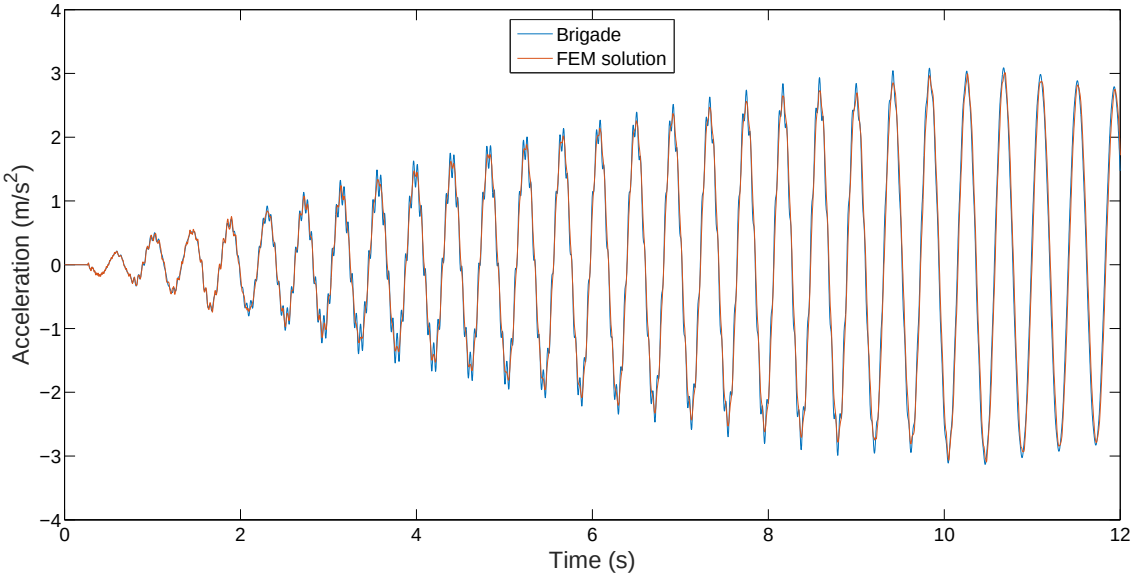

Figure 6.7 – Comparison *Brigade-Solvia* Vertical acceleration at midspan for resonance speed

In the last part of the two figures the free vibration can be appreciated. This part shows how the amplitude is reduced with time due to the damping considered in this comparison.

As shown in fig. 6.6, results for vertical displacements are again very similar between the two solutions and no difference can be observed. Comparing results for acceleration, it can be seen that peak values are slightly higher in *Brigade* solution. When comparing two different FEM models, it is very difficult to get the same solution between them, especially comparing the acceleration where the convergence is hardly achieved. fig. 6.8 shows a close-up of fig. 6.5, where the tendency and shape between the two solutions are also the same.

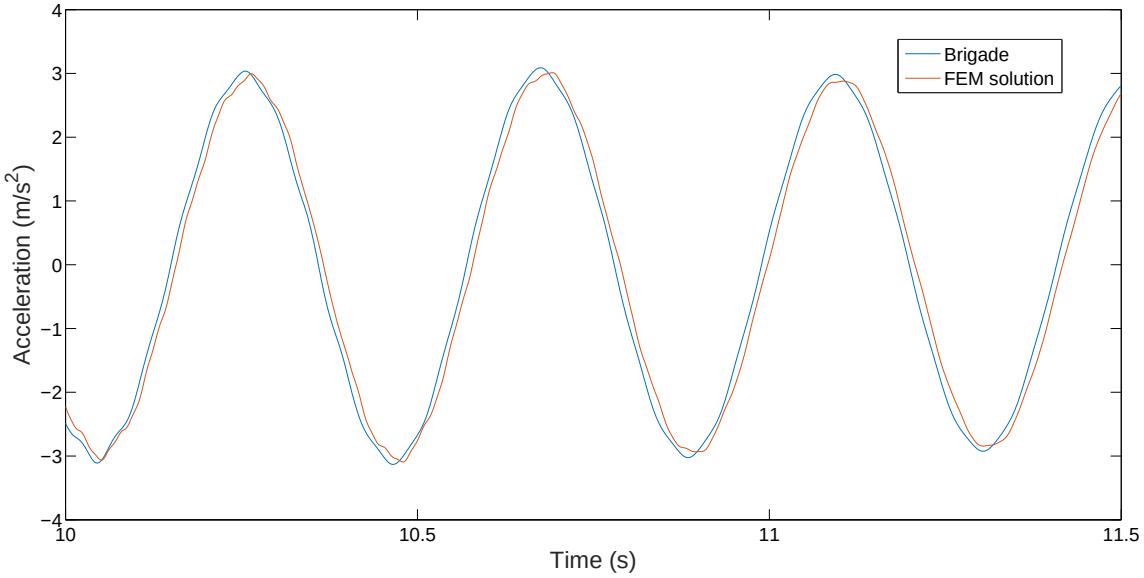

Figure 6.8 – Close-up of comparison *Brigade-Solvia* Vertical acceleration at midspan for resonance speed

After comparing the model with the analytical solution and the alternative FEM model it can be concluded that the model behaves in a proper way. This model can be used then to compare the two different approaches: time-domain and frequency-domain approach. The comparison between them is presented in the next section.

6.3 Comparison between frequency and time domain

In order to implement the frequency domain approach, results obtained with solutions in the time-domain will be compared with results obtained with a frequency analysis method.

6.3.1 Frequency Response Function

For this analysis, the frequency step has to be chosen according to eq. (6.1).

$$\Delta f = \frac{1}{T} \tag{6.1}$$

With Δf the frequency step, and T the total time for the studied phenomenon.

A representation of the FRF matrix's envelope is given in fig. 6.9 for the $Banafjäl$ bridge.

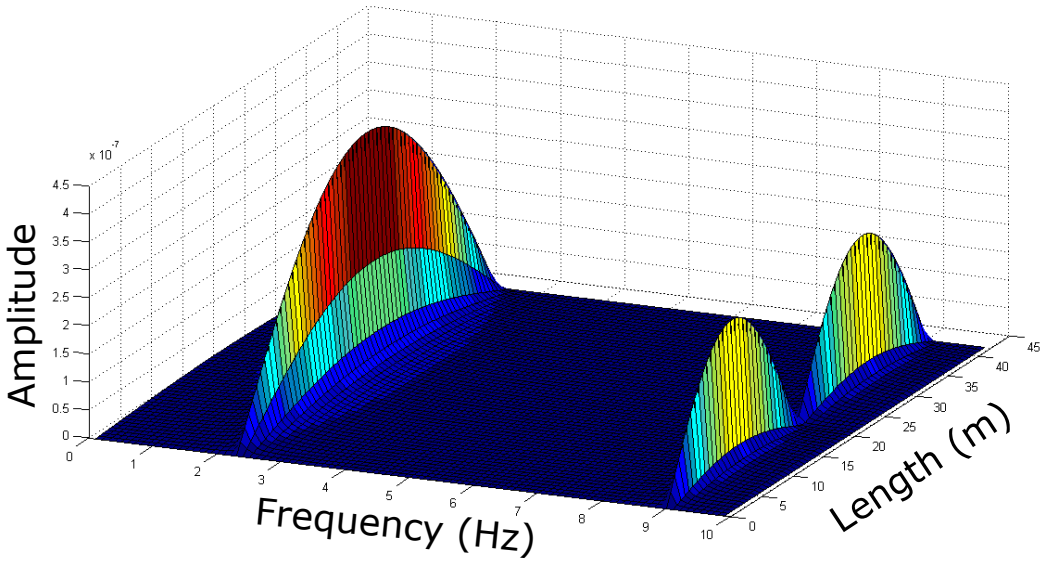

Figure 6.9 – FRF envelop for the *Banafjäl* railway bridge

The two first natural frequencies with the corresponding mode shapes can be seen in fig. 6.9, for a frequency range from 0 to 10 Hz. The maximum amplitude is obtained at the midspan for the first mode of vibration, and at the quarter span for the second one. In addition, the amplitude is close to zero between the eigenfrequencies.

6.3.2 Comparison between the results

For this comparison, displacements and accelerations are compared for the resonance and out of resonance speed, at the midspan. fig. 6.10 and fig. 6.11 results are presented with the frequency analysis for the *Banafjäl* railway bridge at the midspan, together with the ones obtained with a time domain analysis.

Results are similar, although a small difference can be noticed at each peak for the resonance speed. Indeed, in this analysis a frequency range of 50 Hz has been considered with a frequency step $\Delta f = 1/64\ s$, which corresponds to a time step of $\Delta t = 0.01\ s$ larger than the one used in time domain.

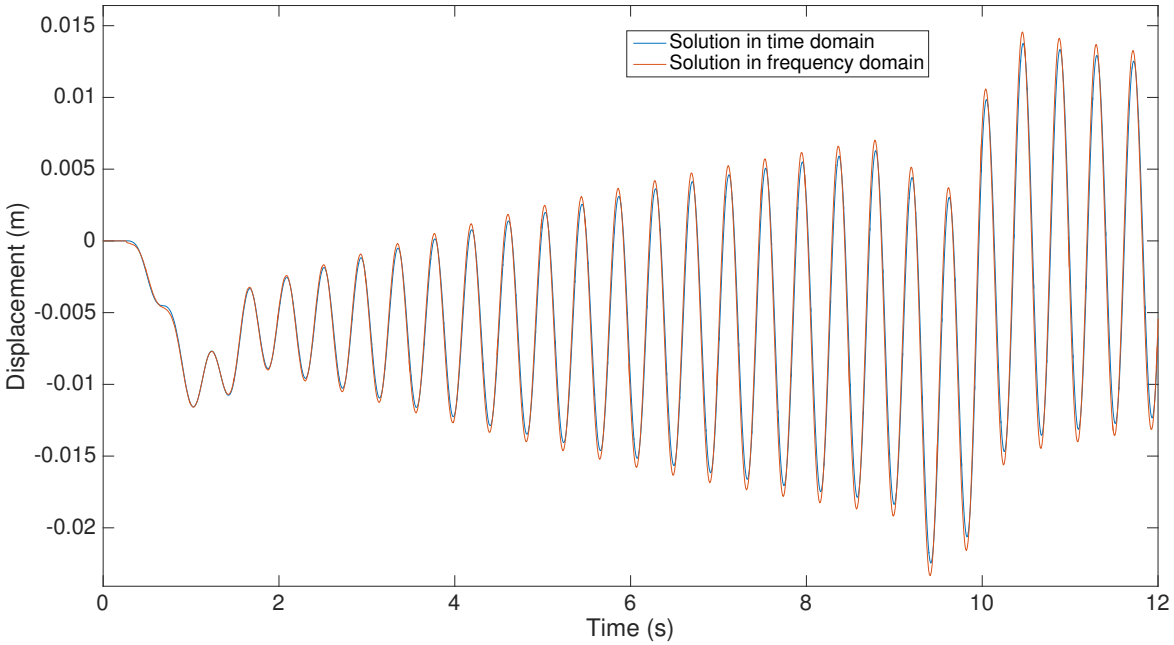

Figure 6.10 – Comparison of the displacement in time domain and in frequency domain - *Banafjäl* bridge - Resonance speed

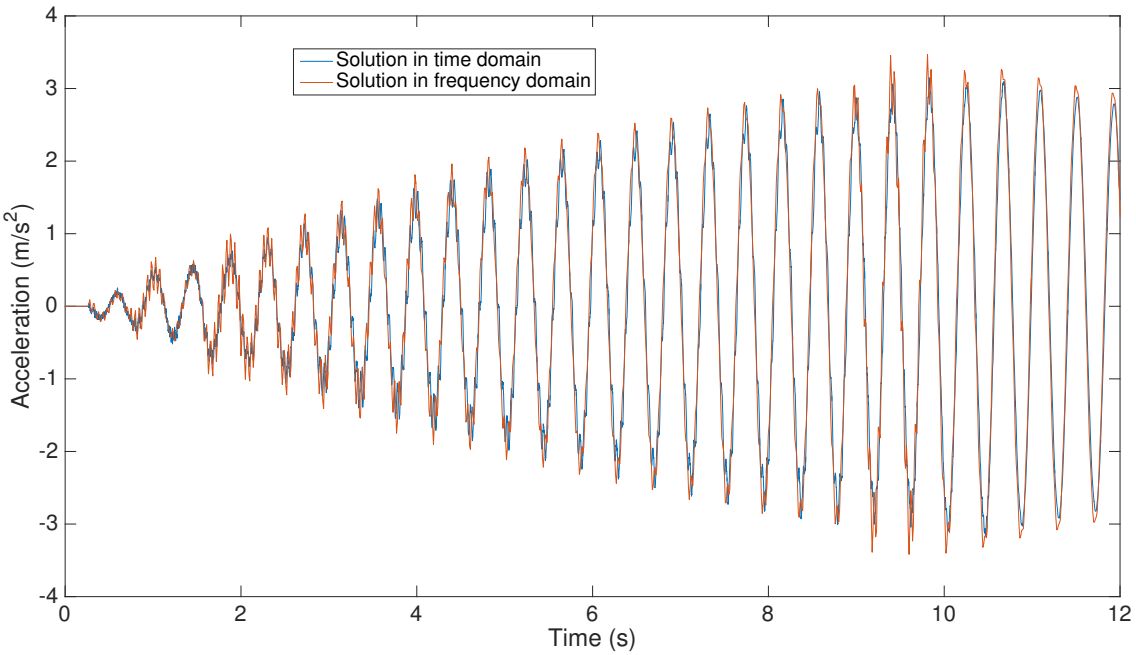

Figure 6.11 – Comparison of the acceleration in time domain and in frequency domain - *Banafjäl* bridge - Resonance speed

6.3.3 Computing time comparison

A comparison of the computing time using both methodologies has been carried out. The aim of this analysis was to figure out the computing time relationship between the frequency approach used and the time domain. In order to simplify the analysis, average cases have been computed extrapolating the resulting time for the other cases. In the following part the assumptions considered are presented.

The extreme cases of span length have been analysed. For a different number of spans, the minimum and maximum span length have been computed. A time step equal to Δt= $0.01s$ has been considered in both methods, in order to obtain the same accuracy. The same number of output points is considered in both approaches, corresponding to the insertion points of the load. The outputs requested in both methodologies are vertical displacement and vertical acceleration.

Regarding the analysis performed, the train load corresponding to the HSLM-A1 has been applied. As previously said, different speeds from 100 km/h to 384 km/h have been computed for the good cases in this project, in order to find the most unfavourable. Since this particular analysis is focused on the computing time, the average speed (242 km/h) has been computed. Then, the computing time for that speed has been counted 143 times, the total amount of speeds considered in the real cases.

The analysis was computed until reaching free vibration in the bridge in order to make sure that the maximum value for the response has been obtained. For this reason, an extra time of 3 seconds has been added to the total time that it takes for the entire train to pass over the bridge.

Under the previous assumptions, the computing time for the different cases has been studied and compared between the two different approaches. fig. 6.12 illustrates the relationship between the difference in computing time for the two methods (where N is the ratio between the time domain solution and the frequency approach), and the total length of the bridge. In Appendix B a table with the detailed computing time is presented.

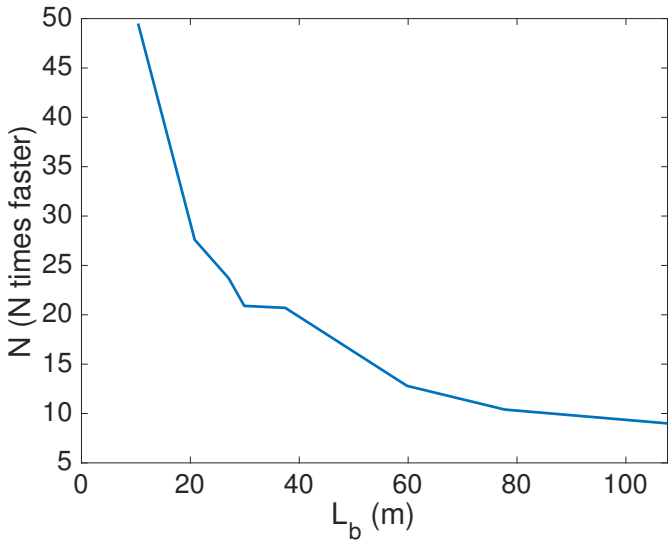

Figure 6.12 – Computing time comparison between a frequency analysis and a time-domain approach

As shown, frequency domain approach is faster than time domain approach for all the cases considered. It can be seen that for short span lengths the frequency approach is between 40 and 50 times faster, while for the larger span lengths this is approximately 10 times faster. The tendency of the graph shows that for larger span lengths the frequency approach would still take less computing time, between 5 and 10 less than the time domain approach.

On one hand, when the frequency domain method is used, most of the CPU-time is related to calculating the FRF. The post process where the train loads are applied is less relevant. For this reason, when a larger span length is considered, the total number of outputs is increased, leading to higher computing time. On the other hand, using the time-domain analysis, each train passage takes some time. Thus, the span length considered does not affect the computing time in a pronounced way.

From this analysis, the methodology used shows to be faster than the alternative. This efficiency is reduced however as the total length of the bridge is increased.

6.3.4 General remarks on the influence of parameters

A frequency analysis is very sensitive to different parameters like the frequency range or the frequency step that can affect the accuracy of the solution. The influence of these parameters on the results will be presented in the following sections.

6.3.4.1 Influence of the frequency range

The frequency range is defined by the maximum value of the frequency that has to be included in the analysis, as an interval from 0 to this value. In this way, changing this value will change the number of modes of vibration considered.

On one hand, underestimating this value can lead to poor results, since the resonance is governed by the first mode of vibration. On the other hand, including high values will increase the computing time in a pronounced way.

Different values for this parameter have been computed for the *Banafjäl* railway bridge at the midspan (fig. 6.13), for a speed of 200 km/h and for the same frequency step.

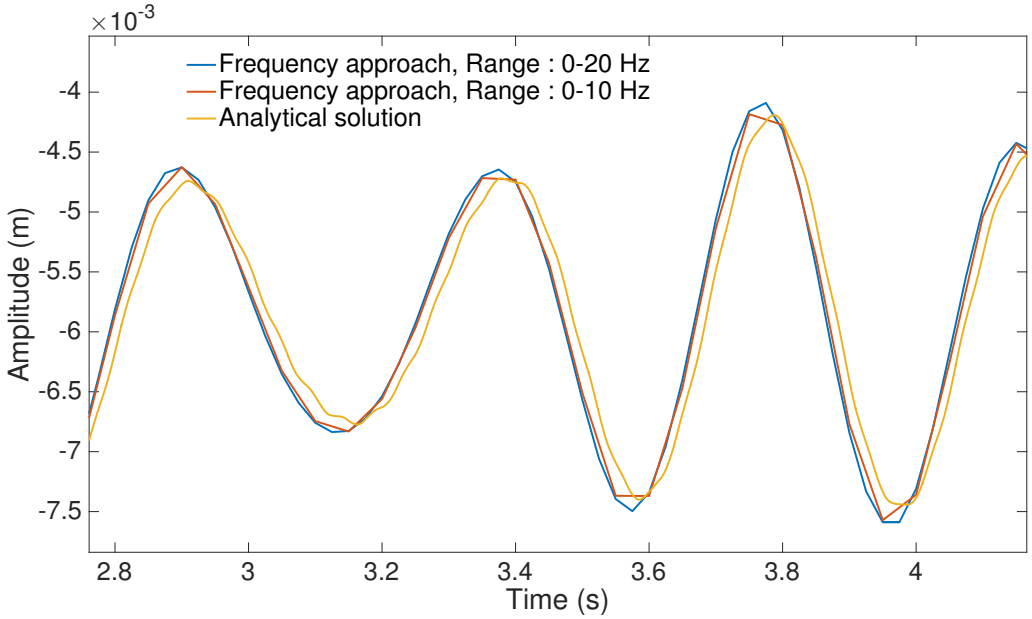

Figure 6.13 – Influence of the frequency range on displacement, v=200 km/h, x=midspan

Increasing the size of the frequency interval tends to make the results smoother for a given frequency step. This is explained by the fact that if Δf is fixed, also the total time T is set. Thus, increasing the frequency step amounts leads to a higher sampling rate and makes displacement smoother, since the time step in time domain is decreased.

However, the difference is more relevant regarding the acceleration as illustrated in fig. 6.14.

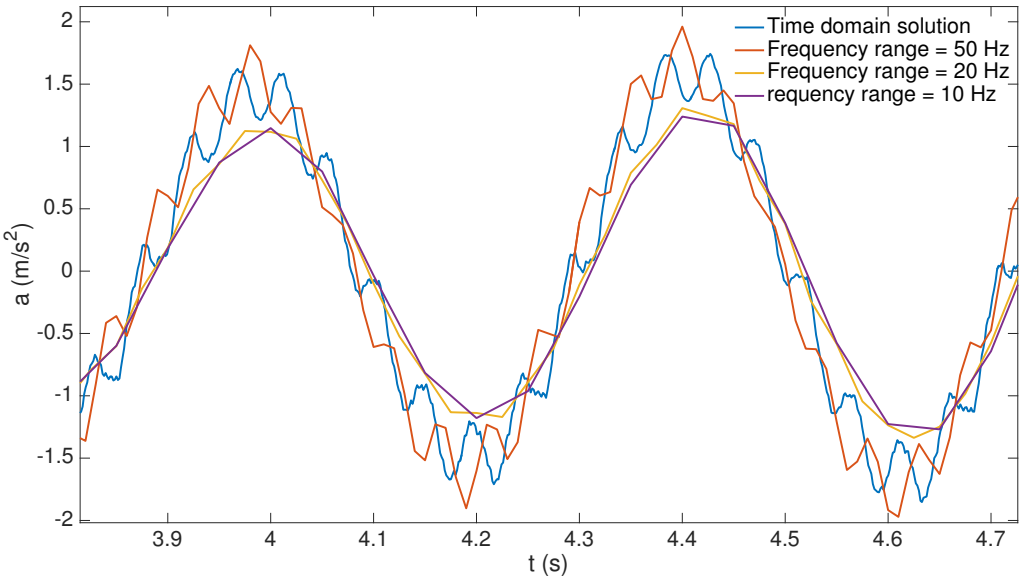

Figure 6.14 – Influence of the frequency range on the acceleration, v=200 km/h, x=midspan

The acceleration involves sharp peaks that require a time step small enough to be represented.

6.3.4.2 Influence of the frequency step

In order to implement a frequency analysis, the frequency step Δf is chosen by defining the total time T according to the relation $\Delta f = \frac{1}{T}$.

Influence of this parameter is illustrated in fig. 6.15 for the same bridge, and for a fixed frequency step.

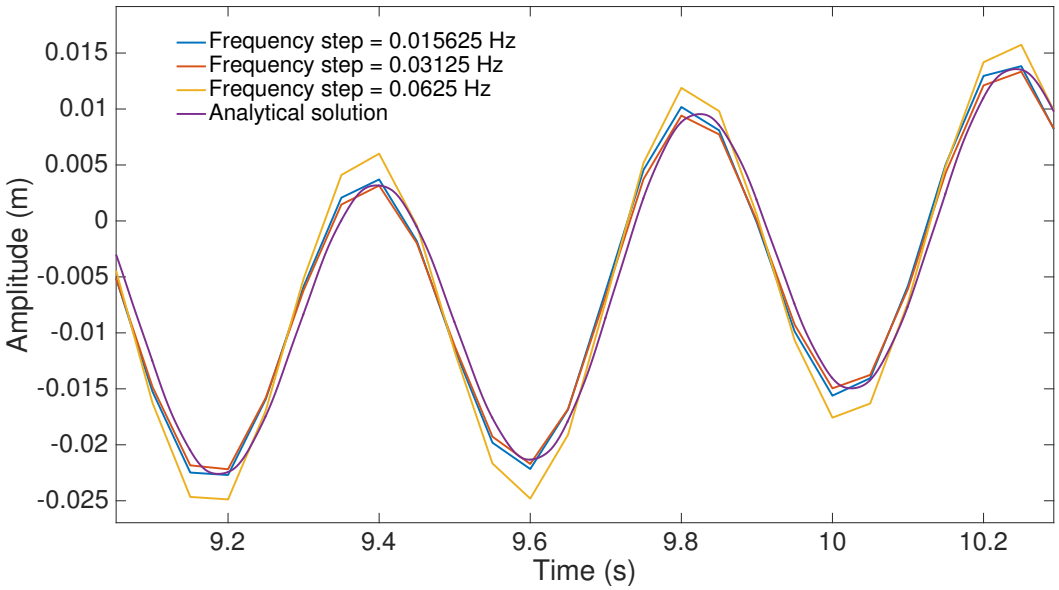

Figure 6.15 – Influence of the frequency step on displacement, v=200 km/h, x=midspan

Convergence of the results in time domain is mainly determined by the frequency step. Indeed, a large frequency step will lead to poor results since some eigenfrequencies might be missed when storing result points. A solution to this problem will be presented later on the thesis.

Chapter 7

Results

7.1 Influence of the mass and the stiffness

A dynamic analysis is very sensitive to mass and stiffness. To study these effects, a simply supported bridge is analysed with a span length (L) of 30 m, a mass (m) of 19 tons and a stiffness (EI) equal to 1.1 GN.m^2. The aim is to study their influence on the maximum vertical deflection and vertical acceleration for a speed range up to 400 km/h, using the train load HSLM-A1.

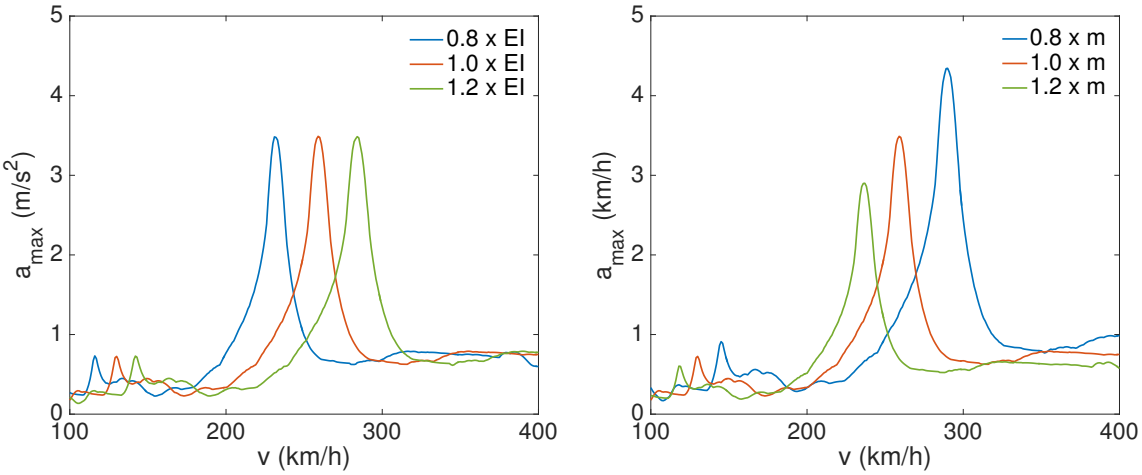

(a) Maximum acceleration, mass fixed

(b) Maximum acceleration, EI fixed

Figure 7.1 – Influence of the stiffness and the mass on the acceleration

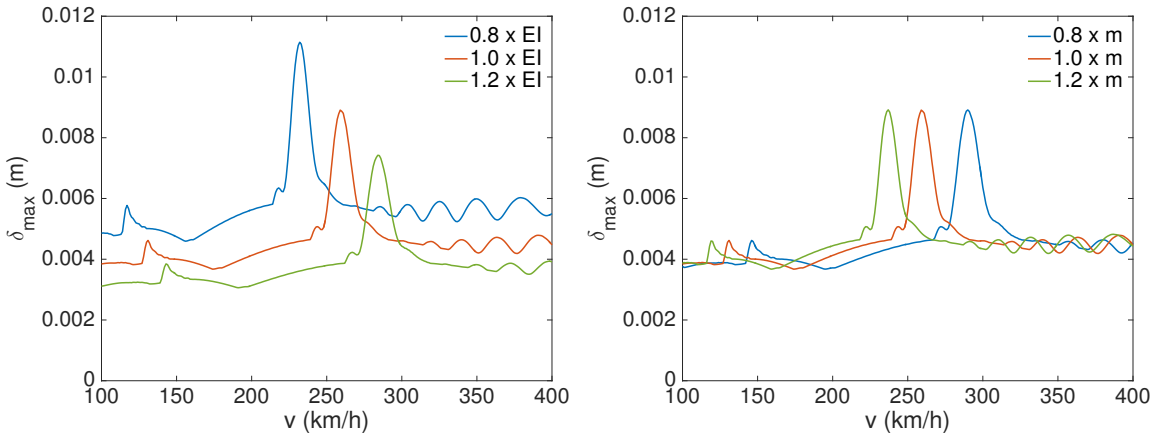

(a) Maximum deflection, mass fixed

(b) Maximum deflection, EI fixed

Figure 7.2 – Influence of the stiffness and the mass on the displacement

On one hand, in fig. 7.1 the acceleration is shown to be inversely proportional to the mass, whereas increasing the stiffness will just translate the acceleration towards higher speeds without changing the values. On the other hand, the displacement is inversely proportional to the stiffness and increasing the mass will translate the deflection towards lower speeds.

7.2 General remarks

For each span length, several thicknesses have been computed with an increment of 5 cm in order to find the optimum thickness fulfilling the dynamic requirements. It is interesting to understand how the maximum acceleration and the maximum deflection behave with changing thickness, which results in a modification of the mass but also the stiffness.

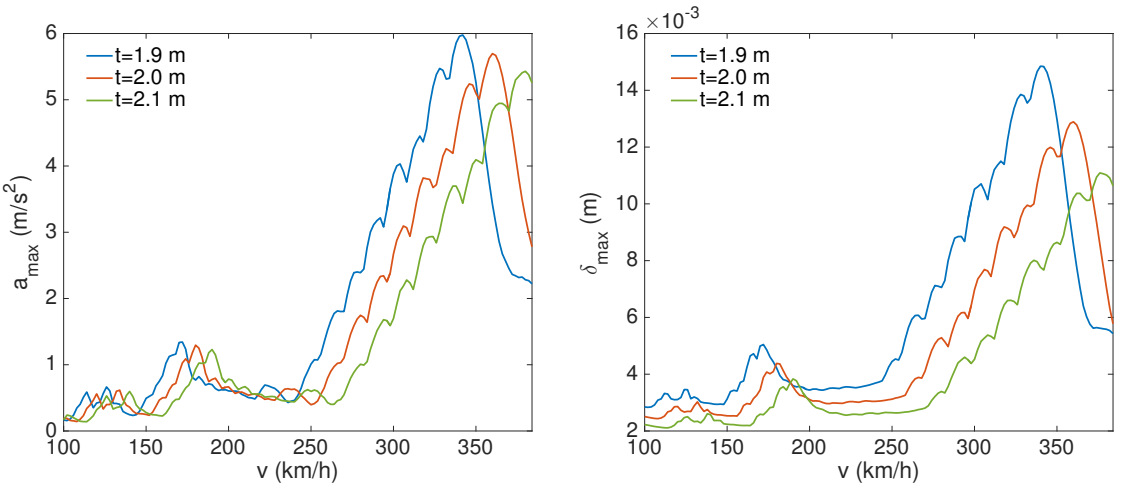

(a) Maximum acceleration

(b) Maximum deflection

Figure 7.3 – Influence of the thickness on the acceleration and the displacement - 1 span slab bridge, L_{span}=28.6 m

Analysing fig. 7.3a and fig. 7.3b, when the thickness is increased, maximum acceleration and deflection are simultaneously pushed to the right with a reduction of the magnitude.

Regarding the maximum acceleration, fig. 7.1a shows that when stiffness is increased (increasing the thickness), results are shifted to the right with the same amplitude, while when mass is increased results are shifted to the left with a reduced amplitude. The fact that the maximum acceleration is finally translated towards higher speeds can be explained when considering the first eigenfrequency of the bridge. Indeed, for a simply supported beam this value can be calculated analytically with eq. (7.1).

It can be seen that n_0 depends on the mass and stiffness. The mass is linearly proportional to the thickness of the deck whereas the stiffness varies with the thickness at the power of three. Thus, when the thickness is increased, n_0 is also increased with a magnitude reduced, as a result of combining the two effects presented in fig. 7.2.

For the deflection, the same phenomenon appears. However, the magnitude is even more reduced since the stiffness is governing the amplitude of the displacement (see fig. 7.2a).

7.3 Design diagrams

Design diagrams presented in fig. 7.4 and in fig. 7.5 have been obtained with 3D models described previously. The thickness t_{min} corresponds to the minimum value that fulfils the dynamic requirements regarding deflection and acceleration, like the first eigenfrequency n_0.

Diagrams have been obtained with an increment of 1.3 m for the span length and 5

centimetres for the thickness. For this reason, some span length thicknesses might be overestimated. Appendix C presents the envelopes for displacement and acceleration corresponding to the minimum thickness obtained for each case, and shows how close the results are to the limit, this can indicate how conservative the thickness is.

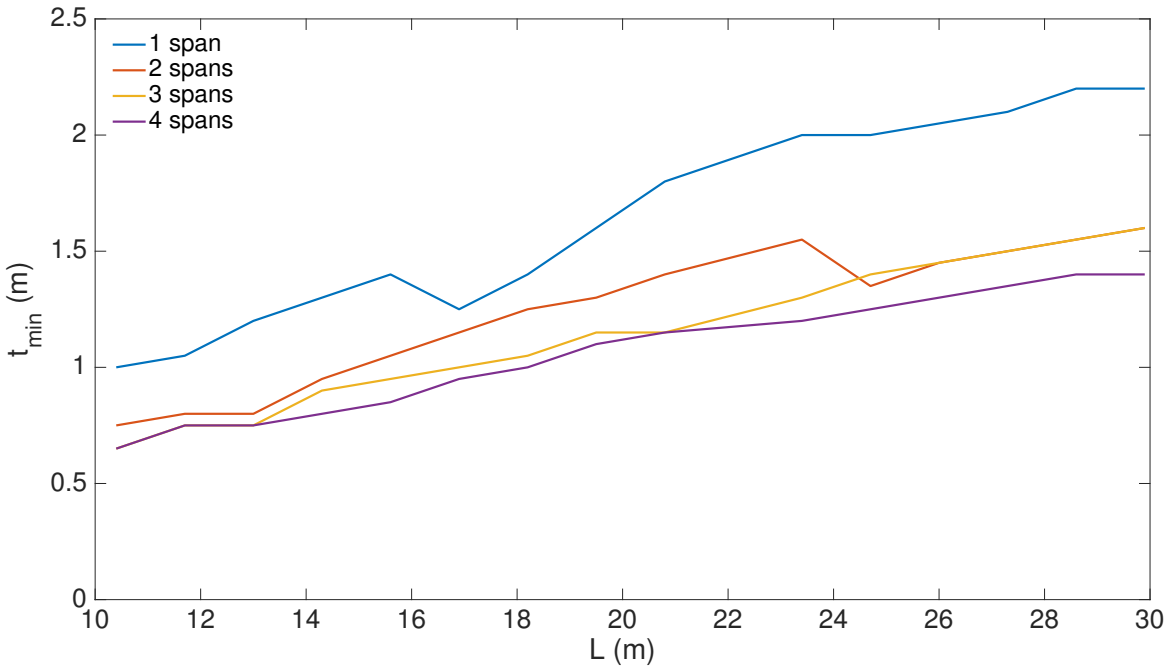

Figure 7.4 – Minimum thickness t_{min} for slab bridges

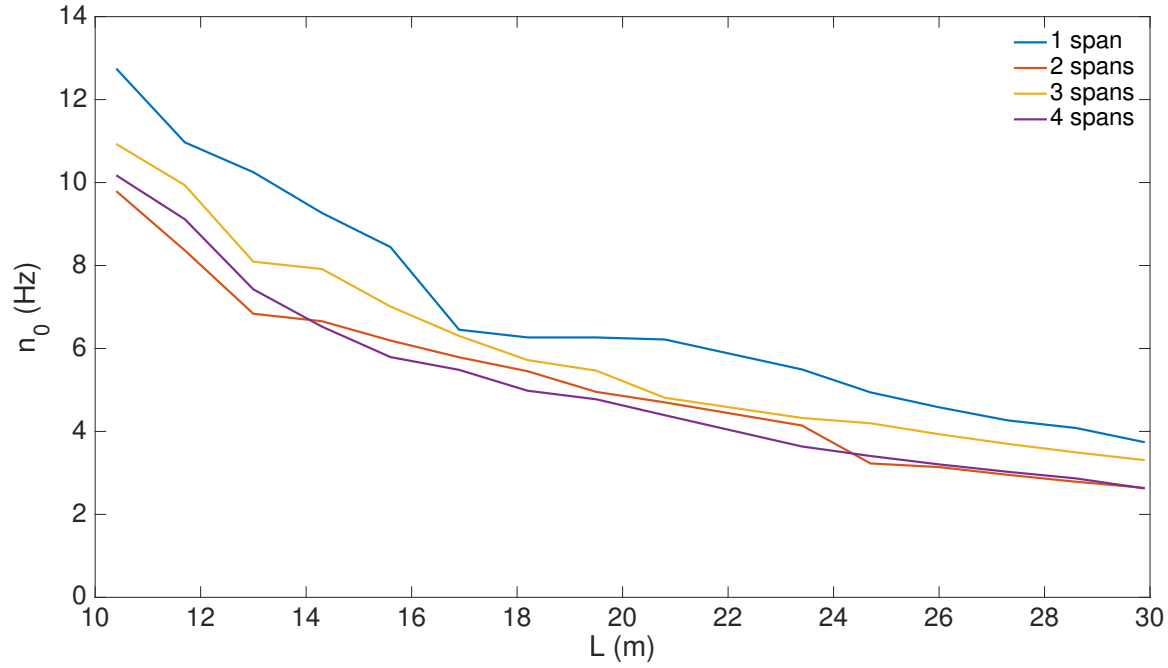

Figure 7.5 – Mimimum first eigenfrequency n_0 for slab bridges

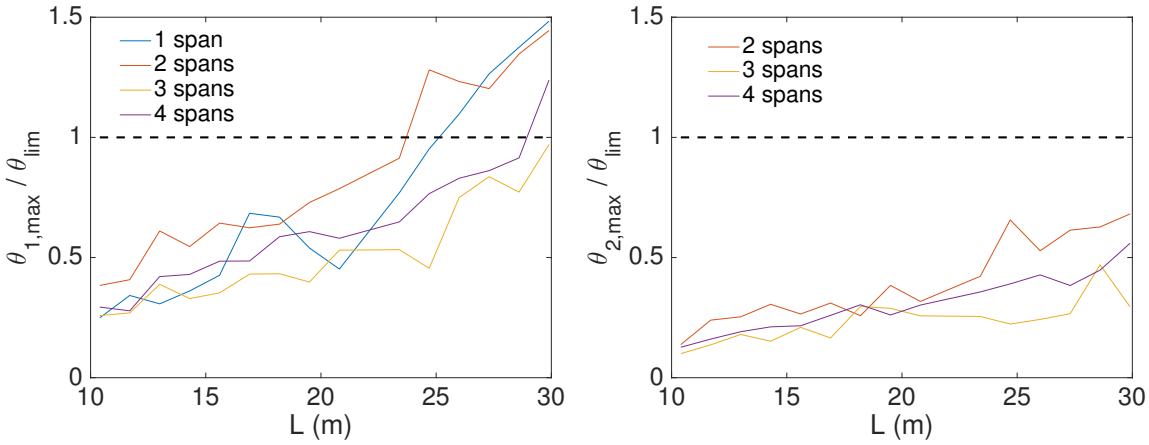

(a) Maximum rotation $\theta_{1,max}$

(b) Maximum rotation $\theta_{2,max}$

Figure 7.6 – Maximum rotations $\theta_{1,max}$ and $\theta_{2,max}$ over the supports

On one hand, fig. 7.4 shows that bridges with larger span lengths require more thickness to fulfil the regulation. In addition, the corresponding first vertical eigenfrequency decreases as the span length increases. On the other hand, bridges with less numbers of spans require more thickness. However, this order is not the same when considering n_0. Indeed, for three and four span bridges where the first and the last span are equal to 0.8xL, they appear to be relatively stiff in comparison with the same cases without considering the span length reduction.

Values for the maximum rotations $\theta_{1,max}$ and $\theta_{2,max}$ of the supports presented in fig. 7.6 are calculated in relation to the maximum rotation allowed (see fig. 3.4). However, since the diagrams are based on displacements and accelerations, the requirements are not always satisfied for $\theta_{1,max}$, whereas they are always fulfilled for $\theta_{2,max}$. Especially for one span and two span bridges with a large span length, demands regarding this parameter are not fulfilled.

Analysing the results, some span lengths are more interesting from a dynamic design point of view. For some points, increasing the span length will result in a decrease of the thickness. This phenomenon is studied for the particular case of two spans with a span length of 25 m.

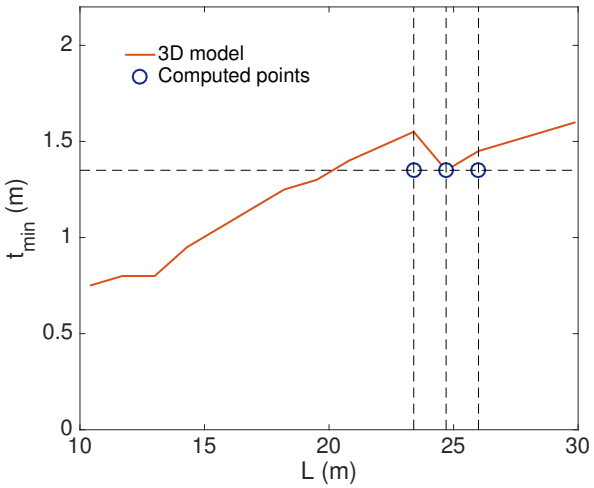

Figure 7.7 – Interesting points from a dynamic point of view

The minimum thickness obtained is equal to 1.35 m for the point located at the bump centre and corresponds to a span length of 24.7 m. To understand this behaviour of the results, the envelopes of the nearest span lengths for acceleration have been computed for the same thickness (i.e for 23.4 m and 26 m) as described in fig. 7.7.

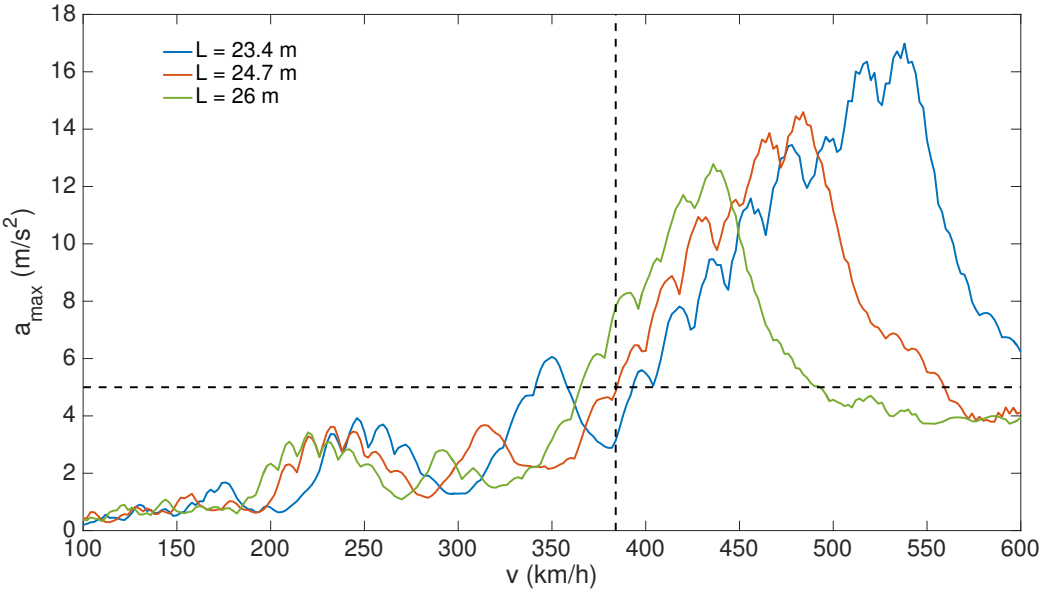

Figure 7.8 – Envelopes for the points presented in fig. 7.7

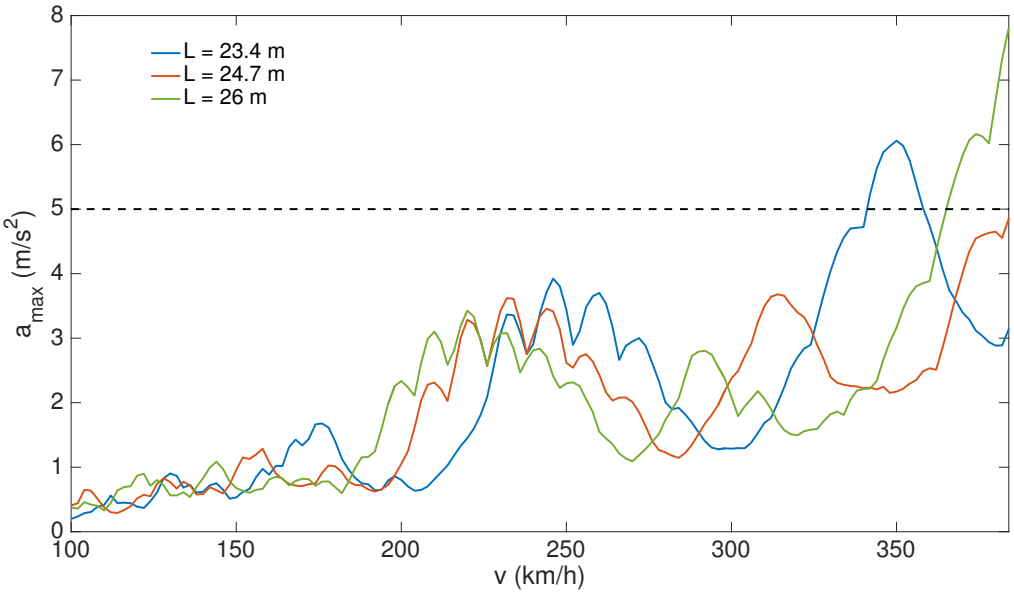

Figure 7.9 – Close-up of fig. 7.8 for a speed range from 100 km/h up to 384 km/h

For the considered thickness, when the span length is increased, the envelopes are shifted towards lower speeds with a magnitude which is also decreased. Thus, peaks corresponding to the resonance speeds and governing the dynamic design are also translated to the left of the diagram. Consequently, for the blue curve in fig. 7.8 corresponding to the first span length, the dynamic design is governed by the second bump. If the third span length is now considered (represented by the green curve), the design is determined by the third bump which is just entering into the interested speed range. In the end, the red curve is between these two bumps and corresponds to a transition between the design peaks. The magnitude of the acceleration is then lower, leading to a lower thickness.

7.4 Contribution of different modes of vibration

7.4.1 Process to separate each mode of vibration

In order to evaluate the contributions of different modes of vibration to the responses obtained for the passage of each HSLM-A train, an analysis has been carried out dissociating each mode shape. The contribution of each eigenfrequency has been considered by applying a band-pass filter to the FRF.

An example of this process is given in fig. 7.11, where from the initial matrix the first mode of vibration is separated by using the filter shown in fig. 7.10. The FRF obtained in fig. 7.11 corresponds to the first eigenfrequency.

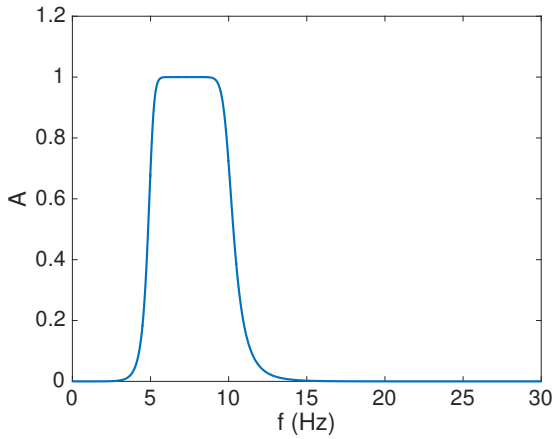

Figure 7.10 – Band-pass filter applied to dissociate each mode of vibration

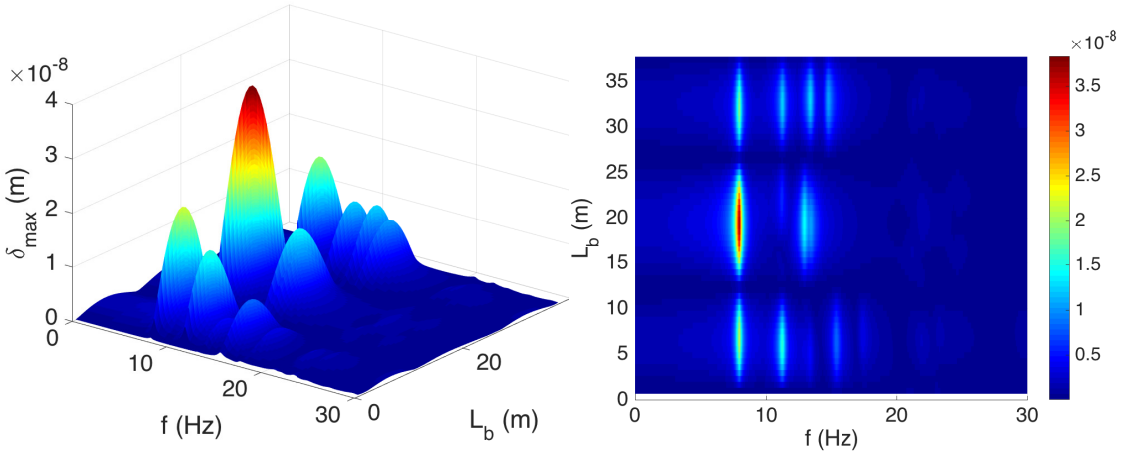

Figure 7.11 – Initial FRF without any filter

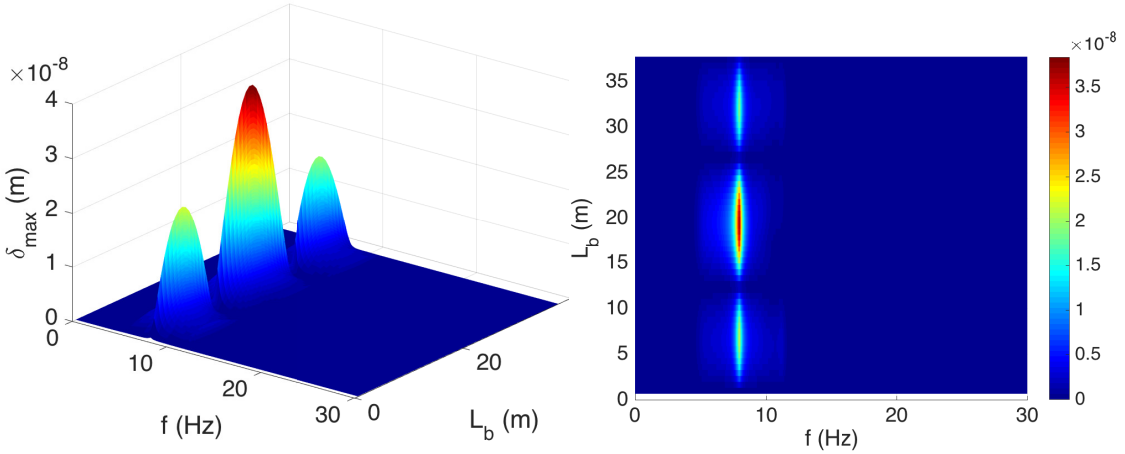

Figure 7.12 – FRF after applying a band-pass filter to separate the first mode of vibration

7.4.2 Contribution of the torsional modes

Afterwards, the HSLM analysis is run for each eigenmode, which allows the evaluation of the contribution of each mode. Appendix E presents the results obtained for different span lengths and number of spans. However, for some cases where the eigenfrequencies are close to each other, the contribution of the mode shape associated might be overestimated due to the band-pass filter applied.

For shorter span lengths, the contribution of torsional modes is more relevant than for larger span lengths.

7.5 Comparisons between 2D and 3D

7.5.1 Natural frequencies comparison

This section presents the results obtained during the frequency analysis performed in *Brigade*. The natural frequencies and corresponding modes of vibration of the bridge have been computed within the frequency range of up to 30 Hz.

The first vertical eigenfrequency (n_0) has been compared with the results from the 2D models. For each number of spans, different span lengths have been compared: L=10 m, L=15 m, L=20 m, L=25 m and L=30 m. The first natural frequency of the 2D model, defined in chapter 2, can be obtained using eq. (7.1).

$$n_0 = \frac{\pi}{2L^2}\sqrt{\frac{EI}{m}} \tag{7.1}$$

In this equation, though, the reduction of span length applied in the outer spans for the cases with 3 and 4 spans is not considered. In order to obtain the corresponding values, a coefficient is applied for those cases. The value obtained is then $n_{0,3spans} \approx 1.2656\, n_0$ and $n_{0,4spans} \approx 1.1565\, n_0$, for 3 and 4 spans respectively. table 7.1 presents the results for the first natural frequency ($n_{0,2D}$) obtained for the 2D models as well as the thickness (h) and material properties (m and EI) used.

Table 7.1 – 2D model properties used for different span length for each number of spans

1 span					
L (m)	**10**	**15**	**20**	**25**	**30**
m (ton/m)	23,37	29,79	35,28	41,62	44,99
EI (GNm^2)	16,28	45,61	89,39	166,31	220,67
h (m)	0,80	1,16	1,48	1,84	2,03
$n_{0,2D}$ (Hz)	13,11	8,64	6,25	5,02	3,87

(a) 1 span

2 spans					
L (m)	**10**	**15**	**20**	**25**	**30**
m (ton/m)	19,76	24,83	29,79	31,04	33,78
EI (GNm^2)	7,92	21,19	45,61	53,93	75,51
h (m)	0,59	0,88	1,16	1,24	1,39
$n_{0,2D}$ (Hz)	9,94	6,45	4,86	3,31	2,61

(b) 2 spans

3 spans					
L (m)	**10**	**15**	**20**	**25**	**30**
m (ton/m)	18,97	22,96	26,27	30,20	33,78
EI (GNm^2)	6,71	15,07	27,01	48,23	75,51
h (m)	0,55	0,77	0,96	1,19	1,39
$n_{0,2D}$ (Hz)	11,82	7,16	5,04	4,02	3,30

(c) 3 spans

4 spans					
L (m)	**10**	**15**	**20**	**25**	**30**
m (ton/m)	18,88	22,56	26,27	28,23	30,83
EI (GNm^2)	6,58	13,96	27,01	36,53	52,45
h (m)	0,54	0,75	0,96	1,08	1,22
$n_{0,2D}$ (Hz)	10,72	6,35	4,60	3,31	2,63

(d) 4 spans

For the cases presented, a 3D frequency analysis has been performed. table 7.2 reports the value for first natural frequency obtained with the 2D and 3D models ($n_{0,2D}$ and $n_{0,3D}$ respectively) and the eigenfrequency corresponding to the first torsional eigenmode (n_T), obtained with the 3D analysis.

Table 7.2 – Eigen-frequencies for different span length for each number of spans

1 span					
L (m)	10	15	20	25	30
$n_{0,2D}$ (Hz)	13,11	8,64	6,25	5,02	3,87
$n_{0,3D}$ (Hz)	10,84	7,54	5,50	4,43	3,42
n_T (Hz)	13,40	14,03	13,87	13,79	13,17

(a) 1 span

2 spans					
L (m)	10	15	20	25	30
$n_{0,2D}$ (Hz)	9,94	6,45	4,86	3,31	2,61
$n_{0,3D}$ (Hz)	8,55	5,64	4,19	2,88	2,26
n_T (Hz)	10,59	10,71	10,83	9,35	8,89

(b) 2 spans

3 spans					
L (m)	10	15	20	25	30
$n_{0,2D}$ (Hz)	11,82	7,16	5,04	4,02	3,30
$n_{0,3D}$ (Hz)	10,31	6,26	4,35	3,46	2,83
n_T (Hz)	10,84	10,40	9,47	9,46	9,32

(c) 3 spans

4 spans					
L (m)	10	15	20	25	30
$n_{0,2D}$ (Hz)	10,72	6,35	4,60	3,31	2,63
$n_{0,3D}$ (Hz)	9,56	5,61	3,97	2,86	2,26
n_T (Hz)	10,33	9,88	9,21	8,28	7,89

(d) 4 spans

As seen in table 7.2, for all the span lengths and number of spans $n_{0,3D} < n_{0,2D}$. This is due to the fact that 3D models are less stiff than 2D models. It can also be noticed that the first eigenmode is never a torsional mode, since the relation $n_T > n_{0,3D}$ is fulfilled for all the cases. Appendix D shows different plots of the modes of vibration corresponding to these natural frequencies presented.

In EN 1991-2, Figure 6.9 presents the requirements to determine if the torsional effects should be considered in the analysis, depending on the value of n_T. If $n_T < 1.2n_0$, then the requirements should be considered. For these studied cases, contributions of torsional modes are not so relevant except for shorter span lengths, where $n_T > n_{0,3D}$.

The loss of stiffness is due to the shear-lag effects and bending moment in the transversal direction. These effects cannot be obtained if the analysis is carried out using 2D models. The 2D models assume a beam theory which is no longer fulfilled when using 3D shell models. These shear-lag effects reduce the section resistance and the general stiffness of the structure. fig. 7.13 shows an example of the 2 spans bridge when the bending moment in the transversal direction takes place.

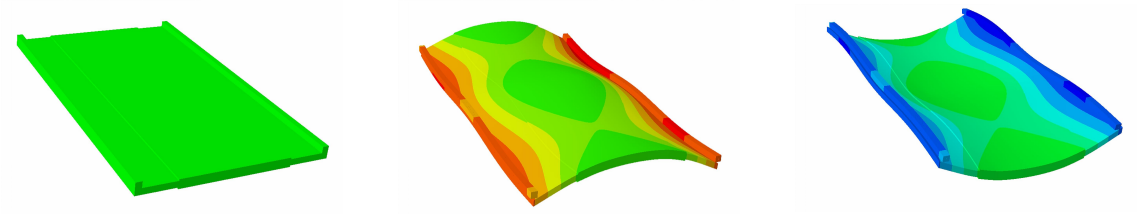

Figure 7.13 – Bending moment in the transversal direction

7.5.2 Comparison of results

In this section there is a comparison between the results for the shell models computed and the 2D beam models. This comparison is based on the design diagrams presented, comparing the minimum thickness to fulfil the regulation and the first vertical eigenfrequency.

fig. 7.14 shows the comparison for each number of spans, where the thickness is plotted for each span length.

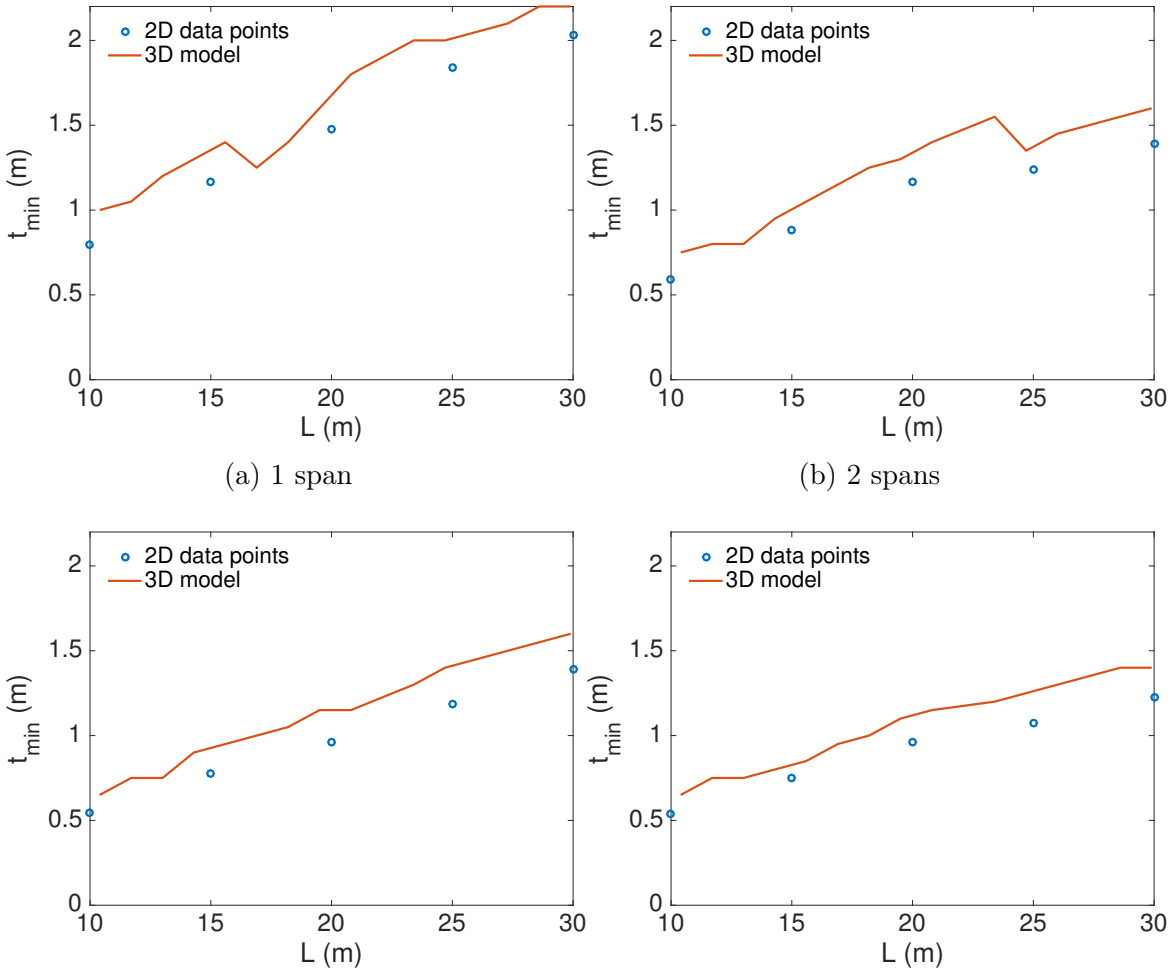

(a) 1 span

(b) 2 spans

(c) 3 spans

(d) 4 spans

Figure 7.14 – Minimum thickness t_{min} for slab bridges

From these figures, the analysis performed with the shell models results in more thickness for all the cases than the value obtained from the 2D beam models. Although for the 2D models not all the cases are plotted, a clear tendency on the results is noticed. For the comparable points, the difference on the value with respect to the shell models is similar for each span length and number of spans.

fig. 7.15 illustrates the comparison of the first vertical natural frequency (n_0) for each number of spans.

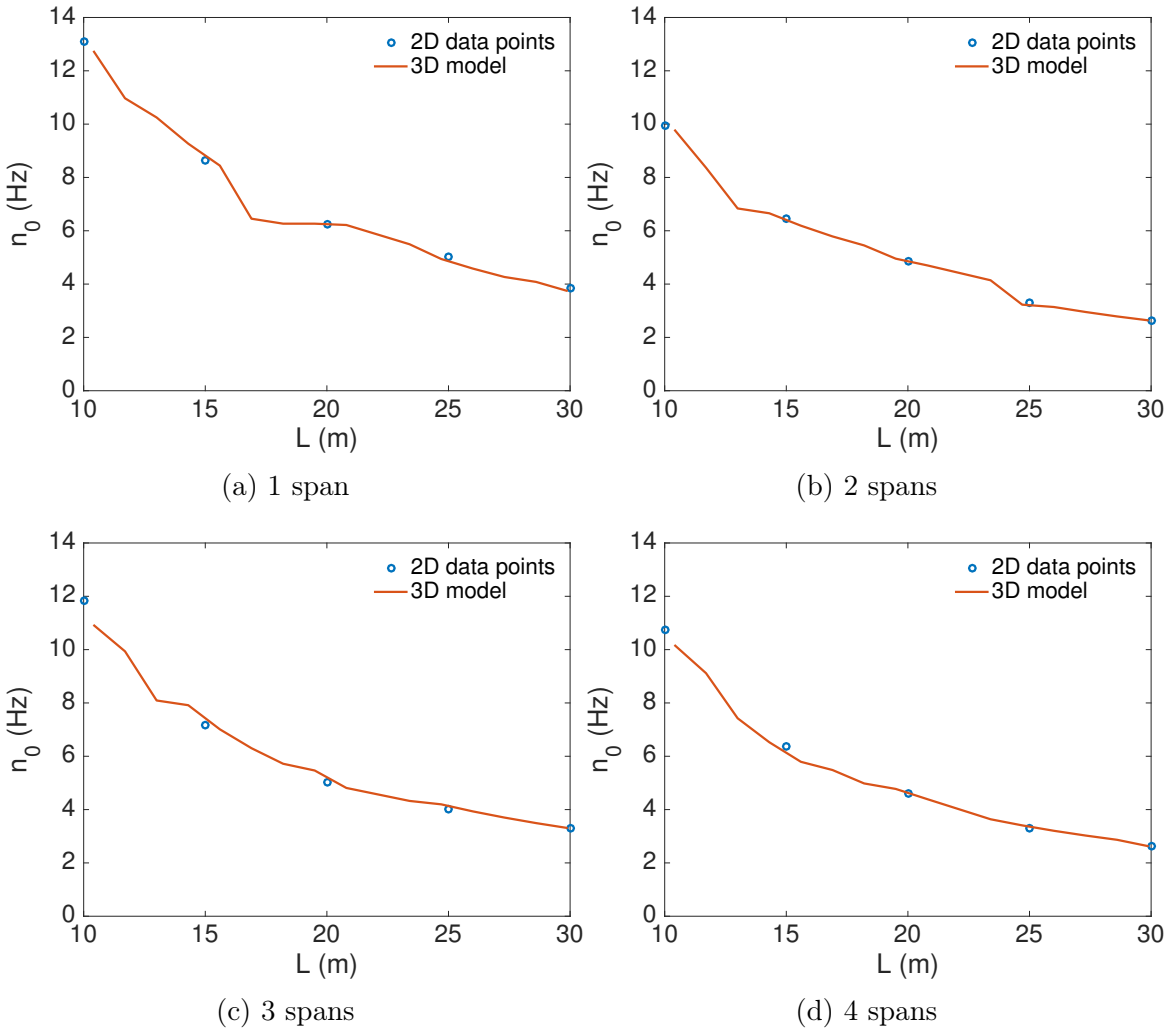

(a) 1 span

(b) 2 spans

(c) 3 spans

(d) 4 spans

Figure 7.15 – First eigenfrequency n_0 for slab bridges

Analysing the results, the values obtained from the two different models are pretty close. Although this natural frequency is computed for cases with different thickness, for each span length and number of spans, the results are similar.

The comparison between the two models on the first vertical eigenfrequency can be explained with the analyses previously performed. On the one hand, when using shell models, there is the stiffness reduction due to the shear-lag effects, which results in a decrease of n_0. On the other hand, more thickness with the shell models is needed in order to fulfil the regulation, which increases the value for n_0. These two factors seem to compensate each other and lead to similar values between 2D and 3D models.

Chapter 8

Conclusions and further research

8.1 Conclusions

The frequency analysis method implemented in this thesis provides a fast way to compute several load systems at different speeds. Thus, this methodology is very convenient for a dynamic parametric study compared to a time domain solution. In addition, this approach can easily be implemented in any programming language. Moreover, in a real design situation the interaction between the soil and the bridge needs to be considered. Some frequency dependent parameters should then be included in the analysis like the damping ratio or impedance functions, that motivate the implementation of this method.

This study shows that 3D models require more thickness compared to 2D beam models. This difference can mainly be explained by two factors. On one hand, contribution of torsional modes affects the total response of a bridge, and on the other hand shear-lag effects play a part in reducing the bending resisting section which leads to larger displacements.

Finally, the contribution of torsional modes varies with the span length. For short span lengths, a 3D dynamic analysis should be performed whereas for large span lengths, 3D effects are less relevant. In any case, shear-lag should be considered.

8.2 Further research

After analysing the results, the computing time saved is reduced when the total length of the bridge is increased. Indeed, when the length of the bridge is increased with 100 meters, the method is 5 times slower. Following the tendency obtained, a study using larger span lengths should be performed verifying that the method is still faster and convenient.

Shear-lag effects should be considered because they have a higher contribution in the difference between the beam and the shell models. Comparing the first vertical

eigenfrequency of the different bridges, it seems that a relation exists between the two different models, thus design diagrams provided by beam models could be used. Further research should be performed to evaluate how they can be considered by defining the correct value of the natural frequency using a shell model, and later use it in the diagrams.

The study that has been performed has been focused on slab bridges analysis, providing a design diagram for the minimum thickness needed to fulfil the criterion of vertical displacement and acceleration for span lengths up to 30 meters. For bridges with larger span lengths this section is no longer convenient due to the thickness needed, and other sections should be taken instead. The study performed in this project should be carried out analysing different sections like beam bridges, to find out if the tendency on the relation with the beam models is the same.

Bibliography

CEN. Eurocode 1: Actions on structures - Part 2: Traffic loads on bridges, 2003.

L. Frýba. *Vibration of solids and structures under moving loads*. Thomas Telford, London, 3. ed. edition, 1999. ISBN 0727727419.

L. Frýba. A rough assessment of railway bridges for high speed trains. *Engineering Structures*, 23(5):548 – 556, 2001. ISSN 0141-0296. doi: http://dx.doi.org/10.1016/S0141-0296(00)00057-2.

HP Gavin. The three-moment equation for continuous beam. Technical report, Technical Report Department of Civil and Environmental Engineering-Duke University, 2009.

Hibbitt, Karlsson, and Sorensen. *ABAQUS/Standard User's Manual*. Pawtucket, 6.6 edition, 2006.

Raid Karoumi. *Course material KTH (AF2011). Structural Dynamics for civil engineers 2008*. Kungliga Tekniska högskolan. Institutionen för byggvetenskap, Stockholm, 2008.

AN Krylov. Mathematical collection of papers of the academy of sciences, vol. 61. *Matematischeskii sbornik Akademii Nauk). Peterburg, Russia.[Transl. Kriloff, AN 1905 Über die erzwungenen Schwingungen von gleichformigen elastischen Staben. Mathematische Annal. 61, 211–234.(doi: 10.1007/BF01457563)]*, 1905.

Joakim Kylén. 2d-model of a portal frame railway bridge for dynamic analysis. 2010.

Jean Lemaitre, Jean-Louis Chaboche, Ahmed Benallal, and Rodrigue Desmorat. *Mécanique des matériaux solides-3eme édition*. Dunod, 2009.

Eugenio Oñate. *Cálculo de estructuras por el método de elementos finitos: análisis elástico lineal*. Centro Internacional de Métodos Numéricos en Ingeniería, 1992.

Christoffer Svedholm and Andreas Andersson. Designdiagram för förenklad dynamisk kontroll av järnvägsbroar. 2016.

Trafikverket. Teknisk systemstandard för höghastighetsbanor, 2014.

Appendix A

Static design calculations

A.1 Materials

A.1.1 Concrete

The concrete used for the static design has the following properties:

- Density : $\rho = 2500kg/m^3$
- Young modulus : $E_c = 34GPa$
- Compression strength : $f_{ck} = 35MPa$
- Tension strength : $f_{tm} = 3.2MPa$

A.1.2 Steel

Reinforcements are made of steel for which the horizontal top branch has no limit in the stress strain relation diagram.

- Young modulus : $E_c = 200GPa$
- Strength : $f_{yk} = 500MPa$

A.2 Critical sections

For each geometry, a general script has been implemented with the help of Matlab to find the critical section, and particularly to determine the internal forces due to the passage of a train.

The self-weight effects are determined with the three moment equation in Matlab, that provides bending moment diagrams and shear diagrams, with the maximum and the minimum value. Here is an example for a 4 spans bridge, with a span length of 20 meters for the main span:

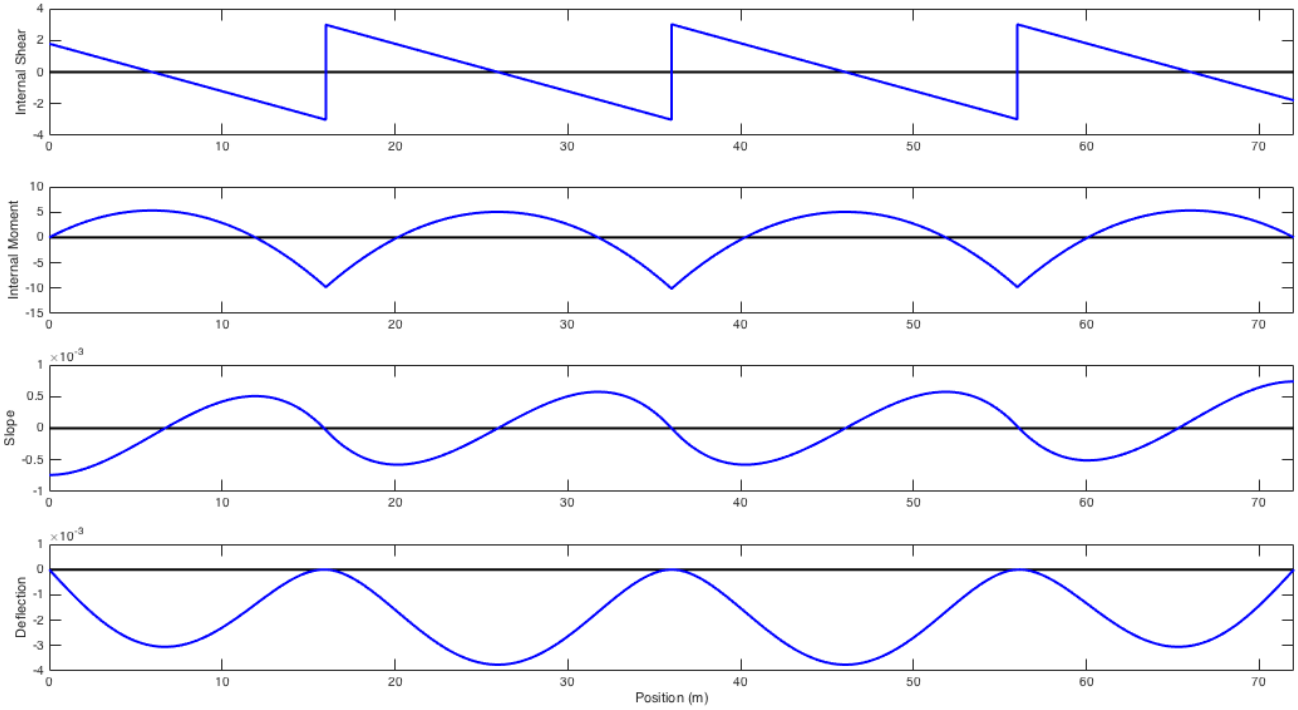

Figure A.1 – Diagrams obtained in Matlab for a 4 span bridge ($L_{span} = 20m,\ h = 1\ m$)

To simulate a moving load representing the LM71 and crossing the bridge, another software has been used. Indeed, Robot Structural Analysis is more convenient to simulate a train passage, and the results can easily be exported. Thus, an increment of 0.65 m is set to determine the forces in the entire deck.

A.3 Static design

A.3.1 Assumptions

The static design is performed for the sections where the bending moment is maximum; that is, at the midspan for 1 span bridges and over the supports for 2 span bridges and more.

The section of the deck is assimilated to a rectangular section with a width b=7m.

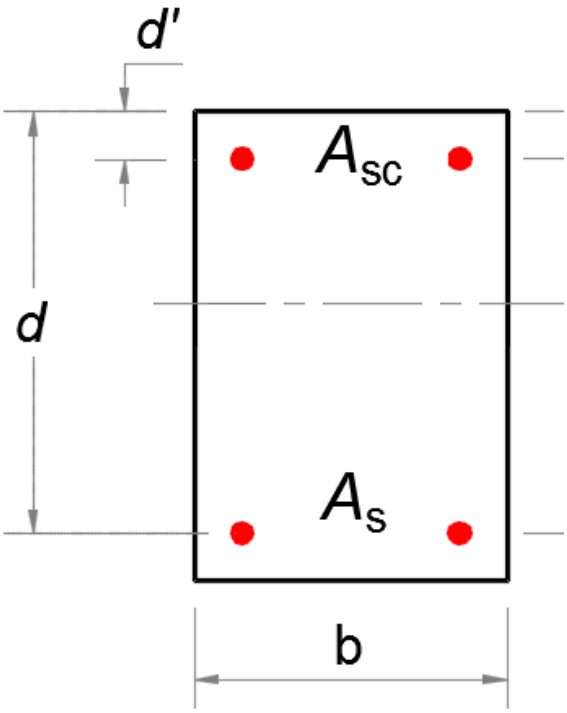

Figure A.2 – Rectangular reinforced concrete section

Asc represents the top reinforcements, and As represents the bottom steel section. Additionally, the distance d has been taken equal to $d = 0.9.h$ and $d' = 0.1.h$ for the design.

The section is then subjected to a bending moment M_{Ed} and to a compressive force N_{Ed}, what means that several cases have to be considered.

A.3.2 Ultimate Limit State

Section entirely compressed

The section is entirely compressed when:

$$e_0 = \frac{M_{Ed}}{N_{Ed}} \in \left[\frac{h}{2} - d; \frac{h}{2} - d'\right] \tag{A.1}$$

Or

$$(d - d')N_{Ed} - M_{As} > (0.337 - \frac{0.81.d'}{h})bh^2 f_{cd} \tag{A.2}$$

With,

$$M_{As} = N_{Ed} + N_{Ed}(d - \frac{h}{2}) \tag{A.3}$$

Then χ has to be calculated as follow:

$$\chi = \frac{0.5 - \frac{d'}{h} - \frac{N_{Ed}(d-d') - M_{As}}{bh^2 f_{cd}}}{\frac{6}{7} - \frac{d'}{h}} \tag{A.4}$$

Now As and Asc are determined with the following expressions:

$$Asc = \frac{M_{As} - M_{c,As}}{f_{yd}(d - d')} \tag{A.5}$$

$$As = \frac{N_{Ed} - bhf_{cd}}{f_{yd}} - Asc \tag{A.6}$$

With,

$$M_{c,As} = bhf_{cd}(d - \frac{h}{2}) \tag{A.7}$$

Section partially compressed

This case appears when $e_0 = \frac{M_{Ed}}{N_{Ed}} \notin \left[\frac{h}{2} - d; \frac{h}{2} - d'\right]$, or when $(d - d')N_{Ed} - M_{As} < (0.337 - \frac{0.81.d'}{h})bh^2 f_{cd}$.

The reinforcements have to be calculated for a section only subjected to a bending moment, and then the normal force will be taken into account.

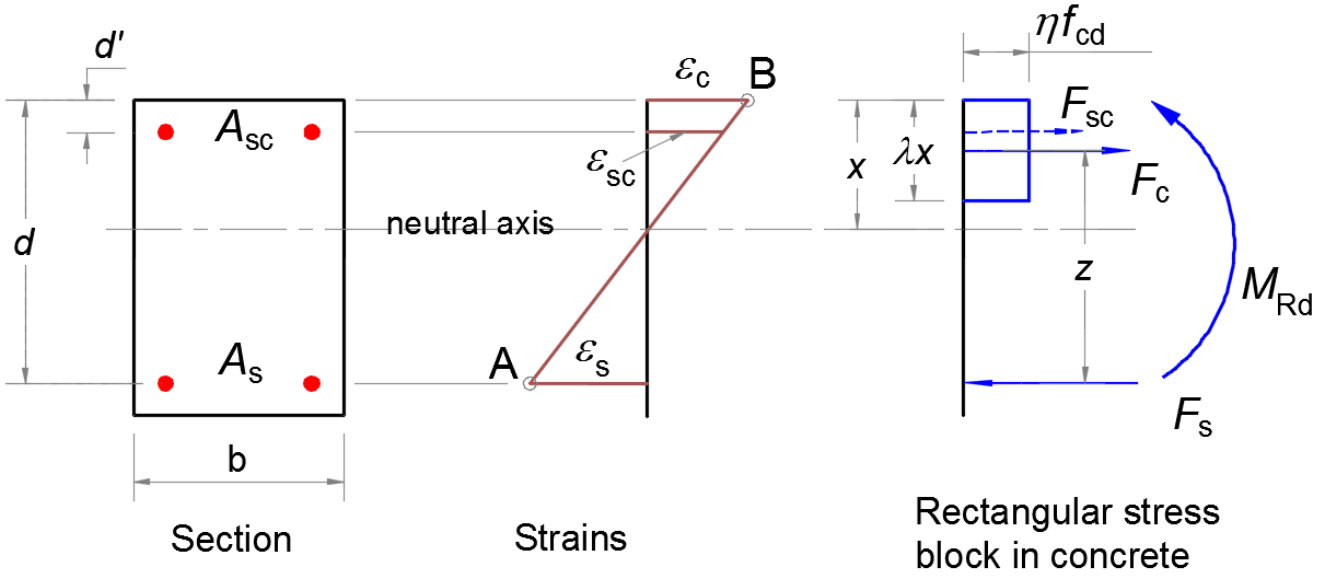

Figure A.3 – Rectangular section in bending at the ULS

$$\mu = \frac{M_{Ed}}{bd^2 f_{cd}} \leq 0.48 \tag{A.8}$$

The position of the neutral axis can then ba calculated:

$$x = 1.25 \cdot (1 - \sqrt{1 - 2\mu}) \tag{A.9}$$

And,

$$As = \frac{0.8dbf_{cd}x}{f_{yd}} \tag{A.10}$$

A.3.3 Serviceability Limit State

Section entirely compressed

As previously, the section is entirely compressed if e, calculated either under rare combination or quasi-permanent combination, satisfy the condition $e \in \left[\frac{-h}{6}; \frac{h}{6}\right]$.

In this case, the center of gravity of the homogenized concrete section is different from the center of gravity of the concrete section, then the homogenized section is calculated:

$$Bh = bh + n(As + Asc) \tag{A.11}$$

Thus, the distance v_s and v_i respectively the distance from the top of the section to the center of gravity of the homogenized section, and from the bottom of the section to this point, are defined:

$$v_s = \frac{\frac{bh^2}{2} + n.Asc.d' + n.As.d}{Bh} \tag{A.12}$$

$$v_i = h - v_s \tag{A.13}$$

The inertia has also to be calculated in order to determine the stresses in the section:

$$I_h = \frac{bv_s^3}{3} + \frac{bv_i^3}{3} + n.Asc.(v_s - d')^2 + n.As.(d - v_i)^2 \tag{A.14}$$

What leads to:

$$\sigma_{c,max} = \frac{N_{Ed}}{Bh} + \frac{M_{Ed}}{Ih} v_s \tag{A.15}$$

$$\sigma_{c,min} = \frac{N_{Ed}}{Bh} - \frac{M_{Ed}}{Ih} v_i \tag{A.16}$$

Section partially compressed

On the contrary, this case appears when $e \notin \left[\frac{-h}{6}; \frac{h}{6}\right]$ (under rare or quasi-permanent loading). In a first time, the distance x_p between the neutral axis and the center of pressure has to be calculated, in order to calculate the stress in the section by solving this equation:

$$x_p^3 + p.x_p + q = 0 \tag{A.17}$$

Where,

$$p = -3c_1^2 + (d - c_1)\frac{6.n.As}{b} - (c_1 - d')\frac{6.n.As'}{b} \tag{A.18}$$

$$q = -2c_1^2 - (d - c_1)^2.\frac{6.n.As}{b} - (c_1 - d')^2.\frac{6.n.As'}{b} \tag{A.19}$$

And $c_1 = x - x_p = d - e_{As}$

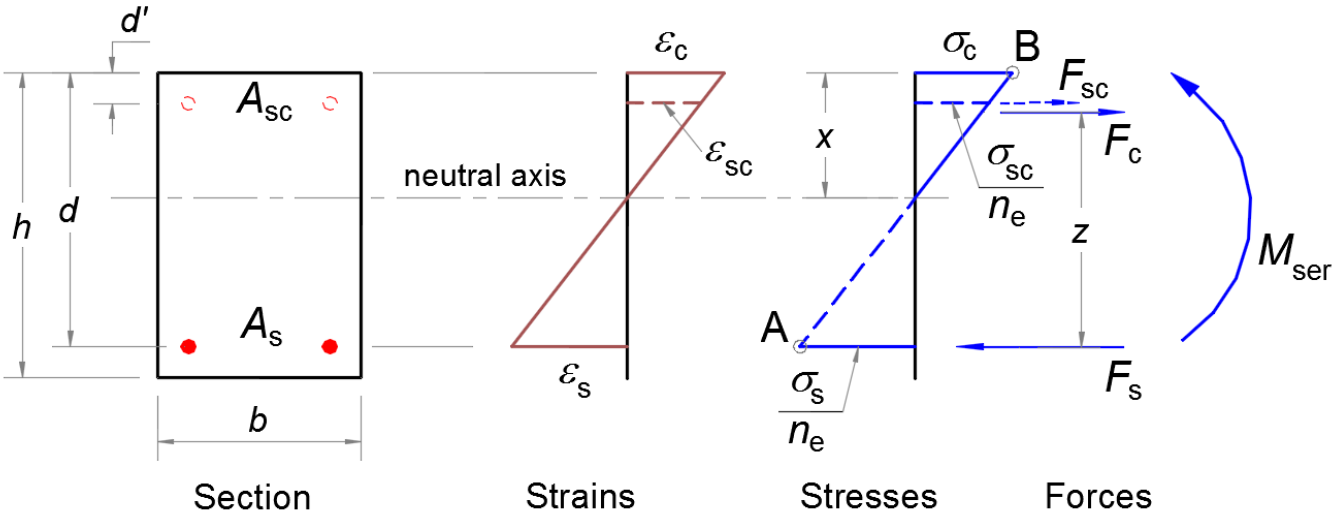

Figure A.4 – Rectangular section in bending at the SLS

Finally, σ_c and σ_s are obtained:

$$\sigma_c = \frac{N_{Ed}.x_p}{I_{hr}}.x \tag{A.20}$$

$$\sigma_s = n.\frac{N_{Ed}.x_p}{I_{hr}}.(d - x) \tag{A.21}$$

Appendix B

Computing time comparison between time and frequency analysis

				COMPUTING TIME					
				TIME APPROACH		FREQUENCY APPROACH			COMPARISON
L (m)	Spans	Total length (m)	Total time (s)	BRIGADE - 1 speed (s)	TOTAL (h)	BRIGADE (s)	MATLAB (s)	TOTAL (h)	Relationship (N times faster)
10,4	1	10,4	9,2	12,4	4,93	7,3	350,6	0,10	49,54
	2	20,8	9,4	13,6	5,40	26,7	678,4	0,20	27,58
	3	27,0	9,5	14,3	5,68	41,1	820,9	0,24	23,72
	4	37,4	9,6	16,1	6,40	72,3	1028,9	0,31	20,91
29,9	1	29,9	9,5	15,1	6,00	73,8	970,6	0,29	20,67
	2	59,8	10,0	20,9	8,30	327	1999,9	0,65	12,84
	3	77,7	10,2	23,5	9,33	575,4	2508,2	0,86	10,90
	4	107,6	10,7	31,1	12,35	1277,7	3643,9	1,37	9,04

Figure B.1 – Computing time comparison detailed

Appendix C

Envelopes for maximum displacement and acceleration

C.1 Results for 1 span

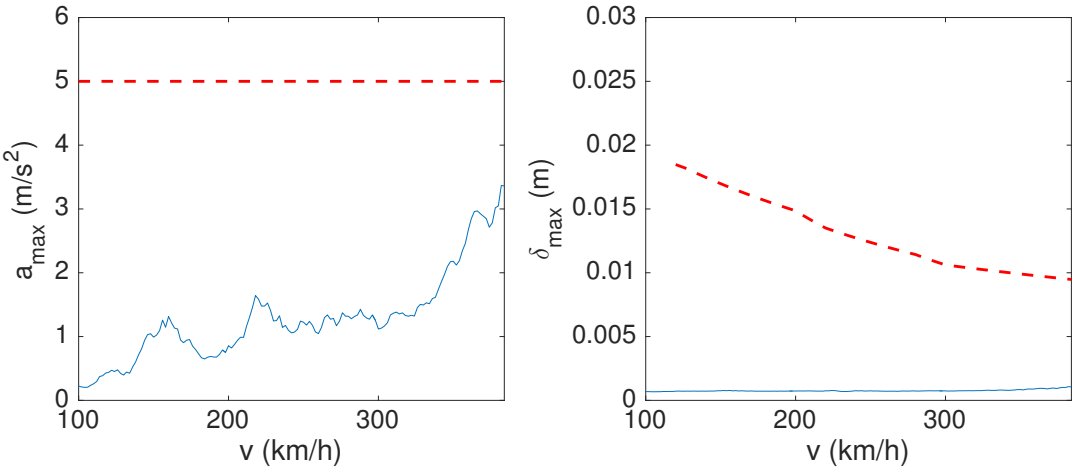

Figure C.1 – 1 span - L=10,4 m

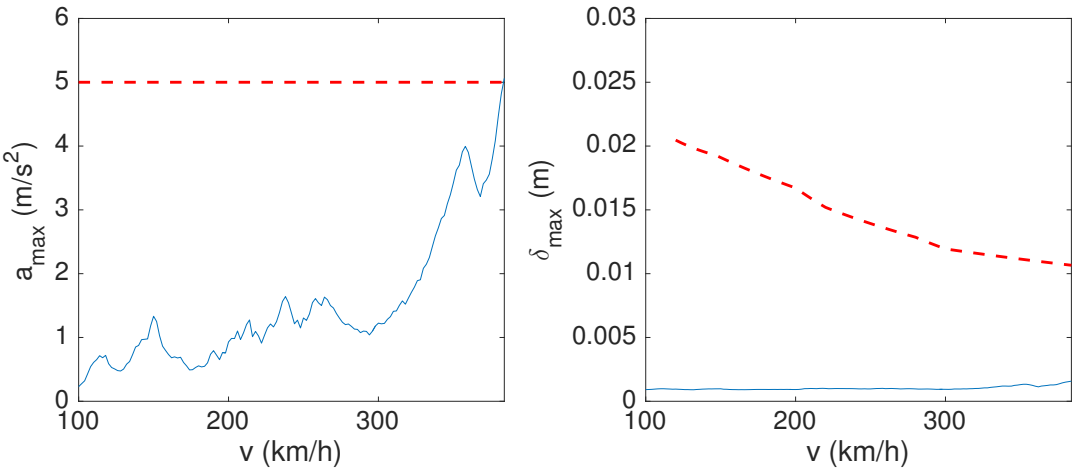

Figure C.2 – 1 span - L=11,7 m

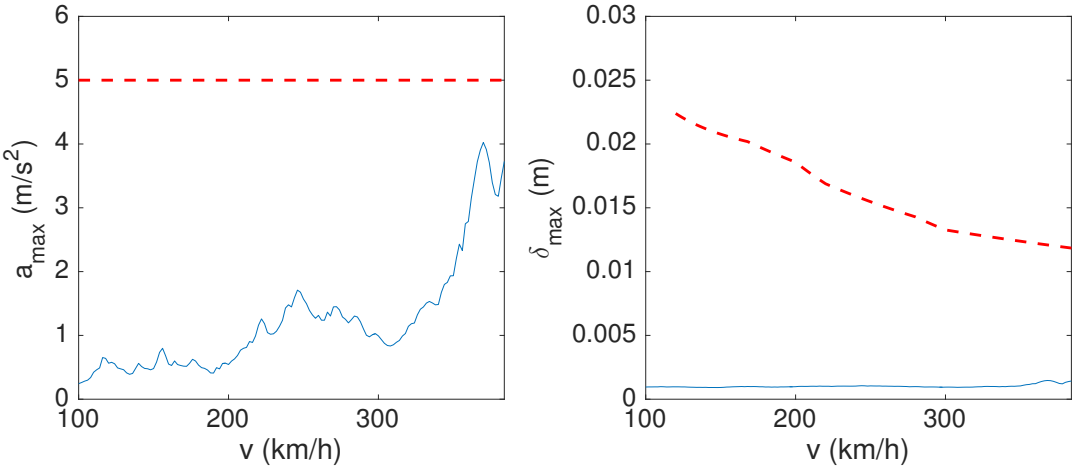

Figure C.3 – 1 span - L=13 m

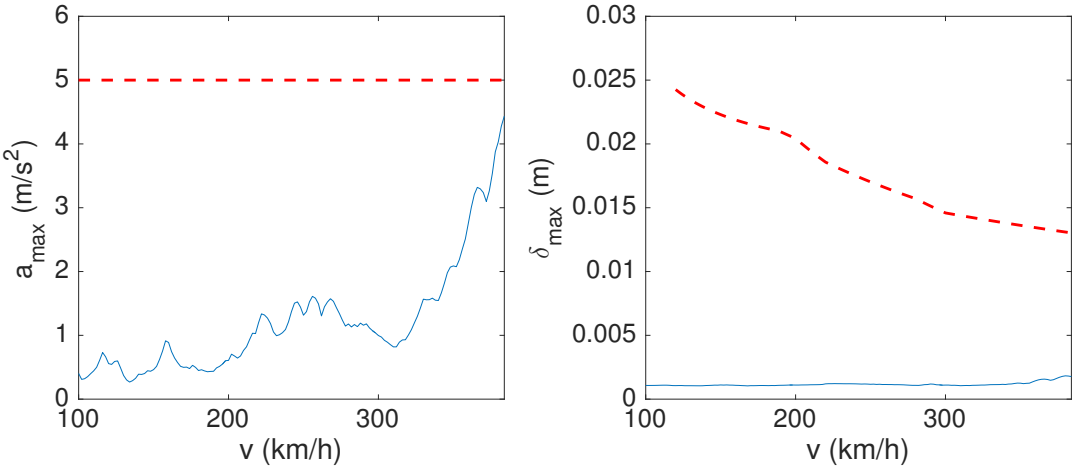

Figure C.4 – 1 span - L=14,3 m

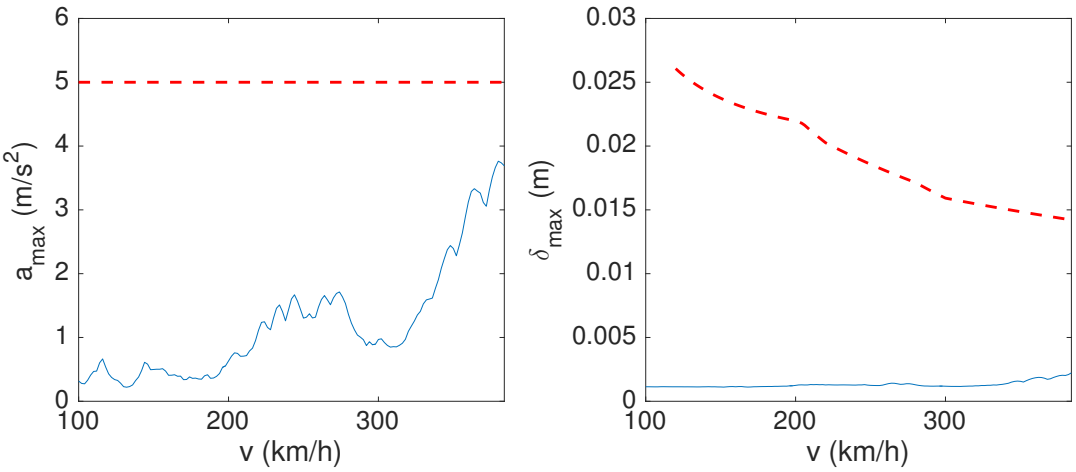

Figure C.5 – 1 span - L=15,6 m

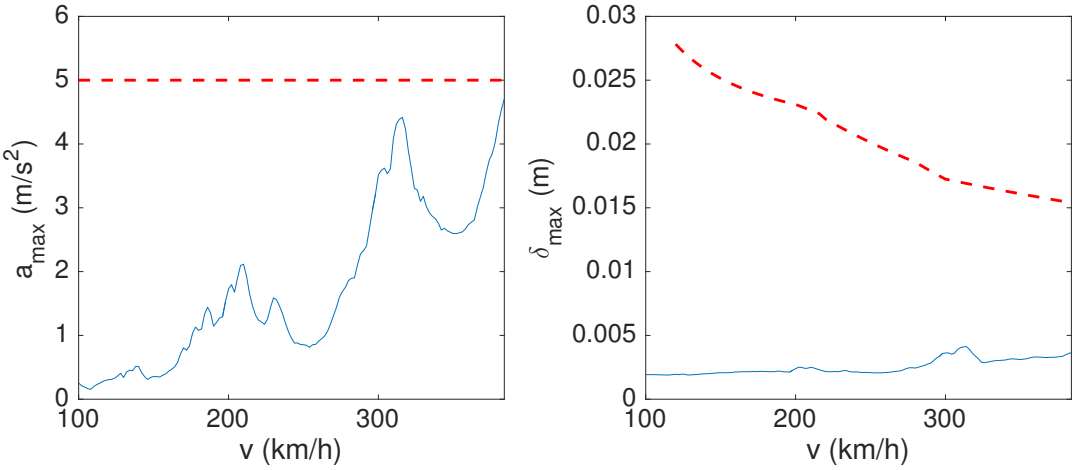

Figure C.6 – 1 span - L=16,9 m

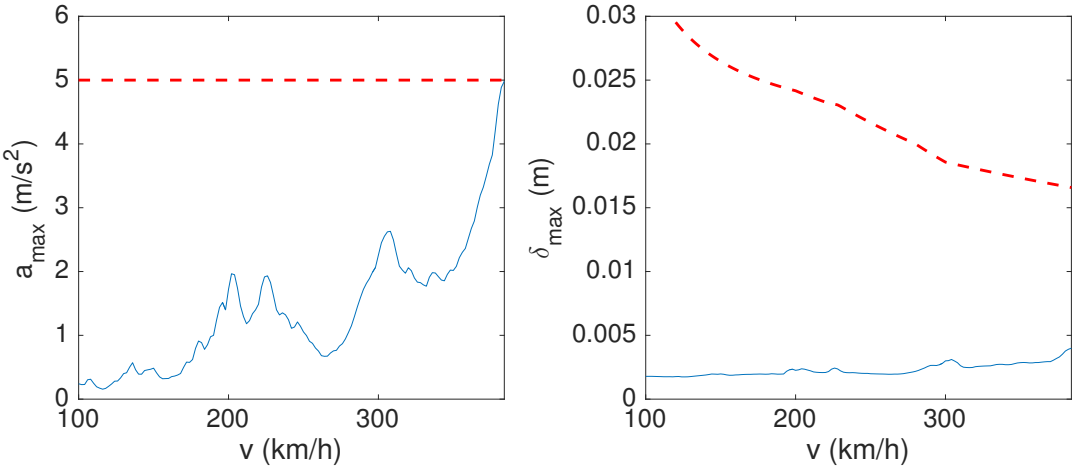

Figure C.7 – 1 span - L=18,2 m

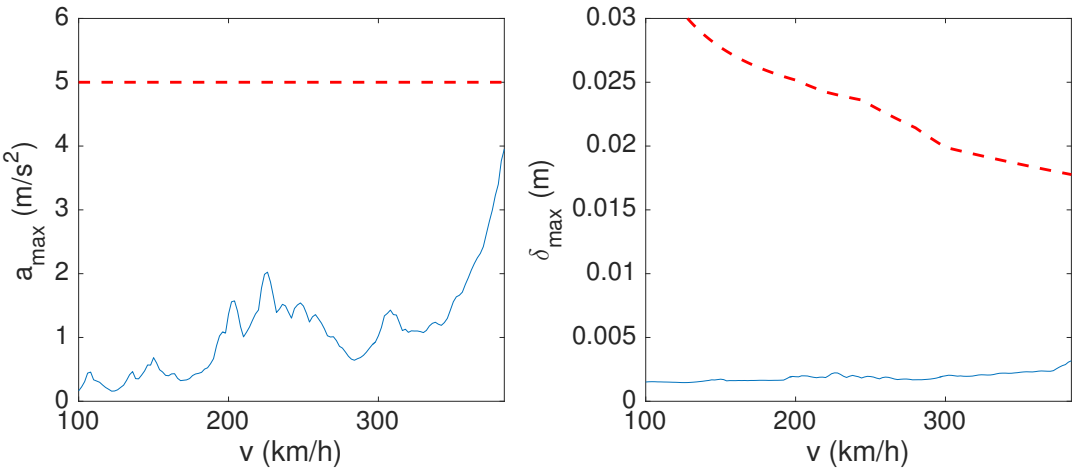

Figure C.8 – 1 span - L=19,5 m

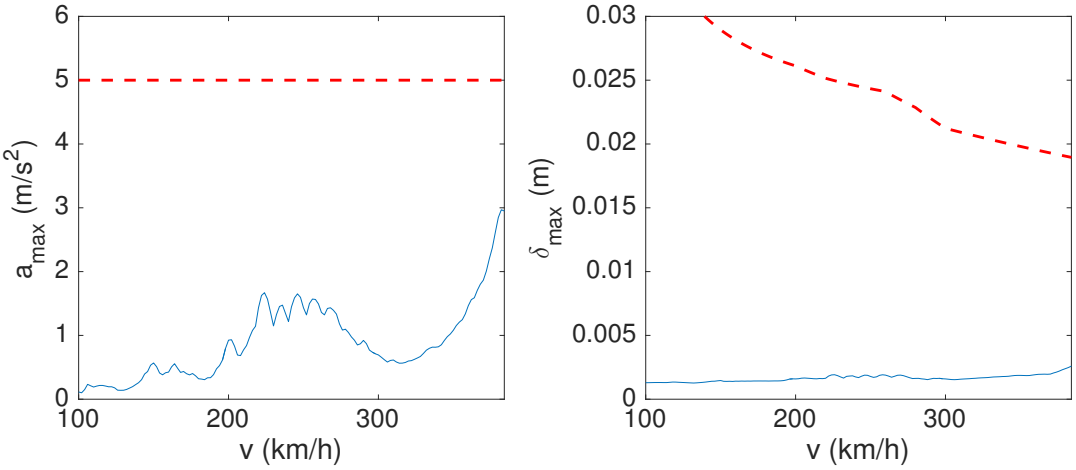

Figure C.9 – 1 span - L=20,8 m

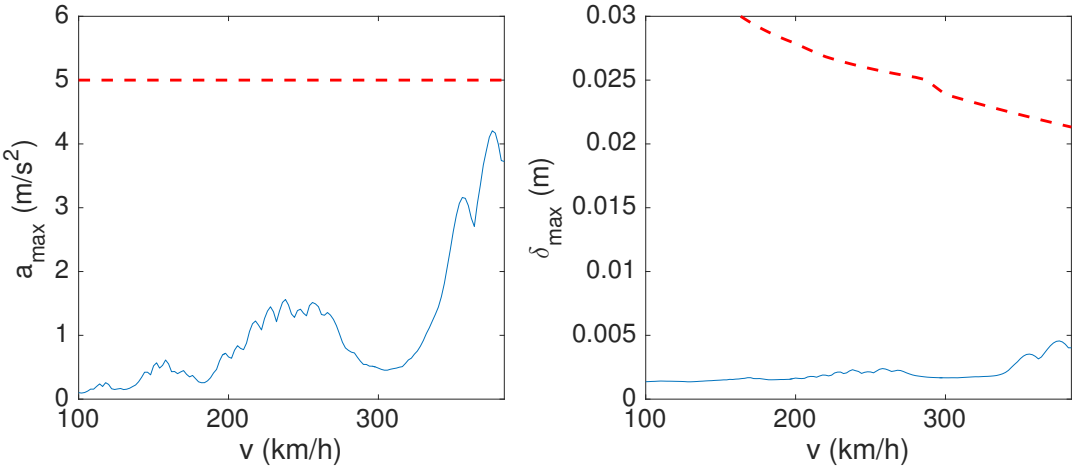

Figure C.10 – 1 span - L=23,4 m

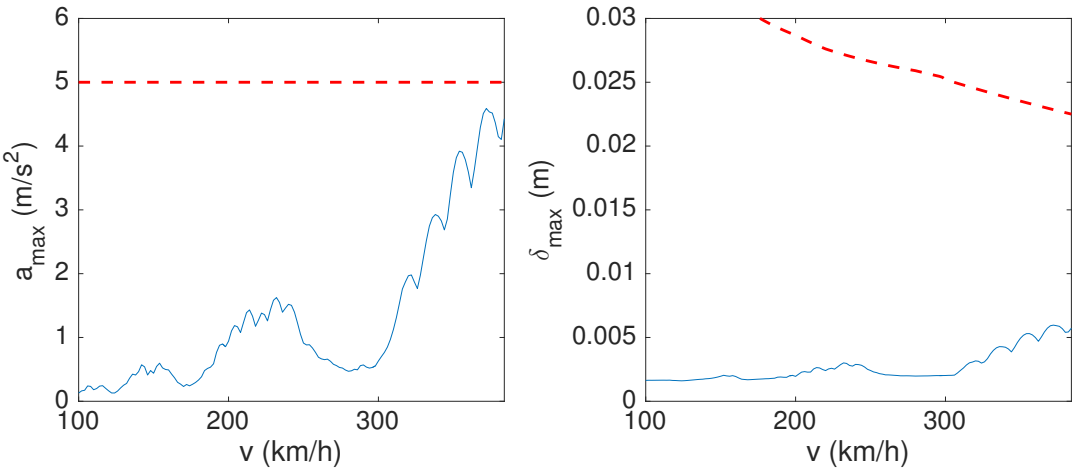

Figure C.11 – 1 span - L=24,7 m

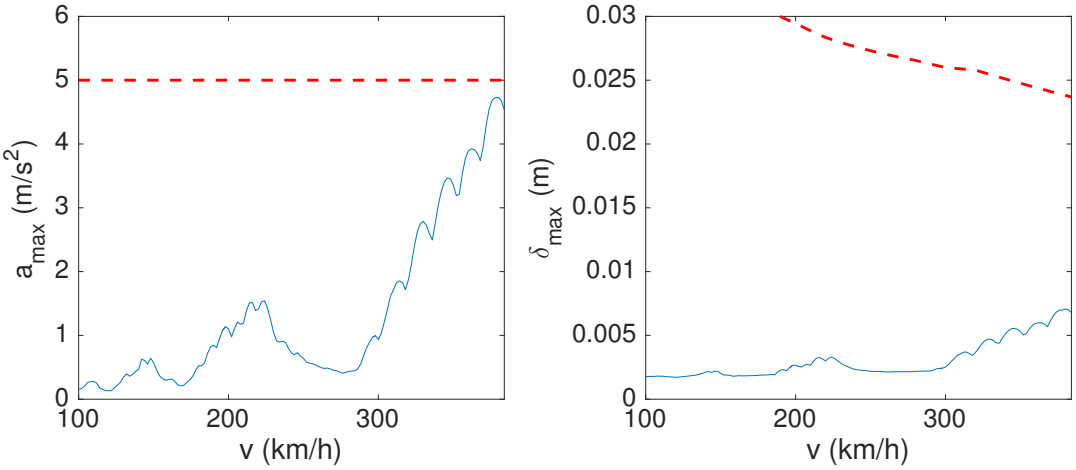

Figure C.12 – 1 span - L=26 m

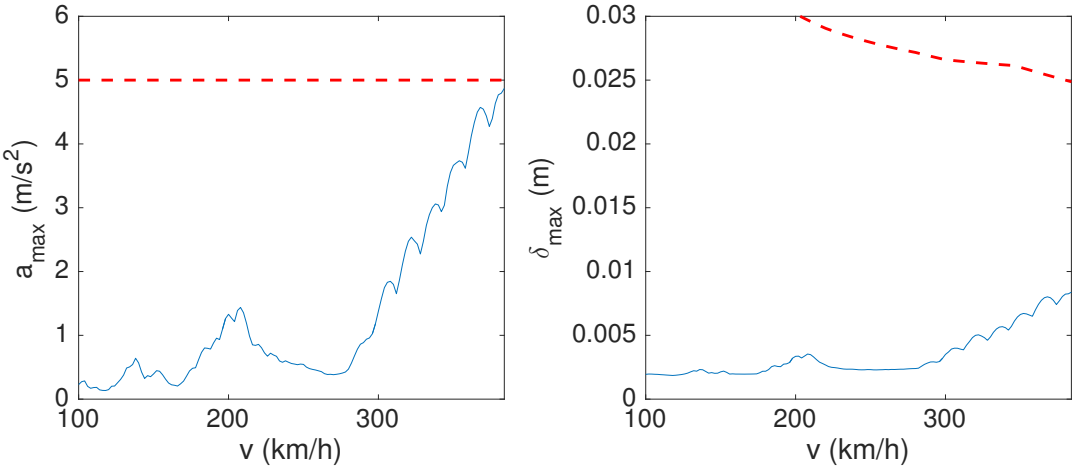

Figure C.13 – 1 span - L=27,3 m

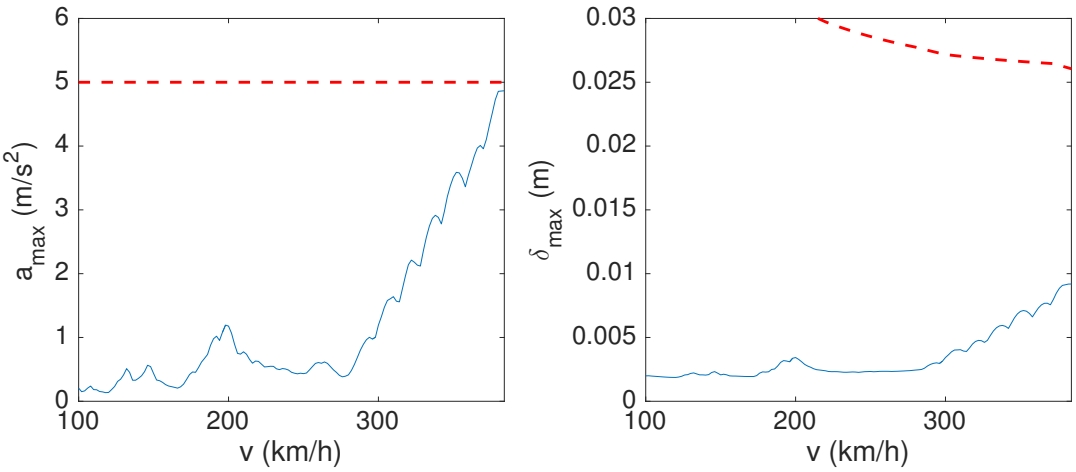

Figure C.14 – 1 span - L=28,6 m

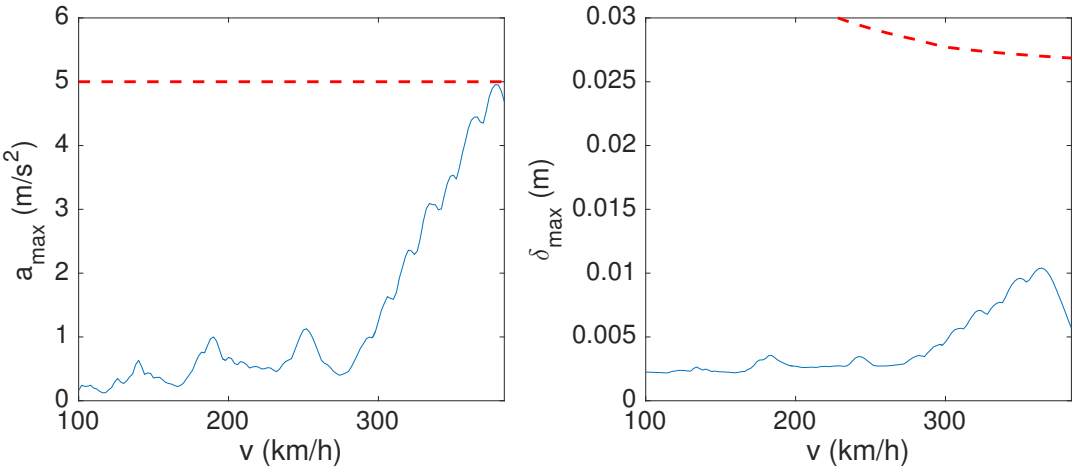

Figure C.15 – 1 span - L=29,9 m

C.2 Results for 2 spans

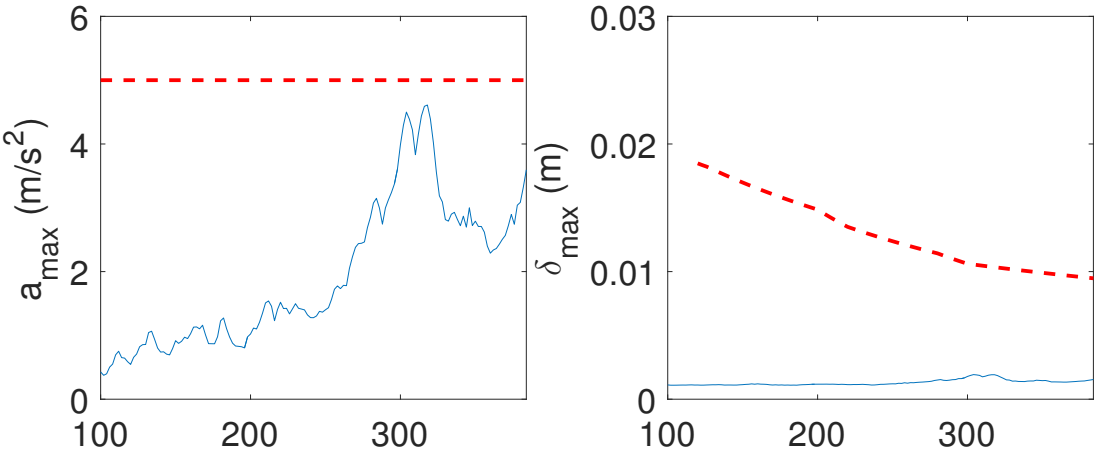

Figure C.16 – 2 spans - L=10,4 m

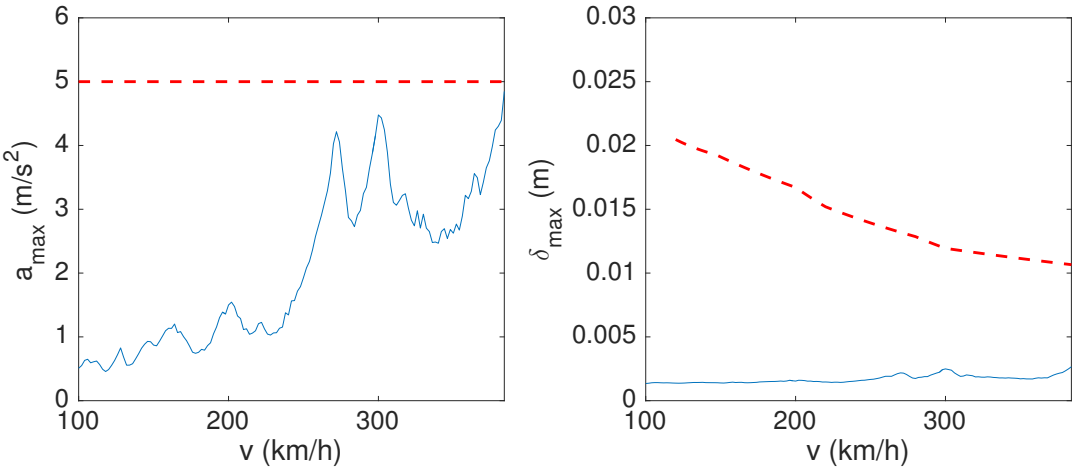

Figure C.17 – 2 spans - L=11,7 m

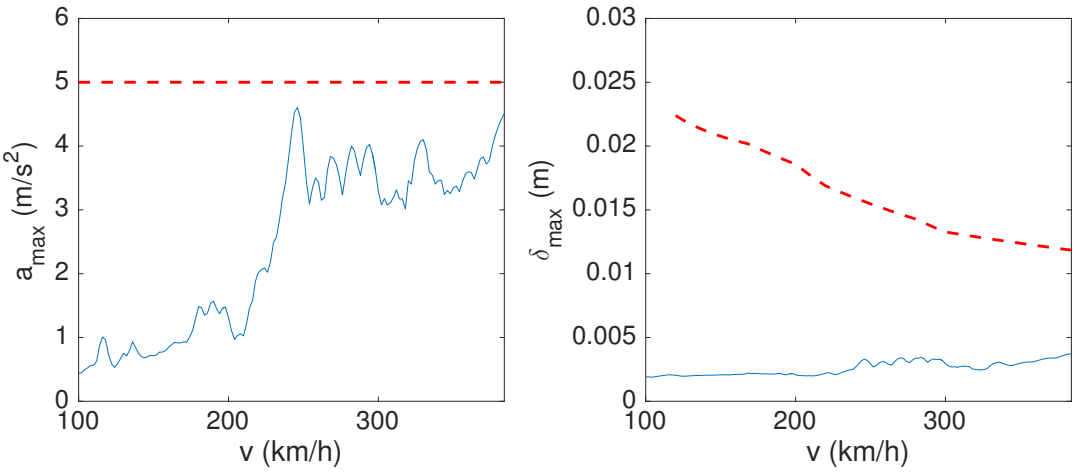

Figure C.18 – 2 spans - L=13 m

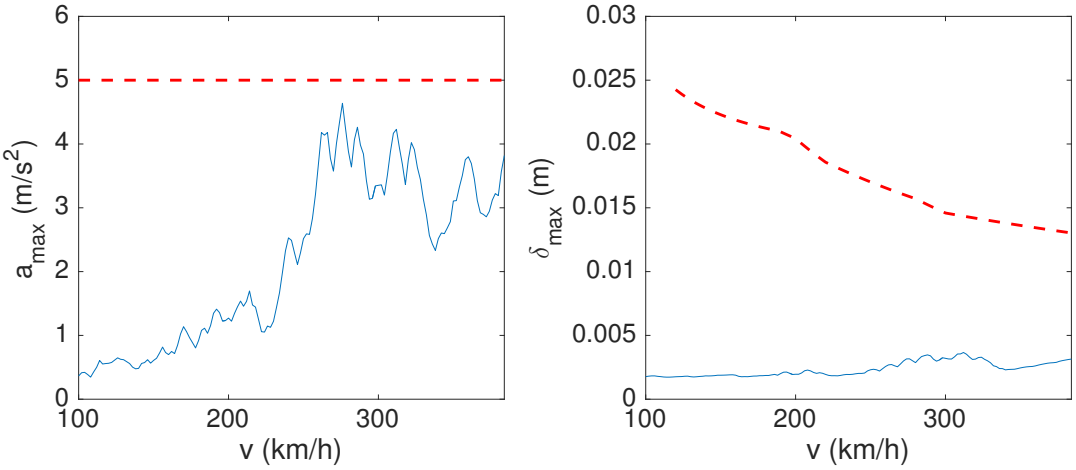

Figure C.19 – 2 spans - L=14,3 m

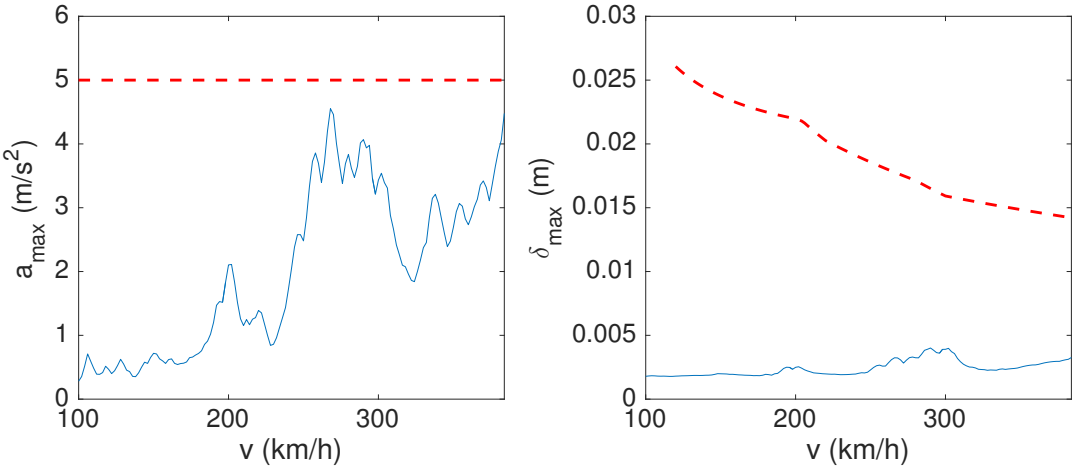

Figure C.20 – 2 spans - L=15,6 m

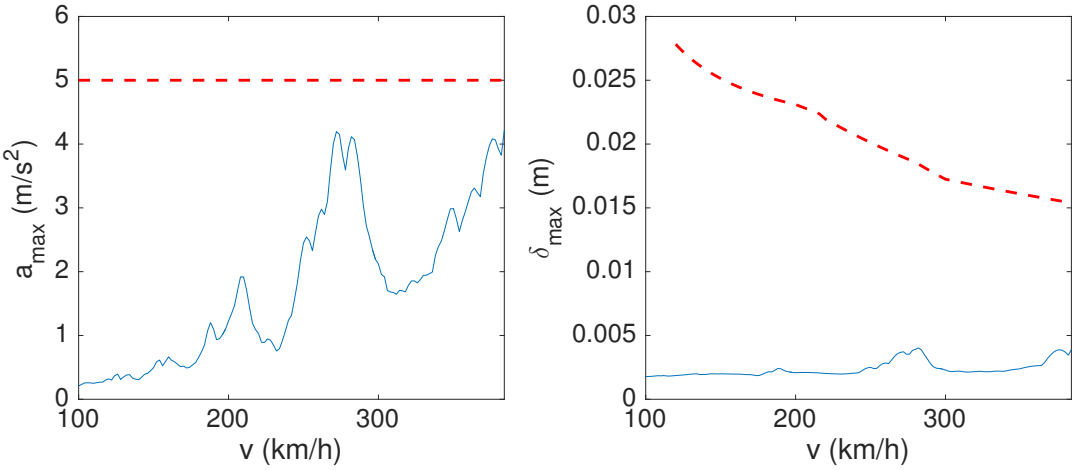

Figure C.21 – 2 spans - L=16,9 m

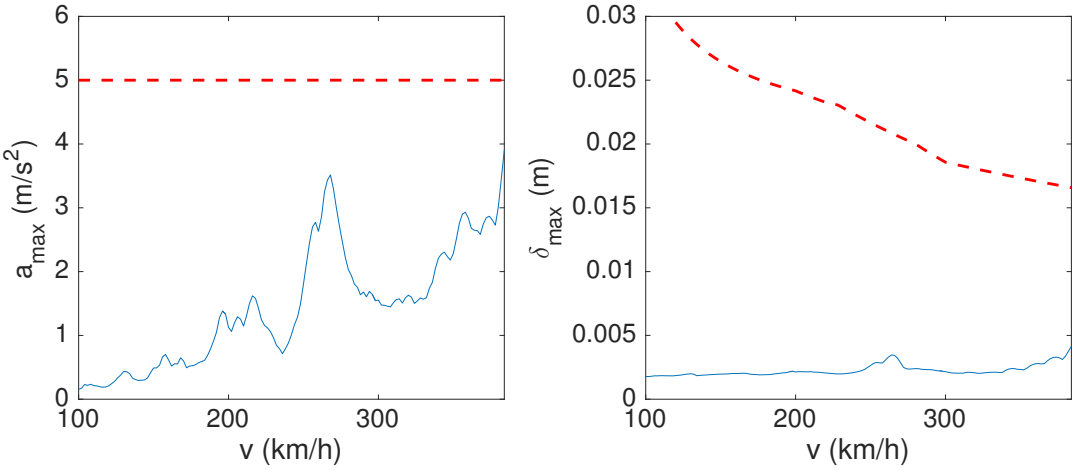

Figure C.22 – 2 spans - L=18,2 m

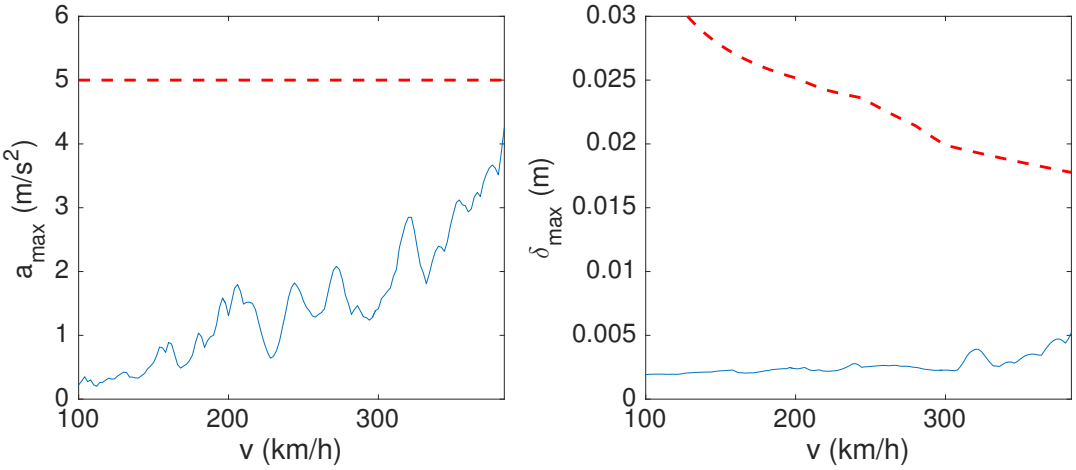

Figure C.23 – 2 spans - L=19,5 m

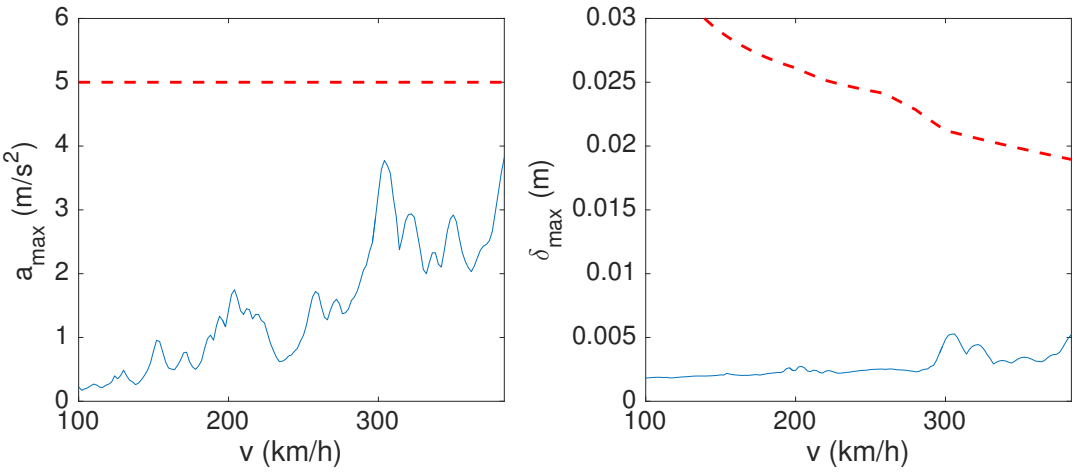

Figure C.24 – 2 spans - L=20,8 m

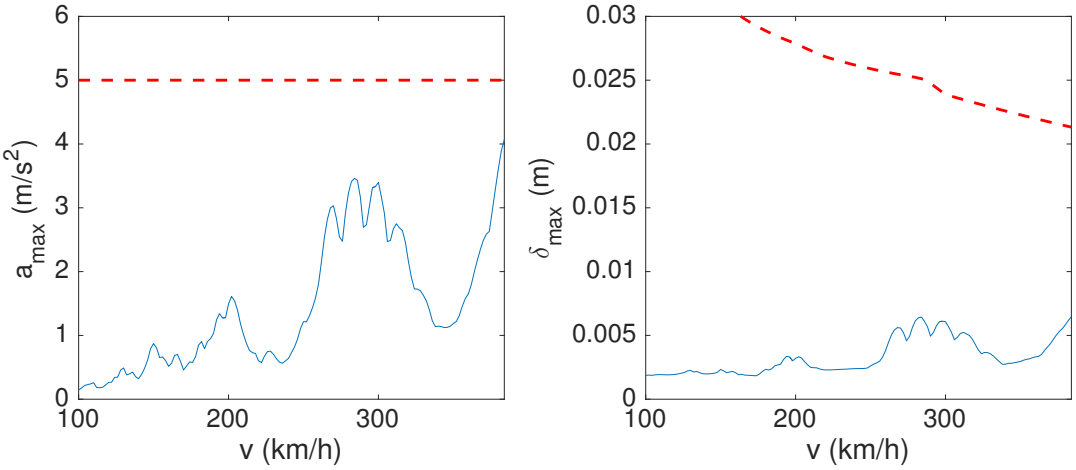

Figure C.25 – 2 spans - L=23,4 m

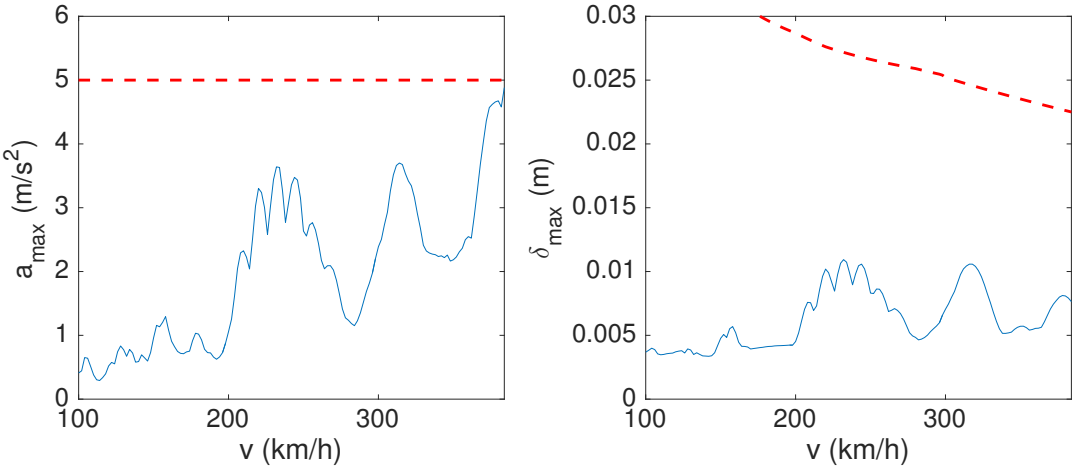

Figure C.26 – 2 spans - L=24,7 m

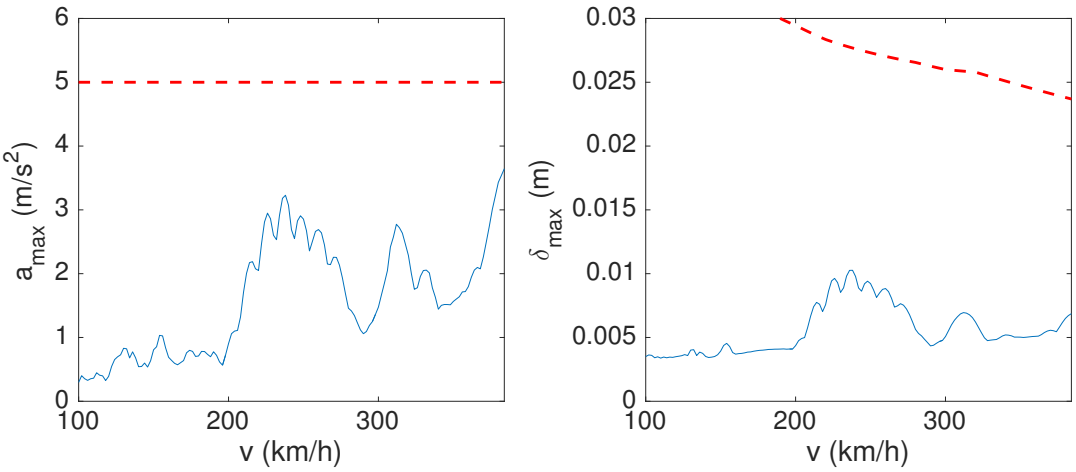

Figure C.27 – 2 spans - L=26 m

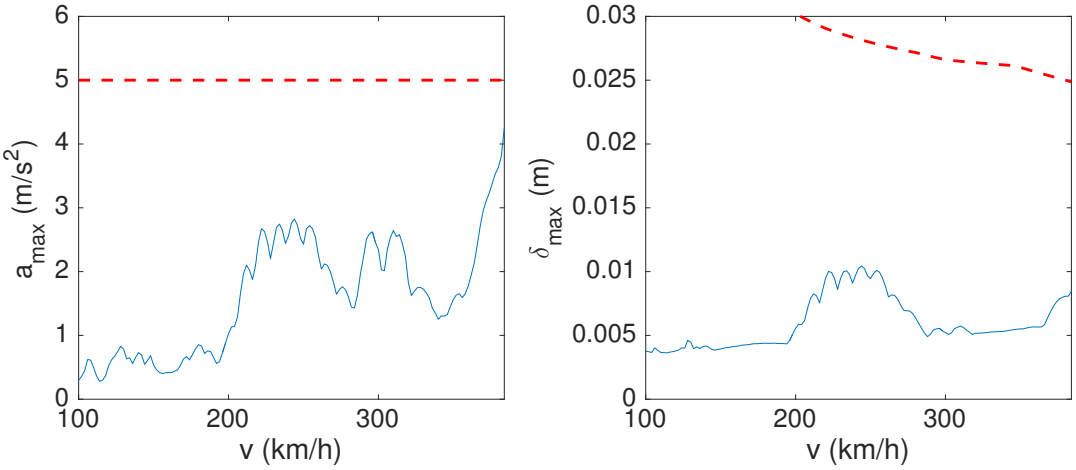

Figure C.28 – 2 spans - L=27,3 m

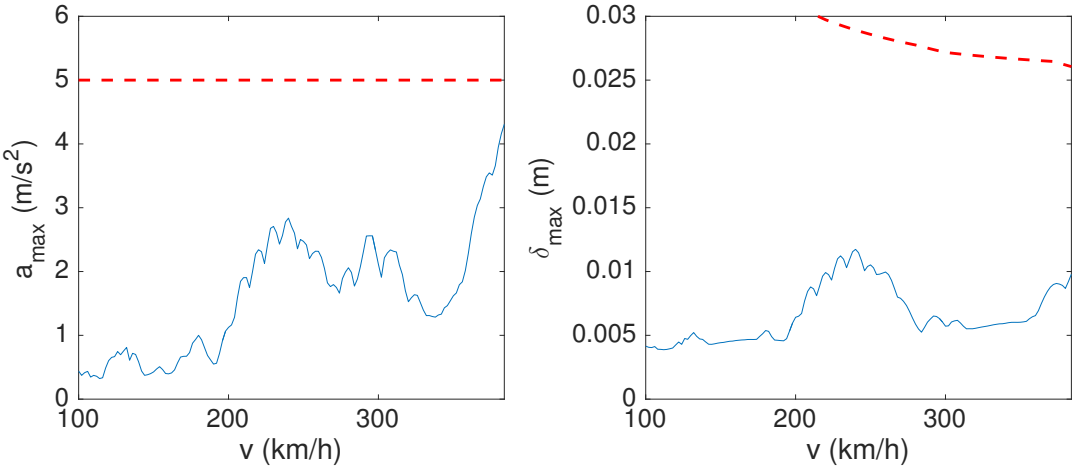

Figure C.29 – 2 spans - L=28,6 m

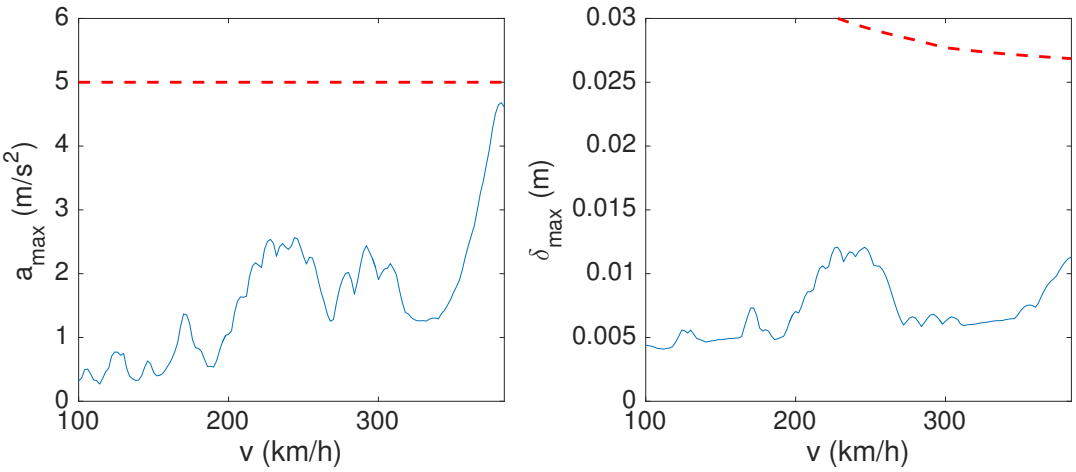

Figure C.30 – 2 spans - L=29,9 m

C.3 Results for 3 spans

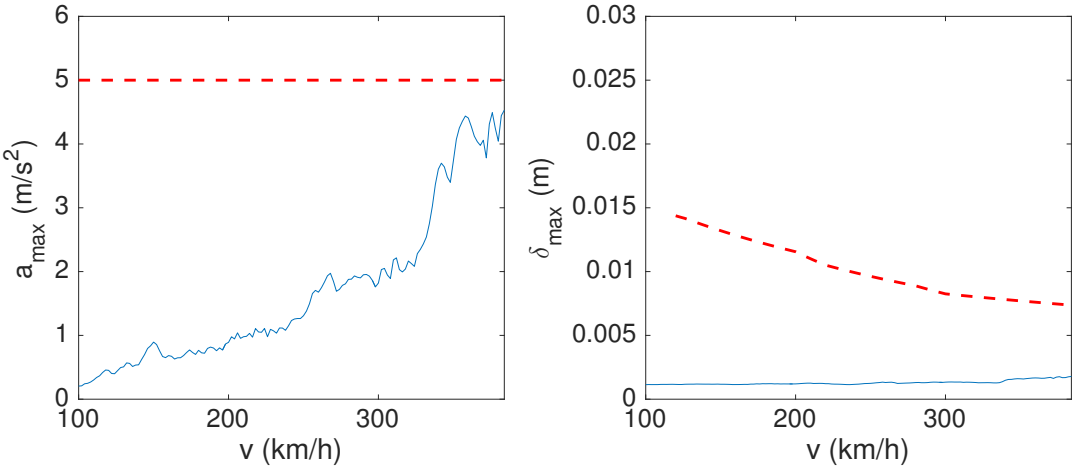

Figure C.31 – 3 spans - L=10,4 m

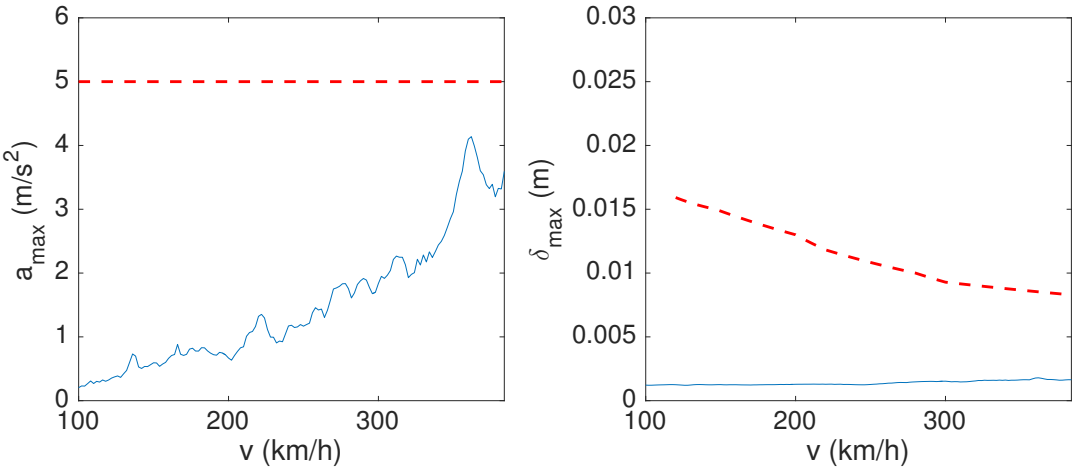

Figure C.32 – 3 spans - L=11,7 m

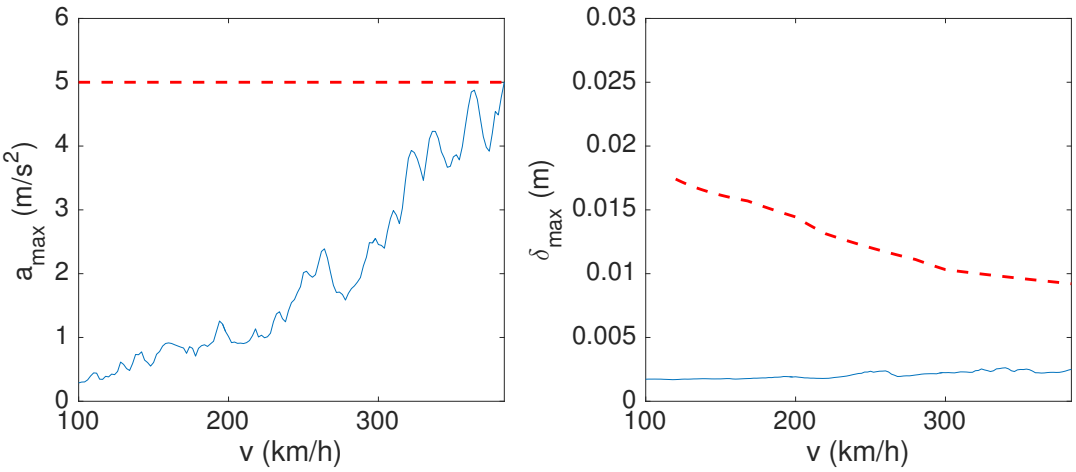

Figure C.33 – 3 spans - L=13 m

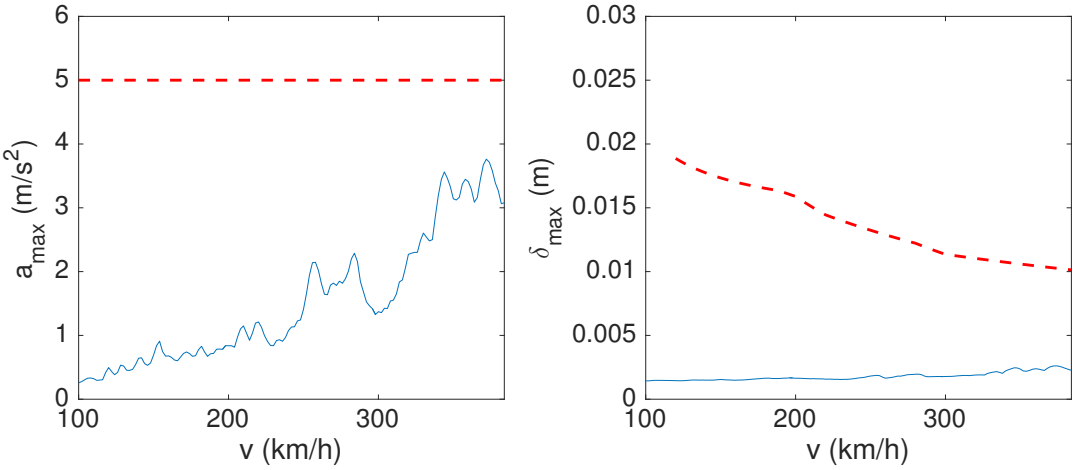

Figure C.34 – 3 spans - L=14,3 m

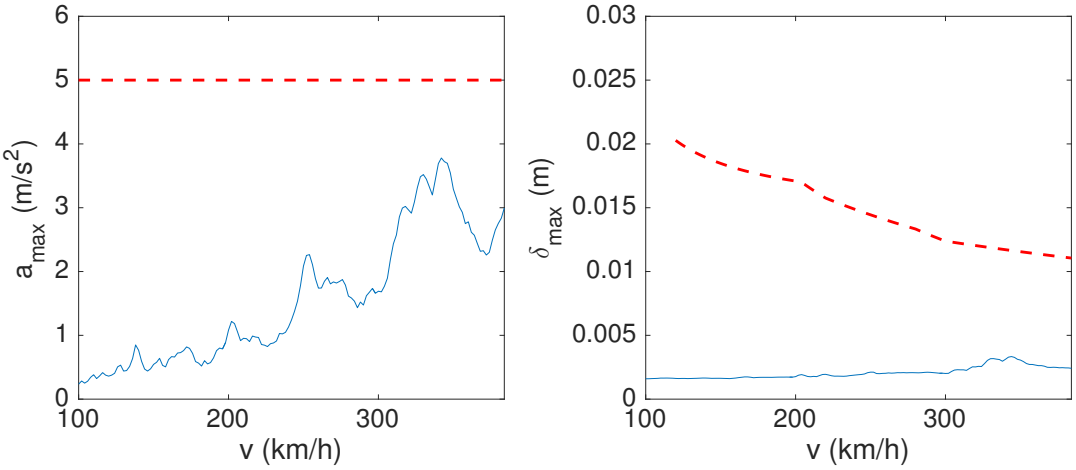

Figure C.35 – 3 spans - L=15,6 m

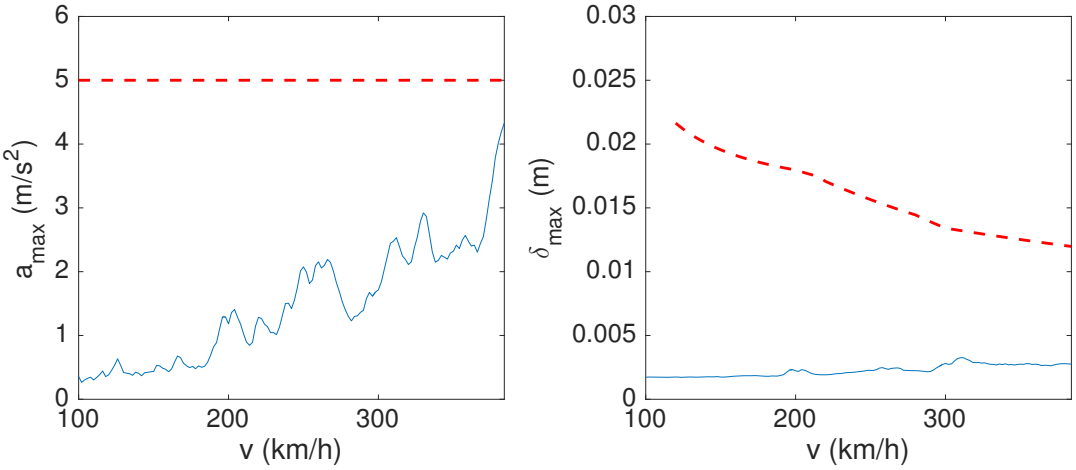

Figure C.36 – 3 spans - L=16,9 m

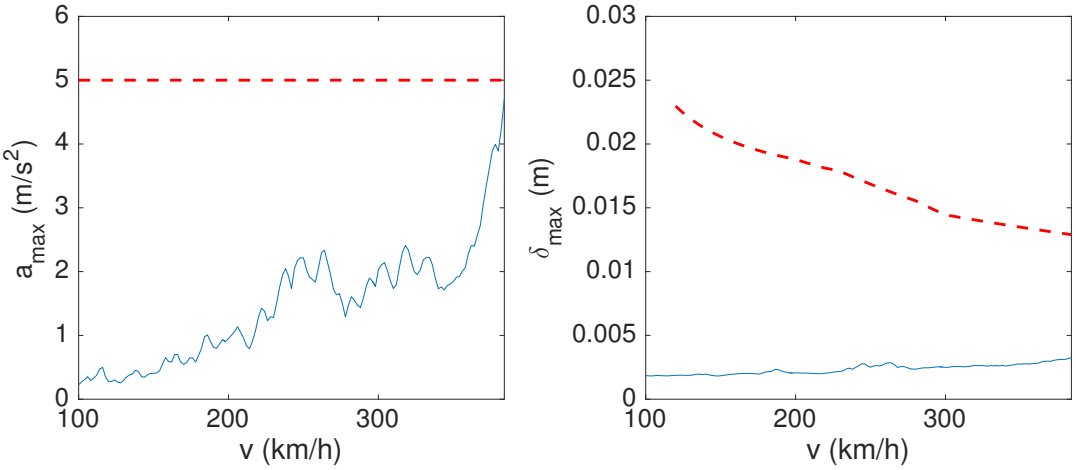

Figure C.37 – 3 spans - L=18,2 m

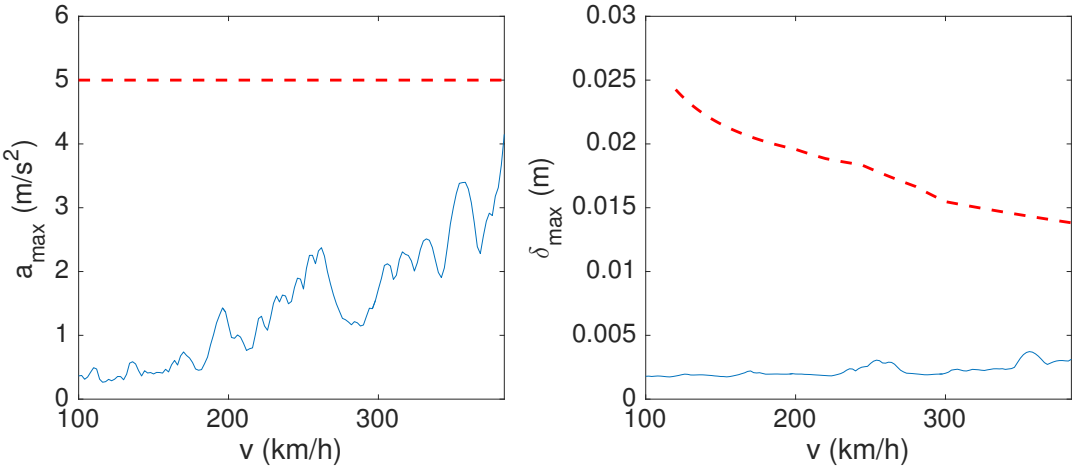

Figure C.38 – 3 spans - L=19,5 m

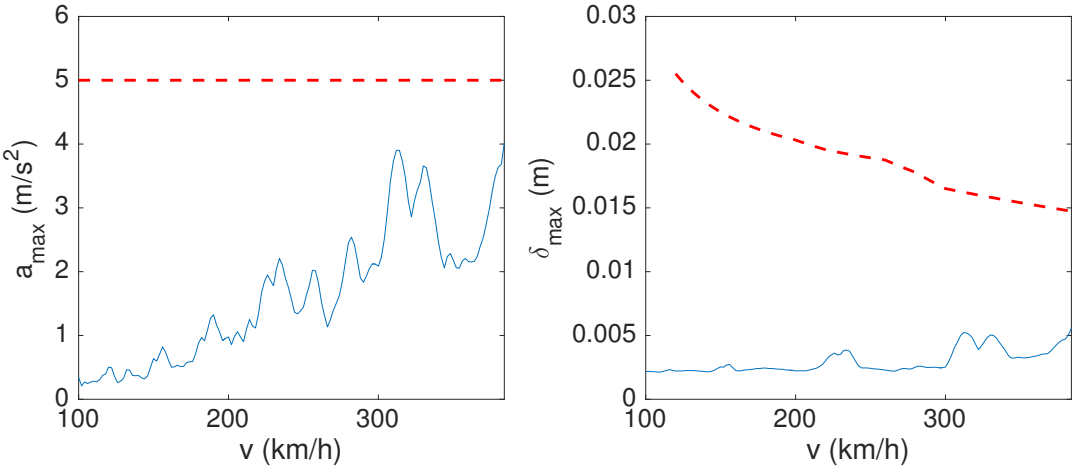

Figure C.39 – 3 spans - L=20,8 m

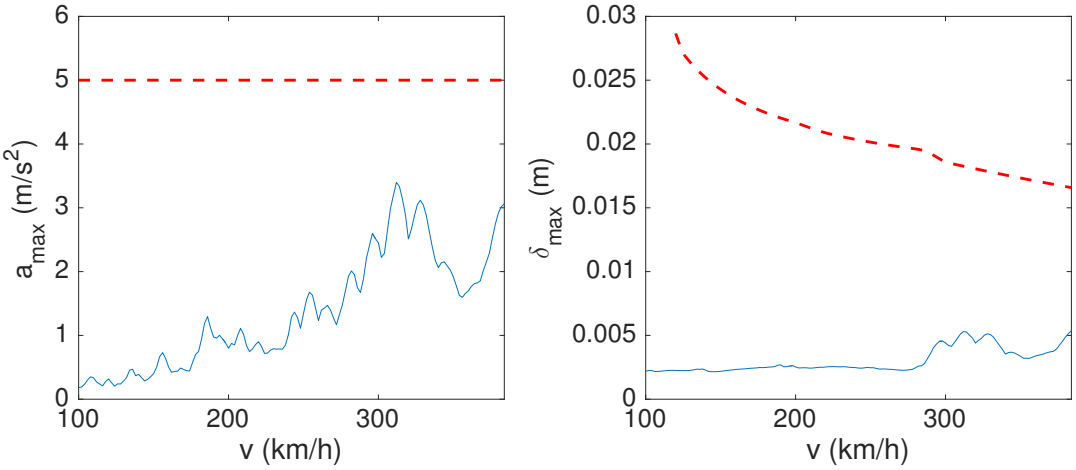

Figure C.40 – 3 spans - L=23,4 m

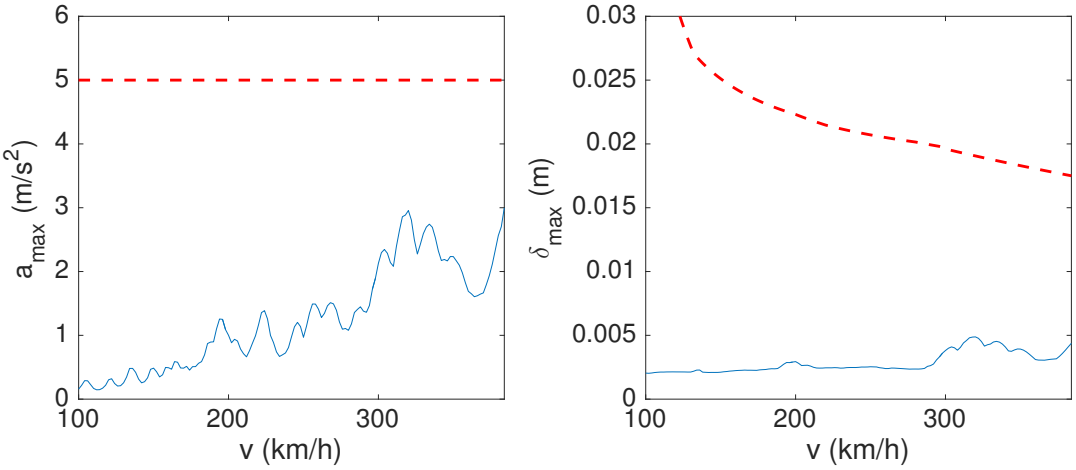

Figure C.41 – 3 spans - L=24,7 m

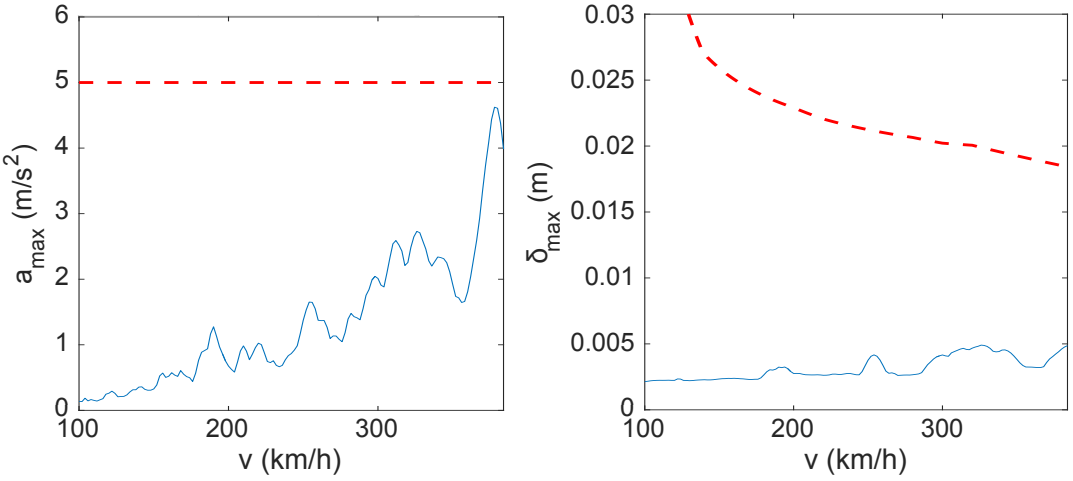

Figure C.42 – 3 spans - L=26 m

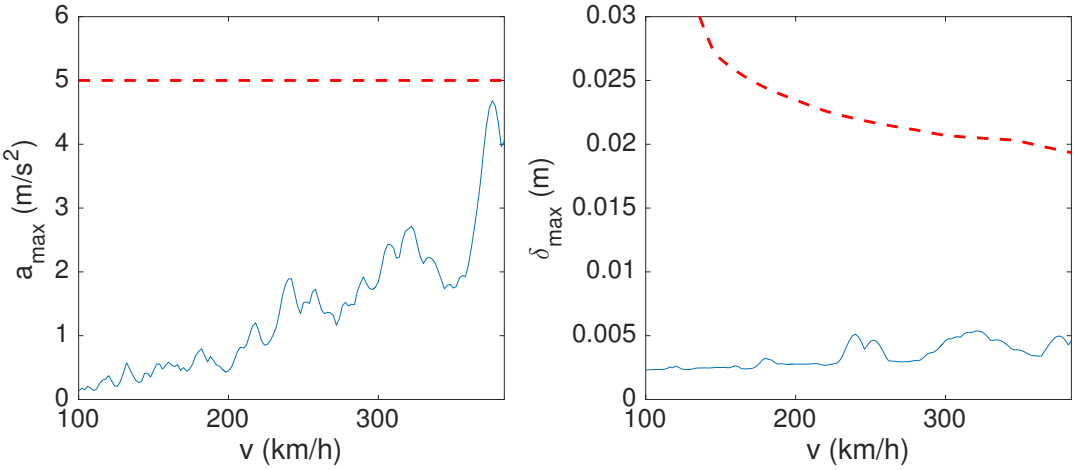

Figure C.43 – 3 spans - L=27,3 m

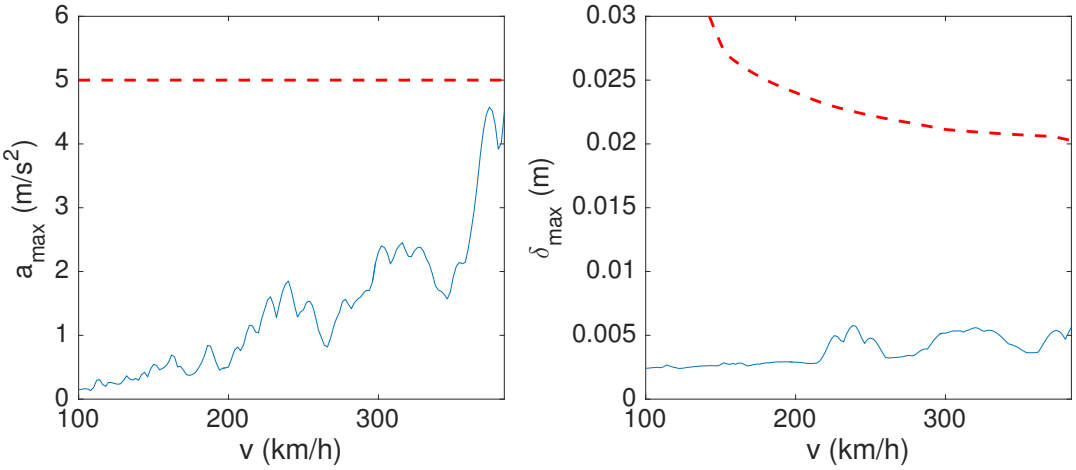

Figure C.44 – 3 spans - L=28,6 m

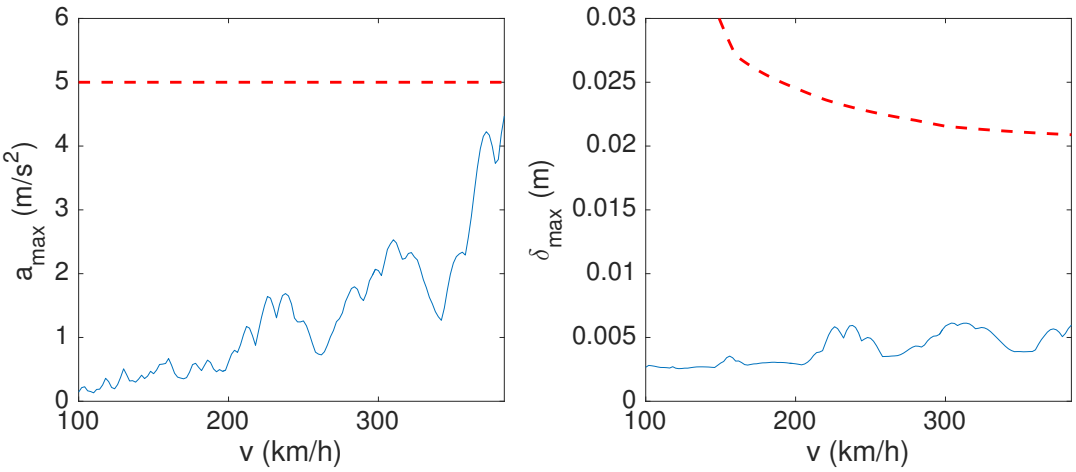

Figure C.45 – 3 spans - L=29,9 m

C.4 Results for 4 spans

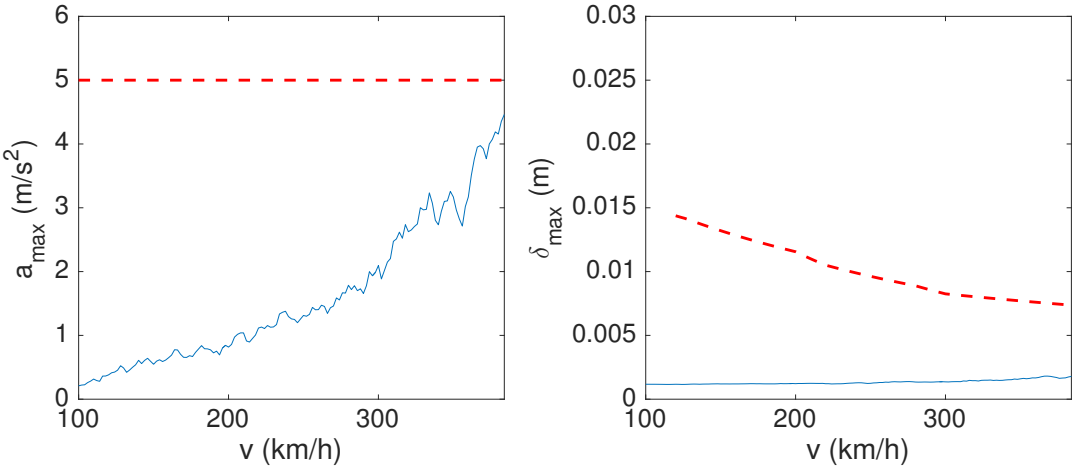

Figure C.46 – 4 spans - L=10,4 m

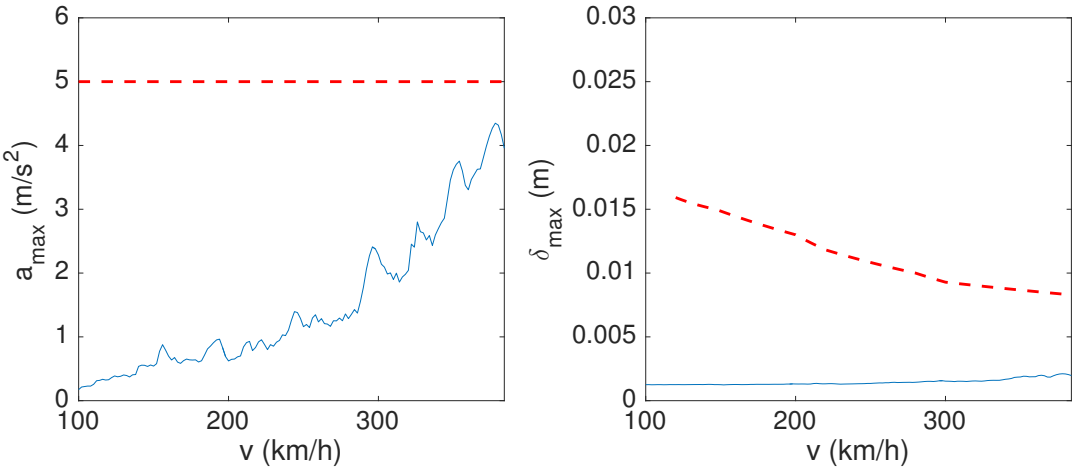

Figure C.47 – 4 spans - L=11,7 m

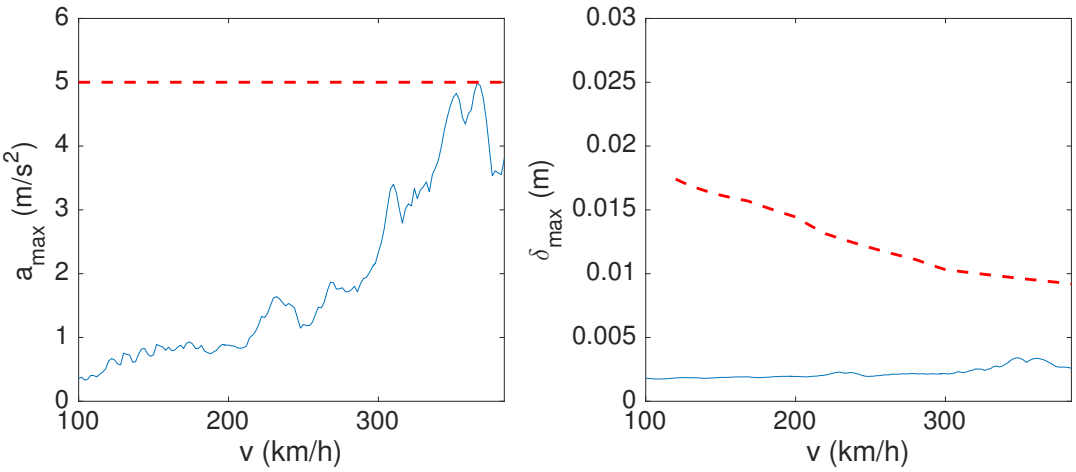

Figure C.48 – 4 spans - L=13 m

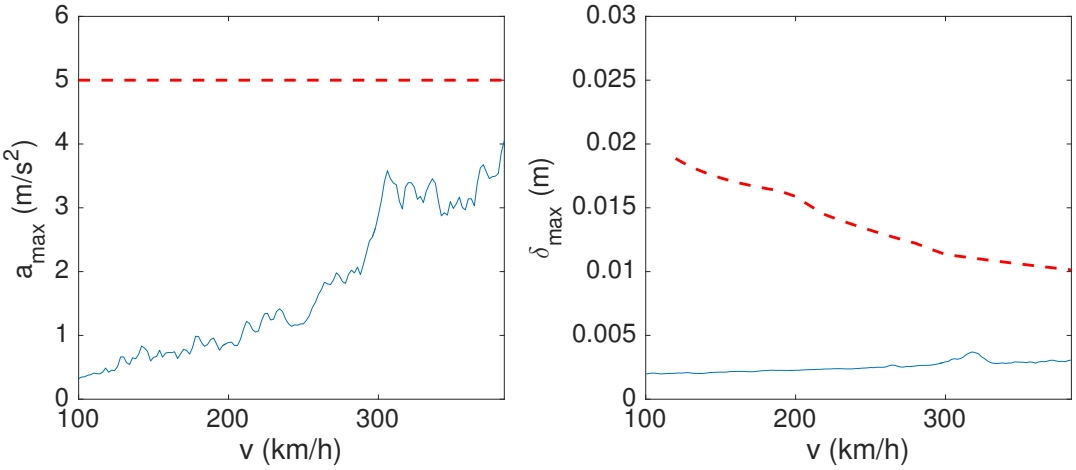

Figure C.49 – 4 spans - L=14,3 m

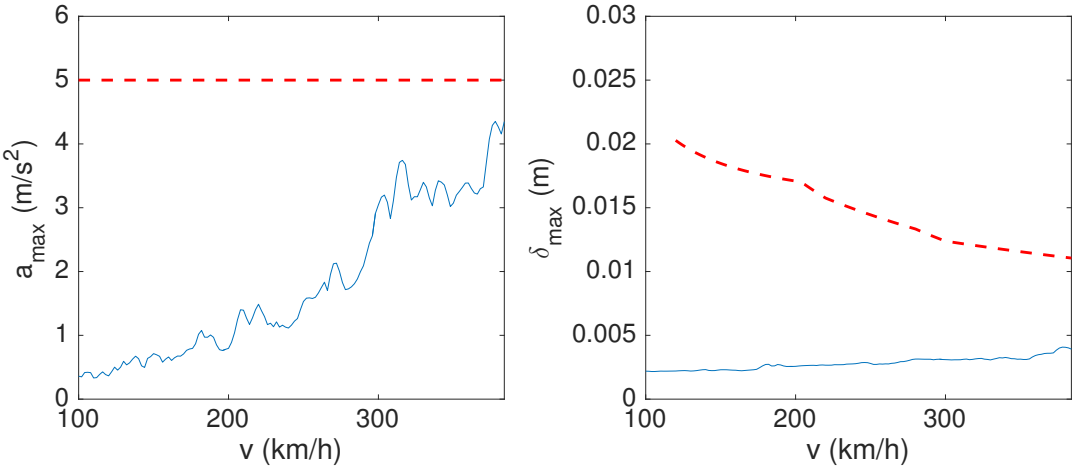

Figure C.50 – 4 spans - L=15,6 m

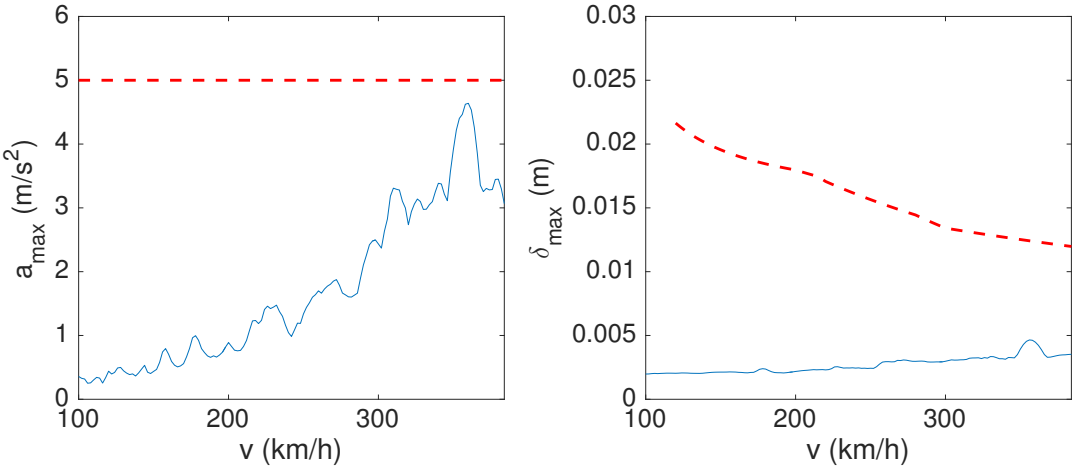

Figure C.51 – 4 spans - L=16,9 m

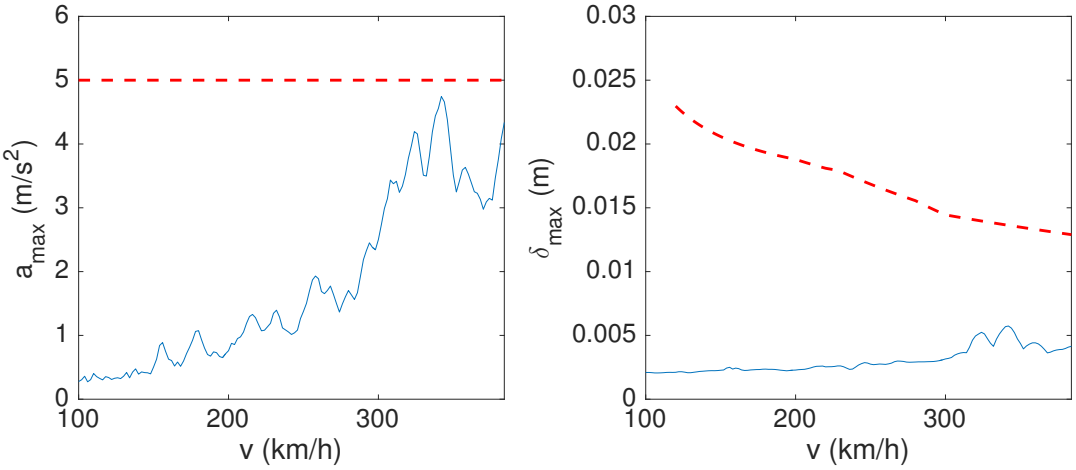

Figure C.52 – 4 spans - L=18,2 m

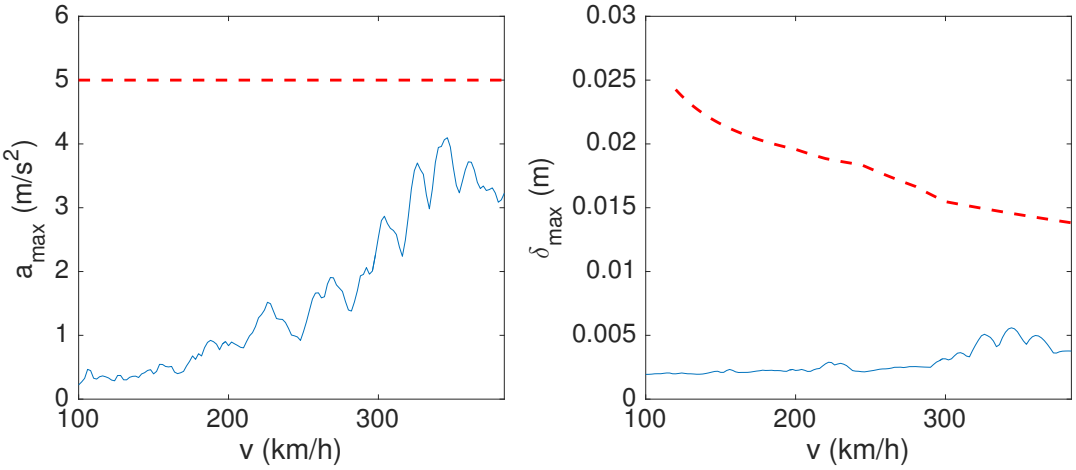

Figure C.53 – 4 spans - L=19,5 m

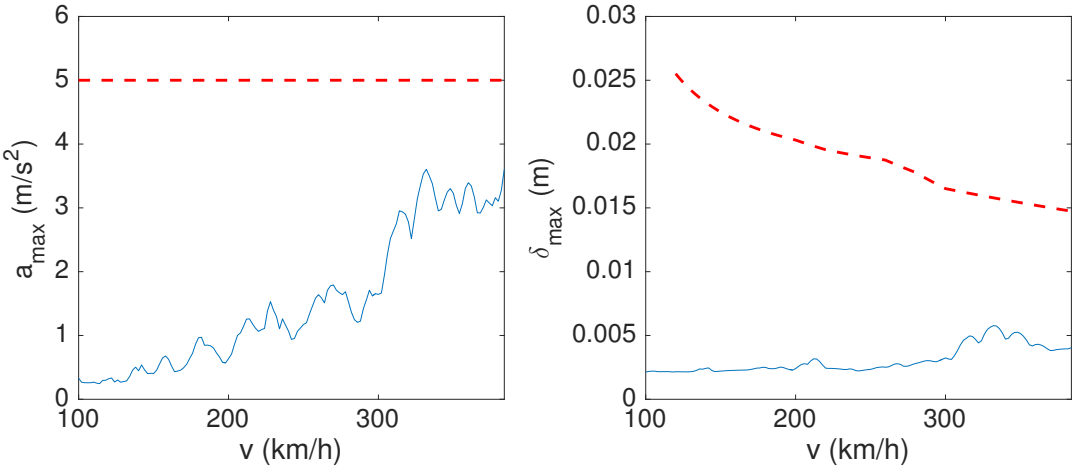

Figure C.54 – 4 spans - L=20,8 m

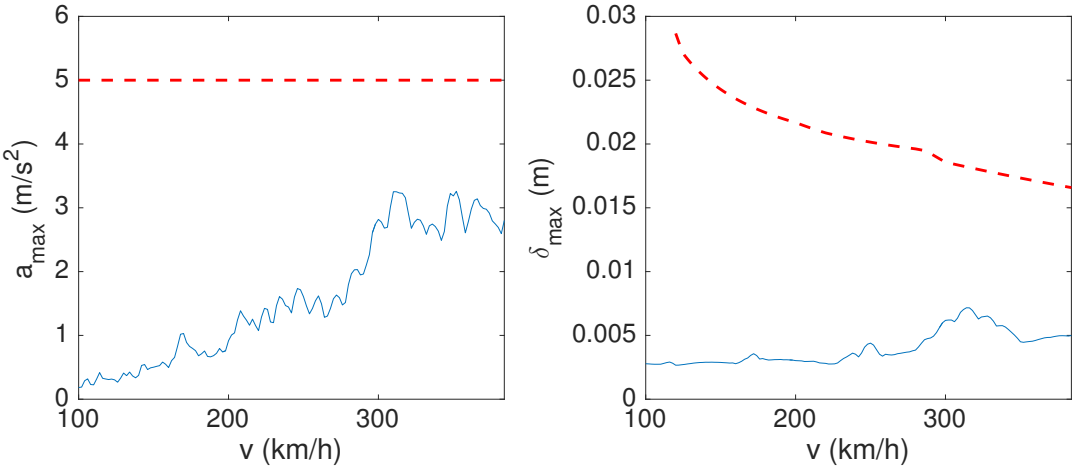

Figure C.55 – 4 spans - L=23,4 m

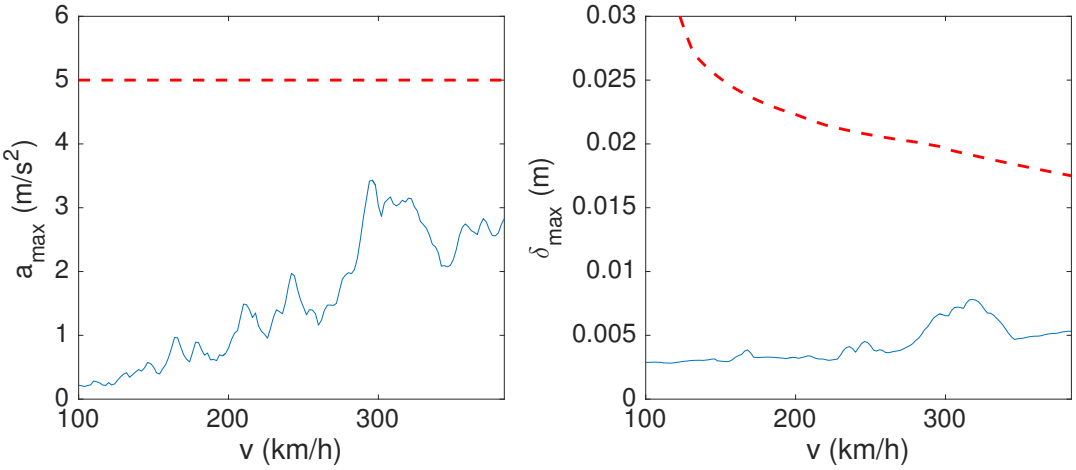

Figure C.56 – 4 spans - L=24,7 m

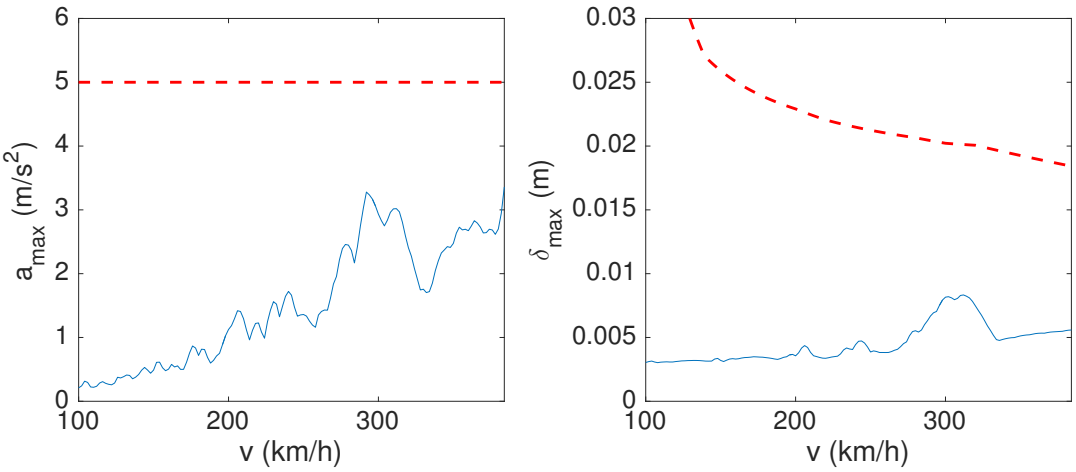

Figure C.57 – 4 spans - L=26 m

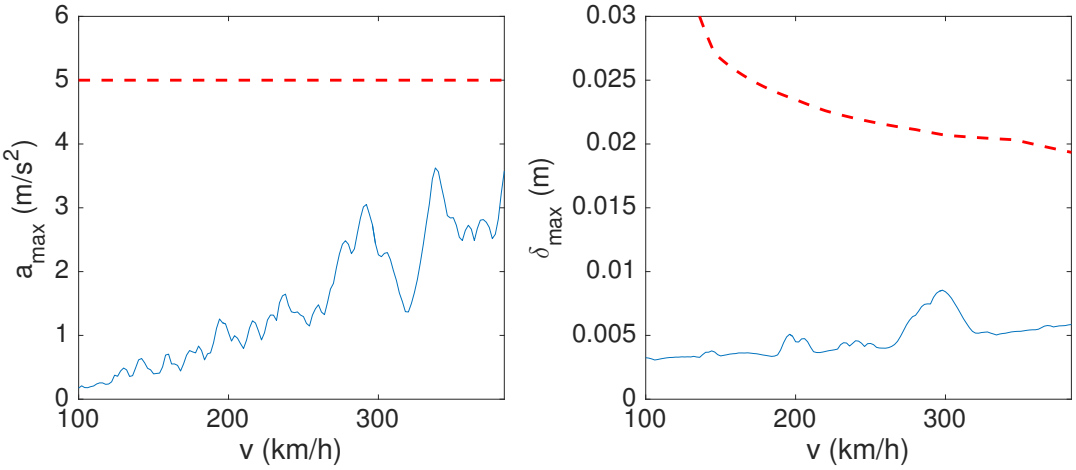

Figure C.58 – 4 spans - L=27,3 m

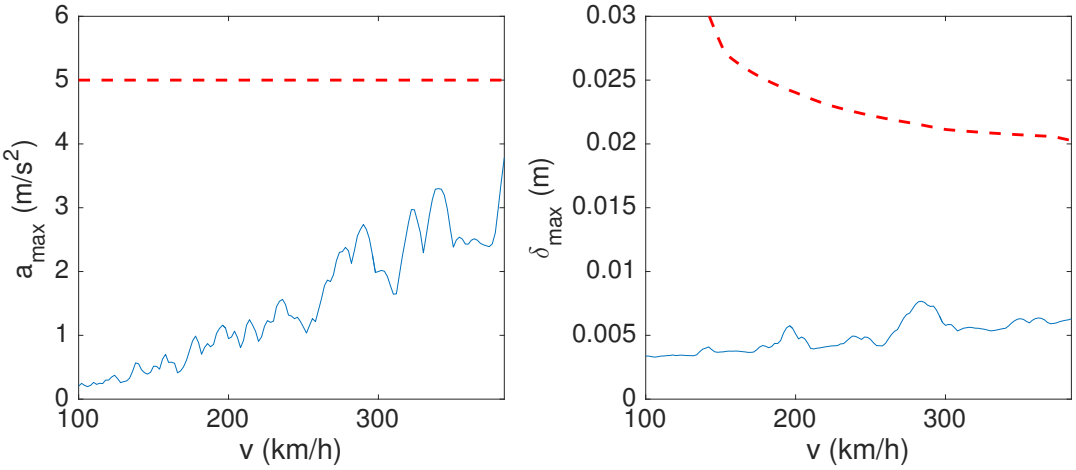

Figure C.59 – 4 spans - L=28,6 m

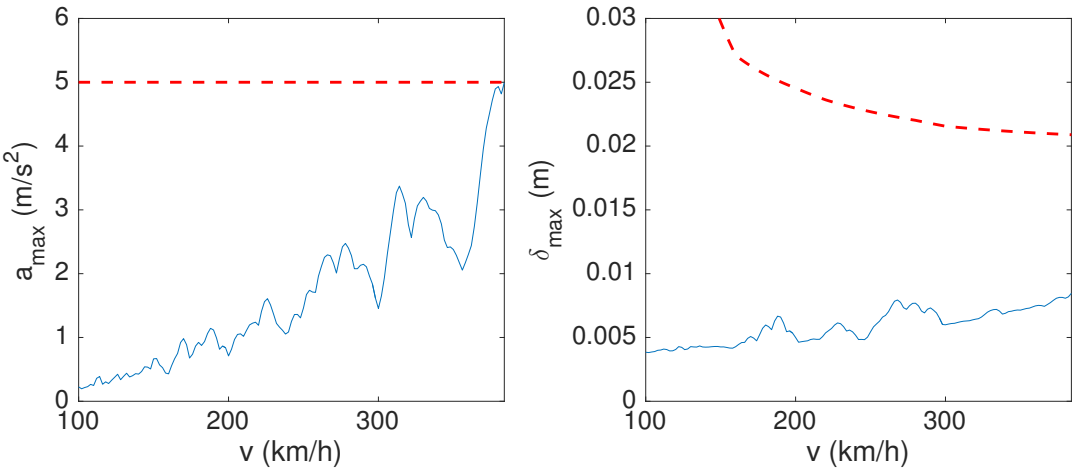

Figure C.60 – 4 spans - L=29,9 m

Appendix D

Mode shapes

D.1 Results for 1 span

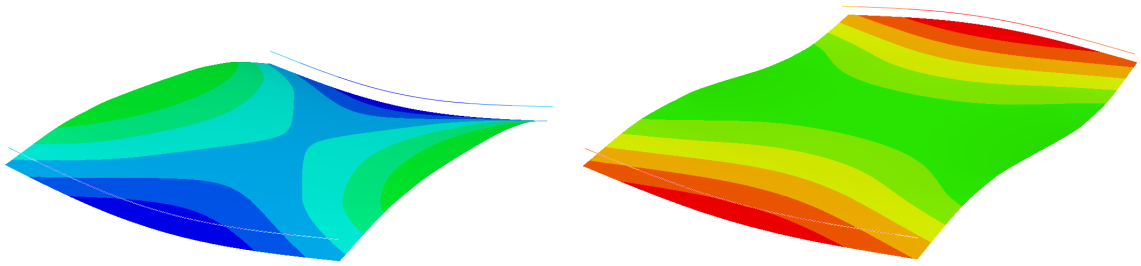

(a) Vertical mode (b) Torsional mode

Figure D.1 – 1 span - L=10 m

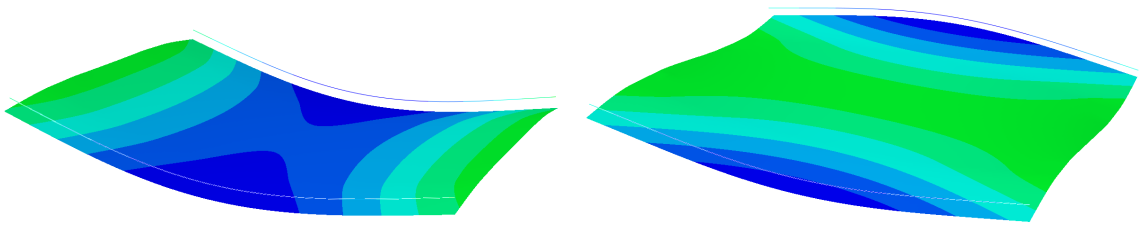

(a) Vertical mode (b) Torsional mode

Figure D.2 – 1 span - L=15 m

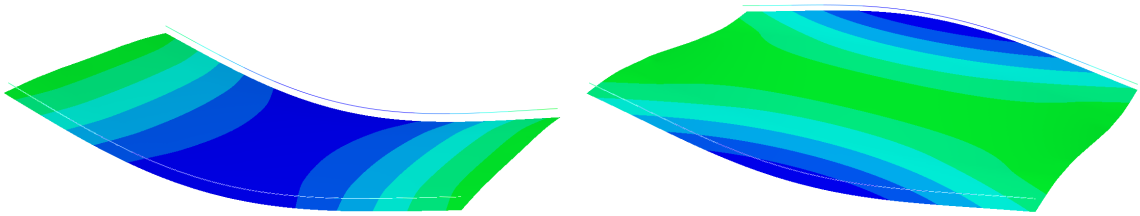

(a) Vertical mode (b) Torsional mode

Figure D.3 – 1 span - L=20 m

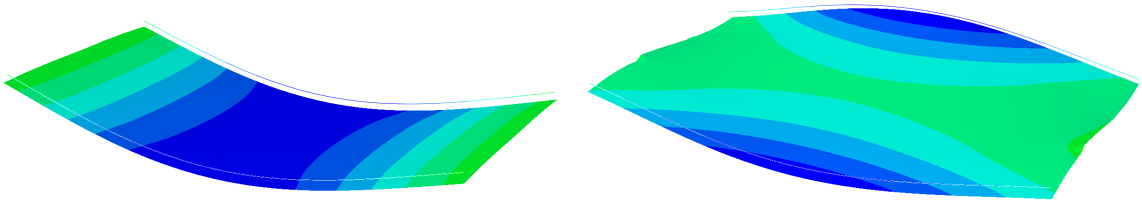

(a) Vertical mode (b) Torsional mode

Figure D.4 – 1 span - L=25 m

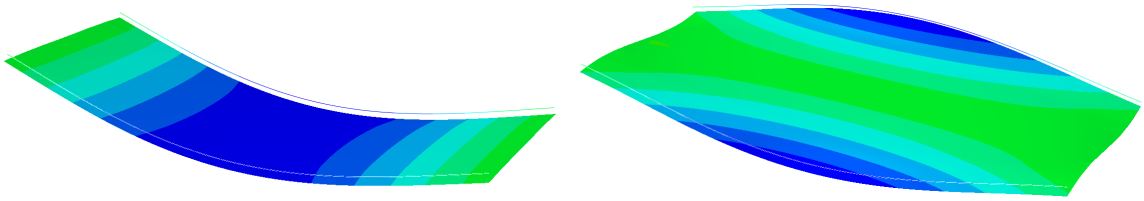

(a) Vertical mode (b) Torsional mode

Figure D.5 – 1 span - L=30 m

D.2 Results for 2 spans

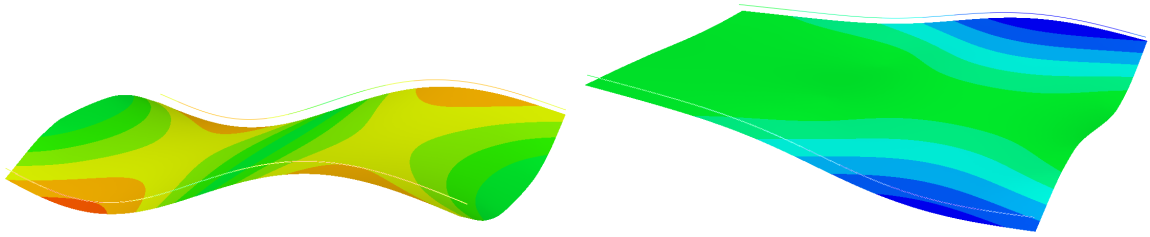

(a) Vertical mode (b) Torsional mode

Figure D.6 – 2 spans - L=10 m

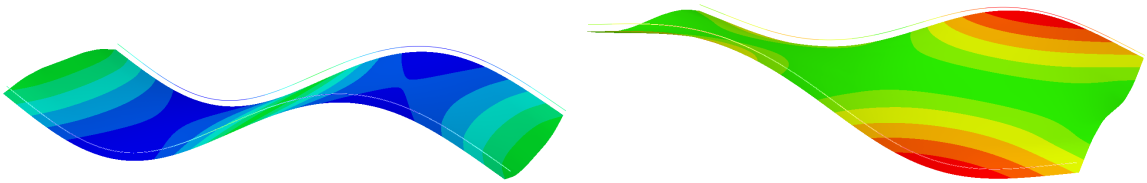

(a) Vertical mode (b) Torsional mode

Figure D.7 – 2 spans - L=15 m

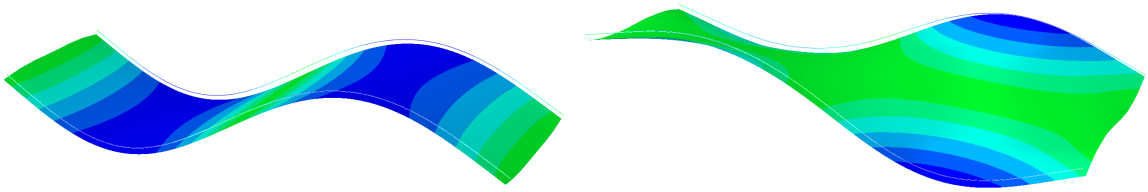

(a) Vertical mode (b) Torsional mode

Figure D.8 – 2 spans - L=20 m

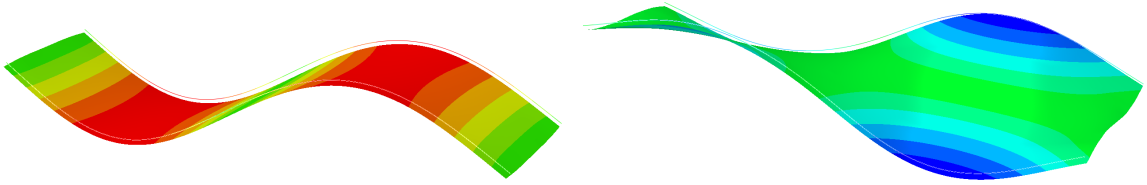

(a) Vertical mode (b) Torsional mode

Figure D.9 – 2 spans - L=25 m

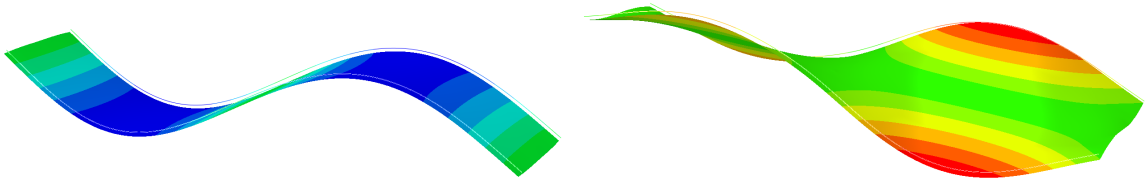

(a) Vertical mode (b) Torsional mode

Figure D.10 – 2 spans - L=30 m

D.3 Results for 3 spans

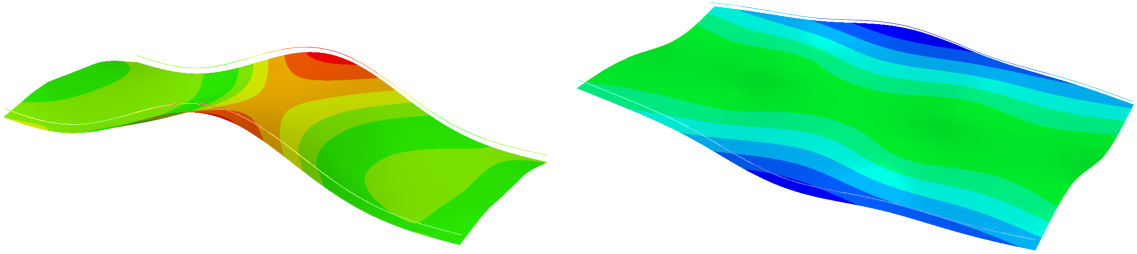

(a) Vertical mode (b) Torsional mode

Figure D.11 – 3 spans - L=10 m

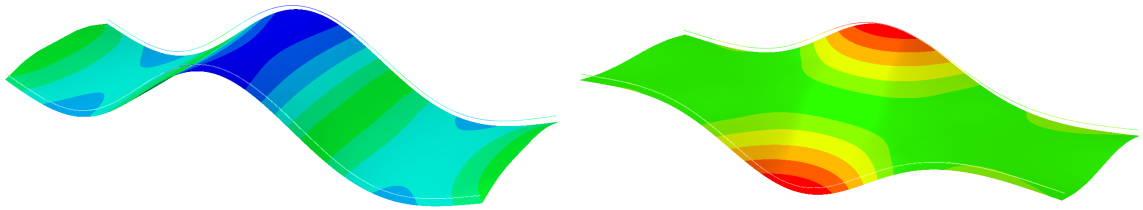

(a) Vertical mode (b) Torsional mode

Figure D.12 – 3 spans - L=15 m

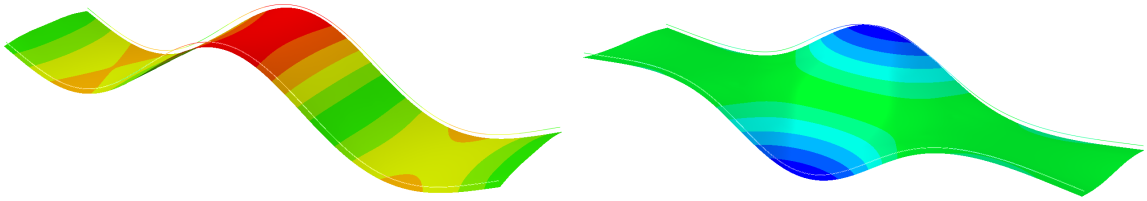

(a) Vertical mode (b) Torsional mode

Figure D.13 – 3 spans - L=20 m

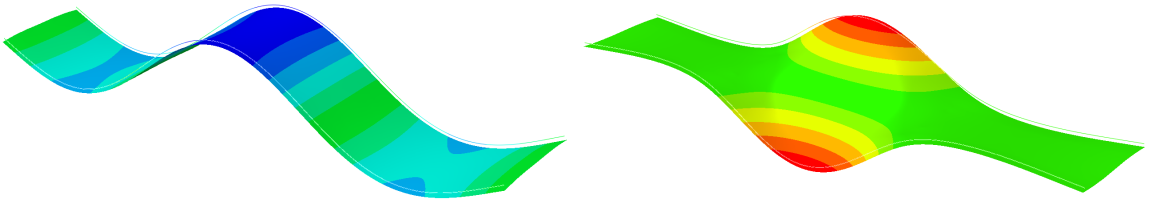

(a) Vertical mode (b) Torsional mode

Figure D.14 – 3 spans - L=25 m

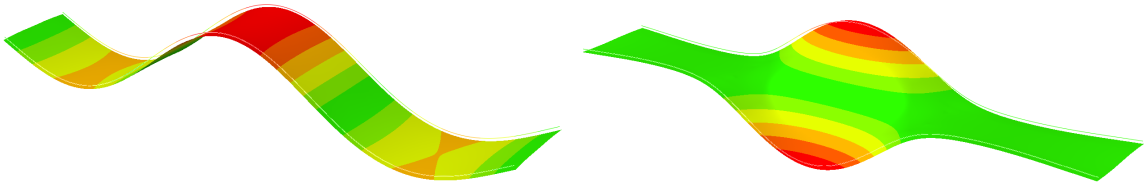

(a) Vertical mode (b) Torsional mode

Figure D.15 – 3 spans - L=30 m

D.4 Results for 4 spans

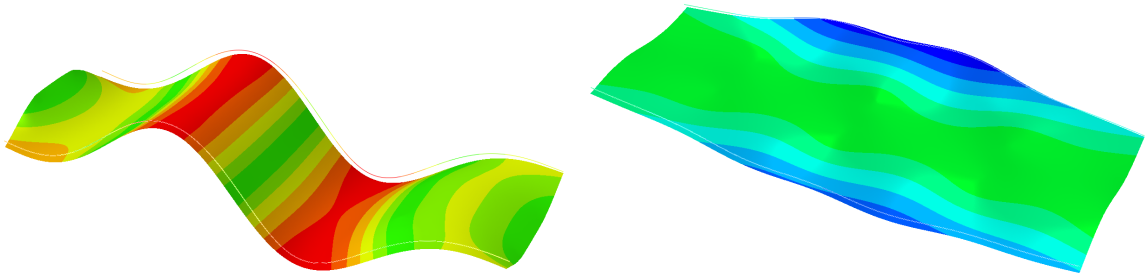

(a) Vertical mode (b) Torsional mode

Figure D.16 – 4 spans - L=10 m

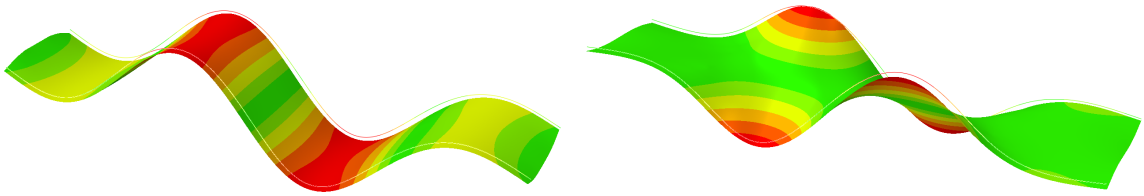

(a) Vertical mode (b) Torsional mode

Figure D.17 – 4 spans - L=15 m

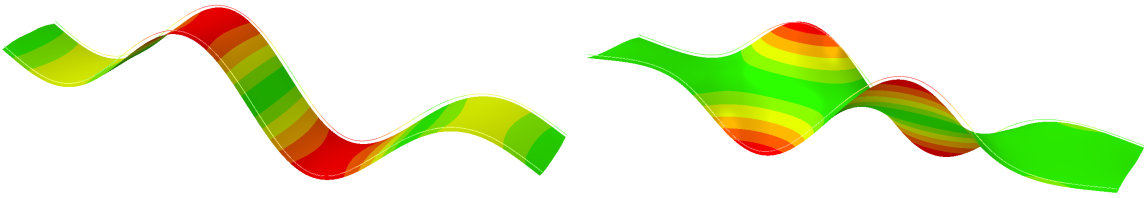

(a) Vertical mode (b) Torsional mode

Figure D.18 – 4 spans - L=20 m

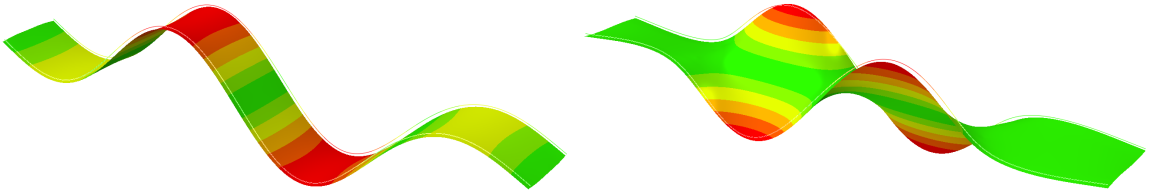

(a) Vertical mode (b) Torsional mode

Figure D.19 – 4 spans - L=25 m

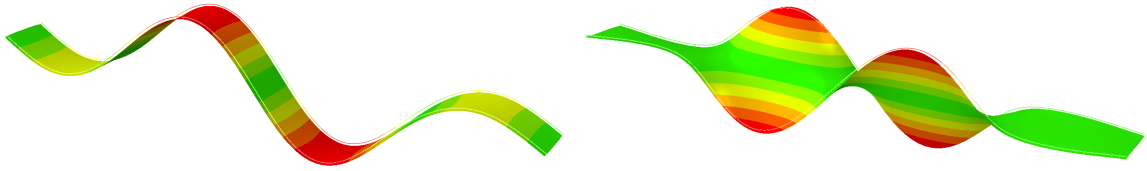

(a) Vertical mode (b) Torsional mode

Figure D.20 – 4 spans - L=30 m

Appendix E

Contributions of different modes of vibration

In this appendix are presented the contributions of different modes of vibration on the total response. In particular, torsional modes coming from 3D models can be compared and quantified. Also, some contributions might be overestimated in some cases due to filters used to dissociate each mode, especially when eigenfrequencies are close to each other.

In each FRF is presented the absolute value of the displacement, obtained after a linear interpolation.

E.1 Results for L=10.4 m

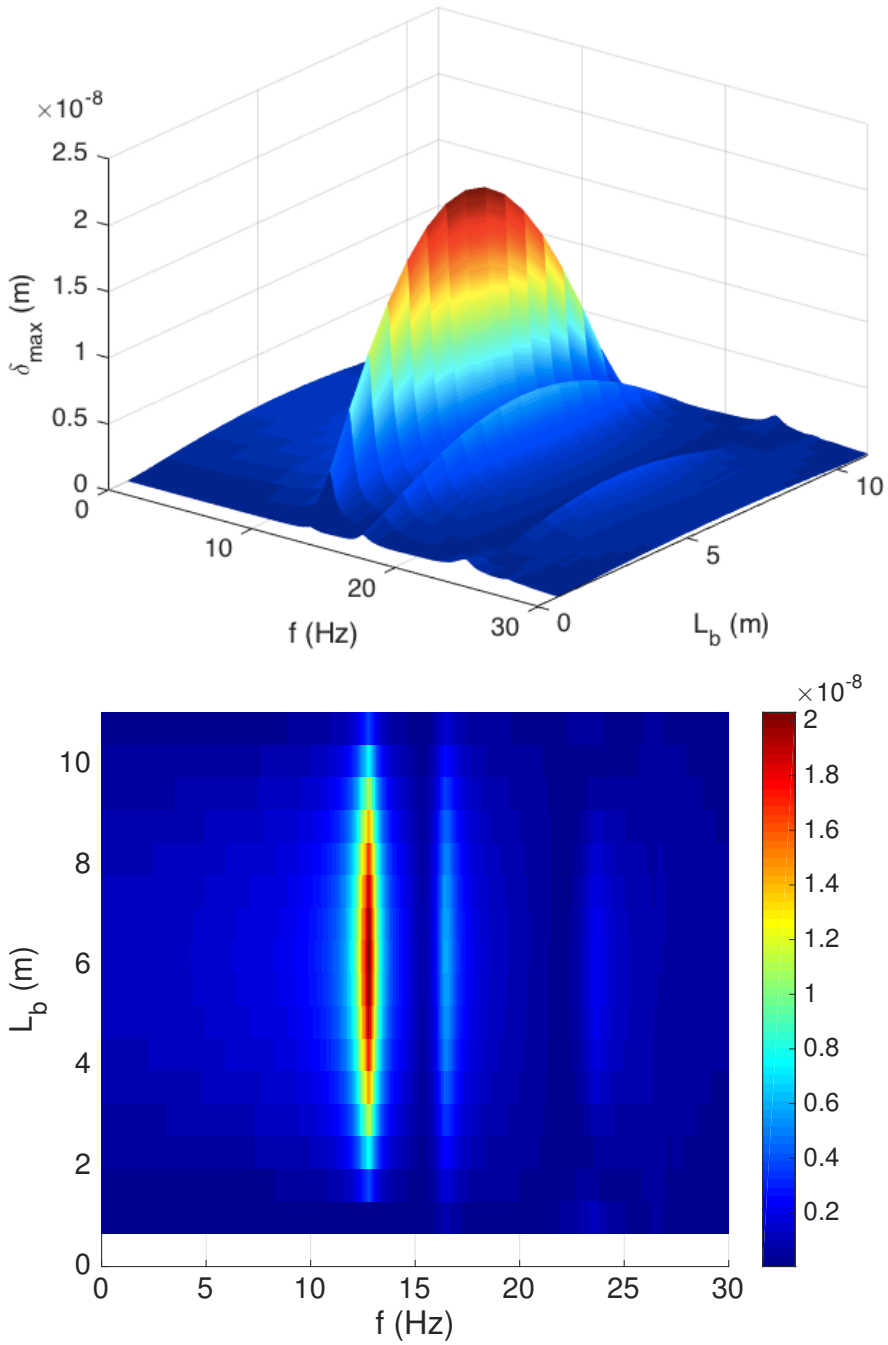

Figure E.1 – FRF - L=10.4 m - 1 span

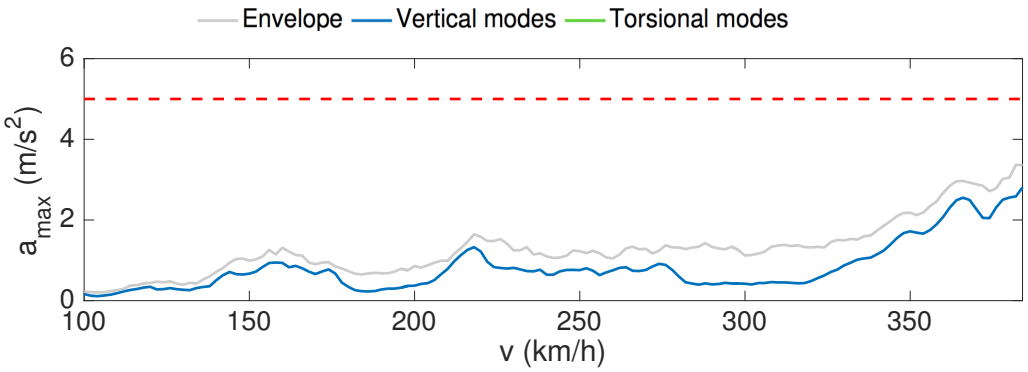

(a) Contribution of the first mode-shape

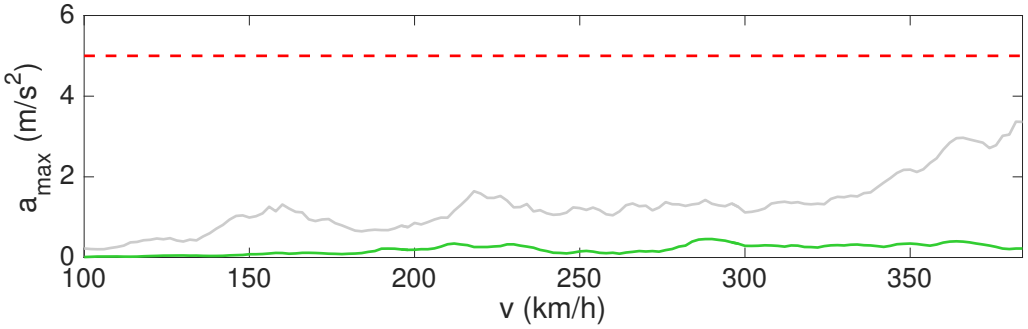

(b) Contribution of the second mode-shape

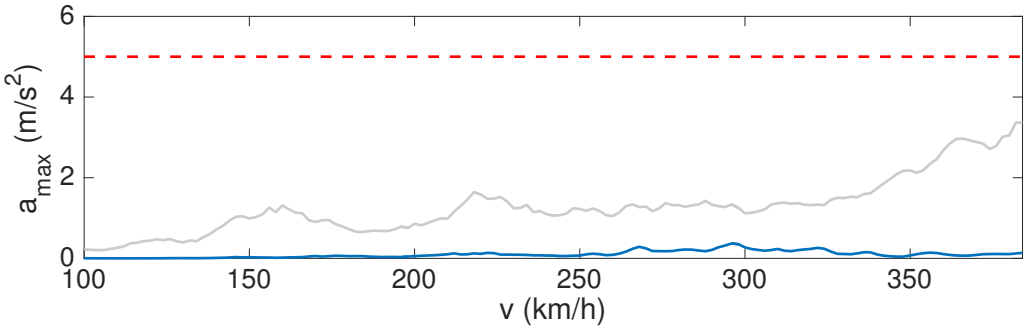

(c) Contribution of the third mode-shape

Figure E.2 – Contribution of different mode-shapes - L=10.4 m - 1 span

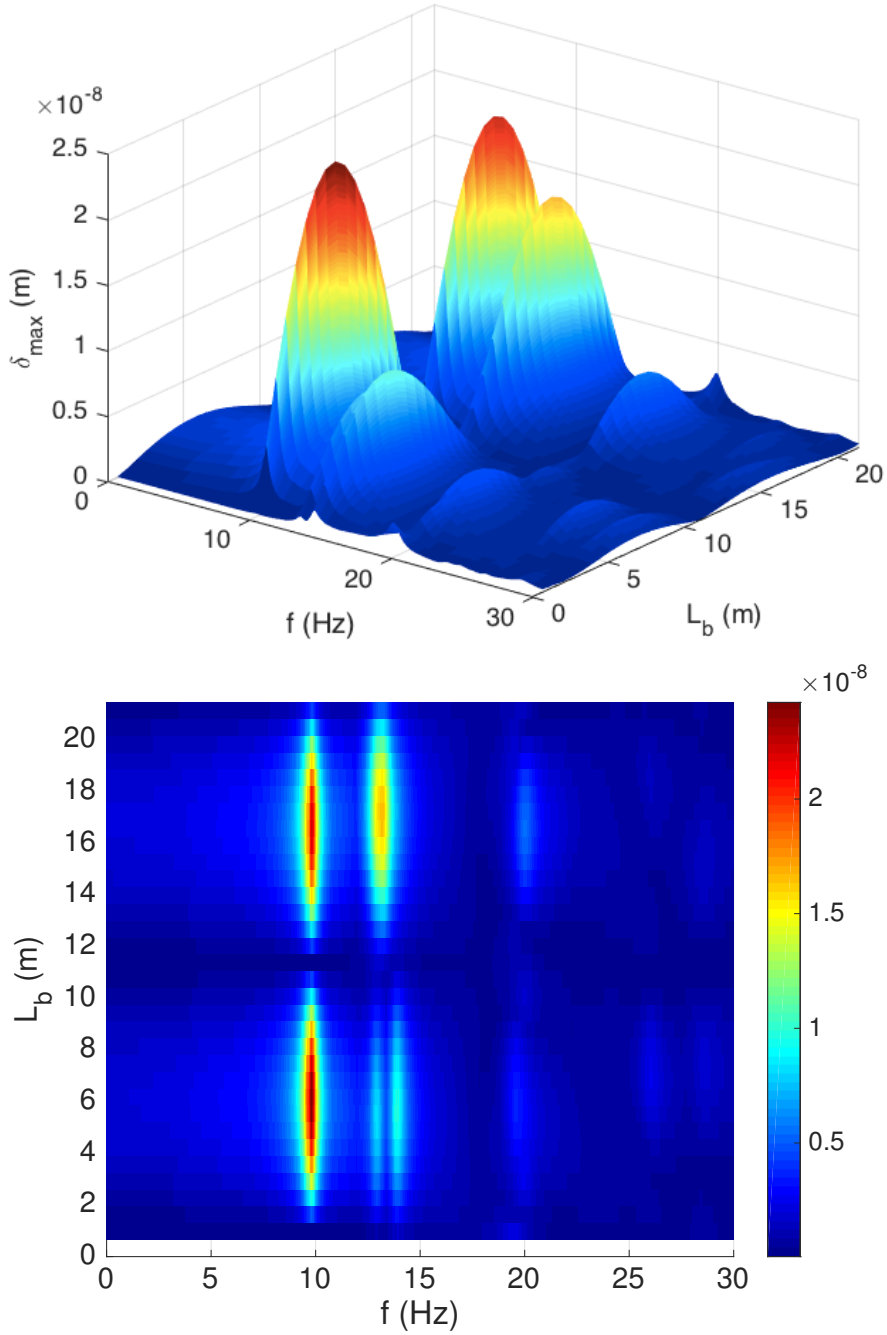

Figure E.3 – FRF - L=10.4 m - 2 spans

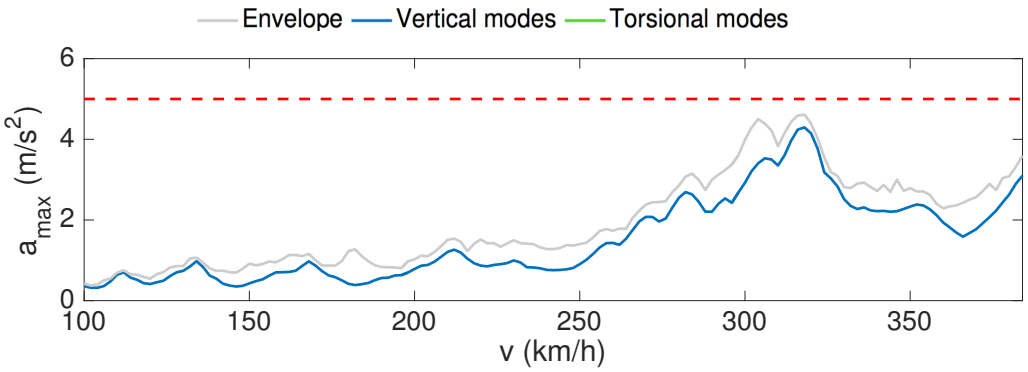

(a) Contribution of the first mode-shape

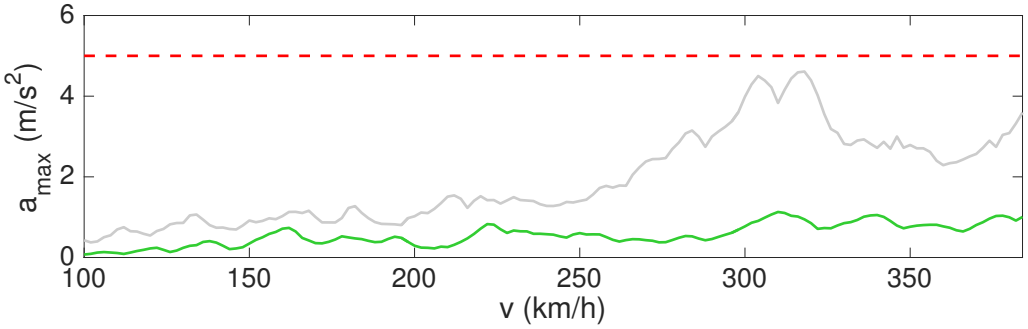

(b) Contribution of the second, third and fourth mode-shapes

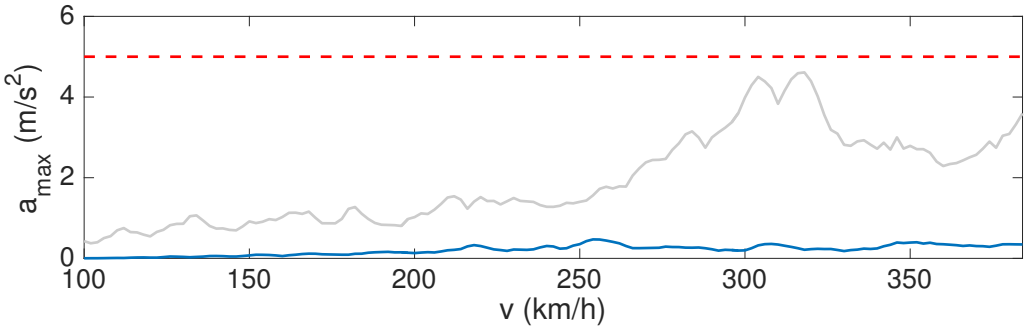

(c) Contribution of the fifth mode-shapes

Figure E.4 – Contribution of different mode-shapes - L=10.4 m - 2 spans

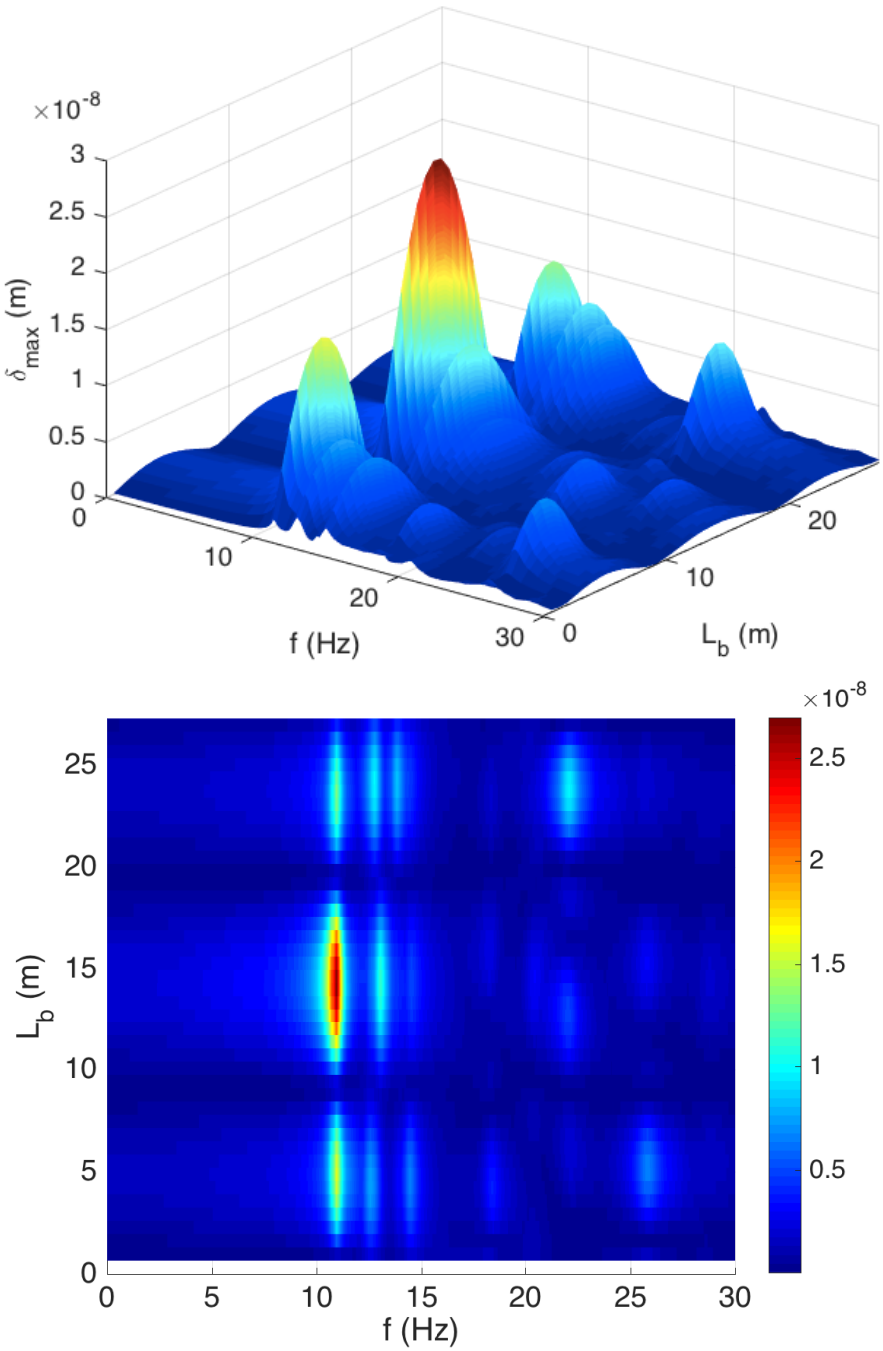

Figure E.5 – FRF - L=10.4 m - 3 spans

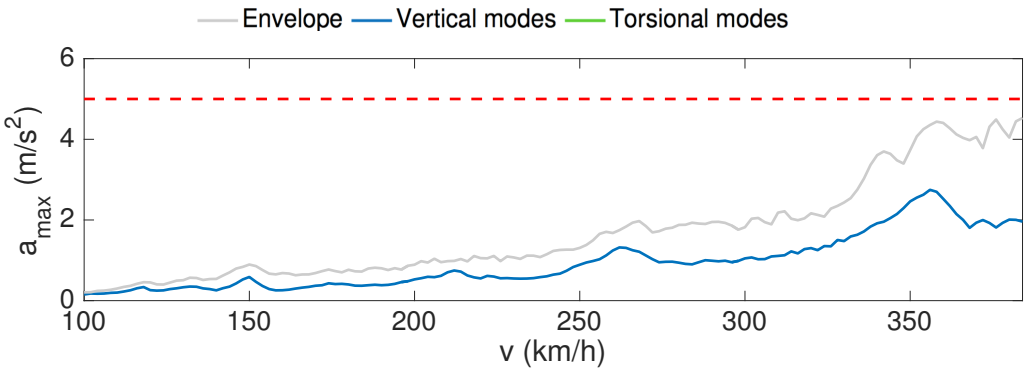

(a) Contribution of the first mode-shape

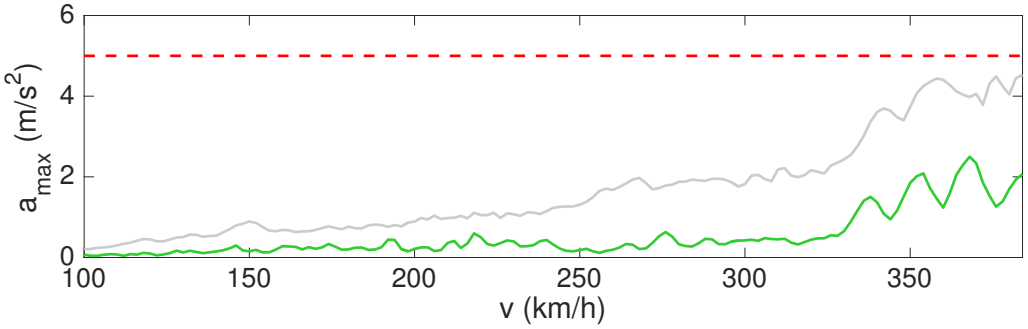

(b) Contribution of the second, third, fourth and fifth mode-shape

Figure E.6 – Contribution of different mode-shapes - L=10.4 m - 3 spans

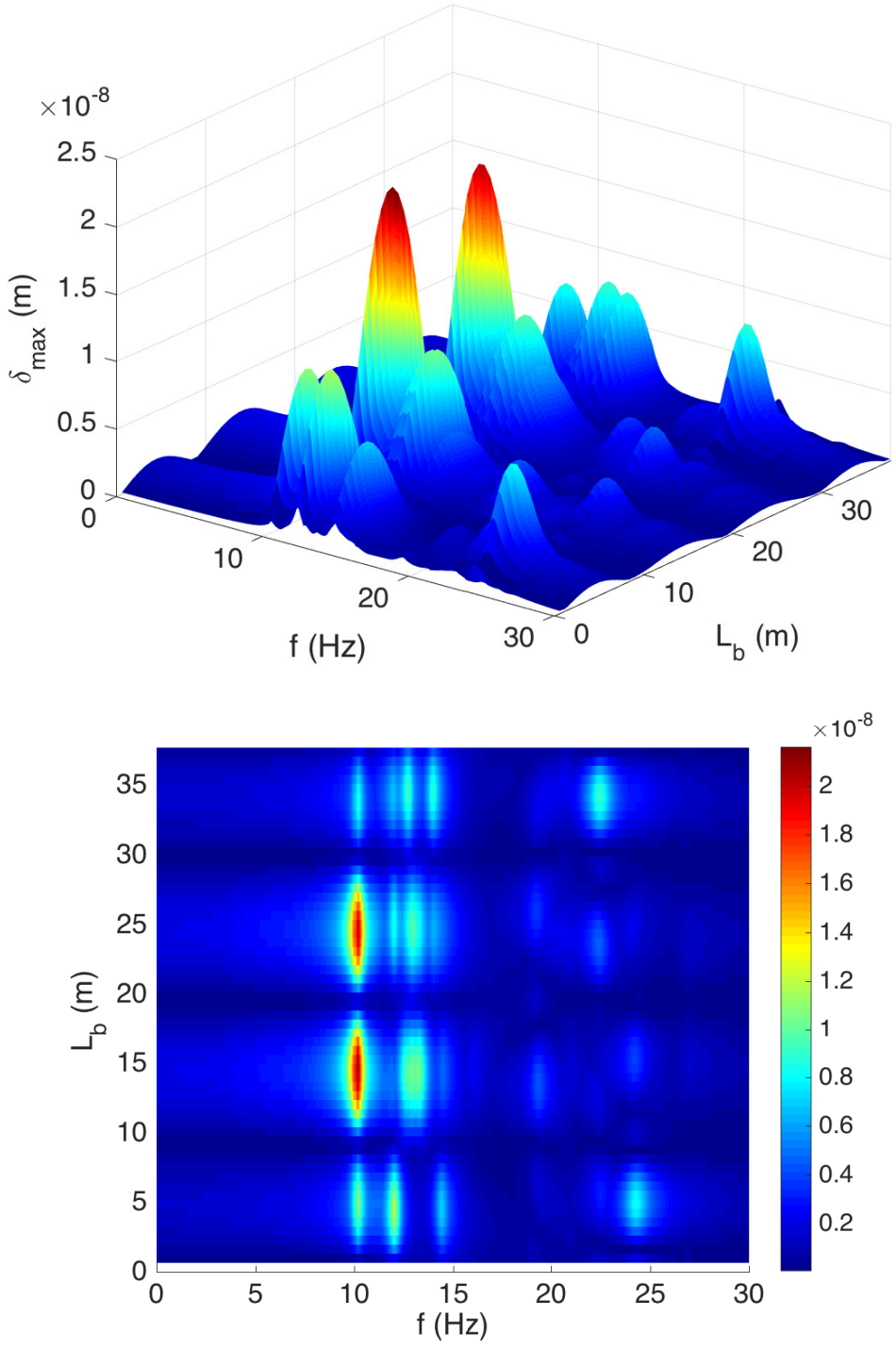

Figure E.7 – FRF - L=10.4 m - 4 spans

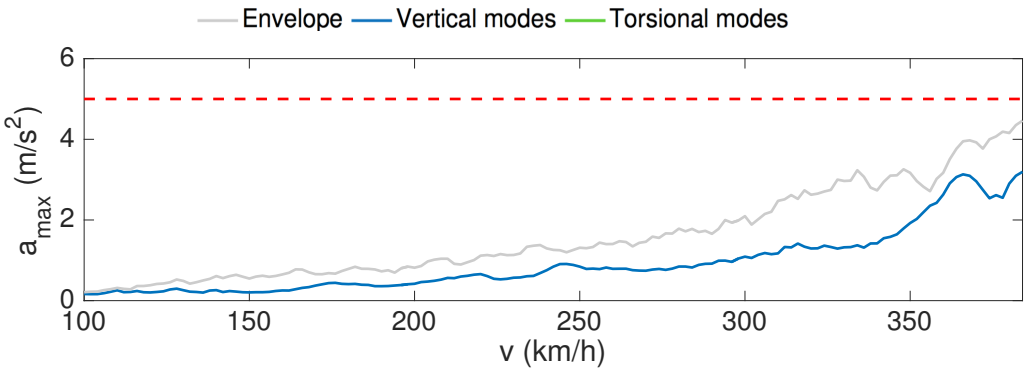

(a) Contribution of the first mode-shape

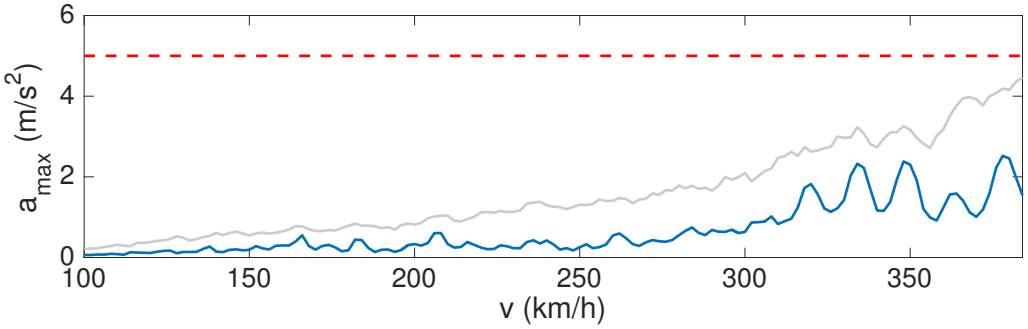

(b) Contribution of the second, third and fourth mode-shape

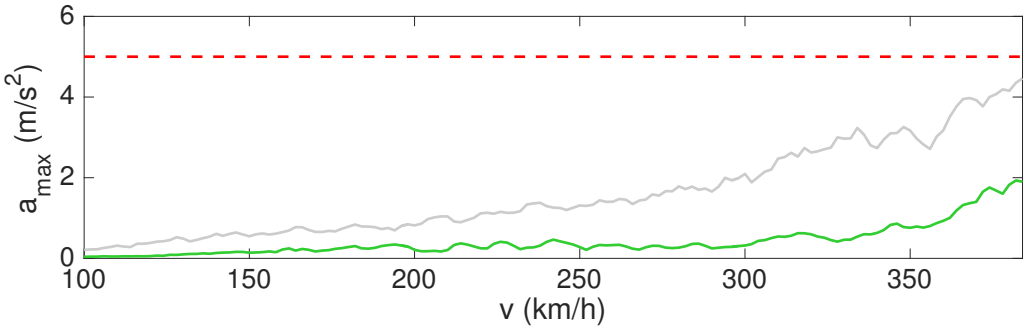

(c) Contribution of the fifth, sixth, seventh and eighth mode-shapes

Figure E.8 – Contribution of different mode-shapes - L=10.4 m - 4 spans

E.2 Results for L=19.5 m

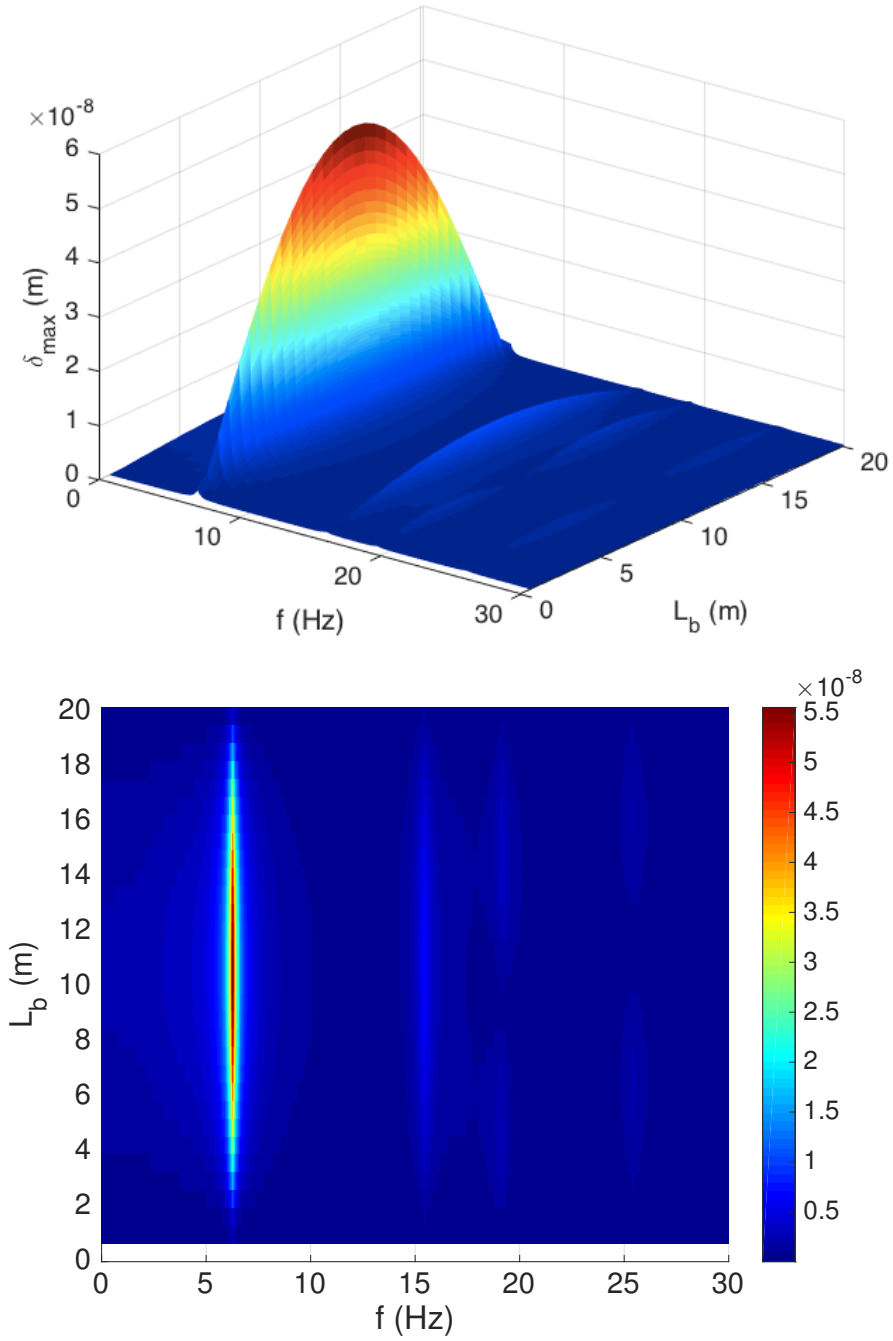

Figure E.9 – FRF - L=19.5 m - 1 span

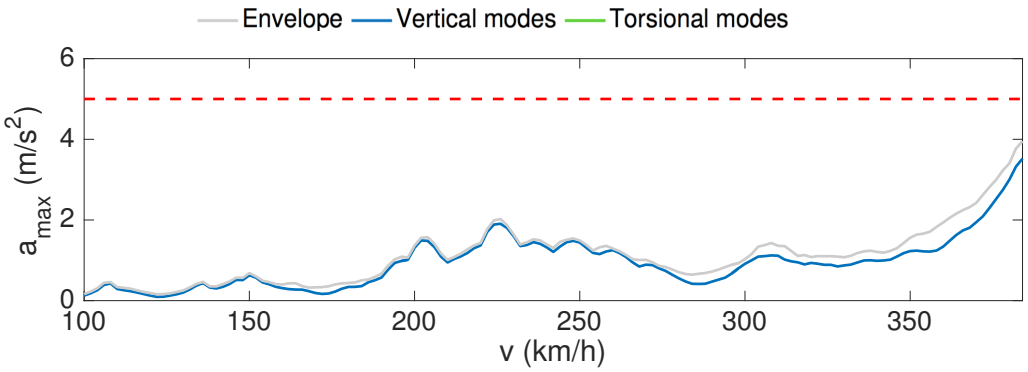

(a) Contribution of the first mode-shape

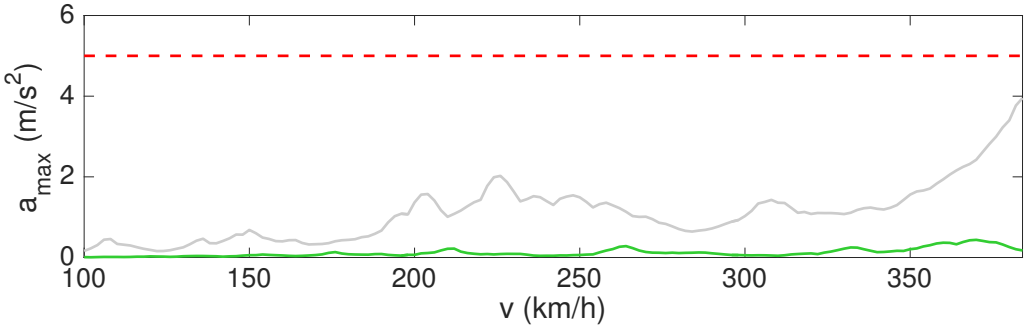

(b) Contribution of the second mode-shape

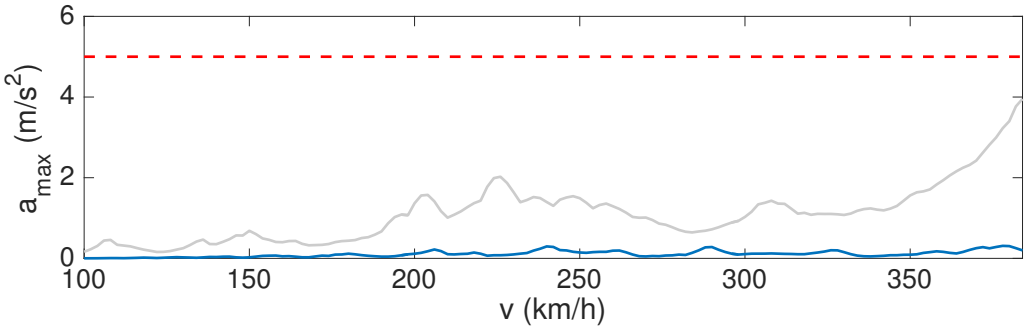

(c) Contribution of the third mode-shape

Figure E.10 – Contribution of different mode-shapes - L=19.5 m - 1 span

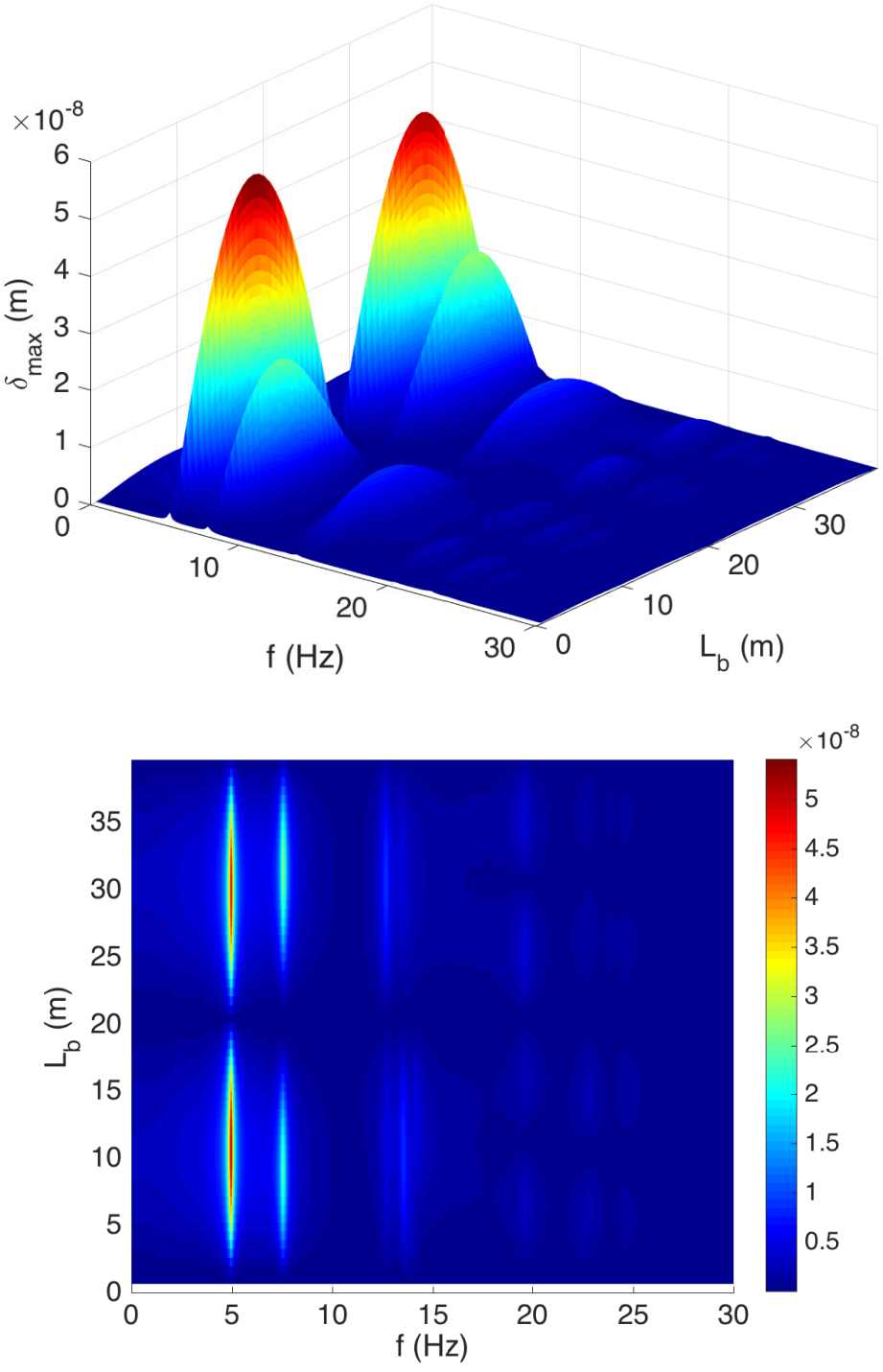

Figure E.11 – FRF - L=19.5 m - 2 spans

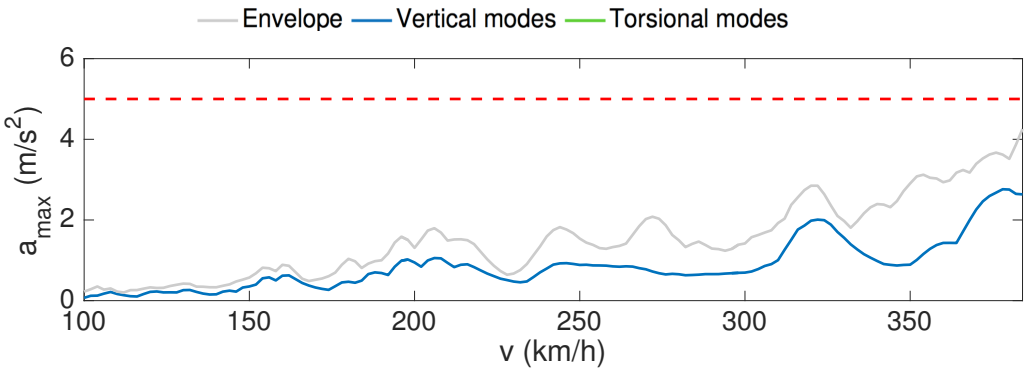

(a) Contribution of the first mode-shape

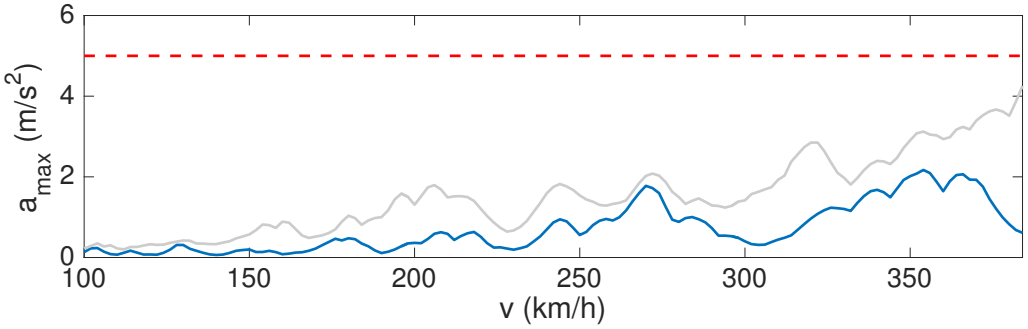

(b) Contribution of the second mode-shape

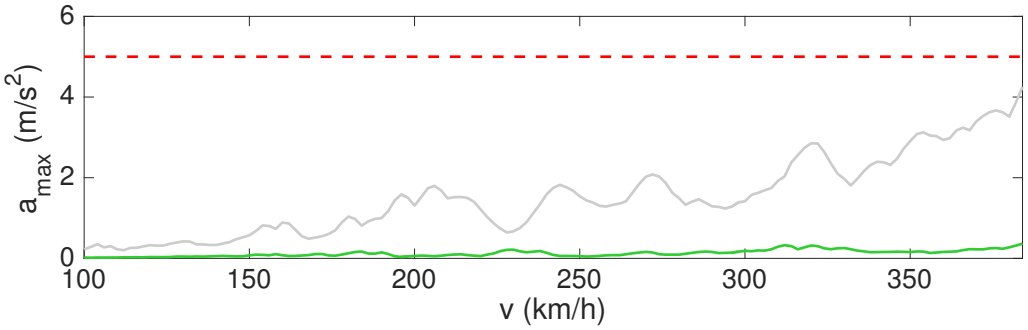

(c) Contribution of the third and fourth mode-shape

Figure E.12 – Contribution of different mode-shapes - L=19.5 m - 2 spans

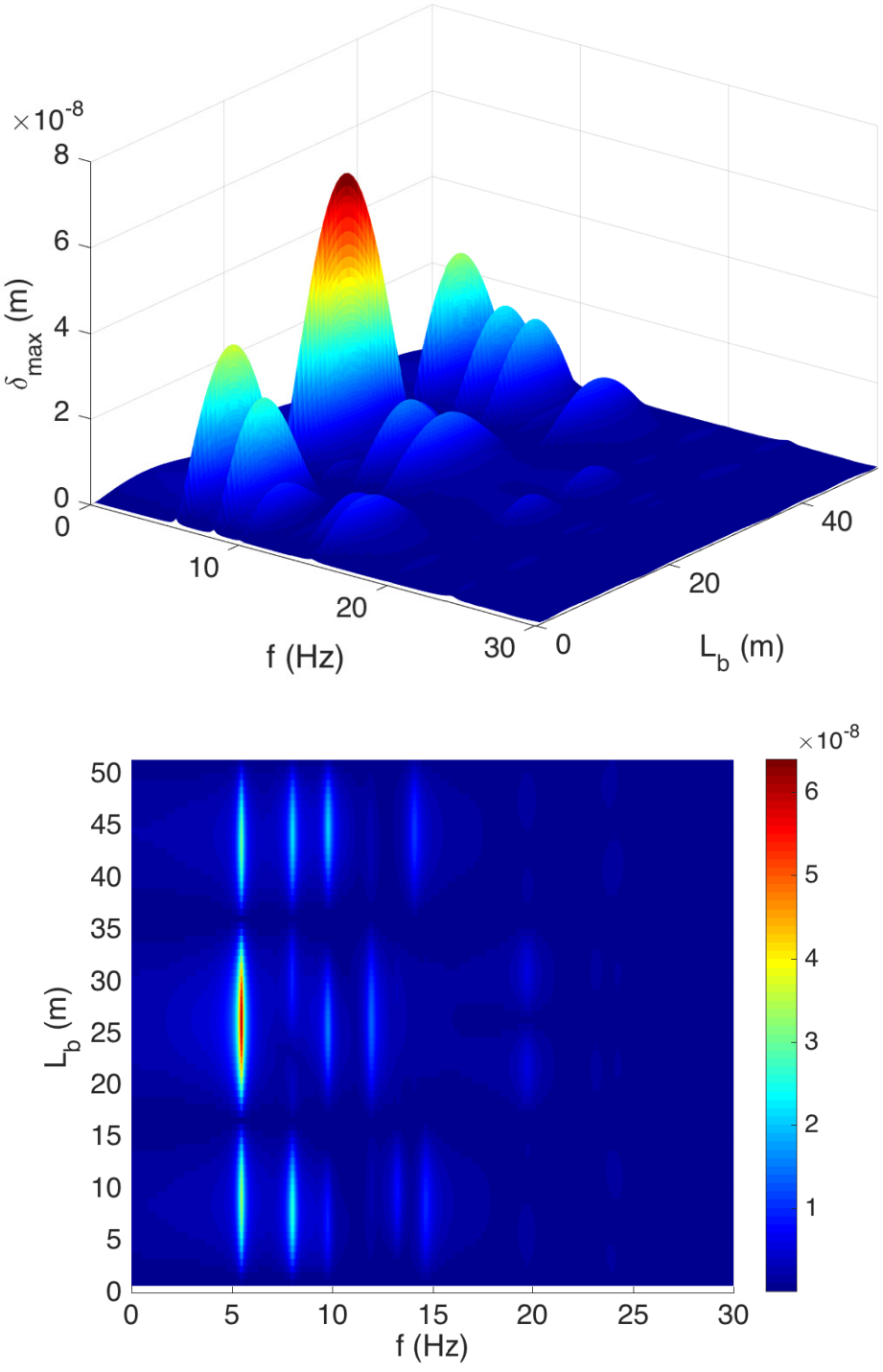

Figure E.13 – FRF - L=19.5 m - 3 spans

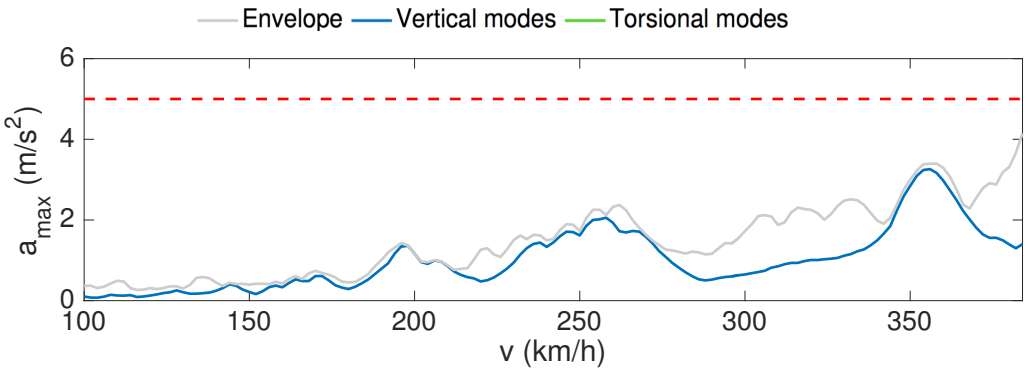

(a) Contribution of the first mode-shape

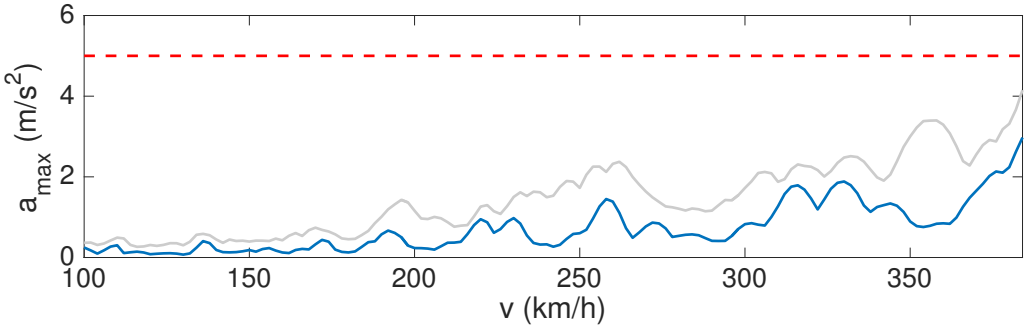

(b) Contribution of the second mode-shape

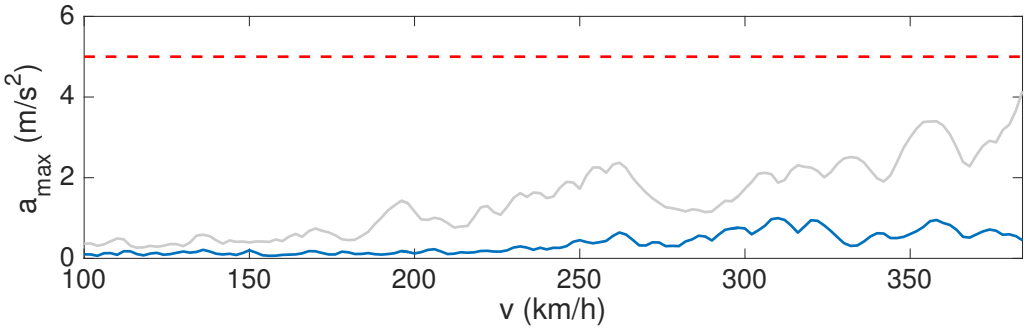

(c) Contribution of the third mode-shape

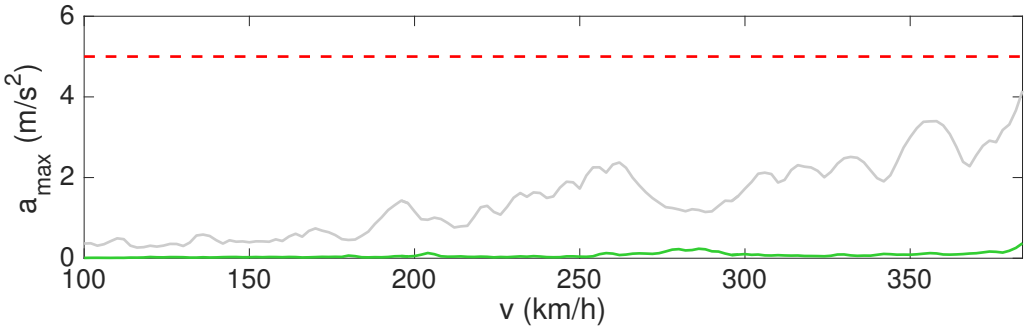

(d) Contribution of the fourth mode-shape

Figure E.14 – Contribution of different mode-shapes - L=19.5 m - 3 spans

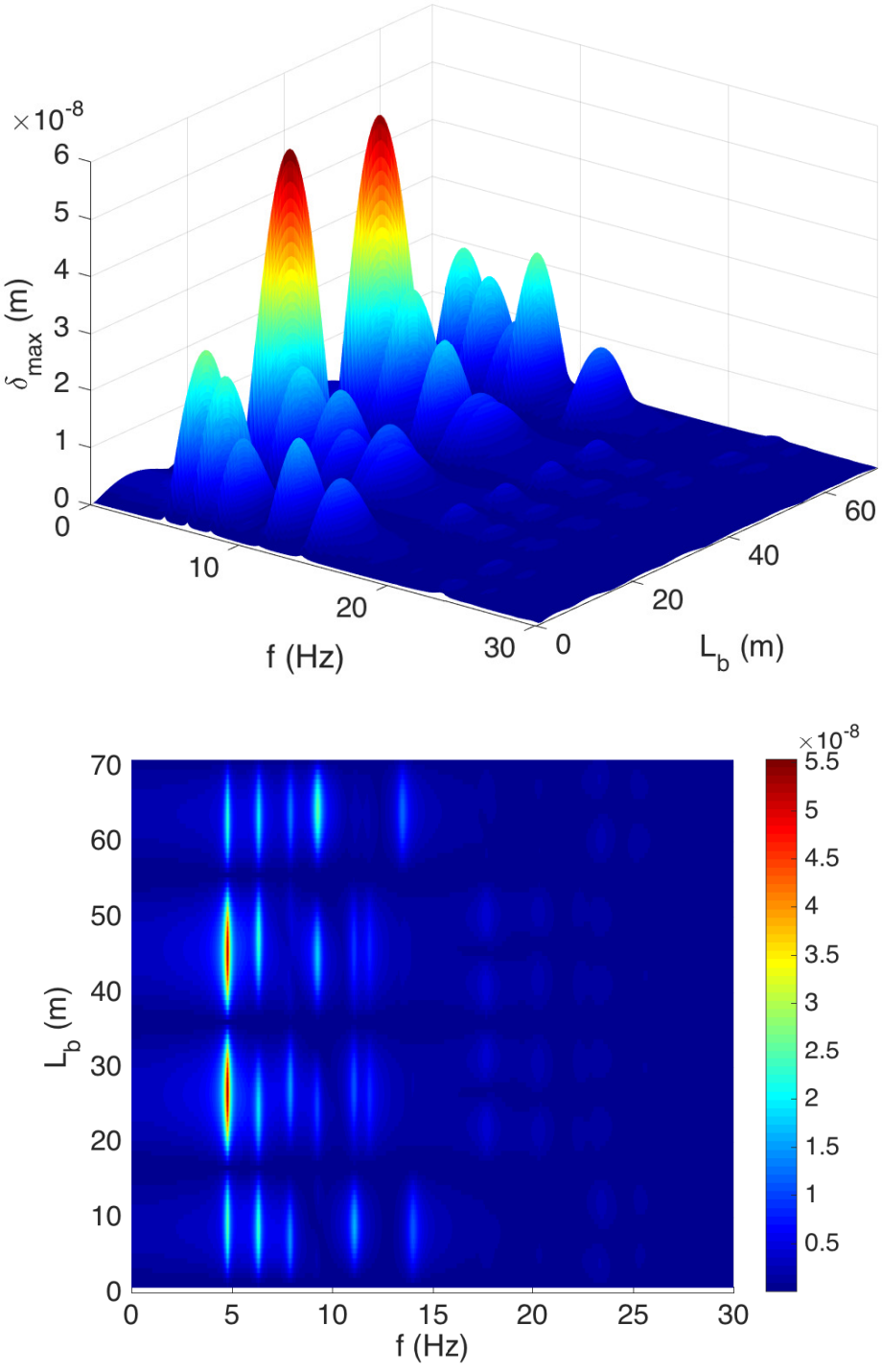

Figure E.15 – FRF - L=19.5 m - 4 spans

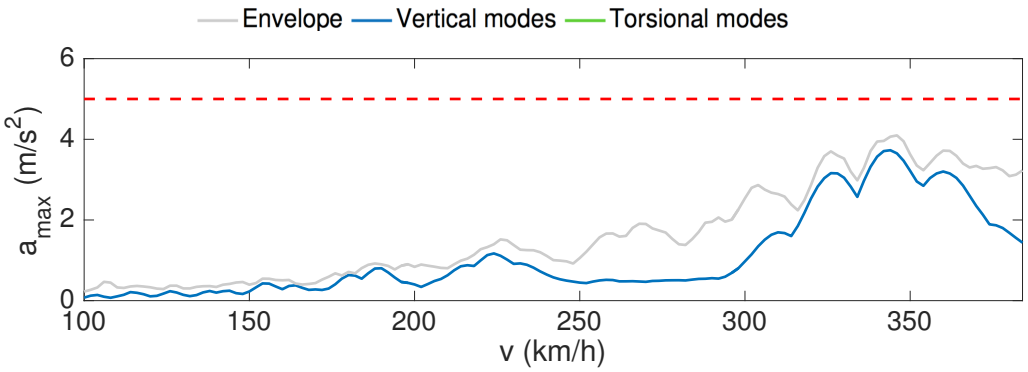

(a) Contribution of the first mode-shape

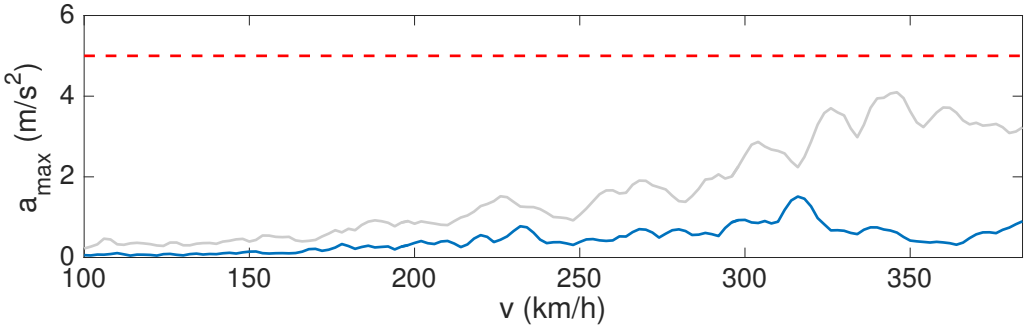

(b) Contribution of the second mode-shape

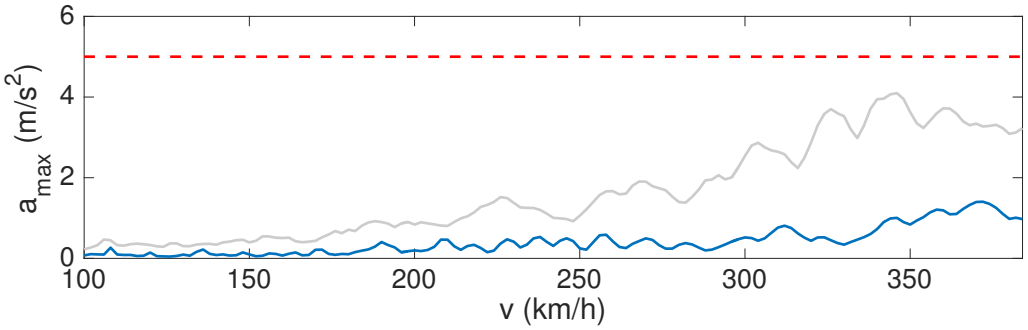

(c) Contribution of the third mode-shape

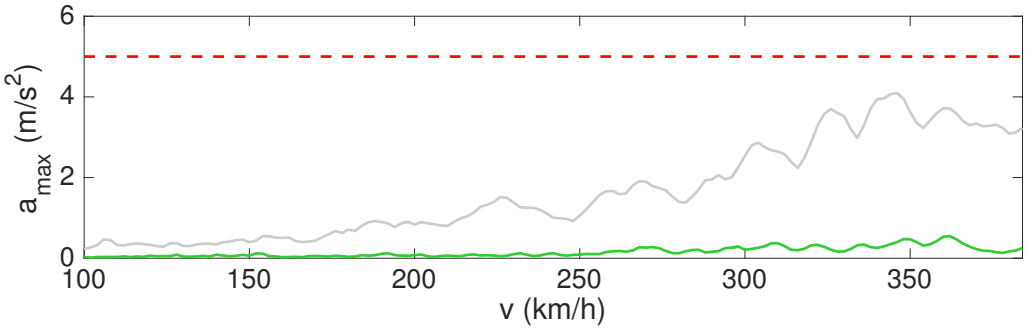

(d) Contribution of the fourth mode-shape

Figure E.16 – Contribution of different mode-shapes - L=19.5 m - 4 spans

E.3 Results for L=29.9 m

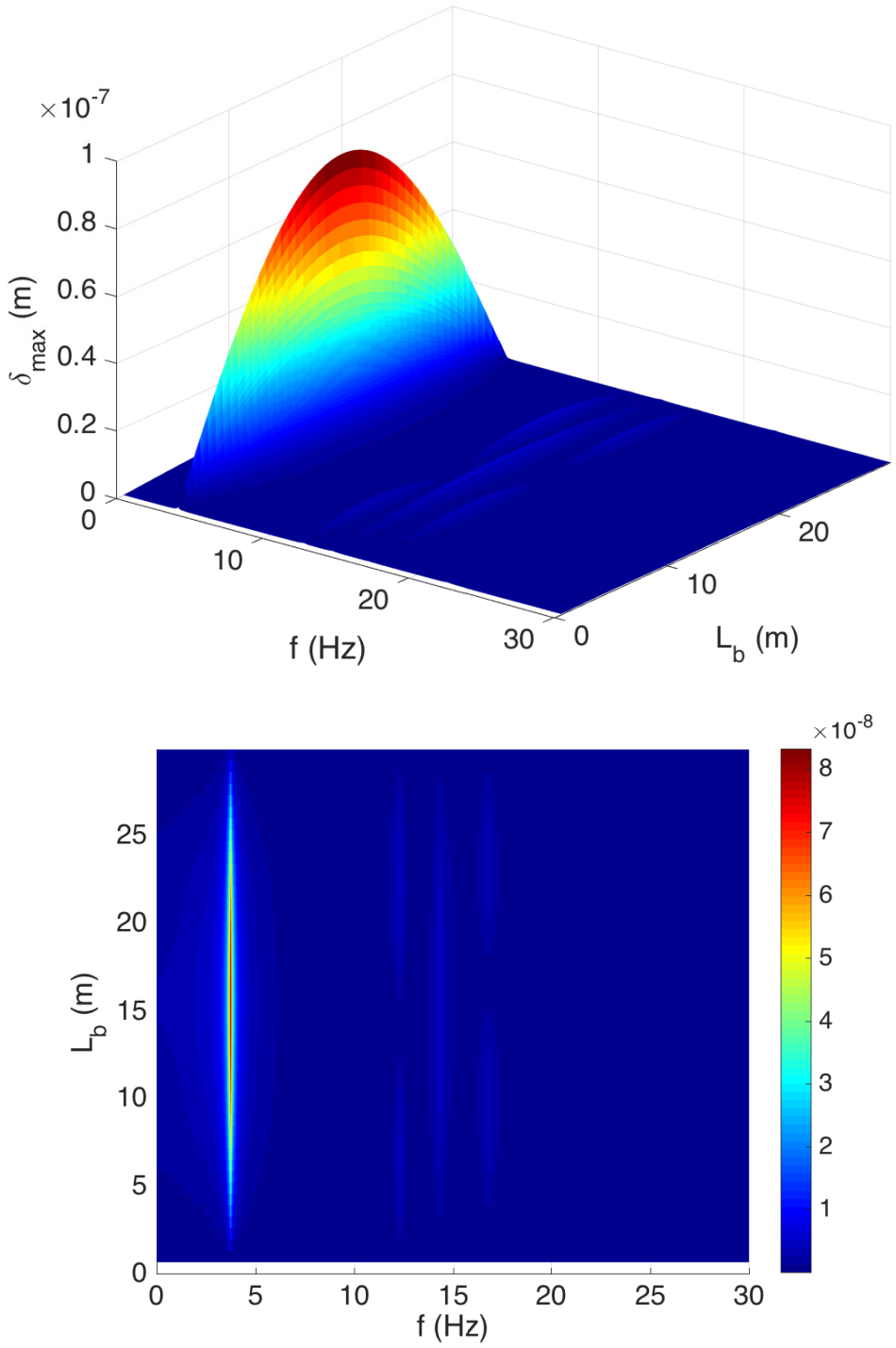

Figure E.17 – FRF - L=29.9 m - 1 span

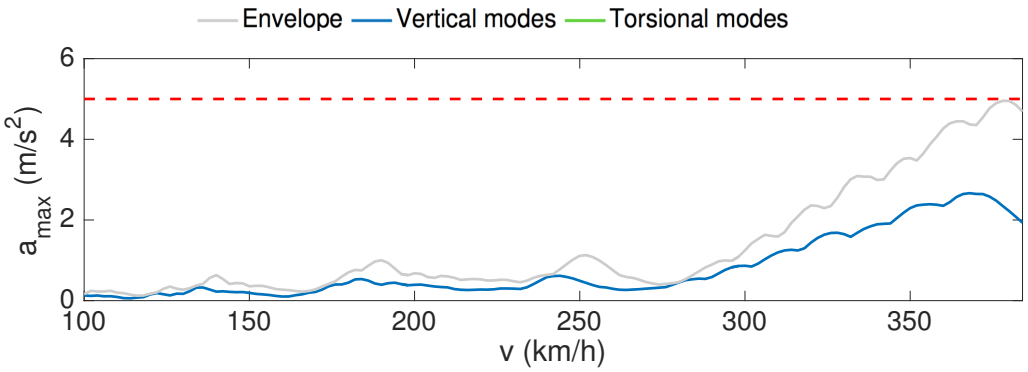

(a) Contribution of the first mode-shape

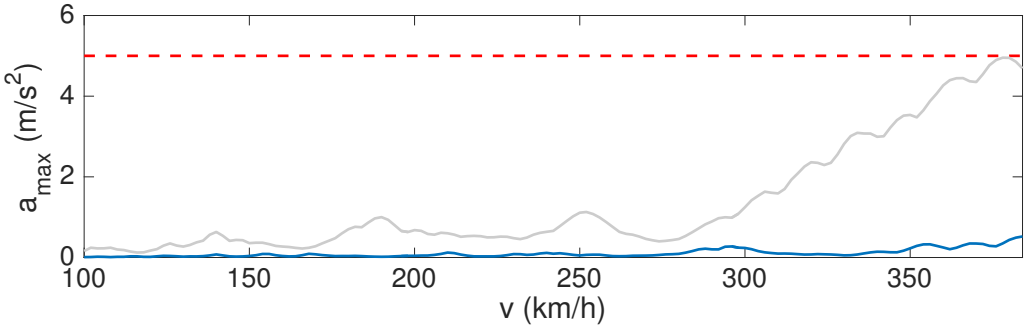

(b) Contribution of the second mode-shape

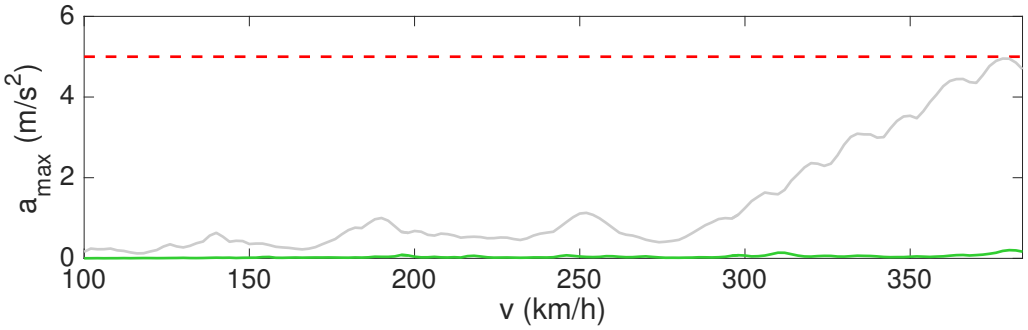

(c) Contribution of the third mode-shape

Figure E.18 – Contribution of different mode-shapes - L=29.9 m - 1 span

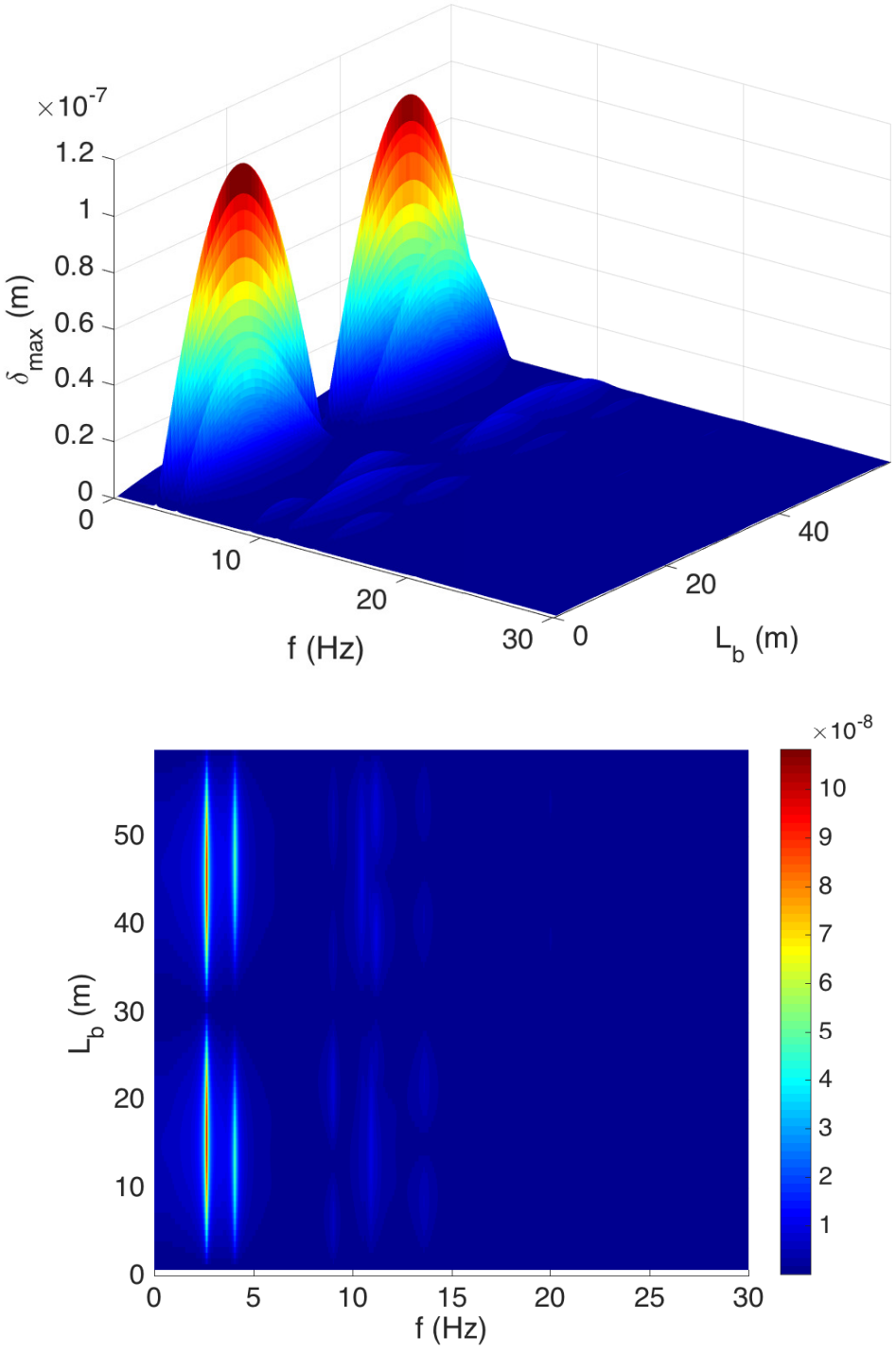

Figure E.19 – FRF - L=29.9 m - 2 spans

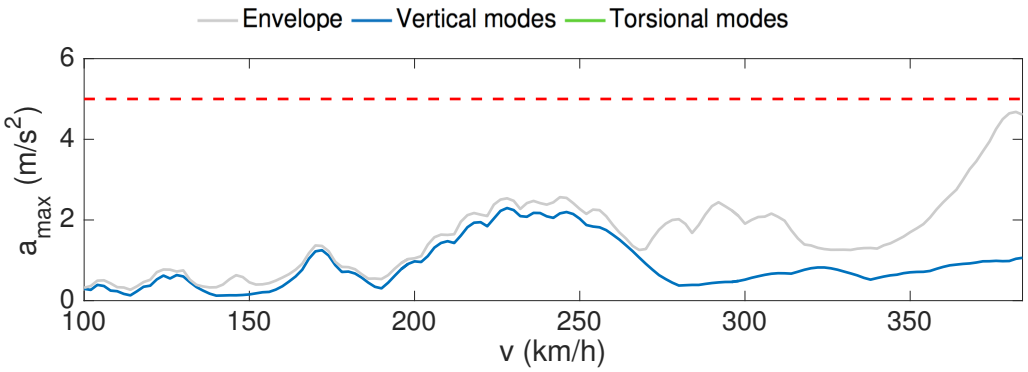

(a) Contribution of the first mode-shape

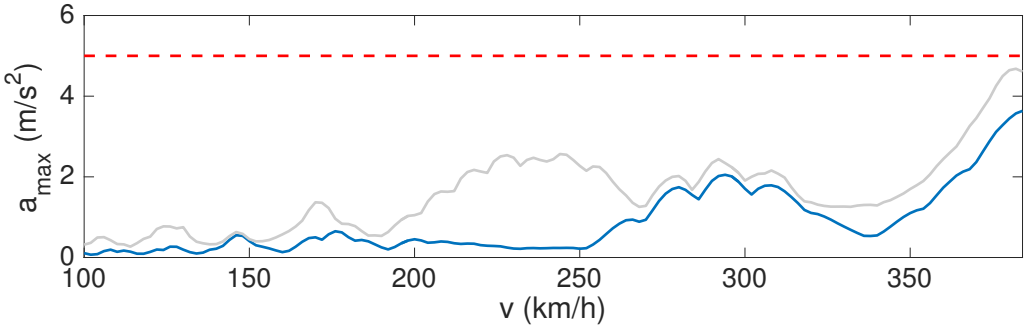

(b) Contribution of the second mode-shape

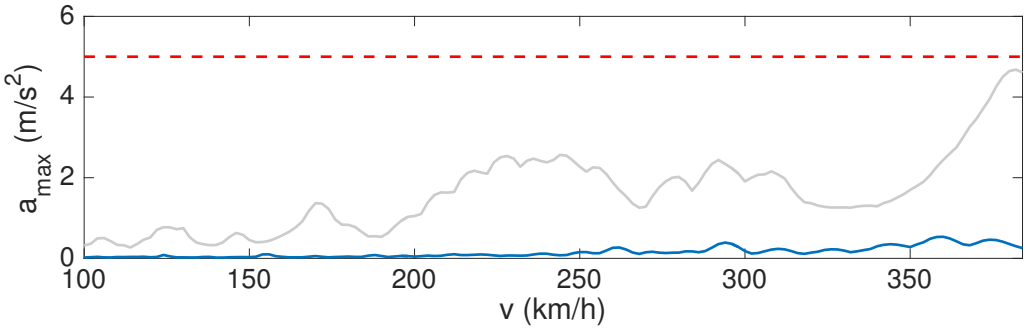

(c) Contribution of the third mode-shape

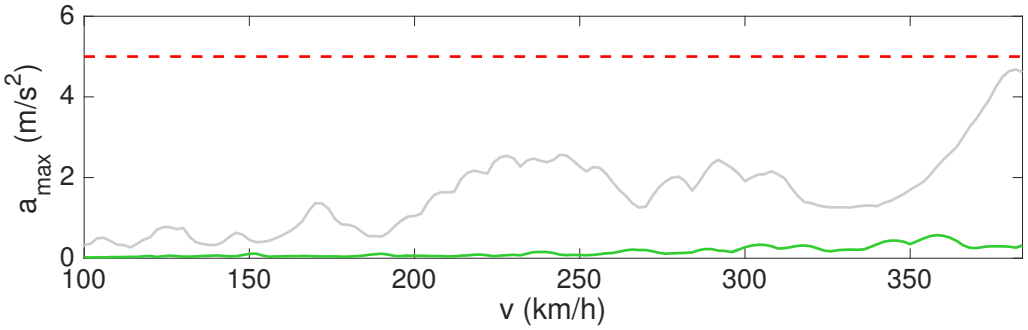

(d) Contribution of the fourth and fifth and sixth mode-shapes

Figure E.20 – Contribution of different mode-shapes - L=29.9 m - 2 spans

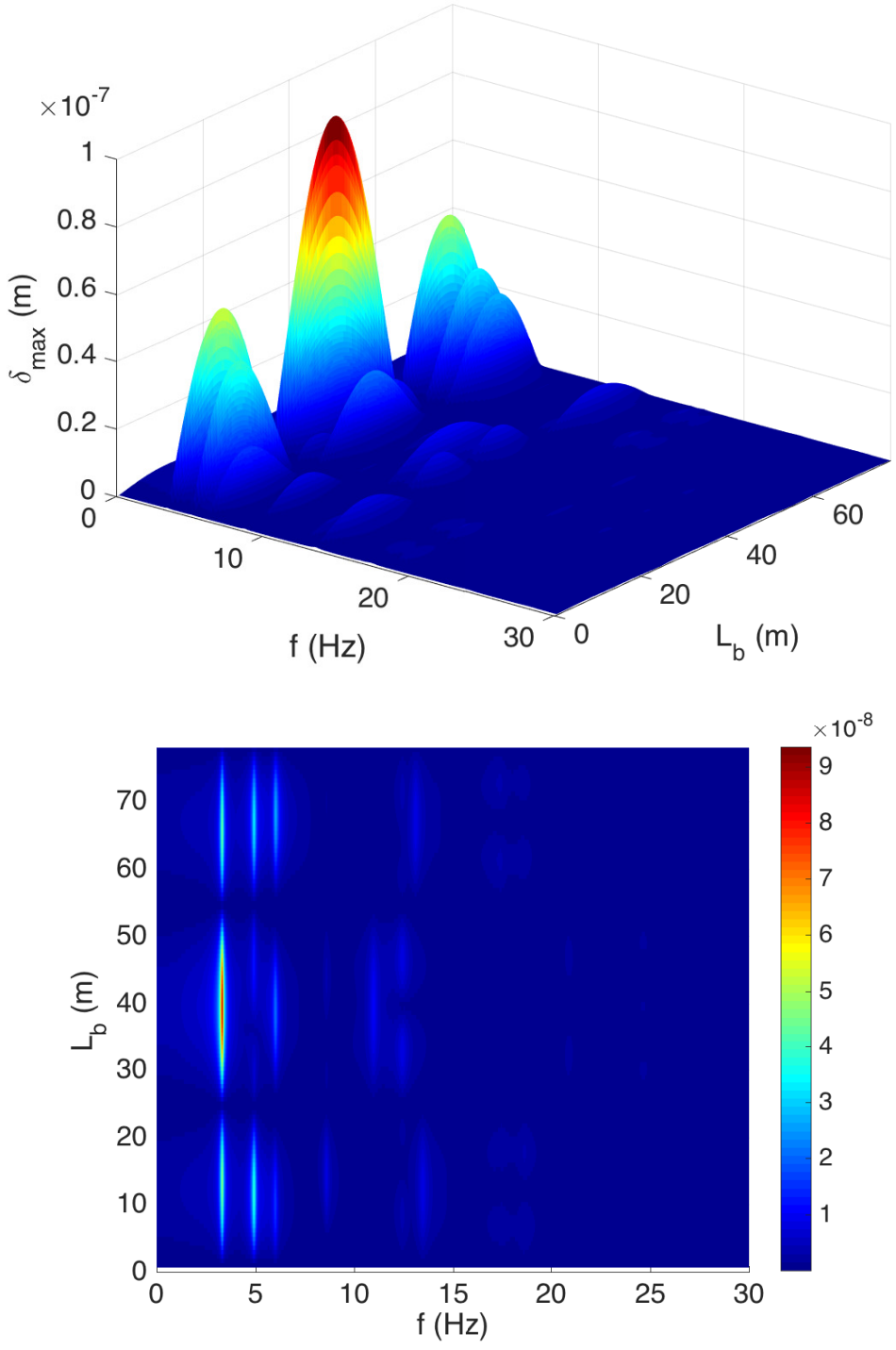

Figure E.21 – FRF - L=29.9 m - 3 spans

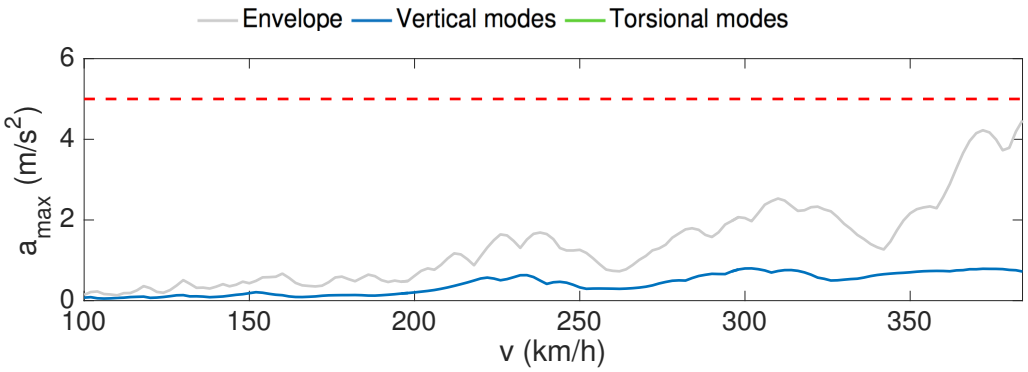

(a) Contribution of the first mode-shape

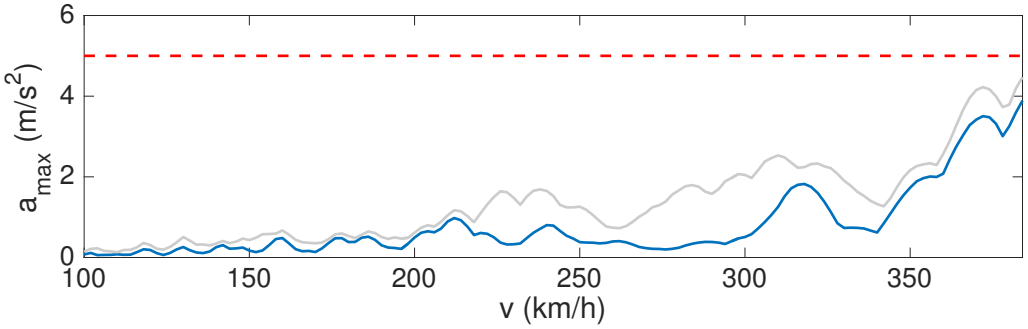

(b) Contribution of the second mode-shape

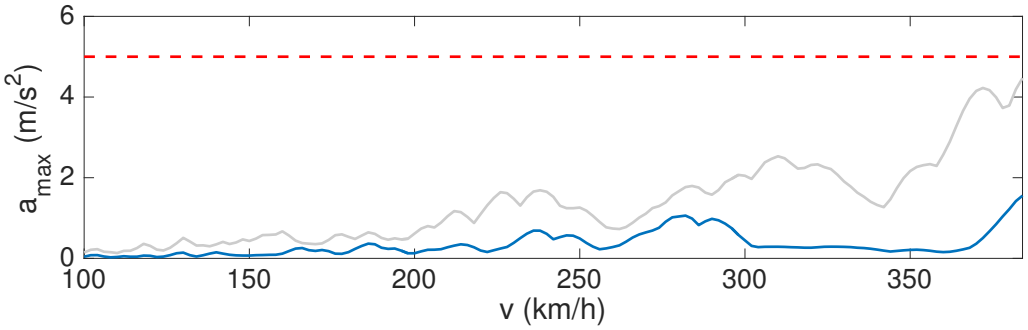

(c) Contribution of the third mode-shape

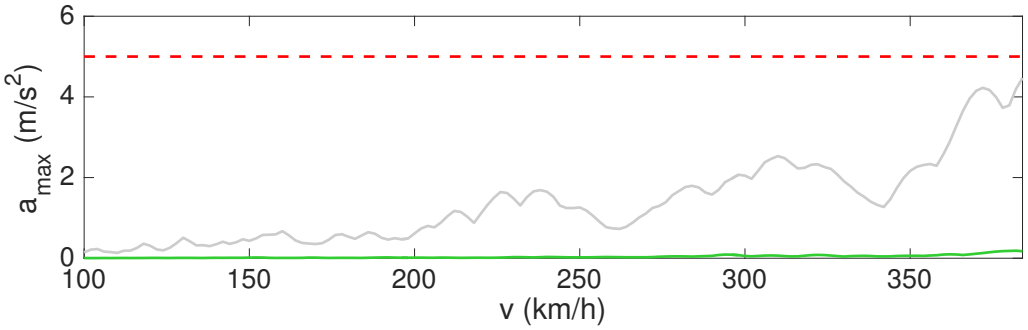

(d) Contribution of the fourth mode-shape

Figure E.22 – Contribution of different mode-shapes - L=29.9 m - 3 spans

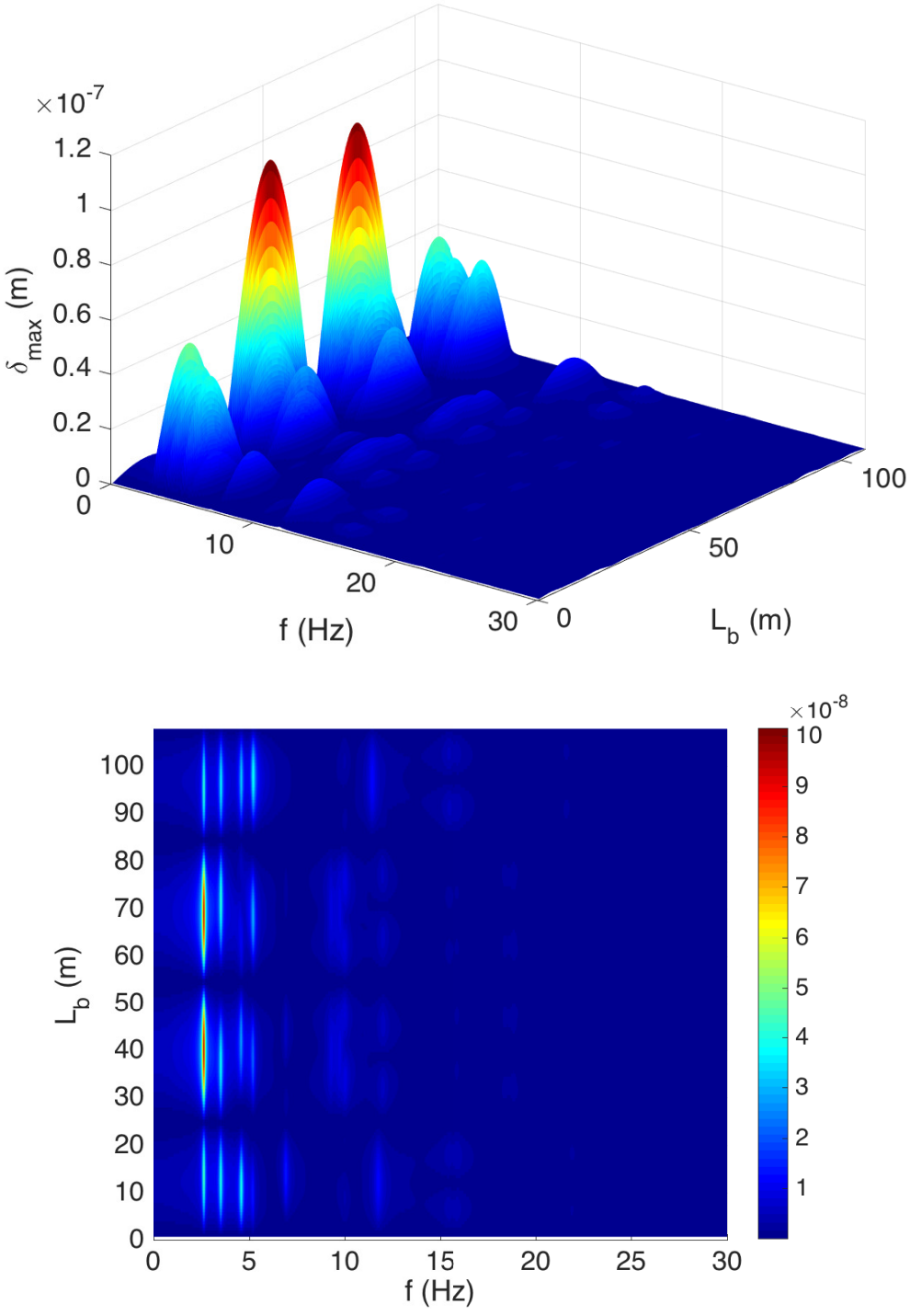

Figure E.23 – FRF - L=29.9 m - 4 spans

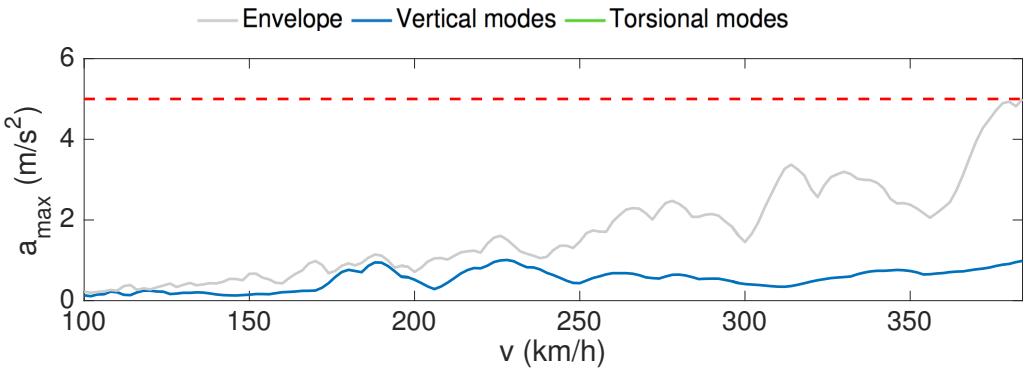

(a) Contribution of the first mode-shape

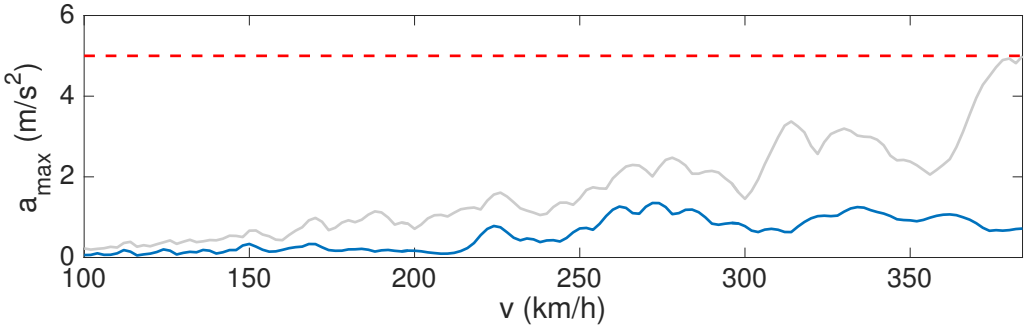

(b) Contribution of the second mode-shape

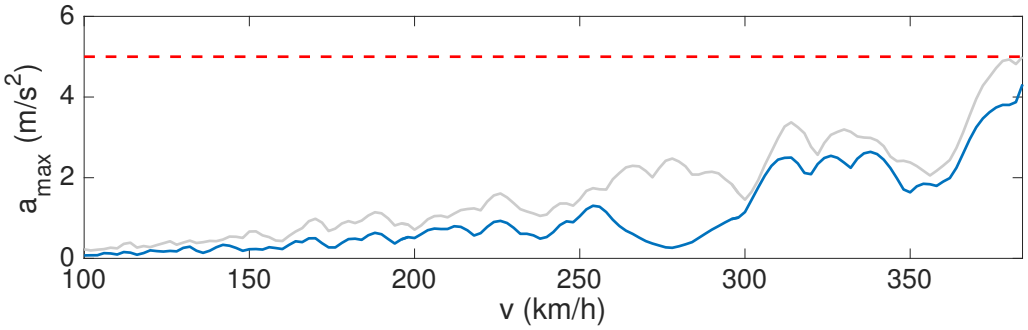

(c) Contribution of the third and fourth mode-shapes

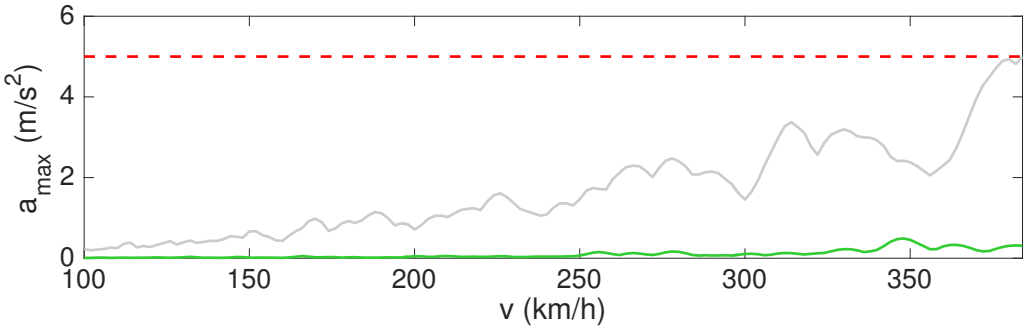

(d) Contribution of the fifth and sixth mode-shapes

Figure E.24 – Contribution of different mode-shapes - L=29.9 m - 4 spans